UNIVERSITY OF PISA

Engineering PhD School “Leonardo da Vinci”

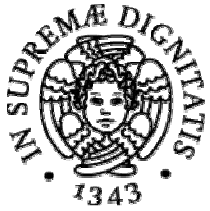

PhD Course in

CHEMICAL ENGINEERING AND MATERIAL SCIENCE

(SSD ING-IND/22)

XXIII cycle

PhD Thesis

Electroactive Materials for Applications in the Field of Wearable Technologies

Author:

Fabia Galantini

Tutors:

Dr. Giuseppe Gallone
Prof. Giovanni Levita
Prof. Danilo De Rossi

(2008 - 2010)

Abstract

The objective of this PhD thesis is to present the most performing EAP-based materials, technologies and devices developed by our lab (Ch.4, 5 and 6) also in collaboration with other research groups (Ch.1, 2 and 3) for sensing, actuating and energy harvesting, with reference to their already demonstrated or potential applicability to electronic textiles and wearable technologies in general.

Over the last decade great strides have been made in the field of wearable technologies: thanks to new discoveries in materials science and miniaturized electronics, tissues and "smart" devices for monitoring vital parameters, rehabilitation and tele-assistance were born. However, a complete and self-powered system, able to exchange information with the external environment, to generate power using the usual movements of the human body (walking, work, sport) and to drive wearable devices, is not yet available on the market and it would find a considerable number of applications (monitoring physiological parameters for athletes and special forces officers in emergency situations, etc.).

After a first survey of the state of the art concerning the so-called "smart materials" and technologies currently available for " wearable " activities, the work has developed on three major directives consisting in: energy generation and storage, sensing and actuation.

Energy generation and storage. An experimental study, conducted mainly during the first year of PhD, has identified possible candidate materials (piezoelectric PVDF, electret PP) for the energy harvesting and subsequent generation of power from movement and gestures by exploiting the piezoelectric properties of selected materials. These materials have been found on the market and processed in laboratory. In collaboration with the University of Pavia, a circuit for the storage of electric charges generated was made. The obtained transduction systems were electromechanically tested and the generation of electric charges has been used to develop a demonstrator generator-LED embedded in a shoe.

Sensing. During the first and second year, different sensor configurations of "dry" piezoelectric PVDF sensors were tested for the monitoring of vital parameters (heart and breathing rate). Such sensors, prepared in collaboration with the University of Lodz (TUL, Poland), our partners in the PROETEX European project (6^{th} FP 2006-2009), were woven into fabrics to be easily integrated into clothing, and their response was studied. Signal intensities comparable to those of common 3M medical electrodes have been observed. A further development of these materials should be turn to reduce noise, while a computational study might deal with the signal filtering and elimination of motion artifacts.

Along with the study of piezoelectric sensors mentioned above, during the third PhD year the production and characterization of dielectric elastomers for sensing applications (artificial skin) was developed too, in collaboration with the Genova DIST (Dipartimento di Informatica, Sistemistica e Telematica). Such elastomers, characterised by high dielectric constants and restrained compressive elastic moduli, were developed in order to act as dielectric medium in piezo-capacitive sensing devices. The obtained materials will be used as artificial skin in robotic systems.

Actuating. In parallel with the two lines described above, the activity was concentrated, throughout the period of PhD, on the development of new dielectric elastomer actuators, to be used as high dielectric constant, low elastic modulus and, especially, low electric driving fields devices so that they can be used once inserted inside the clothing (simplified prototype actuators able to change the porosity / texture of different textiles were developed during the first year of activity for the FLEXIFUNBAR European project (6^{th} FP 2005-2008)). The "blend" approach has been privileged over the "composite" approach, previously studied in the master thesis, and has led to promising results both from the applicative point of view, with an increase in the electromechanical performance, and on a fundamental level, for the implications emerging from the interaction between different phases in the study of dielectric response of partially heterogeneous systems.

Electromechanical encouraging results were then obtained during the second year of activity with the development of silicone/polyurethane (SI/PU) blends prepared by appropriate volume fractions. Further improvements have also been achieved during the third year of doctoral studies, when it was introduced in the same mixtures a third component, the conjugated polymer poly-(3-hexylthiophene-2,5-dyil) (P3HT), already used by our group for its high polarizability in order to increase the dielectric constant of silicon actuators. The obtained samples, dielectrically, mechanically and electromechanically tested, showed that the conjugated polymer leads to a further significant increase in the electromechanical response of the blend only when added at levels of 1 wt%. This polymer shows, in fact, a certain influence on the microscopic distribution of the SI and PU "phases" in the blend. This effect is maximized for the 1 wt% concentration at which the presence of interfaces is maximized and thus a larger surface polarization, combined with the characteristic high polarizability of P3HT, leads to dielectric constant and strain further implementations. Similar increases in performance, compared to pure components, were also found in mixtures prepared using other polyurethanes and silicones adopting, when necessary, appropriate steps to modify the kinetics of reaction (addition of solvents).

The results obtained with this "blending" approach are supported by the Intephase Theory (*IT*), recently introduced to complete the well known Effective Medium Theory (*EMT*) which, although applicable to a variety of particle

composite structures, is not suitable to describe the behaviour of systems where the presence of an interphase between filler and matrix is significant. The IT demonstrates that border regions, showing dielectric characteristics different from those of the starting components, can strongly influence the system performance. Through theoretical and experimental evidence, in fact, it is known that, while the inner parts of the matrix polymer chains are able to adopt a configuration that minimizes spontaneous conformational energy, at the interface they are linked or otherwise conditioned in their movements, giving rise to a region where the electrical properties (in some cases also thermal and mechanical) are different from those of both the pure material composing the mixture.

During the third year, the production and characterization of elastomeric foams with dielectric properties suitable for sensing (artificial skin) and actuating applications were also developed. The electromechanical performance of these polyurethane-based foams, after appropriate polarization under very high electric fields (Corona poling), were compared with those of two commercial products, which were also subjected to corona poling. Studies have been conducted also on the life of the induced polarization produced by poling in the foam and on the influence of electric field exposure time on the final response of the material.

The slightly positive results obtained in terms of increased dielectric constants and strains have opened a new line of activity that represents an innovation in the field of dielectric elastomers, that is the preparation of elastomeric foams with electret properties.

Contents

Introduction

It is accepted opinion today that, in order to provide people with personalised healthcare, support and information, technological advances should be brought closer to the subject by means of easy-to-use wearable interfaces between devices and humans. This can be achieved through multifunctional fabrics, commonly referred as *electronic textiles* (*e-textiles)* or *smart textiles* (these terms will be interchangeable in this thesis), capable of making daily life healthier, safer and more comfortable. Such fabrics are conceived as innovative and high knowledge-content garments, integrating sensing, actuation, electronic and power functions. Due to their multifunctional interactivity, enabled by wearable devices that are flexible and conformable to the human body, e-textiles are considered relevant promoters of a higher quality of life and progress in biomedicine as well as several health-focused disciplines, such as biomonitoring, rehabilitation, telemedicine, teleassistance, ergonomics and sport medicine. Biomonitoring, meaning both body-kinematics and health monitoring (including vital signs detection), would considerably benefit from the implementation of wearable sensorised systems. In addition to sensors, the comfortable embedding into textile substrates of actuators represents a further potentially useful tool for rehabilitation. Actuators may provide enduring mechanical support to lost motory functions (compensation of disabilities) or to their physiotherapeutic restoration. They could be also used to modify textile porosity and promote transpiration.

Electro-active-polymer (EAP) sensors, actuators and transducers, in particular, used in textiles, may be electrically powered and/or controlled by power and electronic devices advantageously embedded in the fabrics. The integration of active electronic components would enable the implementation of closed-loop controls of the system. Furthermore, the possibility of simultaneously detecting a large set of physiological signals and variables and of processing and teletransmitting data would offer a valid tool capable of supporting health professionals in telemedicine and telerehabilitation for remote assistance. The maximum of integration could be represented by the use of wearable energy harvesting devices to supply sensors and actuators without the need of supplementary batteries that should be changed or recharged. Home care of sick or elderly persons, or treatment of individuals in extreme conditions, such as soldiers or astronauts, are just few examples of possible fields of application.

The aim of this work is that of describing how these features, and others mentioned farther on, make electro-active-polymers (EAPs) very promising materials for wearable flexible devices, as demonstrated by materials and prototype components developed by our lab.

In particular, this PhD activity has been focused on the identification of the figures of merit that govern the behaviour of EAPs in order to develop new materials with improved physical characteristics such as dielectric constant and elastic modulus first. All efforts

were made to decrease voltages necessary for actuation and to make EAPs more “energy free”, thus safer, cheaper and more attractive for the global market.

As the reader will notice, the central thread of this PhD thesis will be the attention given to *materials*, each of them considered for its peculiar characteristics. Materials used today and in the past for applications in the field of wearable technologies and materials specifically chosen for this work, with the intent of exploit their potentialities and develop new multifunctional devices. In this regard, particular attention will be given into the text to common dielectric elastomers such as silicones, polyurethanes and blends of them, used as electromechanical transducers, but results obtained with piezoelectric polymers will be reported also.

In Chapter 1 and 2 a look at the State of the Art of wearable technologies and EAPs materials is reported, with some concerns to the theory that governs the physics of EAPs and, among these, dieletric elastomers (DEs), that represent the core of the activity. Chapter 3 is dedicated to the description of the possible different ways to improve the performances of DEs with two completely new proposals coming from our group, the blending of partially miscible low permittivity elastomers to create ad hoc heterogeneous-structures with enhanced permittivities, and the corona charging of elastomer foams to produce electret materials suitable for actuating and sensing applications. Chapter 4, 5 and 6 relates respectively to results obtained during experimental activity and data elaboration regarding the energy generation and storage, the sensing and the actuating, that represent the three topics faced during the PhD. Each of these experimental chapters contains a detailed description of the materials used along with the procedure to prepare and characterise them. Morphological, chemical, mechanical and electro-mechanical analysis are reported and discussed for each of the three topics in a final conclusive paragraph. Chapter 7 finally deals with general conclusions and possible applications for the developed materials and systems in order to give to the reader a global point of view on the results obtained and stimulate comments and new ideas.

I
Theoretical Part

Chapter 1

Wearable Technologies

State of the Art

Reproduced in part from

"Functional Materials for Wearable Sensing, Actuating and Energy Harvesting", De Rossi, D., Carpi, F., Galantini, F., CIMTEC 2008 3rd International Conference Smart Materials, Structures and Systems, vol. 57, pp 247-256, 2008.

and

"Transducer Materials for Wearable Sensing Techniques: a Brief Overview"
Galantini, F., Gallone, G., Danilo De Rossi, *Sens. Lett*., submitted

Since the beginning of history, humans have been feeling the need to bring with them the objects necessary for their survival and support, like weapons, tools and food. The outcomes of the technological progress, in fact, are the means, more or less advanced, that always help man to deal with daily life and work. The tendency to make technology more and more transportable answers needs that are not modern, but as old as man.
In the last years, thanks to recent developments on electronic miniaturization and great results achieved in the field of advanced multifunctional materials, wearable systems for sensing, actuating, communicating and energy harvesting, are spreading around rapidly and their fields of application are constantly growing.
Neverthless, medical measurements are not the only one field in which wearable systems find frequent application [1]. Other common uses include monitoring of athletes during sportive competitions (detection of fouls and collisions, posture recognition, etc.) [1]; gait, impact, movement and sound detection [2]; musical gesture recognition [3]; Braille sensoring [4]; communication of information through light signals (LEDs, optical fibers etc.) [5] or colour changes (thermochromic inks) [6]; energy harvesting form body movements [7] or exposure to solar energy [8].

> *Definition*: Wearable Technologies refer to garments with built-in electronics or electronic devices and to new materials that enable functions far beyond conventional ranges of applications.

In the following, a brief overview of the four applications of wearable technologies, sensing, actuating, energy harvesting and communicating is reported, with particular attention at polymer-based solutions.

1.1 Wearable Sensing

Depending on each specific discipline of application, wearable sensors are made of different materials in a way that they are light, inobtrusive and appropriate for the purpose, as conductive electrodes for the collecting of biosignals [9, 10], electrogoniometers and accelerometers for the recognition of body movements and gait detection [11, 12], etc (Table 1.1).

Electrodes for the recording of biosignals, in particular, as transducers from biochemical signals (ionic) to electronic signals, can be devided in wet, dry, capacitive or insulating electrodes, but such a distinction is not considered here. For a in-depth review about it the reader might refer to [13]. Tab.1.2, later on, reports the main classification of existing wearable electrodes gathered for type of application.

Before to deeply enter the topic a definition of what is a sensor is needed. Generally, recording a *signal* means the presence of a *source* of signal (kynetic, biological, etc...), a *sensitive part*, able to convert the signal received in another form of energy, more easy to be read (usually electrical energy), *connections* (e.g. electrically conducting wires) and a device for the *data processing*. Every material able to transduce energy from one form to another (mechanical to electrical, thermal to mechanical and so on) has to be consider as a *transducer material*. If this converted energy is read by an observer or by an instrument this material is defined as *sensor*.

Typical werable systems consist of miniaturized sensors; these are hold in patches or bandages that can be worn under dresses and connected to a PC by wireless technology. Buffers temporarily gather physiological and biomechanical data that will be sent to a database server through a wireless lan or an internet connection. Data recordered using these systems, can be real-time processed to predict possible worsening of the patient clinical situation or can be analysed to investigate the effect of clinical intervention.

(a) (b) (c)

Figure 1.1. (a) Piezoresistive fabrics by Centro Piaggio; (b) conductive fabric by CSIRO; (c) clothings with integrated i-pod controls by Urban Tool.

Application	***Sensor material***	***Transduction principle***	***Sensitivity/ resolution***	***Embedding tecnique***	***Commercialized products – Companies****	***Drawbacks***	***Ref.***
Physiological parameters detection (breath and heart rate; transcutaneous O_2 pressure, glucose and ions amount in blood, pH, sweat rate...)	Carbon loaded rubber	Piezoresistivity	$G_{f(CLR)}$ = 2,5	Coated fabrics	--	Hysteresis	23
	PPY-coated PU foam		45BPM ca.	Patch in pocket	--	Oxidation=drift with time of R	24
	Carbon coated Nylon66 fibers		G_f =18	Yarns	*Monofilaments* by RESISTAT	Slippage	25
	Ni-plated metal patch	Electronic conduction	--	Band worn in hands	--	On-board power source	26
	FR-4 coated with gold		--	Concentric circles	--	Rigidity	27
	Ag/AgCl ink on a non-woven textile		--	Textile patch	--	Poor durability	6
	TiO_2 coated stainless steel		5μV @ 3Hz	Plate	--	Rigid-flat structure	28
	Ag coated PE and polyester foam		Freq > 5Hz	Patch	--	Pressure dependent	29
	Au/Ti coated silicone		--	Bracelet	*CS series* by Polar	Unstable connection	30
	CNTs		10μV	Rough plate	*Dry Electrodes* by Orbital Res. Inc.	Skin penetration	31
	Nylon insulated Ni-Cr alloy		--	Intramusc. wires	*EMG needle* by AMBU	Skin penetration	32
	Metallic coil	Inductive	--	Coils in sleeve	--	On-board power source	33
	Stainles Steel or Ag coated polyester	Capacitive	--	Patch	*PISeca*™ by PI	Slippage	33
	SiO_2 on silicone		--	Plate		Pressure dependent	29
	Pentacene-Mylar OFET	Field effect	--	Patch	--	--	34
	Glucose oxidase	Oxidation	--	Wristwatch	*GlucoWatch*™ by Cygnus Inc.	ecumbrance	35
	Cellulose bonded hydroxypyrene(sulfonamide)	Fluorescence	--	Ion-permeable membrane	--	On-board ligth source	36
	KCl solution	Potentiometry	0÷8mg/L	Pouch	*3100 WristOx*™ by Nonin	--	37
	Bromocresol purple Cellulose acetate butyrate	pH sensitive H_2O sensitive	pH 4÷8	Waistband	*Humidity sensors* by Philips	Sweat dependent	38
Gait detection	Force sensor-accelerometers	Piezoresistive-Piezocapacitive	--	Shoe insole	By Cedrat, Kistler, Futek, etc...	Bulky	7
	Conductive polymer	Piezoresistive	100g ÷10000g	Shoe insole	*FSR sensors* by Interlink	Low resolution	39
	PVDF stripe	Piezoelectric	--	Shoe insole	--	--	40
Body movements detection	PPy or carbon-loaded rubber	Piezoresistive	$G_{f(PPy)}$ = -13 $G_{f(CLR)}$ = 2,5	Threads in textiles	*SHIMMER*™ by R&D Technologies	Oxidation=Drift with time of R; Hysteresis	41
	Carbon-loaded rubber		$G_{f(CLR)}$ = 2,5	Patches		Hysteresis	23
	Silicon		4°	Silicon die		Bulky	42
	Thermoplastic elastomer-CB composite		Strain ≤ 35%	Patches		Hysteresis	43
	PPy-coated lycra fiber		$G_{f(PPy)}$ = -13	Fibers		Oxidation	44
	Ag plated nylon 66 yarns		3°	Fibers		Hysteresis	45
	Optical fibers – photo diode	Optical signal	--	Elastic bands		On-board power source	46
	Electrogoniometers	Hall effect	--	Knee	*GIB* by Motion Lab Systems	Encumbrance	8
Pressure detection	Silver coated yarns	Piezocapacitive	0 ÷ 10 N/cm^2	Embroidery	*FingerTPS*™ By PPS Inc.	Hysteresis	47
	Cr/Au/Cr coated polyimide diaphragm		± 1 bar	Patches		CTE mismatch	48

Table 1.1. Non exhaustive list of the today's main applications for wearable sensors;

(*) Examples of commercial sensors available for the detection of the corresponding signal are given. They do not necessarily imply the use of the same sensor material or configuration cited in the reference but refer to the particular signal detected and the transduction principle used; BPM=breath per minute; G_F= gauge factor; FR-4=glass reinforced epoxy laminate

(--) Not specified by authors.

1.1.1 EAP-based wearable sensors

This paragraph presents the more performing EAP (Electro-Active Polymers)-based devices developed by our lab and other research groups for sensing with reference to their already demonstrated or potential applicability to electronic textiles.

Electroactive polymers are defined as organic materials capable of responding to an applied electrical stimulus with a change of shape and/or dimensions [14]. This characteristic has enabled their use for polymer based electrically-driven actuation mechanisms, investigated for the development of "artificial muscles" [14]. However, despite the actuation mode, several kinds of EAPs can also work as sensors, electronic components and electrical power sources. Therefore, the term electroactive polymers is today typically used to refer to a class of materials which have multifunctional properties, rather than just the actuating one, as reported in the following.

Most useful devices for wearable sensorised systems can be divided into *active sensors* and *passive sensors*. We classify as active sensors those that intrinsically convert the input energy into a useful electrical potential difference. Differently, those sensors that require an external power source to convert the input into a usable output are defined as passive; they typically work according to a variation of their electrical resistance in response to an applied stimulus.

As showed in Tab.1.2 and 1.3 in the following, EAP-based sensors include piezo-, thermo-, magneto-, chemio- and photo-sensitive polymers.

Transduction principle	**EAPs examples**
Piezoresistivity	Conductor-loaded rubbers Conducting polymers e.g. Polypyrrole (PPy) e.g. Polyaniline (PAni) e.g. Polythiophene (PT) e.g. Polyacetylene (PA) e.g. Pyrolized polyacrylonitrile (PAN)
Thermoresistivity	Poly(p-phenylene vinylene) (PPV)
Magnetoresistivity	Polyacetylene (PA) Pyrolized polyvinylacetate (PVAc)
Chemioresistivity	Polypyrrole (PPy) Polythiophene (PT) Ionic conducting polymers Charge transfer complexes
Photoresistivity	Copper phthalocyanines Polythiophene complexes

Table 1.2. Most used EAPs and macromolecular organics for passive sensors.

Transduction principle	**EAPs examples**
Piezoelectricity	Piezoelectric polymers e.g. Poly(vinylidene Fluoride) (PVDF) e.g. Nylons e.g. Piezoelectric liquid-crystal polymers
Thermoelectricity	Polymer/CNTs composites
Pyroelectricity	Poly(vinylidene Fluoride) (PVDF)
Photoelectricity	Si-Polymer composites Liquid-crystal polymers

Table 1.3. Most used EAPs and macromolecular organics for active sensors.

In the following paragaraphs, a short desctription of the principal categories of EAPs materials, among those cited in the previous tables, is reported.

EAP-Based Wearable Piezoresistive Sensors

In order to endow garments with strain sensing capabilities for the monitoring of body-kinematics, such as position and movement of articulation segments, and for the detection of some vital signs, such as respiration, piezoresistive strain sensors (also known as strain gages) can be advantageously used. These sensors work according to the piezoresistive effect: their electrical resistance is modified by an imposed strain of the material. Most performing piezoresistive EAPs and conventional inorganic counterparts are listed in Table 1.2. In recent years, an innovative technology for wearable EAP based sensors has been developed by our lab, in order to confer strain sensing properties to garments. In particular, two types of piezoresistive polymer materials have been integrated into elastic fabrics: π-electron conjugated conducting polymers and carbon loaded elastomers. The main figures of merit of the developed sensors will be separately described below.

Conducting polymer sensors. Conducting polymers are a class of organic materials able to transport electricity. Since their discovery in the early seventies, several conducting polymers, such as polypyrrole, polyaniline and polythiophene, have been synthesised and their quality has been continuously improved [15]. "E. Piaggio" Research Centre has investigated their use for the development of organic piezoresistive sensors. To this aim, conducting polymer sensors have been fabricated by epitaxial deposition of a thin layer of polypyrrole (PPy) on a Lycra®/cotton fabric [15]. These sensors, showing both piezoresistive and thermoresistive properties [15], have been used by the lab to sensorise a glove and a leotard [15]. Despite the high absolute value of Gauge Factor (GF ~ -12) is suitable for strain gage implementations, two serious problems typically affect PPy-coated fabric sensors. The first one resides in the strong variation with time of their resistance (chemical instability) [15]. The second problem is represented by the long response time: following the application of a sudden mechanical stimulus, the sensor resistance reaches a steady state in a few minutes, strictly limiting the applicability of such devices [16]. Moreover, conducting polymer based sensors are not easily amenable to textile technology. In fact, they would require the problematic insertion in textile processes of tanks for the material synthesis and deposition/coating on fabrics.

Carbon loaded elastomer sensors. A new generation of high-performance strain sensors has been obtained by coating yarns and fabrics with carbon loaded elastomers (CLR), typically consisting of a silicone matrix filled with carbon black powder. Sensors are fabricated on a Lycra®/cotton textile by masked smearing of the conducting mixture. The same polymer/conductor composite is also used as material for the tracks of connection between sensors and an acquisition electronic unit, avoiding the stiffness of conventional metal wires. A GF of about 2.5, quite similar to those of metals, has been measured for CLR-coated fabrics, making this kind of device suitable for high-performance sensing [15]. Moreover, CLR sensors show, as for PPy sensors, thermoresistive properties with reported temperature coefficient of resistance (TCR) of about 0.08 $°C^{-1}$ [15]. Such devices

have been used by us to demonstrate prototype sensorised garments, including gloves, leotards (Fig.1.1), knee bands and sleeves [15]. All these systems are truly wearable fabrics, incorporating compliant polymer sensors, capable of recording body posture and gesture, with no discomfort to the subject wearing the garment and with negligible motion artifacts. Our carbon loaded rubber sensors integrated in the abdominal region of a shirt have also permitted the monitoring of respiratory activity (*respitrace*) with an accuracy comparable to that of conventional sensors in clinical use.

EAP-Based Wearable Piezoelectric Sensors

According to the well-known direct piezoelectric effect, the application of a stress along one of the main axes of a piezoelectric material causes its polarisation, generating net opposite charges on opposite surfaces. The electric potential difference produced by the opposite charge distribution can be detected by embedding the material between two electrodes.

Today's, due to miniaturization of electronics and progress in manufacture technologies, piezoceramic fibers are available [17, 18]. Thanks to this new type of configuration, the range of possible applications for piezoceramics has subsequently spread over [19, 20] allowing applications also in the field of wearable technologies. However, despite their excellent transduction properties, piezoceramics are heavy (d_{PZT}=7.5 g/cm^3 *vs* d_{PVDF}=1.78 g/cm^3) and rigid materials ($c_{33,PZT}$=115 GPa *vs* $c_{33,PVDF}$=10 GPa) for this reason, in the latest two decades, they have been replaced by piezoelectric polymers (PVDF, nylons, etc.) in a lot of applications [21]. The peculiar properties of such a type of polymeric materials were discovered for the first time in seventies by Kawai [22] that first developed PVDF and PVDF copolymer with trifluoroethylene and tetrafluoroethylene with strong piezoelectric activity. More recently Scheimbein et al. have demonstrated piezoelectric activity in a series of semicristalline odd numbered nylons [23], while Nalwa studied piezoelectricity in a series of polythioureas [24, 25] and others verified piezoelectric activity, though much more limited than that of semicrystalline systems, also for polyacrylonitrile (PAN) [26], poly(vinylidenecyanide vinylacetate) (PVDCN/Vac) [27], polyphenylethernitrile (PPEN) [28], poly(1bicyclobutanecarbonitrile) [29] and polyvinylchloride (PVC) [30].

Discovered for the first time in Japan during the late sixties [31], characterized by a low weight and a high piezoelectric compression sensibility, electret polymers also represent today a valid substitute for application in the field of wearable technologies, despite their use is not so diffuse today. In particular, useful charge-storing properties have been found in PE [31], PP [31], PTFE [31], PVDF [21], Teflon®AF [32] and a variety of compounds of Cyclo-Olefine Copolymers COCs [33]. More recently, electret foams of polypropylene PP [34] and PTFE [35] were prepared in order to increase their piezoelectricity basing on a concept by Kirjavainen [36] enhancing the piezoelectric d_{33} coefficient up to 150 pC/N in the case of PTFE [37].

Like non-centrosimmetric crystals, also semicrystalline polar polymers, if subjected to an external stress, provide electric fields proportional to the applied stress. In particular, each

of the three components of the polarization ΔP_i is linearly related to each of the nine components of the stress tensor σ_{jk} following:

$$\Delta P_i = d_{ijk}\sigma_{jk} \quad (1)$$

where d_{ijk} is the third-rank tensor having 27 components called piezoelectric coefficients. For highly oriented poled polymer films (uniaxially oriented films), thanks to the simmetry of the structure, the only non zero piezoelectric coefficients are d_{31}, d_{32}, d_{33}, d_{15} and d_{24} where, for convention, *1*, *2* and *3* indicate respectively the direction of drawing, the direction of the film and the normal to the film surface. For this motive, usually d_{33} is used to identify the sensibility of piezoelectric pressure sensors.
In the table below, a list of some of the well-known applications of piezoelectric materials as wearable sensors is reported. The table contains specific information about PVDF based wearable sensors along with a collection of other piezoelectric polymers applications. Once again, embedding techniques, sensitivity and possible drawbacks are reported for each sensor cited. Due to their structure and their finite internal resistance, piezoelectric materials can be defined as *dynamic sensors* being sensitive to impulse and not to stationary imput.

Piezo Class	Piezo material	Quantity to be detected	Embedding technique	Sensitivity/ Resolution	Drawbacks	Ref.
Piezo ceramics	Lead zirconate titanate	Breath rate Heart rate Pulse echo tech.	Waistband	d_{33} = 37 pC/N	--	79
	AT-cut Quartz	Chemical, biochemical and physical measurands	Stainless steel enclosure in clothes	ng/mm^2	On-board power source	80
	PZT	Arterial pulse	Wristwatch	--	On-board power source	81
	PZT	Kicks	Plastic backing	3÷4 Watts	--	1
	Lead zirconate titanate	Foot contact stress	Silicone embedding in a shoe insole	--	--	82
Piezo PVDF and PVDF copolymers	PVDF	Breath rate Heart rate	Belt	--	Saturation	83
	PVDF	Heart rate	Textile band	--	--	84
	PVDF	Arterial pressure	Wristwatch	$Freq_{cut\text{-}off}$=0,16Hz	--	85
	PVDF	Foot pressure	Insole patches	--	Saturation	86
			Insole disks	d_{33}= 22 pC/N	--	87
	P(VDF-TrFE)		Insole patches	d_{33}=24pC/N	--	88
	PVDF	Tactile feedback Braille reading	Membrane	d_{33}= 10 pC/N	No distinction between solid/ hollow probes	89
	PVDF		Thimble	50÷200 mm/s	--	4
	PVDF	Impact	Vest	--	--	19
Other piezo polymers	FEP* or PC**	Pressure detection	Metallic casing	--	--	90
	PP electret	Tactile feedback	Polyimide substrate	d_{33}= 140 pC/N	--	91
	PP electret	ECG	Strips	--	No quantitative	92

Table 1.4. Non exhaustive list of the today's main applications for piezoelectric wearable sensors. PZT: piezoelectric transducer; (*) fluorinated etilene propilene resin; (**) polycarbonate; (--) not specified by authors.

EAP-Based Wearable Chemio-resistive (-capacitive) Sensors

Monitoring of biochemical fluids is another important field where EAP based devices can play a useful role in order to develop wearable detection systems. Several body fluids, such as sweat, tears, saliva and urine (or even secretions from chronic wounds), carrying biochemical analytes of specific biomedical interest can be easily, non invasively, accessed by using wearable contact devices. These can include patches, medical bandages, handkerchief or diapers made of sensorized textiles. These might be equipped with EAP based sensing elements working according to either the chemioresistive or the chemiocapacitive effects and made of both conjugated polymers and hydrophilic gels. As an example, the European Project *BIOTEX*, now over, was aimed at developing such types of systems [38]. As an observation, it is worth mentioning here that a monitoring of certain biochemicals by means of wearable non-EAP devices has been already demonstrated. Examples include glucose-sensible wrist-watches, such as the GlucoWatch (by Cygnuss, Redwood City, CA) [39], and disposable contact lenses (CIBA VISION, Duluth, GA) [40].

During this PhD activity, prototypes of fabric-embedded PVDF stripes were developed, in collaboration with the University of Potsdam, collecting information about body movements and respiratory rate, in order to approach the coveted fiber-configuration. Together, tests were performed on high dielectric constant elastomers and elastomeric foams to develop piezocapacitive sensor devices for robotics applications (in collaboration with the University of Genova within the european project Roboskin).

1.2 Wearable Actuating

Among the large group of actuator devices (pneumatic, thermic, electromagnetic, magnetic and electric), few are those suitable for wearable applications. In particular, electrical- and thermal-based actuators, thanks to their lightness and capability to be miniaturised and inserted in clothes, have already found several applications in smart dresses.
Different are the possible applications of actuating devices in wearable systems. In healthcare, using piezoelectric micro-actuators as pumps embedded in wristwatch to dispense medicines (e.g. insulin in diabetics) [41]; in rehabilitation, using dielectric elastomers as motors to trains articulations after injuries [42]; in fashion, with SMP (Shape Memory Polymers) or SMA (Shape Memory Alloy) knitted in fabrics to change clothes feature.

Figure 1.2. Shape-memory-alloy (SMA) integrated into textiles; the sleeves roll up when it becomes too warm.

In the following paragraphs a description of the main categories of polymeric actuators for wearable applications is reported.

1.2.1 EAP-Based Wearable Actuators

In order to endow fabrics with motor functions, flexible actuating devices are needed. They share with sensors the necessity of overcoming several technological problems towards textile implementations. The most noticeable challenging issues include the identification of efficient principles of operation and suitable configurations, selection of high-performance materials and implementation of custom fabrication processes.

Fabrics with shape recovery capabilities have been developed by D'Appolonia, by integrating shape memory alloy (Nitinol) fibers with thermal memory effect [43]. Despite this, no successes towards an effective and comfortable embedding of actuating functions into textiles have been substantially reported so far. Electroactive polymer based actuators may be used for such a purpose. Different EAP classes currently under investigation for flexible actuation are listed in Table 1.5. Ionic EAPs can be activated, within a surrounding electrolyte medium, by very low voltages (in the order of 1 V). On the contrary, electronic EAPs require typically high driving voltages (electric fields of the order of 10-100 V/μm for electrostrictive polymers and dielectric elastomers). However, progresses concerning the reduction of their driving fields are currently occurring, as it will be shown further on. Electronic EAPs show, in comparison with the ionic ones, shorter response time and higher efficiency, stability, reliability and durability.

In order to describe the potential applicability of EAP based actuators to electronic textiles, we will select here only one representative material per class among the electronic and ionic electroactive polymers. In particular, we will briefly analyze the current state of the art on two of the most performing types of materials: conducting polymers and dielectric elastomers.

Transduction principle	**EAPs and macromoleculars**
Ionic activation:	
Electro-chemo-mechanical effect	Conducting polymers *e.g.* Polypyrrole (PPy) *e.g.* Polyaniline (PAni) Polyelectrolyte gels *e.g.* Polyacrilonitrile (PAN) Ionic polymer-metal composites (IPMC) Carbon nanotubes (CNT)
Electronic activation:	
Piezoelectricity	See Table 1.6
Electrostriction	Electrostrictive polymer *e.g.* Poly(vinylidene fluoride–trifluoroethylene) (P(VDF-TrFE)) *e.g.* Poly (vinylidene fluoride–hexafluoropropylene) (P(VDF-HFP)) Liquid-crystalline elastomers
Electrostatic effect	Dielectric elastomers *e.g.* Acrylic or silicone rubbers

Table 1.5. Most used EAPs and macromolecular organics for actuation.

Conducting Polymer Actuators. Since many years, conducting polymers have been studied as materials for polymer actuation [15]. For such a purpose they are used as one component of an electrochemical cell, whose base structure includes two electrodes

immersed in an electrolyte. In particular, the active conducting polymer material constitutes one of the two electrodes of the cell. By applying a potential difference between the electrodes, the one made of conducting polymer shows a dimensional variation and works as an actuator (thanks to ion diffusion). Conducting polymer actuators typically exhibit active strains of the order of 1-10%, high active stresses (up to tens of MPa), and low driving electrical potential differences (order of 1 V). Nevertheless, the use of conducting polymers as actuators is typically limited by their short lifetimes and high response times. However, several attempts to overcome these limits are in progress. In order to endow fabrics with actuating functions, fiber-shaped actuators may be particularly useful. Our Research Centre has proposed, at the end of the nineties, conducting polymer fiber actuators constitued by an extruded polyaniline fiber coated with a thin layer of solid polymer electrolyte (e.g. ethylene carbonate (EC)/polyacrilonitrile (PAN)/sodium perchlorate ($NaClO_4$)) and an outer layer of polypyrrole that acts as a counter-electrode. Alternatively, the counter-electrode can consist of a metal wire twisted around the fiber. Actuators with such a fiber-like structure have shown strains of about 0.3% and active stresses of about 3 MPa, for driving voltages lower than 1 V [15].
Conducting polymer fibers have today become more readily available. For instance, Santa Fe Science and Technology Inc. produces polyaniline (PANI) fibers under the trademark of Panion^{TM}. They have been used to fabricate linear actuators: a bundle of Panion^{TM} fibers (operating as an actuating electrode) is inserted into a Panion^{TM} hollow fiber (counter electrode) with a separator/electrolyte medium. This kind of actuator, tested with a [BMIM][BF_4] ionic liquid electrolyte, has reported strains of about 0.3%, stresses of about 1.8 MPa and red-ox cycle lifetimes in excess of 10^4 cycles [15]. These strain and stress values are nearly equal to those reported by our group [15], whereas the achieved higher lifetimes are a demonstration of the above-mentioned beneficial effect of ionic liquid electrolytes.
However, despite these new results, much more work has to be done in order to endow textiles with efficient and reliable actuating functions.

Dielectric Elastomers Actuators. Dielectric elastomers represent the EAP class with the highest achievable active strains (order of 100%), as well as considerably high active stresses (up to 1 MPa) [44]. They consist of insulating rubbery polymers, having a low elastic modulus. When a thin film of such materials is sandwiched between two compliant electrodes (e.g. made of carbon conductive grease) and a high voltage difference is applied between them, the polymer undergoes an electric field sustained deformation, consisting of a thickness squeezing and a related surface expansion [44]. The achievable large deformations are mainly due to a Coulombian effect, established by means of the electrostatic interactions occurring among free charges on the electrodes.In principle, any kind of dielectric material can be subjected to such an electrostatic squeezing. However, it is evident that the corresponding deformations are markedly emphasised by both the compliance of the electrodes and the polymer softness. These two key-features macroscopically distinguish actuating devices made of dielectric elastomers from those based on different electric-field-driven dielectrics, such as piezoelectric or electrostrictive

materials, whose principle of operation is different. Acrylic and silicone rubbers are the most representative materials of the dielectric elastomer class for actuation purposes (Table 1.5). The excellent figures of merit possessed by dielectric elastomers in several respects (high actuation strains and stresses, fast response times, high efficiency, stability, reliability and durability) make them the most performing materials currently available for polymer actuation. The price for achieving these high-level capabilities is represented by the high driving electric fields required (order of 100 V/µm). For a definite polymer thickness, such field levels can be reached by applying high voltages, which may have disadvantages in many applications. In order to reduce the driving electric fields, polymers with a high dielectric constant (or permittivity) are necessary. In fact, the strain generated by a dielelctric elastomer actuator is proportional to both the square of the applied electric field and the material dielectric constant [44].

So far, many configurations for dielectric elastomer actuators have been proposed and demonstrated, including planar, tube, roll, extender, diaphragm and benders [44]. Tube and, mainly, roll actuators are flexible devices potentially suitable to endow fabrics with linear (along a line) actuation functionalities. These actuators elongate under electrical stimulation. Therefore, they are not useful if electrically-activated contractions are requested. For this purpose, we have developed a new type of dielectric elastomer actuator [44], based on a configuration recently patented [44]. It consists of an hollow cylinder of dielectric elastomer (e.g. silicone), having two helical compliant electrodes integrated within its wall. By applying a voltage difference between them, the attraction among opposite charges causes an axial contraction of the actuator [44]. The electromechanical performances of this new type of actuator are currently being studied in our lab.

At present, the need for high driving electric fields limits the diffusion of these transduction materials in some areas of potential application, especially in the case of biomedical disciplines. A reduction of the driving fields may be achieved with new elastomers offering intrinsically superior electromechanical properties. So far, most of attempts in this direction have been focused on the development of composites between elastomer matrixes and high-permittivity ceramic fillers, yielding to limited results. In our laboratories, a different approach was adopted for increasing the electromechanical response of a common type of dielectric elastomer. The technique consisted in blending, rather than loading, the elastomer (poly-dimethyl-siloxane) with a highly polarizable conjugated polymer (undoped poly-hexyl-thiophene). The resulting material was characterised by dielectric spectroscopy, SEM microscopy, tensile mechanical analysis and electromechanical transduction tests. Very low percentages (1-6 wt%) of poly-hexyl-thiophene yielded both an increase of the relative dielectric permittivity and an unexpected reduction of the tensile elastic modulus. Both these factors synergically contributed to a remarkable increase of the electromechanical response, which reached a maximum at 1 wt% content of conjugated polymer. This approach may lead to the development of new types of materials suitable for different applications requiring elastomers with improved electromechanical properties [45].

To dielectric elastomers for actuative purposes is dedicated the most part of this PhD thesis. Theoretical dissertations about physical mechanisms governing the electromechanical actuation of this class of materials, silicones and poliurethane in particular, along with dielectric, mechanical and electromechanical characterization of developed samples, are reported. The blend approach, rather than the more common composite approach, was used to increase the dielectric constant of the elastomeric matrices with good results. Studying actuative properties of poliurethanes, a particular bending configuration was observed and further investigations will be carried on for this class of elastomers to be used in diaphragm and tilt applications (see Chapter 6). Part of the developed samples could be utilized to actuate textile substrates and modifying the mesh size of different tipe of fabrics.

1.3 Wearable Energy harvesting

As the power requirements for microelectronics continue decreasing, environmental and body energy sources can begin to replace batteries in certain wearable subsystems. In this spirit, different devices had been projected and devoloped in the past decade to be inserted into a shoe (where excess energy is readily harvested) and used for generating electrical power "parasitically" while walking. Two of these are piezoelectric in nature: a unimorph strip made from piezoceramic composite material and a stave made from a multilayer laminate of PVDF foil. The third is a shoe-mounted rotary magnetic generator (all by MIT Laboratory). Test results are given for these systems, their relative merits and compromises are discussed, and suggestions are proposed for improvements and potential applications in wearable systems. As a self-powered application example, a system had been built around the piezoelectric shoes that periodically broadcasts a digital RFID as the bearer walks.

(a) (b)

Figure 1.3. (a) Backpack straps harvest energy to power electronics [7]; (b) sportive shoe with integrated piezo-converters for generate electrical power [46].

Physical effect	**EAPs and macromoleculars**
Piezo-electricity	Polyvinylidene fluoride (PVDF) Polyvinylfluoride (PVF) Poly(vinylidene fluoride –trifluoroethylene) (P(VDF-TrFE)) Poly (vinylidene fluoride –hexafluoropropylene) (P(VDF-HFP)) Poly(vinylidene fluoride –tetraflouoroethylene (P(VDF-TFE)). Polyamides (e.g. Nylon-11) Liquid crystalline polymers (flexoelectricity)
Thermo-electricity	Polyacetylene (PA) Polyaniline (PAni) Polypyrrole (PPy) Polythiophene (PT) Polyphthalocyanines Nitrile based polymers
Pyro-electricity	PVDF P(VDF-TrFE) P(VDF-HFP) PVF
Photo-electricity	Polythiophene (PT) Polyaniline (PAni) Polypyrrole (PPy) Poly(N-vinyl carbazole) (PVCZ) Polyacetylene/n-zinc sulfide (PAS) Poly(p-phenylenevinylene) (PPV) Poly(2-vinylpyridine) (P2VP) Oligothiophenes Phthalocyanines

Tabel 1.6. Most used EAPs and Macromolecular Organics for Electrical Energy Generation.

1.3.1 EAP-based Wearable Devices for Energy Harvesting

EAP-Based Piezoelectric Converters.

Piezoelectric materials, able to convert mechanical energy into electrical energy can be used for energy harvesting from human actions. Transducers made of such materials can in fact be advantageously employed to generate electricity from loads applied by daily activities and movements of a human body (e.g. gesture, respiration or locomotion). In particular, one of the possible strategies for the implementation of a comfortable, lightweight and unobtrusive harvesting of energy from gesture and body segment movements consists of the insertion of piezoelectric transducers into clothes, preferably corresponding to articulation joints (e.g. elbow, knee, shoulder). The movement-induced stretching of an electroded piezoelectric strip or fiber will cause the generation of a useful electric potential difference across the device. Similarly, energy can be harvested from breathing, by embedding into clothes band-like transducers around the chest, capable to exploit the rhythmic variation of its circumference. These examples indicate that, for these tasks, piezoelectric polymers can be better candidate materials than piezoceramics, because of their higher flexibility (e.g. the elastic modulus of polyvinylidene fluoride (PVDF) is one order of magnitude lower than that of lead zirconate titanate (PZT)). However, the price for achieving with piezopolymers a better fitting of mechanical requirements is paid with a piezoelectric effect resulting weaker than in piezoceramics (e.g. the piezoelectric constant of PVDF is one order of magnitude lower than that of PZT).

Dielectric Elastomer Converters.

A different kind of heel-strike generators capable of harvesting energy from walking has been proposed by Stanford Research Institute (SRI), by using dielectric elastomers [47]. The operation principle underlying this kind of transducers is the following. Compliant electrodes (e.g. made of carbon grease) are fabricated on a dielectric elastomer film (typically an acrylic polymer or a silicone rubber) in order to realise a compliant capacitor. When the deformable capacitor is compressed (e.g. by the heel pressure on the floor) an external generator supplies a bias high voltage, which charges the electrodes. After the removal of the mechanical pressure (e.g. the shoe is lifted), the film elastically relaxes toward the original dimensions, decreasing the device capacitance (the thickness increases, while the electrode area decreases). As a result, the voltage across the device is increased (with respect to its original bias value) and the related electrical energy can be delivered to a load. Therefore, this transducer is capable of converting mechanical elastic energy into electrical energy. Based on this principle, the generation of energy densities up to 0.4 J/g has been demonstrated [47]. However, these interesting performances (superior to those achievable with piezoelectric converters) have their price: such devices require additional external sources of bias high voltages. This feature can limit the usefulness of dielectric elastomer generators with respect to the piezoelectric ones.

Inertial (or Kinetic) Converters.

For the sake of completeness on the panorama of human mechanical energy transduction systems potentially useful in smart textiles, with no or least discomfort for the wearer, we focus here the attention on devices able to transduce kinetic energy into electricity (inertial power generators). As an example, they are used in self-powered wristwatches, which take energy from the arm motion of the user during daily activities [48]. These watches typically embed small mechanical components, having a spindle-mounted magnetic mass, whose rotation, activated by the wearer movements, induces electrical currents. More generally, inertial generators (either rotational or linear) exploit inertial-forces-induced accelerations of a mass with respect to its housing, which originate electrical energy by electro-magnetic induction (if magnetised) or by stressing a piezoelectric material [49]. The first feasibility studies for applications of this kind of power sources in the field of electronic textiles are in course [50].

EAP-Based Thermoelectric Converters.

Thermoelectric transducers, known as thermocouples, are devices capable of generating electricity from a temperature gradient. They work according to the Seebeck effect, which consists of the generation of an electric potential difference within a circuit including two different metals, or semiconductors (p-n couples), whose junctions are kept at different temperatures. The most used organic and inorganic materials for thermocouples are listed in Table VI of [15]. The thermoelectric effect in organic materials has been studied mostly in conducting polymers [51] and in carbon/polymer composites [52]. The figure of merit conventionally used to evaluate the thermoelectric properties of a thermocouple is the product ZT, where T is the absolute temperature and Z is a material parameter, defined as

$Z=S^2\sigma/k$, where S is the Seebeck coefficient, σ is the electrical conductivity and k is the thermal conductivity. High-performance inorganic thermoelectric power generators made of Bi_2Te_3/Sb_2Te_3 have demonstrated *ZT* values of about 2.4 [52], while nanocomposites of conjugated polymers have shown recently very competitive *ZT* values of about 1 [51].
The human body's heat, in particular, is a very interesting potential source of energy. Body heat power dissipated with daily activities varies from about 80 W during sleeping up to about 1500 W while running [15].

EAP-Based Pyroelectric Converters.

One material is defined 'pyroelectric' if it shows a temperature-dependent spontaneous polarisation (pyroelectric effect). Therefore, a pyroelectric material subjected to a temperature variation modifies the amount of opposite charges located on opposite surfaces. As for piezoelectric generators, these charges can be harvested by two electrodes applied to the material (capacitor-like configuration).
All pyroelectric and piezoelectric materials are also ferroelectric. Therefore, most used organic and inorganic pyroelectric materials are common into the piezoelectric list too. Pyroelectric properties are shown by several electroactive polymers [53]. PVDF and P(VDF-TrFE)) are the most performing ones, having typical pyroelectric coefficients of about 25 $\mu C/m^2K$ and 40 $\mu C/m^2K$, respectively [53]. For comparison with inorganic materials, we mention that PZT offers a coefficient of 380 $\mu C/m^2K$ [53]. Interesting performances have been obtained by mixing pyroelectric ceramics with pyroelectric polymers, in order to develop flexible active composite structures. Since a variation in the spontaneous polarisation of pyroelectric materials occurs when they are heated, they may find potential applications for the harvesting of energy from body heat. However, this use has not been developed yet and they are typically employed as thermal (infrared) radiation sensors [53].

EAP-Based Photoelectric Converters.

The photoelectric effect can be exploited for the development of photovoltaic cells able to produce electric energy from electromagnetic radiation. This effect consists of a light-induced dislodging of electrons from atoms. In particular, light absorbed by a photoelectric material generates a pair of negative and positive electric charges (electrons and holes, respectively), which can be collected by two electrodes, originating an electric potential difference.
The typical structure of an organic photovoltaic cell is identical to that of an organic light emitting diode. A slightly different structure is presented by the so-called photoelectrochemical cells, which include an electrolyte layer coupled to the photoelectric polymer layer [54]. Solar cells are a common example of photovoltaic cells employed to transduce solar energy into electricity. The first photovoltaic cells fabricated onto flexible plastic supports have reached the market [15]. However, the higher flexibility offered by all-organic cells is encouraging the development of photovoltaic generators based on several EAP semiconductors, such as conjugated polymers [54]. Nevertheless, due to their lower efficiency of charge carrier photogeneration and higher electrical resistivity (lower

mobility of charge carriers), the energy conversion efficiency of organic photovoltaic devices is still lower than that of the best inorganic semiconductors. In particular, the highest reported conversion efficiencies for organic cells are lower than 3% [54], corresponding to about one tenth of those enabled by the best solar cells available today, made of inorganic semiconductors [15]. Although studies on the fabrication of flexible photovoltaic devices by coating fibers with inorganic semiconductors have been reported, such as cadmium sulfide coated trylene threads [15], the advantageous union of the interesting mechanical and semiconducting properties shown by organic materials spur their use for flexible photovoltaic generators. Therefore, it is not surprising that, as for organic electroluminescent devices or organic transistors, the development of organic photovoltaic cells is collecting considerable attention and financial resources. Existing devices today make realistic to foresee for this kind of technology potential applications in electronic textiles for energy harvesting from both natural or artificial environmental light sources.

Electrokinetic Converters.

Finally, we mention here another energy conversion mechanism. It consists of the electrokinetic effect, consisting in the generation of an electric potential from the flux of an electrolyte inside a charged conduit subjected to a pressure difference. Attention for this effect, which was largely studied some decades ago [55], is renewed, mainly due to improvements in microfabrication technologies [15]. Highly attractive conversion efficiencies (up to 12%) have been reported [15]. These outcomes encourage the development of new wearable transduction systems possibly made of flexible polymer materials (e.g. based on Nafion membranes), in appropriate locations (e.g. shoes).

During PhD activity, experiments with piezelectric polymers have been carried out in order to develop devices for the energy harvesting from human walk. An electrical circuit has been designed and optimized in collaboration with the University of Pavia to collect charges from the electromechanical conversion and power a LED.

1.4 Wearable Communicating

Fashion and functionality are synergistically melted together in wearable systems used as multimedia displays; they can reflects the emotional status of the wearer by changing their appearance according to the changes in the physical or emotional state of the user. Computationally controlled garments and accessories can detect the need for expression and transmit messages appropriate for the context. Thus, wearables both enhance the expressive abilities of the self and enhance the usability of the clothes. Wearables define a new relation between wearers and garments, and propose new directions for fashion. Coloured LEDs to inform about user condition (body temperature, Fig.1.4b) and send messages with clothes (Fig.1.4c), lasers in eyewear to be always informed and connected [56] by Microvision.

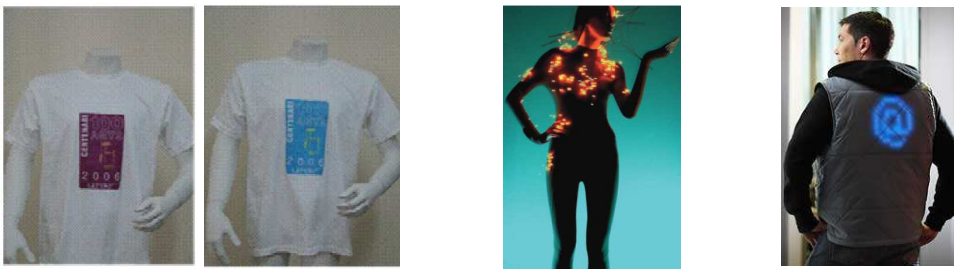

(a) (b) (c)

Figure 1.4. (a) thermochromic ink printed on the fabrics by Chromatic Technologies Ink; (b) FRISON, body suit to sense changes on the skin and to create an LED visual output, by Philips Research; (c) LUMALIVE jacket, colored and flexible light-emitting diodes integrated in the textiles, Philips Research.

1.4.1 EAP-based Wearable Devices for Communication

Thermochromic or photochromic inks, susceptible to ambient and consumer conditions, temperature in particular, have been using in the last decades to exchange information and communicate in wearable systems (Fig.1.4a). In particular, polymers and organic macromolecules, thanks to their lightness and easiness of processability, are attractive to be inserted in miniaturized devices. Liquid crystals for knitted displays for example, or smart inks to enrich clothes, but they will be not object of the present study.
Thermochromic reversible inks, for example, are colored below the activation temperature and they are clear or lightly colored above the activation temperature. In addition to standard 15 C°, 31 C° (body-heat activated), and 45 C° sensitive products, custom products with transition temperatures between -5 C° and 65 C° can be formulated upon request.

1.5 Conclusions

Advantages deriving from the exploitation of intrinsic multifunctional properties of several electroactive materials have been shown. In particular, most performing EAP based sensors, actuators and power sources currently under development have been described, with reference to their potential or demonstrated implementation in fabric based configurations. The near-future developments of such EAP based e-textiles open new challenges. One of them concerns the improvement of the wearability of electroactive polymer devices by means of textile-compatible configurations and shapes, preferably in fiber form, along with decreased driving voltages. However, the integration into fabrics of EAP based distributed sensing, actuating and power functions represents, in our opinion, one of the means of having great potentialities for the development of completely wearable electronic textiles.

1.6 References

[1] Chi H. *et al*., *IEEE Pervasive Computing*, 4, 3, 47-53, 2005
[2] Park C. *et al*., *IEEE International Conference on Pervasive Computing and Communications*, 2006
[3] Dubost G. *et al*., Ann. Arbor., MI: Scholarly Publishing Office, University of Michigan Library, 2002
[4] Miyata K. *et al*., *IEEE/RAS-EMBS International Conference on Biomedical Robotics and Biomechatronics*, 93-98, 2006
[5] De Rossi D. *et al*., *Sensors & Sensing in biology & Engineering*, J. Secomb Ed. New York: Springer Verlag, 381-394, 2003
[6] http://www.ctiinks.com/
[7] Granstrom *et al*., *Smart Materials and Structures*, 16, 1810-1820, 2007
[8] Brunelli D. *et al*., An Efficient Solar Energy Harvester for Wireless Sensor Nodes, *EDAA*, 2008
[9] Pola T. *et al*., Textile electrodes in ECG measurement, *ISSNIP-07 Third International Conference of Intelligent Sensors, Sensor Networks an Information Processing*, Melbourne, Australia, 2007
[10] Kang T. H. *et al*., *IEEE transactions on biomedical engineering*, 55, 1, 188-195, 2008
[11] Tao L. *et al*., Development of a wearable sensor system for human dynamics analysis, Dissertation, Kochi University of Technology, Japan, 2006
[12] Kyriazis V. *et al*., *Journal of Orthopaedics and Traumatology*, 2, 1, 1-6, 2001
[13] Searle A. *et al*., *Physiological Measurements*, 21, 2 , 271-283, 2000
[14] Bar-Cohen Y. Ed. *Electroactive polymer (EAP) Actuators as artificial muscles. Reality, potential, and Challenges*, Washington: SPIE, 2001
[15] Carpi F. *et al*., Electroactive polymer-based devices for e-textiles in biomedicine, *IEEE Transactions of Information Technology in Biomedicine*, 9, 3, 2005
[16]. Scilingo E. P. *et al*., *IEEE Sensors Journal*, 3, 4, 460-467, 2003
[17] Qiu J. *et al*., *Smart Materials and Structures*, 12, 331-337, 2003
[18] Yoon C. B. *et al*., *Journal of the American Ceramic Society*, 89, 4, 1333-1336, 2006
[19] Qin Y. *et al*., *Nature*, 451, 809-314, 2008
[20] Sun D. C. *et al*., *Journal of Sound and Vibration*, 241, 2, 297-314, 2001
[21] Lang S. B. *et al*., *Applied Physics A*, 85, 125-134, 2006
[22] Kawai H. *et al*., *Japanese Journal of Applied Physics*, 8, 975-977, 1969
[23] Scheinbeim J. I. *et al*., *Journal of Applied Phys*ics, 52, 5939, 1981
[24] Nalwa H. S. *et al*., *Proceedings of Nuclear Physics and Solids State Physics Symposium*, 21C, 712, 1978
[25] Fukada E. *et al*., in Ferroelectric Polymers, Chemistry, Physiscs and Application, H.S. Nalwa Ed., Marcel Dekker Inc., New York, p.353, 1995
[26] Ueda H. *et al*., *Polymer Journal*, 16, 9, 661, 1984
[27] Jo Y. S. *et al*., *Polymers*, 28, 9, 1583-1588, 1987
[28] Tasaka S. *et al*., *Polymers*, 30, 1639, 1989

[29] Hall H. K. Jr.1 *et al*., *Polymer Bullettin*, 17, 2, 135, 1987
[30] Mopsik F. I. *et al*., *J. Applied Physiscs*, 46, 4204, 1975
[31] Sessler G. M. *et al*., Electrets, Springer-Verlag, New York, 1980
[32] Gunther P. *et al*., *Annual Report, Conference on Electrical Insulating and dielectric Phenomena*, pp. 197-202, IEEE Service Center, Piscataway, NJ, 1993
[33] Sessler G. M. et al., *Annual Report, Conference on Electrical Insulation and Dielectric Phenomena*, pp. 467-470, IEEE Service Center, Piscataway, NJ, 1997
[34] Paajanen M. *et al*., *Journal of Physics D*, 34, 2482-2488, 2001
[35] Gerhard-Multhaupt R. *et al*., *Proceedings, 10th International Symposium on electrets*, IEEE Service Center, Piscataway, NJ, 1999
[36] Kirjavainen K. *et al*., US Patent n. 4.654.546, 1987
[37] Kunstler W. *et al*., *Applied Physics A*, 70, 5-8, 2000
[38] http://www.biotex-eu.com
[39] Tamada J. A. *et al*., *IEEE American Medical Association*, 282, 19, 1839-1844
[40] Scherick W. *et al*., *Journal*, 24, 4, 216-9, 1998
[41] http://www.microdysis.com/TechInstrumentWatch.aspx
[42] Carpi F. *et al*., Elastomeric contractile actuators for hand rehabilitation splints, in *Proceedings of Smart Structures and Materials 2008: Electroactive Polymer Actuators and Devices*, Y. Bar-Cohen, editor, SPIE 2008
[43] Carosio S. *et al*., *Proc. of International Workshop: New Generation of Wearable Systems for e-Health: Towards a Revolution of Citizens' Health and Life Style Management*, Lucca, Italy, pp. 271-280, 2003
[44] Pelrine R. *et al*., *Science*, 287, 836-839, 2000
[45] Carpi, F. *et al*., *Advanced Functional Material*, 18, 235-241, 2008
[46] Kymissis, J. *et al*., *Proceedings of the 2nd International Symposium on Wearable Computers*, Pittsburgh, PA, 132-139, 1998
[47] Perline E. et al, Generator mode: devices and applications, in *Dielectric Elastomers as Electromechancial transducers*, Carpi F., et al. Ed., 2008
[48] http://www.seiko-kinetic-watches.com
[49] El-hami M. *et al*., *Sensor and Actuators A*, 92, 335-342, 2001
[50] Büren T. *et al*., *Proceedings of the Seventh IEEE International Symposium on Wearable Computers*, 22-24, 2003
[51] Feng J. *et al*., *Synthetic Metals*, 135-136, 55-56, 2003
[52] Venkatasubramanian R. *et al*., *Nature*, 413, 597-602, 2001
[53] Bauer S. *et al*., *IEEE Transactions on Dielectrics and Electrical Insulations*, 3, 6, 647-476, 1996
[54] Wallace G. *et al*., *Cemical Innovation*, 30, 4, 15-21, 2000
[55] Angrist S. W., *Direct Energy Conversion* , Allyn and Bacon Inc. 1977
[56] http://www.microvision.com/wearable_displays/mobile.html

Chapter 2

Electro-active Materials

2.1 Definition

Electro-active materials are materials that exhibits a change in size, shape, colour or in some physical property (refractive index, electrical resistivity, viscosity, etc.) when stimulated by an electric field. The most common applications of this type of materials are in actuators and sensors, according to the Table 2.1, reported below.

The majority of historical actuators and sensors are made of ceramic piezoelectric materials, for instance the well-known barium titanate ($BaTiO_3$), used as dielectric material for ceramic capacitors and as piezoelectric material for microphones; the lead zirconate titanate ($Pb(Zr_xTi_{1-x})O_3$), also known as PZT, and its lanthanum-doped form called lead lanthanum zirconate titanate ($Pb_{0.83}La_{0.17}(Zr_{0.3}Ti_{0.7})_{0.9575}O_3$), in short PLZT, used to make ultrasounds and other sensors and actuators as well as high-value ceramics capacitors and FRAM (Ferroelectric Random Access Memory) chips. PZT is also used in the manufacture of ceramic resonators for reference timing in electronic circuitry [1]. Nevertheless, while these materials are able to withstand large forces, they commonly only deform for fractions of a percent. In the late 1990s, it has been demonstrated that some polymeric materials can exhibit up to a 380% strain [2], like the acrylic elastomer VHB 4910 (by 3M Company, St. Paul, Minnesota, USA), so a new market emerged for synthetic materials and elastomers replaced ceramics in a lot of actuative sectors, in particular concerning robotic and human mimic applications.

Table 2.1, in the following, reports the main classes of electroactive materials along with indication of the type of response and few possible applications. The physical processes driving the electromechanical response of ceramic and elastomeric materials, used for this work, are described in the following paragraph. Hybrid systems will not be treated here even if their behaviour can easily be deduced from that of constituents, inorganic and organic materials. For a deep discussion on the argument please refer to [3].

Class	Materials	Type of Response	Typical applications
Inorganic	Piezoceramics Carbon Nanotubes (CNTs) Cadmium zinc telluride	Actuation, sensing Actuation Electro-optic	Micromotors, sensors Microactuators Infrared lasers
Organic	Conducting polymers (Tab 1.2) Poly(*p*-phenylene) + $FeCl_3$ in SI oil Viologens	Actuation Electro-rheologic Electro-chromism	Micromotors Clutches, dampers etc. Displays
Hybrid	Gels IPMC (ionic polymer-metal composites) Urea-coated- nanoparticles of Ba/Ti-Oxalate in SI oil	Actuation-bending Actuation-bending Electro-rheologic	Micromotors Micromotors Clutches, dampers etc.

Table 2.1. Non exhaustive list of electro-active materials collected for nature.

2.2 Electro-active ceramics

The word ceramics is derived from *Keramos* [1], the Greek word for potter's clay or ware made form clay and fire, and can simply be interpreted as "pottery". Pottery is based on clay and other siliceous minerals that can be conveniently fired in the 900-1200° temperature range. Pottery owes its usefulness to its shapability by numerous methods and its chemical stability after firing.

The evolution from pottery to electronic components has broadened the term "ceramics" so that today it is sometimes used to cover all inorganic non-metallic materials.

Whilst the obvious characteristic of ceramics in electrical use in the first half of the twentieth century was that of chemical stability and high resistivity, it was evident that the possible range of properties was extremely wide. For example for the ferroelectric ceramics as barium titanate and other niobates and tantalates of similar structure. A ferroeletric crystal possesses a unique polar axis that can be switched in direction by an external field. The extent of alignment of the polar axes of the crystallites in a ceramic is limited by the ramdomness in orientation of the crystallites themselves but is sufficient to convert a polycrystalline isotropic body into a polar one. This polarity results in piezoelectric, pyroelectric and electro-optic behaviour that can be utilized in sonars, ultrasonic cleaners, infrared detectors and light processors.

2.2.1 Piezoelectric ceramics

A sub-class of electro-active ceramics is that of piezoelectric ceramics.

In the mid-18th century Carl Linnaeus and Franz Aepinus studied the capability of certain materials to generate electric potential in response to a temperature change, the so called pyroelectric effect. Drawing on this knowledge, both René Just Haüy and Antoine César Becquerel posited a relationship between mechanical stress and electric charge but experiments by both proved inconclusive. The first demonstration of the direct piezoelectric effect was in 1880 by the brothers Pierre Curie and Jacques Curie. They combined their knowledge of pyroelectricity (Carl Linnaeus and Franz Aepinus, mid-18th century) with their understanding of the underlying crystal structures that gave rise to pyroelectricity to predict crystal behavior, and demonstrated the effect using crystals

of tourmaline, quartz, topaz, canesugar, and Rochelle salt (sodium potassium tartrate tetrahydrate). Quartz and Rochelle salt exhibited the most piezoelectricity.
The converse effect was mathematically deduced from fundamental thermodynamic principles by Gabriel Lippmann in 1881 [4]. The Curies immediately confirmed the existence of the converse effect, and went on to obtain quantitative proof of the complete reversibility of electro-elasto-mechanical deformations in piezoelectric crystals.
For the next few decades, piezoelectricity remained something of a laboratory curiosity. More work was done to explore and define the crystal structures that exhibited piezoelectricity. This culminated in 1910 with the publication of Woldemar Voigt's *Lehrbuch der Kristallphysik* (Textbook on Crystal Physics), which described the 20 natural crystal classes capable of piezoelectricity, and rigorously defined the piezoelectric constants using tensor analysis.
Specifically, the word piezoelectricity means electricity resulting from pressure. It is derived from the Greek *piezo* or *piezein* (πιέζειν), which means to squeeze or press, and *electric* or *electron* (ήλεκτρον), which stands for amber, an ancient source of electric charge.

- **Piezoelectricity** is due to the charge which accumulates in certain solid materials (notably crystals, certain ceramics, and biological matter such as bone, DNA and various proteins) in response to applied mechanical strain.

The piezoelectric effect is understood as the linear electromechanical interaction between the mechanical and the electrical state in crystalline materials with no inversion symmetry [5], and it is a reversible process in that materials exhibiting the direct piezoelectric effect (the internal generation of electrical charge resulting from an applied mechanical force) also exhibit the reverse piezoelectric effect (the internal generation of a mechanical force resulting from an applied electrical field). For example, lead zirconate titanate crystals will generate measurable piezoelectricity when their static structure is deformed by about 0.1% of the original dimension. Conversely, lead zirconate titanate crystals will change about 0.1% of their static dimension when an external electric field is applied to the material. Usually, accordingly to the scheme below, piezoelectric ceramics are used as sensors, working in the direct mode, and as actuators, working in the reverse mode.

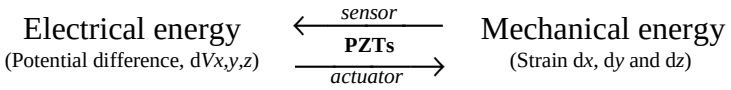

Piezoelectricity is found in useful applications such as the production and detection of sound, generation of high voltages, electronic frequency generation, microbalances, and ultra fine focusing of optical assemblies. It is also the basis of a number of scientific instrumental techniques with atomic resolution, the scanning probe microscopies such as STM (Scanning Tunneling Microscopy), AFM (Atomic Force Microscopy), SNOM (Near Field Scanning Optical Microscopy) etc, and everyday uses such as acting as the ignition source for cigarette lighters and push-start propane barbecues.

2.2.1.1 An electrical approach

The nature of the piezoelectric effect is closely related to the occurrence of electric dipole moments in solids. The latter may either be induced for ions on crystal lattice sites with asymmetric charge surroundings (as in $BaTiO_3$ and PZTs) or may directly be carried by molecular groups (as in cane sugar). The dipole density or polarization (dimensionality [Cm/m^3]) may easily be calculated for crystals by summing up the dipole moments per volume of the crystallographic unit cell. As every dipole is a vector, the dipole density ***P*** is also a vector or a directed quantity. Dipoles near each other tend to be aligned in regions called Weiss domains. The domains are usually randomly oriented, but can be aligned during *poling* (not the same as magnetic poling), a process by which a strong electric field is applied across the material, usually at elevated temperatures.

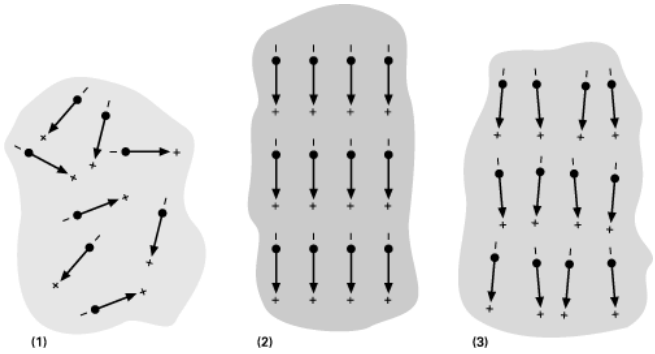

Figure 2.2. (1) Electric dipoles in Weiss domains: unpoled ferroelectric ceramic; (2) during and (3) after poling (piezoelectric ceramic).

Of decisive importance for the piezoelectric effect is the change of polarization ***P*** when applying a mechanical stress. This might either be caused by a re-configuration of the dipole-inducing surrounding or by re-orientation of molecular dipole moments under the influence of the external stress. Piezoelectricity may then manifest in a variation of the polarization strength, its direction or both, with the details depending on the orientation of ***P*** within the crystal, the crystal symmetry and the applied mechanical stress. The change in ***P*** appears as a variation of surface charge density upon the crystal faces, i.e. as a variation of the electrical field extending between the faces, since the units of surface charge density and polarization are the same, $C/m^2] = [Cm/m^3]$. However, piezoelectricity is not caused by a change in charge density on the surface, but by dipole density in the bulk. For example, a 1 cm^3 cube of quartz with 2 kN (500 lbf) of correctly applied force can produce a voltage of 12500 V.

2.2.1.2 An electro-mechanical approach

The piezoelectric effect is a linear electromechanical effect where the mechanical strain (*S*) and stress (*T*) are coupled to the electric field (*E*) and displacement (or charge density *D*) linearly

$$S = dE \tag{2.1}$$

$$D = dT \tag{2.2}$$

In the literature [6], the effect in Eq.(2.1) is often known as the converse piezoelectric effect and Eq.(2.2) as the direct piezoelectric effect. The variable *d* in the equation reported is the piezoelectric coefficient. Adding the linear elastic (Hook's law) and dielectric relations to Eq.(2.1) and writing it out in the full tensor form, we will have the piezoelectric constitutive equations

$$S_{ij} = d_{ijk}E_k + s^E_{ijkl}T_{kl} \tag{2.3}$$

$$D_i = \varepsilon^T_{ik}E_k + d_{ijkl}T_{kl} \tag{2.4}$$

where *s* is the elastic compliance, ε is the dielectric permittivity and i, j, k, l =1-3. In the equation, the convention in which repeated indices are summed is used. The superscript *E* and *T* refer to the condition under which those quantities are measured. That is, compliance is measured under a constant electric field (short circuit conditions) and dielectric constant under a constant stress. Due to the electromechanical coupling in a piezoelectric material, the elastic compliance under a constant electric field can be very different from that under constant charge. In order to write the elastic and piezoelectric tensors in the form of a matrix array, a compressed matrix notation is introduced. In the matrix notation *ij* or *kl* is replaced by *p* or *q* according to [6], so

$$11 \to 1,\ \ 22 \to 2,\ \ 33 \to 3,\ \ 23 or 32 \to 4,\ \ 31 or 13 \to 5,\ \text{and}\ 12 or 21 \to 6$$

Eqs.(2.3) and (2.4) are the complete costitutive equations for a piezoelectric material. For a given piezoelectric material, the number of independent parameters can be reduced using simmetry relations in the material. For instance, for an unstretched and poled material which has a point group ∞m, the piezoelectric coefficient, the dielectric permittivity ($\varepsilon_{ij}=K_{ij}\varepsilon_0$, where K_{ij} is the relative permittivity and ε_0 is the vacuum permittivity), and elastic compliance matrices are

$$\begin{bmatrix} 0 & 0 & 0 & 0 & d_{15} & 0 \\ 0 & 0 & 0 & d_{15} & 0 & 0 \\ d_{31} & d_{31} & d_{33} & 0 & 0 & 0 \end{bmatrix}, \begin{bmatrix} K_{11} & 0 & 0 \\ 0 & K_{11} & 0 \\ 0 & 0 & K_{33} \end{bmatrix}, \begin{bmatrix} s_{11} & s_{12} & s_{13} & 0 & 0 & 0 \\ s_{12} & s_{11} & s_{13} & 0 & 0 & 0 \\ s_{13} & s_{13} & s_{33} & 0 & 0 & 0 \\ 0 & 0 & 0 & s_{44} & 0 & 0 \\ 0 & 0 & 0 & 0 & s_{44} & 0 \\ 0 & 0 & 0 & 0 & 0 & s_{66} \end{bmatrix} \tag{2.5}$$

with $s_{66}=2(s_{11}-s_{12})$ and the 3-direction is the material poling direction.

During this PhD activity we prepared some $BaTiO_3$ circular tablets sintering the ferroelectric powder and poling the obtained samples under a high external electric field

(about 2kV/μm for 10mins at 140°C). The effect of the polarization on the electromechanical behaviour of the piezo-tablets to be used as energy harvesting devices in wearable systems, has been tested via dielectric and mechanical characterization, as reported in Cap.4. Prototypes of devices able to convert passive energy by human walk to batteries were prepared and a an electrical circuit for the accumulation of electrical cherges was developed and used to switch on a LED after a series of pulses.

2.2.1.3 Barium Titanate

Barium Titanate ($BaTiO_3$), one of the well known piezoelectric ceramic material, presents a paraelectric cubic phase above 130°C, temperature called Curie point. Between 130°C and 0°C the tetragonal phase is stable and the spontaneous polarization is along [001] direction. Between 0°C and -90°C the ferroelectric rhombohedral phase is stable with polarization along [110].
Decreasing temperature below -90°C transition from rhombohedral phase to orthorhombic phase takes place with polarization axis along [111].

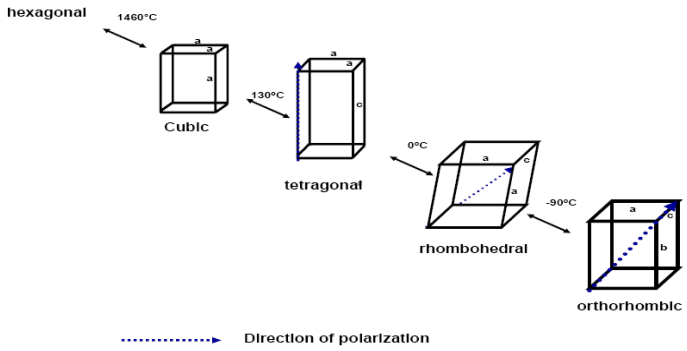

Figure 2.2. Phase transitions in BaTiO3 crystals.

For these reasons, in order to poling the $BaTiO_3$ powder, it is necessary to heat it above its Curie temperature and orient all crystals along the same axis (the axis of the applied external electric field.

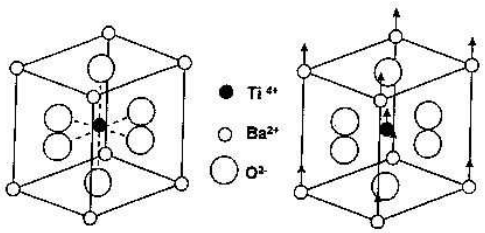

Figure 2.3. $BaTiO_3$ piezoelectric elementary cell; (1) before poling, cubic structure(2) after poling, tetragonal structure.

2.3 Electro-active polymers (EAPs)

The field of EAPs emerged back in 1880, when Wilhelm Roentgen designed an experiment in which he tested the effect of an electrical current on the mechanical properties of a rubber band [7]. The rubber band was fixed at one end and was attached to a mass at the other. It was then charged and discharged to study the change in length with electrical current. Sacerdote followed up on Roentgen's experiment by formulating a theory on strain response to an applied electric field in 1899 [7]. It wasn't until the year 1925 that the first piezoelectric polymer was discovered (Electret). Electret was formed by combining carnauba wax, rosin and beeswax, and then cooling the solution while it is subject to an applied DC electrical bias. The mixture would then solidify into a polymeric material that exhibited a piezoelectric effect.

Polymers that respond to environmental conditions other than an applied electrical current have also been a large part of this area of study. In 1949, Katchalsky et. al. demonstrated that when collagen filaments are dipped in acid or alkali solutions they would respond with a change in volume[7]. The collagen filaments were found to expand in an acidic solution and contract in an alkali solution. Although other stimuli (such as pH) have been investigated, due to its easiness and practicality most research has been devoted to developing polymers that respond to electrical stimuli in order to mimic biological systems.

It wasn't until the late 1960s when the next major breakthrough in EAPs was observed. In 1969, Kawai was able to demonstrate that polyvinylidene fluoride (PVDF) exhibits a large piezoelectric effect[7]. This sparked research interest in developing other polymers systems that would show a similar effect. In 1977, the first electrically conducting polymers were discovered by Hideki Shirakawa et.al [8]. Shirakawa along with Alan Mac Diarmid and Alan Heeger demonstrated that polyacetylene was electrically conductive, and that by doping it with iodine vapor, they could enhance its conductivity by 8 orders of magnitude. Thus the conductance was close to that of a metal. By the late 1980s a number of other polymers had been shown to exhibit a piezoelectric effect or were demonstrated to be conductive.

In the early 1990s, ionic polymer-metal composites were developed and shown to exhibit electroactive properties far superior to previous EAPs. The major advantage of IPMCs was that they were able to show activation (deformation) at voltages as low as 1 or 2 volts[7]. This is orders of magnitude less than any previous EAP. Not only was the activation energy for these materials much lower, but they could also undergo much larger deformations. IMPCs were shown to exhibit anywhere up to 380% strain, orders of magnitude larger than previously developed EAPs [2]. In 1999, Yoseph Bar-Cohen, proposed the Arm wrestling Match of EAP Robotic Arm Against Human Challenge[7]. This was a challenge in which research groups around the world competed to design a robotic arm consisting of EAP muscles that could defeat a human in an arm wrestling match. The first challenge was held at the Electroactive Polymer Actuators and Devices Conference in 2005 [7]. Another major milestone of the field is that the first commercially developed device including EAPs as an artificial muscle was produced in 2002 by Eamex

in Japan [2]. This device was a fish that is able to swim on its own, moving its tail using an EAPmuscle. But the progress in practical development is not satisfactory, possibly due to misleading in fundamental research [9].

EAPs Mechanism	**Materials**	ε_{max} **[%]**	P_{max} **[MPa]**	d_{EE} **[J/g]**	**Drawbacks**
Ionic	Conducting polymers: PANI	10	450	23	Low speed resp.; Low efficiency
	Gels: Polyelectrolites	>40	0.3	0.06	Low speed resp.; Low actuative P
	Ionic Polymer-Metal Composite: Nafion	0.5-3.3	1.0	0.025	Low speed resp.; Low efficiency
Electronic	Ferroelectric polymers: Liquid Crystals Polymers (LCP)	>35	>0.3	>0.10	Low strains
	Piezoelectric polymers: PVDF	0.1	4.8	0.0024	Low strains
	Electrostrictive polymers: Silicone	32	0.21	0.0034	
	Polyurethane	11	1.9	0.1	Low strains
	P(VDF-TrFE)	4.3	43	0.49	
	Dielectric elastomers: Acrilic	380	7.2	3.4	Low actuative pressures
	Silicone	120	0.3-3.2	0.75	

Table 2.2. Main classification of EAPs and their performance (ε=strain; P=active pressure; d_{EE}=elastic energy density).

2.3.1 Dielectric elastomers

Among the broad class of EAPs, dielectric elastomers (DEs) are described as electrically insulating materials able to convert electrical energy to mechanical energy and *vice versa*. More specifically, DEs are "actuators" (electromechanical transducers), when they transduce electrical energy to mechanical energy (shape change), and "generators", when they transduce mechanical energy to electrical energy.

Electrical energy (Potential difference, dV*x*,*y*,*z*) ⟵ *sensor* **DEs** *actuator* ⟶ Mechanical energy (Strain d*x*, d*y* and d*z*)

The basic structure of DEs, shown in Fig.2.4, is quite simple. A polymer film, typically, but not necessarily, an elastomer, is sandwiched between two compliant electrodes able to stretch and contract with the polymer during the actuation mechanism; a lot of different configurations for actuation in compression or expansion have been developed so far. For a deep insight into the argument please refer to [10].

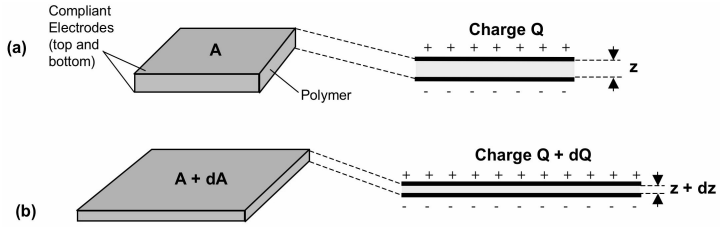

Figure 2.4. DEs in the actuation mode, before the application of the external electric field (a) and after (b). Changes of shape are exagerated for clarity.

The behaviour and physics of DEs can be derived in a number of ways. Methods involving tensors are perhaps the most general, and several excellent analysis using tensors have been developed [11].

2.3.1.1 A mechanical approach

The forces induced into dielectric elastomers as a consequence of the application of an external electric field have two different origins:

- **Electrostriction**: due to the redistribution of atoms and molecules in a dielectric material when it is placed in an electric field
- **Maxwell stress**: due to the Coulumbian attraction among the free opposite charges laying onto the electrodes that squeeze the elastomer

Both mechanisms are described in the following.

Electrostrictive effect. The electrostrictive effect, differently from piezoeletric effect, is a quadratic dependence of strain or stress on the polarization *P* and exist in all materials [12]

$$S_{ij} = Q_{ijkl} P_k P_l \tag{2.6}$$

where *S* is the mechanical strain, *Q* the charge-related electrostrictive coefficient and *i, j, k, l* = 1÷3. For an isotropic polymer:

$$S_3 = Q_{33} P^2 \tag{2.7}$$

$$S_1 = Q_{13} P^2 \tag{2.8}$$

where S_3 and S_1 are the strains parallel and perpendicular to the polarization direction, known as the longitudinal and transverse strains, respectively.
For an isotropic polymer, experimental evidence and theoretical consideration indicate that $Q_{33}<0$ and $Q_{13}>0$ [13, 14]. Hence, for a polymer, an increase in polarization will result in a contraction along the polarization direction.
For a linear dielectric polymer, the polarization is related to the dielectric permittivity as:

$$P = \varepsilon_0(\varepsilon - 1)E \tag{2.9}$$

where ε is the dielectric permittivity of the elastomer, ε_0 is the vacuum dielectric permittivity ($8{,}85\times10^{-12}$ F/m). Hence, Eq.(2.6) can be converted into

$$S = Q(\varepsilon - \varepsilon_0)^2 E^2 = ME^2 \tag{2.10}$$

where *M* is known as the electric-field-related electrostriction coefficient. For an isotropic solid, the longitudinal strain is $S_3=M_{33}E^2$ and the transverse strain $S_1=M_{13}E^2$. Therefore, for an isotropic polymer, $M_{33}<0$ and $M_{13}>0$. that is, it will contract along the thickness direction and expand along the film direction when an electric field is applied across the thickness.
For electromechanical applications, as the case of the present work, electromechanical coupling factor *k*, wich measures the efficiency of the material in converting energy

between the electric and mechanical forms, is one of the most important parameters [6], being:

k_1^2 = converted mechanical energy / input electric energy
k_2^2 = converted electrical energy / input mechanic energy

In electromechanical applications, an electric field is applied along a certain direction and the electromechanical actuation along the same direction or another direction is used. The coupling factor depends on the direction of the electric field and the mechanical strain (or stress) direction. Hence, for electromechanical EAPs, there are many electromechanical coupling factors, depending on the combination of the directions of electric and mechanical variables. For example, a polymer actuator can be made with the electric field along the 3-direction, while the actuation is along the same direction. In this case, the coupling factor is the longitudinal electromechanical coupling factor k_{33} which is related to the piezoelectric coefficient d_{33} and the elastic compliance s_{33} as:

$$k_{33}^2 = \frac{d_{33}^2}{\varepsilon_{33}^T s_{33}^E} \tag{2.11}$$

On the other hand, if the mechanical actuation is along the direction perpendicular to the applied electric field (the 1-direction, for instance), the coupling factor is k_{31} and

$$k_{31}^2 = \frac{d_{31}^2}{\varepsilon_{33}^T s_{11}^E} \tag{2.12}$$

The coupling factor can also be related to the material coefficient measured under different conditions. For example, the elastic compliance s_{33}^E is related to s_{33}^D (measured under constant charge or open circuit condition) as

$$s_{33}^D = (1 - k_{33}^2)^2 s_{33}^E \tag{2.13}$$

where D is the displacement or charge density of the system.
Therefore, a polymer with a large coupling factor will see a large difference in the elastic compliance when used under different external electric boundary conditions, which may be utilized to tune the elastic modulus of the polymeric material by varying the electric conditions.

Maxwell Stress effect. Analogous to the electrostriction, where the strain is approximately proportional to the square of the electric field strenght, there is onother electromechanical actuation mehcanism whose strain response is also approximately proportional to the square of the eletric field strength. That is the electrostatic force (maxwell stress)-induced strain, which can be quite significant in soft polymer elastomers.
The general expression for the Maxwell stress for a dielectric material has been derived as [15, 16]:

$$T_{ij}^M = -E_i D_j + \frac{1}{2}\delta_{ij} D_k E_k \tag{2.14}$$

where T is the stress, δ_{ij}=1 (Kronecker identity tensor) when i=j and δ_{ij}=0 otherwise. Using $D_i=\varepsilon_{ij}E_j$, Eq.(2.9) can be rewritten as:

$$T_{ij}^{M} = -\varepsilon_{jm}E_iE_m + \frac{1}{2}\delta_{ij}\varepsilon_{kl}E_lE_k \tag{2.15}$$

therefore, the strain due to the Maxwell stress in a dielectric material is

$$S_{ij} = -(s_{ijkm}\varepsilon_{ml} - \frac{1}{2}\delta_{ij}s_{ijmn}\varepsilon_{kl})E_lE_k \tag{2.16}$$

which has the same form of the electrostriction (Eq.(2.10)). For an isotropic solid without mechanical constraints, the longitudinal strain induced by the Maxwell stress is

$$S_3 = S_{33} = -\frac{1}{2}\varepsilon(s_{11} - 2s_{12})E_3^2 \tag{2.17}$$

and the transverse strain is

$$S_1 = S_{11} = -\frac{1}{2}\varepsilon s_{11}E_3^2 \tag{2.18}$$

in Eq.(2.17) and (2.18), we have made use of the fact that for an isotropic polymer, the dielectric tensor is reduced to one constant: ε. For a polymer with Poisson's ratio equal to one half, Eq.(2.17) becomes

$$S_3 = -\varepsilon s_{11}E_3^2 \tag{2.19}$$

Analogous to the electrostriction in an isotropic polymer, the Maxwell stress causes contraction along the field direction; and for a soft polymer (a large elastic compliance), the Maxwell stress induced strain (here it is called Maxwell strain) can be significant. For large strains, Eq.(2.19) should be modified to the form

$$Y\ln\left(\frac{d_0}{d}\right) = \varepsilon\left(\frac{V}{d}\right)^2 \tag{2.20}$$

where d_0 is the initial film thickness, d is the final film thickness, Y is the Joung's modulus ($Y=1/s_{11}$) and V is the applied voltage. These espressions show that for a soft polymer elastomer under high field, the Maxwell stress induced strain can be quite high. For an isotropic material, it has been shown that a thickness strain of 40% can be induced by the Maxwell stress effect before the mechanical instability occurs [17]. However, for anisotropic materials or materials with nonlinear elastic behavior, the analysis of the mehcanical instability should be modified, which may lead to a strain level higher than 40% before the mechanical instability occurs.

Descending form Eq.(2.19) is the expression of the actuative stress or pressure:

$$T_3 = p_3 = -\varepsilon E_3^2 \tag{2.21}$$

where $T=p$ is the compressive stress or pressure exerted over an area A through a displacement dz necessary to provide mechanical work equal to the actual work on the polymer.

$$-Apdz = dW \tag{2.22}$$

where W is the mechanical work done by or on the electric charges via the field pressure.

2.3.1.2 An electrical approach

The electromechanical transduction properties of any dielectric elastomer are intrinsically regulated by the dielectric permittivity of the material. This parameter proportionally controls both the achievable active stresses and strains. Accordingly, a suitable increase of the material permittivity may provide a valuable means to improve the performance of a dielectric elastomer actuator. This paragraph provides a brief overview of the most known and applied mixing rules governing the dielectric behavior of materials and composites in order to provide an overview of the available methods for increasing the permittivity of a dielectric elastomer.

As reported in §2.3.1.1, the electromechanical response of a dielectric elastomer actuator is determined by the actual compressive stress p [18]:

$$p = \varepsilon_0 \varepsilon E^2 \tag{2.23}$$

where ε_0=8.854 pF/m is the dielectric permittivity of vacuum, $\vec{E}$ is the applied electric field and ε is the relative dielectric permittivity of the elastomer.

Modifying a polymer matrix in order to increase its dielectric permittivity means acting on the dipolar moments of the material and, therefore, on its polarisation vector $\vec{P}$ [19]. This vector is related to the field vector $\vec{E}$ by the following expression:

$$\vec{P}(\omega) = \varepsilon_0 (\varepsilon(\omega) - 1)\vec{E}(\omega) \tag{2.24}$$

where ω is the angular frequency of the ac electric field. Deviations from the linear behaviour expressed by Eq.(2.9) are likely to be observed at sufficiently high electric fields, when also higher order terms of $\vec{E}(\omega)$ must be taken into account. The frequency dependence of Eq.(2.9) reflects the possible existence of dispersive behaviours somewhere in the electromagnetic spectrum. In any case, the relative dielectric permittivity is a frequency dependent complex quantity:

$$\varepsilon^*(\omega) = \varepsilon'(\omega) - j\varepsilon''(\omega) \tag{2.25}$$

$\varepsilon'(\omega)$ and $\varepsilon''(\omega)$ being its real and imaginary parts, respectively. The real part $\varepsilon'(\omega)$ is always different from zero and represents the contribution to the polarisation responsible for the energy storage into the material. In order to stress its substantial independence from the electric field, it is often referred to as the *relative dielectric constant* of a material. The imaginary part $\varepsilon''(\omega)$, usually called *loss factor*, accounts for possible dissipative effects and its frequency spectrum differs from zero only in coincidence to dispersive regions.

Sometimes, the dissipative behaviour is characterized by means of the so-called *loss angle* $\delta(\omega)$ and it is defined as $\mathrm{tg}\delta(\omega)=\varepsilon''(\omega)/\varepsilon'(\omega)$.

In a homogeneous medium, the polarisation $\vec{P}$, and thus also $\varepsilon^*(\omega)$, arises as a combination of various contributions. One main contribution comes from the deformational polarisability of the material, which is the mutual displacement of oppositely charged particles, like electrons nuclei and ions, under the action of the applied field. Associated with such a polarisation mechanism, dispersive phenomena may arise from different physical processes occurring at electronic, atomic or ionic level. Since they involve interactions with quantum energy levels, the associated frequency response is characterised by a resonant-like behaviour. On the other hand, if the material molecules already possess permanent dipole moments, say $\vec{\mu}$, these individually interact with the field $\vec{E}$ through a potential energy $U=-\vec{\mu}\cdot\vec{E}$, which drives each dipole to orientate itself parallel to the field. Such orientational polarisability represents the second important contribution to the global polarisation $\vec{P}$. Nevertheless, additional dispersive processes may originate from the limited mobility of the permanent dipoles, resulting in a frequency response typical of relaxation phenomena. Due to the very different time scales involved, resonant phenomena determine dispersive behaviours at infrared frequencies and above, while relaxation phenomena show up at much lower frequencies; they are particularly evident in the case, for instance, of highly polar liquids (e.g. water), resins and polymers. In addition to such deformational and orientational contributions to polarisation (whose associated properties in the following will be referred to as "bulk" or "intrinsic"), also a limited displacement (diffusion) of possible space charges may give rise to a polarisation; this, in turn, may be responsible for energy dissipation inside a heterogeneous system. This is the case, for example, of the relaxation phenomena associated to the so-called Maxwell-Wagner (or interfacial) polarisation. It takes place when surface charges accumulate at interfaces between a dielectric matrix and other phases with different electrical properties (i.e. electrodes, inclusions, defects, fillers, impurities). Moreover, the dissipation of energy may be increased if the material, either homogeneous or heterogeneous, exhibits a finite dc electrical conductivity σ_{dc}, which may originate, for example, from diffusion of impurity ions (electrophoresis). Differently from metals, electrical conduction in dielectrics is an activated process, and thus σ_{dc} results to increase with temperature.

All these different contributions sum up to give an effective relative complex dielectric permittivity ε_{eff}^*, which may be defined in a very general form as follows:

$$\varepsilon_{eff}^*(\omega)=\varepsilon^*(\omega)+\sum_i\varepsilon_{MW,i}^*(\omega)-j\left(\frac{\sigma_{dc}}{\omega\varepsilon_0}\right)=\left(\varepsilon'(\omega)+\sum_i\varepsilon'_{MW,i}(\omega)\right)-j\left(\varepsilon''(\omega)+\sum_i\varepsilon''_{MW,i}(\omega)+\frac{\sigma_{dc}}{\omega\varepsilon_0}\right) \tag{2.26}$$

where each term $\varepsilon_{MW,i}^*$ accounts for an *i*-th interfacial contribution. It is worth stressing that all the dispersive phenomena associated to the intrinsic polarisation are accounted for by $\varepsilon^*(\omega)$ in Eq.(4). In particular, since the time scale of dielectric elastomer actuation is never shorter than the period associated to radio waves, we are here mainly concerned with the dielectric properties of materials well below infrared frequencies, where any dispersive

behaviour of the deformational polarisation is absent. Thus, the bulk permittivity $\varepsilon^*(\omega)$ can be thought as being composed by a constant real term representing the "low frequency limit" (relaxed) value of the deformational permittivity, plus a frequency dependent component which accounts for the dispersive behaviour of the orientational polarisation of the system. In presence of multiple intrinsic relaxations, $\varepsilon^*(\omega)$ can be expressed as a superposition of individual contributions. Indeed, each relaxation process, either orientational or interfacial, can be analytically described by means of a proper relaxation function. In the simplest case of a material consisting of identical and non-interacting dipoles, whose relaxation is characterised by a unique time constant τ, Debye derived the relaxation function for the complex permittivity in the associated dispersion region [20]. In the frequency domain, the Debye model brings to the well-known formula:

$$\varepsilon^*(\omega) = \varepsilon_\infty + \frac{\varepsilon_s - \varepsilon_\infty}{1 + j\omega\tau} \tag{2.27}$$

where ε_s and ε_∞ respectively represent the static (relaxed) and the high frequency (unrelaxed) values of the permittivity, with respect to the considered process. For a material showing a unique dipolar relaxation in its whole spectrum, ε_∞ in turn coincides with the aforementioned relaxed value of the deformational permittivity. Eq.(2.27) can be splitted in its real and imaginary parts and then equivalently expressed by the following pair of equations:

$$\begin{cases} \varepsilon'(\omega) = \varepsilon_\infty + \dfrac{\varepsilon_s - \varepsilon_\infty}{1 + \omega^2\tau^2} \\ \varepsilon''(\omega) = \dfrac{(\varepsilon_s - \varepsilon_\infty)\omega\tau}{1 + \omega^2\tau^2} \end{cases} \tag{2.28}$$

Due to the very simplistic assumptions it is based on, it can appear obvious that the Debye model is found to fail in describing relaxation phenomena in complex. Thus, Havriliak and Negami proposed a more general formula [21]. Though derived by a phenomenological approach, it has the merit of including the possibility of a distribution of different time constants through the introduction in Eq.(2.27) of two *shape parameters* α and β:

$$\varepsilon^*(\omega) = \varepsilon_\infty + \frac{(\varepsilon_s - \varepsilon_\infty)}{\left[1 + (j\omega\tau)^{1-\alpha}\right]^\beta} \quad (0 < \alpha < 1,\ 0 < \beta < 1) \tag{2.29}$$

For our purposes, the occurrence of a dispersive process of any nature in the frequency region of interest, represents a drawback. In order to advantageously exploit a dielectric elastomer as an actuation material, the effective loss factor should be kept as low as possible. In fact, losses not only waste part of the input energy, but they also worsen the insulation properties of the material. In particular, for any dielectric material it is possible to identify a threshold electric field, which generates irreversible modifications in the medium accompanied by the onset of an intense and disruptive flow of charges. Such a sudden loss of insulation due to a very high electric field is named *dielectric breakdown* of the material. The minimum field responsible for such effect is called *breakdown field* or *breakdown strength*, E_{break}. In most polymers, E_{break} is included in the range 10^6 - 10^8 V/m.

It represents the analogous of the mechanical fracture threshold for a material subjected to an external load. Although dielectric breakdown phenomena are object of intense studies since the first half of the last century [22], physical models allowing reliable predictions of E_{break} are still not available. In fact, several are the possible causes and processes related to dielectric breakdown; these include purity level, processing methods, working conditions, environmental conditions, and mechanical solicitations [23]. However, it is generally accepted that mechanisms responsible for dielectric discharges can have both thermal and intrinsic (bulk) origin. In the first case, both dielectric polarization and conduction losses determine a temperature increase of the material. Indeed, the power density W dissipated into the dielectric medium, at expenses of the electric field, is proportional to $\varepsilon_{eff}''(\omega)$:

$$W \propto \omega \left|\vec{E}\right|^2 \varepsilon''_{eff}(\omega) \tag{2.30}$$

Such a heating, in turn, enhances the conductivity in a self-amplified process with catastrophic consequences; in fact, the amount of heat that the material is not able to dissipate drives it to the breakdown. As a second possibility, breakdown may be related to an avalanche discharge process that begins with the promotion of few valence electrons to the conduction band. These electrons, being accelerated by the applied electric field, strike against other valence electrons, driving them to the conduction band by a kinetic energy transfer; as this process of charge carriers multiplication goes on, the current flow grows rapidly in the dielectric and the material can locally melt and pierce. For further information on the argument read [24].

2.3.1.3 Theory of electromechanical transduction in DEs: recent remarks

In the last few years, after the first irruptive success obtained by DEAs and the numerous developed applications, some theories have come out reconsidering the relations used to describe the physics of DEAs. In particular, Suo Z. [25] pointed out two aspects:

- when two electric charges are placed inside a dielectric solid, the force between them is not a measurable quantity: for deformable dielectric solids, unconstrained in the space, the electric force can be neither defined nor measured.

- when a dielectric solid deforms, the true electric field and true electric displacement are nor work conjugates.

In brief, Suo states that only for ideal “liquid-like” dielectric elastomers the Maxwell stress is valid and that a more general model can represent both the Maxwell stress and electrostriction.
Wissler M, and Mazza E. [26] during the same year added:

- dielectric constant ε is not a constant parameter but it decreases with increasing pre-stretch ratio λ (from 4.7 to 2.6 for VHB 4910 pre-stretched at λ=5).

In the following, a new relation between pressure p and electric field E is reported for a system with dielectric constant ε varying with the strain dz.

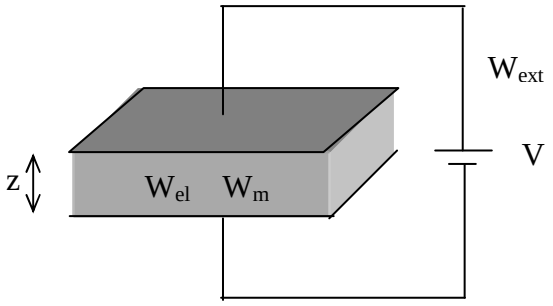

Figure 2.5. Electromechanical coupling in a dielectric elastomer actuator.

The energy balance for a closed electromechanical system for an incremental deformation dz is given by the following equation [26]:

$$\frac{dW_{ext}(z)}{dz} = \frac{dW_{el}(z)}{dz} + \frac{dW_m(z)}{dz} \tag{2.31}$$

where W_{ext} is the supplied energy, W_{el} the supplied electrical energy and W_m the mechanical energy. W_{ext}, as the electrical energy from the power source, can be rewritten as:

$$\frac{dW}{dz} = V(z)\frac{dQ(z)}{dz} \tag{2.32}$$

with V as the electric voltage and Q the supplied charge, being the time derivative of the energy from the power source related to current I and voltage V as (chain rule):

$$\frac{dW_{ext}}{dt} = VI = V\frac{dQ}{dt} \tag{2.33}$$

Where t is time.
Q and V are linked as $Q(z)=C(z)V(z)$ with the capacitance C defined as

$$C = \frac{\varepsilon_0\varepsilon_r A}{z} = \frac{\varepsilon_0\varepsilon_r Vol_0}{z^2} \tag{2.34}$$

Where (2.33) is the active electrode area and $Vol_0=Az$ is the elastomer active volume which remains constant during deformation. The variation of charge Q with z can thus be written as:

$$\frac{dQ(z)}{dz} = \varepsilon_0\varepsilon_r Vol_0 \frac{d}{dz}\left(\frac{V(z)}{z^2}\right) = \frac{\varepsilon_0\varepsilon_r Vol_0}{z^2}\left(\frac{dV}{dz} - 2\frac{V}{z}\right) \tag{2.35}$$

Combining Eq.(2.33) and (2.35) we have.

$$\frac{dW_{ext}}{dz} = \frac{\varepsilon_0\varepsilon_r Vol_0 V}{z^2}\left(\frac{dV}{dz} - 2\frac{V}{z}\right) \tag{2.36}$$

Therefore, if, as proved by Wissler and Mazza [26], ε varies with the strain, we must change Eq.(2.35) considering that

$$Q(z) = C(z)V(z) = \frac{\varepsilon_0\varepsilon_r(z)Vol_0}{z^2}\cdot V(z) \tag{2.37}$$

so

$$\frac{dQ(z)}{dz} = Vol_0\left(\frac{\varepsilon_0\varepsilon_r' z^2 - 2\varepsilon_0\varepsilon_r z}{z^4}V(z) + \frac{\varepsilon_0\varepsilon_r V'}{z^2}\right) \tag{2.38}$$

and

$$\frac{dW_{ext}}{dz} = V \cdot Vol_0\left[\left(\frac{\varepsilon_0\varepsilon_r'}{z^2} - \frac{2\varepsilon_0\varepsilon_r}{z^3}\right)\cdot V + \varepsilon_0\varepsilon_r\frac{V'}{z^2}\right] \tag{2.39}$$

Similarly, the energy W_{el} stored by the electric field in the capacitor is:

$$W_{el} = \frac{1}{2}C(z)V(z)^2 = \frac{1}{2}\frac{\varepsilon_0\varepsilon_r(z)}{z^2}V(z)^2 \tag{2.40}$$

$$\frac{dW_{el}}{dz} = \frac{Vol_0}{2}\left[\frac{\varepsilon_0\varepsilon_r(z)' z_2 - 2\varepsilon z}{z^4}V^2 + \varepsilon\frac{2VV'}{z^2}\right] = \frac{Vol_0 V}{2}\left[\frac{\varepsilon_0\varepsilon_r' V}{z^2} - \frac{2\varepsilon_0\varepsilon_r V}{z^3} + \frac{2\varepsilon_0\varepsilon_r V'}{z^2}\right] \tag{2.41}$$

Finally, subtracting Eq.(2.39) form Eq.(2.41) we obtain the derivative of the mechanical energy

$$\frac{dW_m}{dz} = -\frac{V^2 Vol_0}{2z^2}\left[\varepsilon_0\varepsilon_r' - \frac{2\varepsilon_0\varepsilon_r}{z}\right] \tag{2.42}$$

At this point, calculating the external electrostatic pressure p_z acting on the film we get

$$p_z = -\frac{dW_m}{dz}\frac{1}{A(z)} = -\frac{dW_m}{dz}\frac{z}{A_0 z_0} = \varepsilon_0\varepsilon_r E^2 - \frac{1}{2}\varepsilon_0\varepsilon_r' z E^2 \tag{2.43}$$

which differs from equation obtained by Perline [18] for the second term. Considering ε constant with strain, in fact, Perline in 1998 got Eq.(2.44)

$$p_z = \varepsilon_0\varepsilon_r E^2 \tag{2.44}$$

In his work, Wissler and Mazza specify that there are papers presenting experimental data about the non-dependence of the dielectric constant on strain [27] and that their work should be studied in depth to verify also if there is a dependence on the elastomeric material itself.

2.3.1.4 A chemical approach

The empirical definition of an elastomer is a macromolecular material that deforms substantially when exposed to small mechanical loads [28, 29, 30]. Furthermore, the material almost recovers its original shape shortly after the load has been released. A more physical definition is that an elastomer is a crosslinked polymer material above its glass transition temperature. Three common types of elastoms are chemically crosslinked (vulcanized) rubbers, physically crosslinked thermoplastic elastomers, and polymers of sufficiently high chain length, where entanglements serve as physical crosslinks.
A wealth of information exists on the mechanical properties of elastomers as described in the following chapters. The dielectric properties and especially electric breakdown

properties are less understood. It generally holds for any polymer that polar groups increase the dielectric constant, and at the same time increase ionic conductance and lowers chain mobility and hence raise the glass transition temperature (T_g). Poly(dimethylsiloxane) (PDMS) is an example of a polymer with low relative dielectric constant – typically between 2.5 and 3 – high dielectric breakdown strength and high chain mobility. Polyurethanes (PUs), which contain several polar groups compared to PDMS, follow the general trend: they have relative dielectric constant in the range 3-10, they have much higher ionic conductivity at especially elevated temperatures and hence lower dielectric strength. Finally, PUs have glass transition temperatures much above those of silicones. The acrylic elastomer used in VHB™ 4910 from 3M™ deviates from the general trends by possessing extremely high dielectric strength when stretched, and at the same time, a relative high dielectric constant, which has been shown to be dependent on stretching [31].

In general, the dielectric constant is proportional to the density of polarisable groups and decreases with increasing temperature due to thermal expansion. The variations in time of the dielectric constant and elastic modulus instead share a common origin. The effects are dominated by relaxations of the polymer – reorientation of the polymer chains under stress or in an electric field. The α-relaxation is associated with the glass transition of amorphous polymers. As the temperature service ranges of elastomers are well above T_g, the relaxation typically occurs in microseconds or faster, and the relaxation poses no restriction to the speed of dielectric elastomer actuators or influence their properties. In polymer melts, entanglements form an important contribution to the viscoelastic properties and the disentanglement time – the time it takes a polymer chain to reptate out of its tube [32] - defines a slow relaxation process in milliseconds to seconds. In a network, the chains are fixed through chemical crosslinks; they can no more relax through reptation along their tube, and most of the entanglements are trapped. Only free ends – so called dangling ends – and substructures attached to those can relax through a kind of breathing motion. This motion requires a strong deformation of the chain and is order of magnitudes slower than reptation motion in a melt [33].

These relaxations of dangling ends are responsible for the slow – seconds to days - viscoelastic response observed in most elastomers.

The affine model for rubber elasticity (see below) states that the elastic modulus is proportional to the density of elastic active polymer chains and the temperature. For a room temperature vulcanized PDMS the decrease in density due to thermal expansion approximately balance the temperature proportionality. The modulus is almost constant over a wide temperature range.

Elastomers possess properties of both solids and liquids, and therefore elastomers have many applications in the field of soft solids, e.g. as vibration sinks in electronics, medical implants or adhesives. Permanent, chemical, physical, or topological crosslinks contribute to the elastic behavior, whereas long polymer chains contribute to the viscous behavior of the material. The elasticity of elastomers are generally speaking governed by the length of elastic active chains – that is the average molecular weight of chains between crosslinks (M_x) measured in quantities of the molecular entanglement weight (M_e), which is a

temperature dependent characteristic material property. Generally speaking, elastomers with $M_x/M_e<1$ are rigid, and elastomers with $M_x/M_e>1$ are soft. Traditionally the elasticity is measured by the elastic modulus (G) or the Young's modulus (Y). For an elastomer, the relation between the two is:

$$Y = 3G \tag{2.45}$$

The premise for traditional theories of rubber elasticity is that network chains stretch as simple Gaussian random coils and that their contributions to the modulus are additive. Models of elastomers in the 'phantom' limit (in which the chains are assumed to be devoid of material properties) were developed by James and Guth [34]. In such a phantom network, it is assumed that the chains move freely through one another, and that the only contribution to the elasticity arises from the network connectivity. The phantom model predicts the modulus to be proportional to the inverse of the molecular weight of the elastic active chain:

$$G_{ph} = (\nu - \mu)RT = (1 - \frac{2}{f})\frac{\rho}{M_x}RT \tag{2.46}$$

where μ is moles of junctions per unit volume given by $2\nu/f$ with f being the functionality of the crosslinker, ν is moles of elastic chains per unit volume, R is the gas constant, T the absolute temperature, and ρ the density of the elastomer.

In an affine network, on the other hand, the end-to-end chain vectors are assumed to transform affinely with the macroscopic deformation. The affine model does not take into account the functionality of the crosslinking agent:

$$G_{af} = \nu RT = \frac{\rho}{M_x}RT \tag{2.47}$$

It can be seen that for high functionalities, the affine and the phantom model coincide. The phantom and affine limits of deformation are two extreme cases, and experimental stress-strain measurements suggest that low-molecular PDMS networks exhibit properties between these two limits. The network is predicted to be more affine-like at small deformations and more phantom-like at larger deformations. Contributions to the modulus from topological constraints along the contour of the polymer chains are not considered in the two above models, and these so-called entanglements contribute significantly to the elastic modulus when the molecular weight of the PDMS prepolymer is increased. Langley [35] and Graessley [36] developed a phenomenological model with an additional term introduced to allow for the contribution from entanglements. The result of the model can be expressed as:

$$G_{LG} = (\nu - h\mu)RT + G_o T_E \tag{2.48}$$

where h is an empirical parameter between 0 and 1, G_o is the plateau modulus of the melt of uncrosslinked, high molecular weight prepolymer, and T_E is the proportion of the maximum concentration of topological constraints that contribute to the modulus, the so-called trapping factor. This result indicates that with increased molecular weight of PDMS, a plateau is obtained:

$$G_{M\to\infty} = G_o T_E \tag{2.49}$$

The molecular entanglement weight M_E is determined from the equilibrium modulus of long, linear chains G_o as:

$$G_o = \frac{\rho}{M_e} RT \tag{2.50}$$

The time-dependence of soft materials is usually described in terms of the storage modulus $G'(\omega)$ and the loss modulus $G''(\omega)$, where ω is the frequency of the applied stress in oscillatory shear experiments. The time-dependent behavior of elastomers may be very complex. For the completely crosslinked rubber, the material behaves as an ideal spring, i.e. $G'(\omega)$=G and $G''(\omega)$=0, which means that the elastic modulus is constant and that there is no viscous dissipation in the material. However, real elastomers will always have some extent of viscous dissipation since ideal crosslinking is very hard to obtain. Very soft elastomers will in general have a storage modulus approaching the entanglement modulus of the corresponding linear polymer as given by Eq.(2.50). The time-dependent properties are often described by the so-called loss function:

$$\tan(\delta)(\omega) = \frac{G''(\omega)}{G'(\omega)} \tag{2.51}$$

When $\tan(\delta)$<1, the material is mainly elastic, and when $\tan(\delta)$>1 the material is mainly viscous at the given frequency. For certain applications it is favorable for the material to be viscous at a given frequency and to be elastic at another frequency e.g. in applications where conformability and stability are wanted. This can for example be obtained by choosing network reactants with certain chemical structures and lengths. There exist a variety of elastomers and common commercially available elastomers operating at room temperature include polyisoprenes (also known as synthetic rubber), silicones, polyurethanes, and polyacrylates. Within the different types of elastomers, one can obtain very different properties by adding side groups to the polymer, which influences the glass forming properties and the dynamics of the elastomer. Another way to alter the properties of elastomers is to swell the elastomer in a compatible solvent. This is an easy method to obtain fast-responding, soft materials.

Styrene-butadiene rubber (SBR) is the most important synthetic rubber and the most widely used rubber in the world. SBRs are obtained by the emulsion polymerization of butadiene and styrene in varying ratios. Unlike natural rubber, SBR does not crystallize upon stretching and therefore it has low tensile strength unless reinforced. The major use for SBR is in tires and tire products. Silicone elastomers possess extraordinary properties due to the special characteristics of the silicon oxygen bonds in their backbone. The silicon oxygen bond is much stronger than the carbon-carbon bond of organic polymers, which makes silicones better electric insulators and more resistant to oxidation. Furthermore, the silicon-oxygen chain is easily twisted, and the organic side groups can rotate freely around the bonds, which gives rise to very flexible materials even at room temperature. This can be visualized by each silicone molecule occupying its own space, preventing close contact with its neighbours and as a result, silicones have weak forces of attraction, low freezing points, and low surface tension. These properties have rendered silicones ideal for variety

of specialized uses where high tear strength is not required. Silicone elastomers retain their elasticity, strength and flexibility in temperatures ranging from approximately -60ºC to higher than 300ºC, which clearly makes silicone elastomers capable of working under extreme conditions. Speciality grades are even elastic down to -60ºC. Other elastomers such as isoprenes become brittle below room temperature and degrade or decomposite at elevated temperatures. Polyurethane (PU) networks find large applicability in a wide range of areas including e.g. medical devices, mattresses, and components to the automotive industry. PU elastomers are of interest because of their versatility and variety of properties and uses. They can be used as liquids or solids in a number of manufacturing methods.

A new trend in polymeric networks has emerged, namely the so-called interpenetrating networks (IPNs), where mixtures of two or more crosslinked networks are held physically together via entanglements. The combination of two dissimilar polymers provides a convenient route for the modification of properties to meet specific needs. The combination of varied chemical types of polymeric networks in different compositions, often resulting in controlled different morphologies, has produced IPNs with properties that show synergism between the two components. Plastic material may attain improved toughness with an elastomeric component as the minor phase and a reinforced elastomer may result if the phase proportions are reversed [37]. An example of IPNs is the poly(ether urethane)/poly(ethyl methacrylate) (PU/PEMA) system where Young's moduli in the range of 1 MPa (100% PUR) to 800 MPa (100% PEMA) were observed depending on the mixing ratio of the two components [38]. By altering the ratio of the two components one can also change the dynamic response of the elastomer since the two polymers will relax at two different frequencies due to the large difference in their glass transition temperatures, which is illustrated in Fig.3.1.

The vulcanization

The crosslinking reaction (also known as vulcanization) of polymers into elastomers can be performed in several ways. The traditional way of producing hard rubbers is radical vulcanization where the crosslinks are introduced randomly along the chain. However, if more controlled properties and soft materials are wanted, end-linked addition curing systems are favorable since the distance between crosslinks can be controlled and there are no byproducts. The distance between crosslinks can also be controlled in condensation curing systems such as OH-chemistry, but during the crosslinking water will be produced and side-reactions may occur. End-linked curing systems consist in general of a crosslinker with 3 or more reactive groups per chain (denoted functionality *f*, $f \geq 3$), a polymer with a reactive group positioned at both ends, and a catalyst. The properties of the resulting elastomer can furthermore be optimized by adding volatile or non-volatile solvent, chain extenders, resins or other polymers interfering either chemically or physically with the network [39].

In general, the reactants are all linear and during the vulcanization, the viscosity of the reaction mixture is increased. It is well-known that the zero-shear-rate viscosities of linear polymer melts depend on the molecular weight in a non-simple way. For molecular

weights below a critical molecular weight (M_c) there is linear dependency but for molecular weights above M_c, the scaling is stronger:

$$\eta_o(M,T) = K(T)M, \qquad M < M_c \tag{2.52}$$

$$\eta_o(M,T) = K(T)M^{3.4}, \qquad M > M_c \tag{2.53}$$

where $K(T)$ is a temperature dependent material constant. During the vulcanization, the viscosity of the reaction mixture will change dramatically, because the molecules grow longer and more branched and thereby one can get an idea of the degree of crosslinking. The viscosity and the elastic modulus are closely related, so one can follow the development of the elastic modulus as function of reaction time. The gelation point is defined as the time when there is a transition from mainly viscous to mainly elastic, i.e. when $G'(t)=G''(t)$ and it usually occurs at where the curve is steepest [40]. Elastomers below the gelation threshold may seem stable, but on longer timescales such as weeks they will flow, i.e. $G'(t\rightarrow\infty)=0$. For elastomers above the gelation threshold, the elastic modulus will reach a plateau on long timescales, i.e. $G'(t\rightarrow\infty)=G_o$. However, for most traditional networks the reaction time is not a real parameter. For certain silicone networks catalyzed by platinum catalyst, the vulcanization can be stopped by cooling down the reaction mixture and thereby inhibit the catalyst, which stops the network formation at a given time to give certain properties of the elastomer. However, the resulting elastomer can not be applied at elevated temperatures without the vulcanization proceeding further to the final harder elastomer. In the same way as with reaction time, the stoichiometry can be used to obtain networks below and above the gelation threshold. The stoichiometric imbalance is a more versatile parameter to optimize a material rather than the reaction time, and from the figure it is obvious that the stoichiometric imbalance has large influence on the properties of the elastomer. With the same reactants one can obtain elastomers ranging from extremely soft and fragile to hard and durable. Another issue is the stability of the material since for most applications it is important to have exceeded the gelation point such that the material is stable with time, i.e. $G(\omega\rightarrow 0)>0$. Systems just below the gelation threshold will usually behave as elastomers under normal usage but on long time scales such as several days or weeks, they will flow since the elasticity arises from entanglements between hyperbranched structures without the continuous three-dimensional structure and the material can therefore flow upon storage.

Swollen networks

One can obtain very favorable properties of elastomers by swelling, either before or after the vulcanization. The most applicable method is to mix the reactants with the swelling agent before the vulcanization process (pre-swelling) since swelling afterwards can cause uneven elastomers as a result of small imperfections within the initial 'dry' elastomer. However, it can be favorable to swell the cured elastomer since pre-swelling may lead to extra soft and fragile networks. This is due to the dilution of trapped entanglements, which is significant for pre-swelling [41]. When pre-swelling is applied, the two contributions to the elastic modulus scale with the volume fraction of polymer in the elastic network, ν, as:

$$G_c \sim \nu, \qquad G_E \sim \nu^n \tag{2.54}$$

Where n is a parameter with value $n \approx 2.4$ for well-entangled networks [42]. If swelling is performed after curing, one may expect:

$$G \sim G_c \sim G_E \sim \nu \tag{2.55}$$

Soft elastomers reacted from unstoichiometric reacting mixtures generally consist of a large fraction of so-called dangling material, i.e. material chemically attached to the network but which is not elastically active, except on short time-scales. This fraction will give rise to dynamics with a characteristic relaxation time which scales as:

$$\tau \sim \mathrm{e}^{k\nu M_d / M_E} \tag{2.56}$$

Here k is a constant and M_d is the average molar weight of dangling material. From this it is obvious that the swelling plays a tremendous role on the dynamics of the resulting swollen elastomer. The relaxation time of the elastically active network fraction is also decreased due to dynamic dilution effects [43] as well as the so-called strangulation or tight-mesh effect [44].

Another method to produce soft elastomers is to pre-swell the elastomer reactants by a volatile solvent and then remove the solvent after vulcanization. Thereby one has reduced the entanglement contribution [41]:

$$G = \frac{G_{c,o}}{\varphi} + \frac{G_{E,0}}{\varphi} = G_c + T_E G_0 \varphi^{n-1} \tag{2.57}$$

The dynamic properties will however be comparable to a traditional network without any swelling agent present during or after the vulcanization.

Processing

Elastomers can be processed in different ways. The processing may however interfere with the resulting properties, e.g. solvent casting leads to softer elastomers than obtained from coating the reaction mixture without any volatile solvent present. This is due to the reduction in the concentration of physical entanglements in the elastomer when volatile solvent is present [41]. Furthermore the mixing process may influence the elastic modulus of the network since it introduces local or over-all alignment of the molecules. From this, it is clear that the processing of the elastomers influences the properties of the elastomer, and it can therefore be used as a parameter to optimize the material.

Environmental Considerations

An actuator must maintain acceptable performance over the range of environmental conditions it might encounter. In most cases, the environmental conditions of interest are temperature and humidity. In some other applications, such as usage in space, factors such as radiation (e.g., solar), outgassing, and chemical compatibility may be important.

Dielectric elastomers such as acrylics and silicones have not yet been rigorously tested for performance and lifetime over a range of temperatures and humidities, although some studies have been performed. Further, projections can be based on knowledge of the basic physical phenomena. The physical basis of the electromechanical response of dielectric elastomers is electrostatics. Electrostatic forces do not themselves vary with temperature or

other environmental factors, so that one can focus on the mechanical and electrical properties of dielectric elastomers in estimating their environmental tolerance. If these properties are not themselves adversely affected by environmental conditions, then the actuator itself will not be affected.

Silicones are intriguing because they not only exhibit good performance, but also exhibit stable mechanical properties over a fairly wide range of temperatures. For example, one silicone (CF19-2186, NuSil Corporation, Carpinteria, California) has been shown to have similar performance over a temperature range of –65 ºC to 240 ºC [45]. While we do not expect the material to sustain its maximum performance over such a temperature range, we do expect that acceptable performance can be sustained over the range of temperatures seen in many applications. Another silicone rubber was shown to be capable of operation at temperatures below –100 °C [45].

Silicones are also known to have low rates of moisture absorption, so changes in humidity should not affect performance significantly.

Acrylic dielectric elastomer does not have as large a temperature range as the silicones. They have been shown to operate over a range of –10 °C to 80 °C, enough for many applications.

To some extent, it is possible to select a dielectric elastomer material with a desired temperature range. For example, if high-temperature operation is important, one would likely select a silicone rather than an acrylic.

While normal atmospheric variations in the humidity are not expected to greatly affect the performance of some dielectric elastomer materials, except for polyurethanes [46], long-term immersion might require coatings of moisture-proof materials. It is of course critical that the actuator be designed so that moisture cannot create a short circuit across the electrodes. Since the electrodes are exposed to high voltage, even a small amount of moisture could create a short.

2.3.1.5 Silicones

History

Silicones are defined as polymers comprising alternate silicon and oxygen atoms in which the silicon atoms are joined to organic groups [47]. The following types of structures come within this definition:

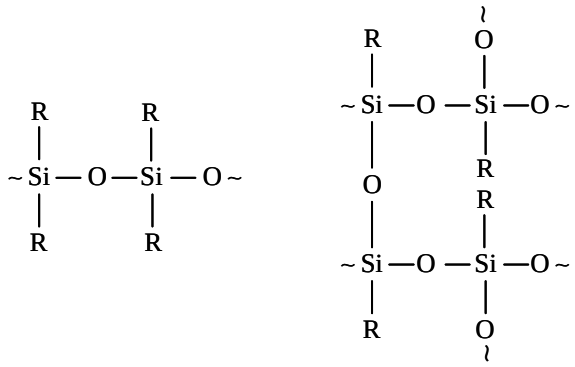

Figure 2.6. Typical linear (left) and network (right) silicone structure.

and both linear and network silicones find technological use. It is convenient to classify the silicones which are of commercial interest into three groups, namely fluids, elastomers and resins, but only elastomers will be treated here.

The possibility of the existence of organaosilicon compounds was first noted in 1840 by Dumas. In 1863, Friedel and Craft prepared the first organosilicon compound, tetraethylsilane, by the reaction of diethylzinc with silicon tetrachloride:

$$2Zn(C_2H_5)_2 + SiCl_4 \rightarrow Si(C_2H_5)_4 + 2ZnCl_2$$

Nevetheless, it is generally agreed that the foundation of organosilicon chemistry were reallay laid by Kipping (University College, Nottingham, UK) during the period 1899-1944. however, his investigations were concerned almost exclusively with non-polymeric compounds and it is unlikely that Kipping foresaw any commercial application of his work. Indeed, the resinous materials which were frequently encountered were regarded merely as troublesome. Commercial interest in silicon polymers developed in the 1930s during searches for heat-resistant electrical insulating materials. Research was carried out by the Corning Glass Works (USA) and the General Electric Co. (USA) end silicone resins were developed. It also became evident that these polymers had potential use in many other fields. The manufacture of silicones was started by Dow Corning Corp. (USA) in 1943 and by the General Electric Co. (USA) in 1946.

Elastomeric silicones.

Chemistry. In particular, silicone elastomers are based on linear polymers which are analogous to the fluids but which have higher molecular weight. As with other elastomeric materials, it is necessary to cross-link the linear polymers in order to obtain characteristic elastic properties. General purpose elastomers are based on polydimethylsiloxanes but special purpose materials which contain a small proportion of groups other than methyl are also available. These various products are vinyl silicone elastomers, phenyl silicone elastomers, nitrile silicone elastomers, fluorosilicone elastomers, room temperature

vulcanizing (RTV) silicone elastomers and borosilicones. For this PhD activity a RTV silicone elastomer was used.

Like other types of silicone elastomers, RTV are based essentially on polydimethylsiloxanes. Their distinguishing feature is that the siloxane chains of the basic gums are terminated by silanol groups which are reactive and readily participate in cross-linking reactions. Also, the gums generally have molecular weights in the range 10^4-10^5, which is much lower than that used for heat-cured materials. In fact, the lowest molecular weight polymers are free-flowing liquids which can be fabricated by casting techniques. Low molecular weight, hydroxyl-terminated polydimethylsiloxanes may be prepared by hydrolysing dimethyldichlorosilane in the presence of small quantities of a base, e.g. calcium carbonate. The base is added continuously and neutralizes the hydrochloric acid formed and thus protects the silanol groups from further condensation. The gums may be converted to rubber-like products by reaction with an alkoxysilane such as a tetralkoxysilane, trialkoxysilane or polyalkoxysiloxane. By a suitable choice of catalyst, cure may be effected at room temperature in times ranging form 10 minutes to 24 hours; stannous octoate and dibutyltin dilaurate are particurarly satisfactory. The reactions which take place with tetraethoxysilane illustrate the cross-linking process:

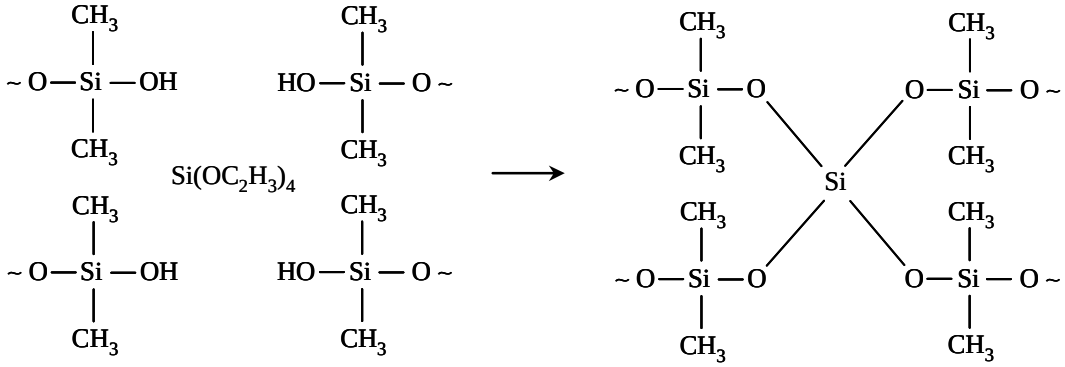

Figure 2.7. Tetraethoxysilane formation.

Alternatively, the silanol-terminated gums may be cured by the use of polysiloxane containing silanic hydrogen:

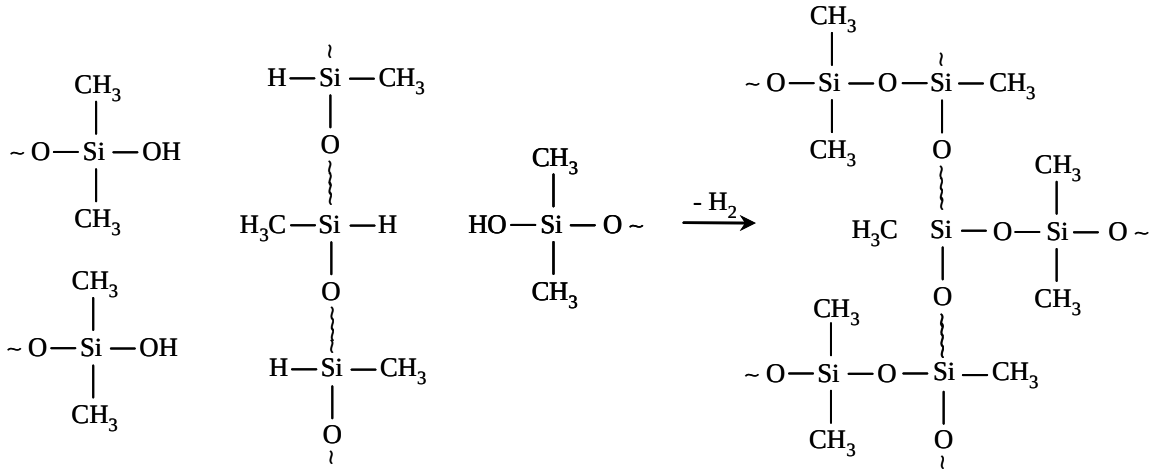

Figure 2.8. Cure in the presence of polysiloxane containing silanic hydrogen.

This reaction also take place in the presence of metallic salt catalyst. The products obtained in this way have good strength but since hydrogen is evolved during cure this type of system is generally used for treatment of substrates such as paper, where only thin films are involved.

The RTV elastomers described above are 'two-pack' systems, i.e. they are supplied as two separate components which must be mixed together prior to use. The first part contains the silanol-terminated gum and the second part contains the catalyst; the cross-linking agent may be present in either part.

General properties. The outstanding property of silicones in their thermal stability. In general, the polymers can be hated in air to about 200°C without appreciable change in properties. This stability is attributable to the relatively high bond strengths found in the polymers.

Bond	**Bond Energy (kJ/mol)**
Si-O	444
C-H	414
C-O	360
C-C	348
Si-C	318
Si-H	318
Si-Si	222

Table 2.3. Bond energies of various carbon and silicon bonds.

It is interesting to note that, in contrast to carbon, the ability of silicon to form catenated compounds is limited, although a few high molecular weight polysilanes have been prepared [48]. The low energy of the Si-Si bond indicated that such chains are less thermodynamically stable than the corresponding carbon chains.

Although the Si-O bond has good thermal stability, its relatively high ionic character (51%) renders it easily cleaved by strong acids and bases (as in equilibration reactions).

The presence of electropositive silicon atoms in the main chain might be expected to lead to dipole interactions with neighbouring chains, resulting in brittle, glass-like behaviour. However, the unusually large Si-O-Si bond angle permits very free rotation about the Si-O bond and the organic substituents occupy a large effective volume. Thus close packing is not possible and chain interactions are diminished. A further characteristic property of all silicones, fundamental for dielectric applications, is that they are water repellent due to the sheath of hydrophobic organic substituents which encases the polymer backbone. Related to this property is the 'non-stick' behaviour of silicone surfaces.

The mechanical properties of silicone elastomers at room temperature are inferior to those of other elastomers. For example, natural rubber vulcanizates normally has tensile strength in the range 21-28 MPa whilst the corresponding range for general purpose heat-cured silicones is only 3,5-7,0 MPa (room temperature-cured material is usually inferior). This low strength results form the small intermolecular attraction between silicone chains and from the highly coiled nature of the chain entanglement. However, the mechanical

properties of silicone elastomers at elevated temperatures are greatly superior to those of other elastomers (except fluoro elastomers).

Silicone elastomers have good electrical insulating properties, especially if the decomposition products of the vulcanizing agent are removed by heating the vulcanizate after cure. Silicone elastomers are unaffected by oxygen and ozone on natural ageing and, because of their water repellency, are not seriously affected by aqueous solutions of most chemical reagents. They are attacked by strong acids and alkalis. General purpose elastomers are swollen by aliphatic, aromatic and chlorinated hydrocarbons but much improved resistance is shown by nitrile- and fluorine-containing silicones. In general, room temperature cured materials have lower solvent resistance.

Electromechanical applications. In the last decades silicone elastomers have found applications in some field of robotics and electronics as electromechanical actuators (ved. Cap 1). The best overall results till now, in terms of achievable strains, have been obtained with silicone rubber films (based on a polydimethyl siloxane backbone) and an acrylate elastomer, specifically that of the 3M Company (St. Paul, Minnesota, USA) VHB acrylic series.

The tables at the end of the chapter summarize the measured performance of the best silicones and acrylics.

During the last decades, from the discovery of the DEAs on, improvements have been made thanks to the discovery of new materials and improved electrodes. Nevertheless, much of the improvement in material performance is due to the discovery of the importance of prestrain, that is, the initial strain loading condition. The introduction of a high amount of prestrain (produced by stretching and holding the film in tension before measurements are made) can significantly increase the maximum strain and pressures that can be generated within a given film [49]. Per Eq.(2.23), the maximum pressure depends on the square of the applied electric field.

In acrylic, the effect of prestrian on breakdown strength is even more dramatic. From no prestrain to a biaxial prestrain of 500% $\times$ 500%, the practical breakdown field in dielectric elastomers increased by almost 10 times [50].

It should be noted that the stretch need not be uniform in both in-plane directions. In the latter case, the film tends to actuate primarily in the direction with lower strain. The principal reason for this observed effect is due to the increase in the local elastic modulus of the material in the direction of the higher prestrain. The film would tend to deform more in the softer, less prestrained direction. Geometric edge constraints can also produce strains almost exclusively in one direction. For example, if the actuation area is a thin line that spans the width of the rigid frame, then the in-plane strain will be produced almost exclusively in the transverse in-plane direction (orthogonal to the long direction of the line), provided that the actuated stress does not exceed the prestrain stress in the width direction. When such a geometric constraint is combined with anisotropic prestrain, extremely large strains in a single direction have been observed.

Dynamic Response. Although, as Tab.2.4 indicates, both silicones and acrylics have demonstrated response at high frequencies, the dynamic response of silicones and acrylics

can differ greatly. It is therefore worth looking more closely at dynamic response issues. This discussion is adapted from [51].

The overall efficiency of an actuator is affected by the electrical and mechanical losses within the material as well as losses in the electric driver circuitry. These losses in the drive circuitry reflect, to some extent, the ability of the actuator to convert a high percentage of the applied electrical energy to mechanical work and thus depend on the fundamental properties of the actuator. The efficiency of silicone-based elastomers is related to the electrical and mechanical loss factors, δ_e and δ_m, respectively, as

$$\eta_e = 1 /(1 + \pi\tan\delta_e) , \quad \eta_m = 1 /(1 + \pi\tan\delta_m) \tag{2.58}$$

It appears that the mechanical losses dominate the electrical losses, although more data are needed to measure the electrical dissipation factor at low frequencies. At low frequencies, the leakage of charge across the polymer film can dominate the electrical losses. In such cases the electrical efficiency may be approximated by

$$\eta_e = 1 /(1+Y / 2 ((\varepsilon_r \varepsilon_o E)^2 \rho f)) \tag{2.59}$$

where ρ is the bulk resistivity of the polymer and f is the frequency in hertz. That the electrical efficiency is dependent on frequency is not surprising. The relative amount of energy lost from electrical leakage increases with the amount of time that the voltage is applied across the electrodes during an actuation cycle.

The efficiency of the electric driver circuit can be included in the overall efficiency by consideration of the electromechanical coupling efficiency k^2. (The square of k is used for consistency with the conventional nomenclature for piezoelectrics.) The electromechanical coupling factor is defined as follows:

k^2 = energy converted into mechanical work per cycle/electrical energy applied per cycle

Materials with low coupling efficiencies are difficult to operate efficiently even if there is no intrinsic energy loss mechanism (low electrical and mechanical loss factors), because low coupling requires a large amount of electrical energy to be removed or recovered from the actuator relative to the work output. Even with high-efficiency (e.g., 90% efficient) recovery circuits, if the coupling is too low, too much energy is lost in the recovery electronics, relative to the work output per cycle.

Coupling efficiency is often difficult to measure directly, but we can use the electrostatic model (in which the permittivity of the material does not change) to estimate the dielectric elastomer coupling efficiency, based on the capacitance change for the given strain (assuming no losses). This analysis, given by [52], yields

$$k^2 = - 2 s_z - s_z^2 \tag{2.60}$$

The efficiency of the actuator, based on the coupling factor and the efficiency of the electric driver circuit in recovering charge, is

$$\eta_d = k^2 / [1- \eta_{\text{rec}}(1- k^2)] , \tag{2.61}$$

where η_{rec} is the efficiency of the driver circuit. Note that if no charge recovery is used ($\eta_{\text{rec}} = 0$), the maximum efficiency of the actuator is $\eta_d = k^2$.

(The mechanical and electrical losses usually are included in k^2, that is, multiply k^2 of Eq.(2.61) by η_e η_m; however, in order to isolate the effect of energy recovery, we have treated them separately.)
The overall efficiency is

$$\eta_t = \eta_e \eta_m \eta_d \tag{2.62}$$

Typical estimated efficiencies of the best dielectric elastomer materials are shown in Tab.2.6.
The overall efficiency, based on Eq.(2.62), assumes 90% energy recovery and uses the average values for electrical and mechanical issues. Note that the coupling efficiencies are given under conditions of maximum strain and are likely to be greater than the efficiencies produced in practical actuators. Nonetheless, the overall efficiencies are competitive with or better than those of other field-activated materials.
The speed of response cannot easily be calculated from the measurable material properties because many different factors come into play, including the actuator size and configuration as well as the driving electronics. Nonetheless, some simple observations and calculations can provide rough estimates. We also present some simple direct measurements of the speed of response.
We first note that the electromechanical response is produced by the electrostatic forces on the electrodes, so no significant delay should be associated with an intrinsic response mechanism of the polymer. This assumption is supported by the fact that the dielectric constant of the materials does not change appreciably over the range of 100 Hz to 100 kHz. The fundamental limitation in response speed would then be due to the speed at which the pressure wave can propagate through the material (basically the speed of sound). Since the individual polymer layers are thin, this propagation time can be less than a millionth of a second. More typically, the limitation on the speed of response is due to the mechanical resonance of the actuator and driven load.
Other response speed limitations arise from the RC time constant of the actuator. Typical surface resistivities of our electrodes are on the order of tens to hundreds to thousands of ohms, so the RC time constant need not be a limiting factor for most small devices. For example, a 10 cm^2 area of silicone film that is 50 μm thick could achieve a 1 kHz response bandwidth with electrodes whose surface resistivities exceed 10^5 Ω. The speed of response, based on the RC time constant, is size dependent (the capacitance scales with the film area). However, the individual electrodes could be comprised of many individual film areas that are electrically connected in parallel, so as to effectively reduce the surface resistivity of the individual electrodes. For example, electrically connecting in parallel the electrodes of many individual film layers of a multilayer actuator would have this effect. However, this approach could also be used on individual electrodes: thin higher conductivity traces could be used to distribute charge over the surface of an electrode and thereby reduce the effective resistance. This “structured electrode” approach is described in more detail by Kornbluh et al. [52]. Since the RC time constant can be manipulated by the actuator design, it is not a fundamental limitation on the speed of response of the technology.

The silicone produced an essentially flat strain response up to about 400 Hz, with a resonance peak at about 1425 Hz. The response rolls off above this resonance point, as would be expected with the introduction of higher modes. The observed resonant peak corresponds closely to that predicted from the fundamental resonance of the in-plane strain response, based on a simplified lumped parameter model (where we have assumed that the characteristic length is equal to the diameter of the circular area and the driven load of inactive material that has a mass equal to half that of the active material).
This correspondence suggests that mechanical resonance of the system due to the elasticity and mass (density) of the material is indeed the limiting factor in response speed. The results also suggest that the elastic modulus and loss factor do not increase significantly at frequencies up to 3 or 4 kHz, which in turn suggests that we can maintain good efficiency at frequencies up to this limit.
In addition to the higher frequency effects discussed above, dielectric elastomer materials are subject to creep or stress relaxation.
Creep and stress relaxation is known to be particularly small in silicones (for an elastomer). Fortunately, many actuator designs, such as those that use push-pull or antagonistic pairs configurations can minimize creep.

2.3.1.6 Polyurethanes

History

Polyurethanes are defined as polymers which contain urethane groups (-NH-CO-O-) in the main polymer chain [47]. However, it is to be noted that in technologically useful polymers of this type the urethane group is not usually the principal group present; other groups such as ester, ether, amide and urea groups are generally contained in the polymer chain in appreciable number.
Several kinds of polyurethanes are of commercial significance and are conveniently classified into the following major types – flexible foams; rigid foams; integral foams; elastomers; surface coatings; and adhesives. In this chapter only elastomers and flexible foams will be treated as used during the PhD activity.
The commercial development of polyurethanes dates from 1937 when O. Bayer (I. G. Farbenindustrie and later Farbenfabriken Bayer, Germany) found that reaction of diisocyanates and glycols gave polyurethanes with properties which made them of interest as plastics and fibres. Further intensive research into polyurethanes soon indicated that the materials showed promise as adhesives, rigid foams and surface coatings. These various applications reached moderate commercial importance in Germany during the second World War, but were not recognized elsewhere at this time. After the war, Allied intelligence teams reported on these activities and interest in polyurethanes was established in the UK and USA although commercial development was slow. Bayer again became active in the polyurethane field and developed elastomers (1950) and flexible foams (1952).

Chemistry

The urethane group results form the interaction of an isocyanate and a hydroxyl compound:

$$R - NCO + HO - R` \rightarrow R - NH - CO - O - R`$$

It will be apparent that this reaction leads to polyurethanes when multifunctional reactants are used. When a diisocyanate and a diol react together a linear polyurethane is obtained whilst a diisocyanate and a polyhydric compound (polyol) lead to a cross-linked polymer. A cross-linked polyurethane could also be derived form a compound containing three or more isocyanate groups and a diol but this approach is of limited commercial importance.

Thus diisocyanates and diols and polyols are the principal raw materials used in the manufacture of polyurethanes.

Chain extenders (functionality=2) and cross linkers (functionality=3 or greater) are low molecular weight hydroxyl and amine terminated compounds that play an important role in the polymer morphology of polyurethane fibres, elastomers, adhesives, and certain integral skin and microcellular foams. The elastomeric properties of these materials are derived from the phase separation of the hard and soft copolymer segments of the polymer, such that the urethane hard segment domains serve as cross-links between the amorphous polyether (or polyester) soft segment domains. This phase separation occurs because the mainly non-polar, low melting soft segments are incompatible with the polar, high melting hard segments. The soft segments, which are formed from high molecular weight polyols, are mobile and are normally present in coiled formation, while the hard segments, which are formed from the isocyanate and chain extenders, are stiff and immobile. Because the hard segments are covalently coupled to the soft segments, they inhibit plastic flow of the polymer chains, thus creating elastomeric resiliency. Upon mechanical deformation, a portion of the soft segments are stressed by uncoiling, and the hard segments become aligned in the stress direction. This reorientation of the hard segments and consequent powerful hydrogen bonding contributes to high tensile strength, elongation, and tear resistance values [53, 54, 55, 56, 57], The choice of chain extender also determines flexural, heat, and chemical resistance properties. The most important chain extenders are ethylene glycol, 1,4-butanediol (1,4-BDO or BDO), 1,6-hexanediol, cyclohexane dimethanol and hydroquinone bis(2-hydroxyethyl) ether (HQEE). All of these glycols form polyurethanes that phase separate well and form well defined hard segment domains, and are melt processable.

Cast elastomers.

Solid polyurethanes elastomers, as distinct form flexible foams, may be divided into three categories, namely cast, millable and thermoplastic elastomers. Here, as used in the PhD activity, only cast elastomers will be treated.

In the casting technique a liquid reaction mixture comprising low molecular weight material is poured into a heated mould, wherein the material is converted to a solid, high molecular weight elastomeric product.

The most obvious method of preparing polyurethane elastomers of this type is to cast a mixture of diisocyanate and slightly branched polyester or polyether. In a typical process, a

mixture of the polyester and isocyanate is degassed by heating at 70°C under reduced pressure. The mixture is then poured into a cylindrical mould (in which a roller spindle is located) and heated at 110°C for 2-3 hours. Although elastomers of this type possess properties (such as resilience and solvent resistance) they are characterized by rather poor mechanical strength which restricts wider utilization. The reason for this inferiority is probably because the branch units in the polyester restrict intermolecular attraction. This limitation is overcome when the elastomer is cast from a mixture consisting of a linear polyester or polyether, diisocyanate and glycol or diamine. The product is a pre-polymer which is, in effect, a mixture of isocyanate-terminated polymer and unreacted diisocyanate. The pre-polymer is then mixed with either a glycol (e.g. 1,4-butanediol or 1,6-hexanediol) or diamine (which is usually a deactivated amine such as 3,3'-dichloro-4,4'-diaminodiphenylmethane (MOCA)). The mixture is poured into a heated mould where it quickly sets. After about 30 mins the casting is removed from the mould and cured at about 110°C for 24 hours.

The reactions which occur when a glycol is used in the above operations are not fully understood, but it is thought that firstly the glycol reacts with the isocyanate-terminated pre-polymer to give an extended polymer containing glycol-urethane links. The amount of glycol used is slightly less than that required to react with all the isocyanate groups in the prepolymer and so the extended polymer is isocyanate terminated.

The chemical properties of cast polyurethane elastomers are similar to those of flexible foams . of particular importance is the outstanding resistance to aliphatic hydrocarbon fuels and oils and to oxygen and ozone. Aromatic and chlorinated solvents cause some swelling.

Foams. Polyurethane foams are produced by forming a polyurethane polymer con-currently with a gas evolution process. Provided these two processes are balanced, bubbles of gas are trapped in the polymer matrix as it is formed and a cellular product results. The matching of the two reactions is essential for the formation of satisfactory foams. If the evolutions of gas is too rapid, the foam initially rises well but then collapses because polymerization has not proceeded sufficiently to give a matrix string enough to retain the gas. If polymerization is too fast, the foam does not rise adequately.

By selection of appropriate reactants, it is possible to prepare foams of varying degrees of cross-linking. Slightly cross-linked products are flexible whilst highly cross-linked products are rigid. Both flexible and rigid poly-urethane foams are of commercial importance.

The gas used in the production of flexible foams is usually carbon dioxide formed by the interaction of isocyanate and water. In a system containing a diisocyanate, a polyol and water, two principal reactions proceed simultaneously, namely:

diisocyanate + polyol = polyurethane
diisocyanate + water = carbon dioxide

as indicated above, a satisfactory foam is obtained only if these two reactions are in step. Although choice of temperature and reactant permit a measure of control over the reactions, much broader control may be exercised through the use of catalysts.

Tolylene is usually the preferred isocyanate for the productionb of flexible polyurethane foams. As previously mentioned, flexible foams are based either on polyester or polyethers; polyether foams account for about 90% of current flexible foam output.
Flexible polyurethane foams are open-cell structures which are usually produced with densities in the range 24-48 kg/m^3. Flexible polyurethane foams have good dry heat stability, withstanding temperatures up to 150°C for long periods without serious loss of strength. Above this temperature the formation of biuret and allophanate cross-links is reversed and there is a reduction in load bearing properties.

Bending. Similarly to Ionic Polymer-Metal Composites (IPMCs), polyurethanes are able to bend under the application of an external electric field [58]. Bending electrostriction was reported by Kawai in 1967 and 1970 [59, 60]. He reported that a polyurethane film would bend by applying an electric field and its deformation was proportional to the square of the electric field. However, the mechanism leading to bending are not yet well understood and the details remains uncertain. In their recent papers, Watanabe *et al*. [61] reported that the bending deformation might result from an asymmetric distribution of space charge formed by a space-charge-limited current. However this may not be the complete story because the bending disappears quickly once the applied field is removed, while the space charge distribution an only evolve more slowly. There has not been any theoretical model that satisfactorily explains the mechanism of bending electrostriction of the polyurethane film in a quantitative way.
After the first publications on the arguments, several attempts have been done in order to use this particular behaviour of polyurethanes to develop actuator with enhanced bending performance, adding for example salts to the matrix [61], or studying the hysteresis effect of actuators used in frequency-driven devices. In particular Watanabe in 2000 [62] demonstrated that the ionic polarization formed by a prior electric-field application influences the next bending electrostriction, but the relation correlating the direction of the bending and the polarity of the electric wave has not been clarified yet.
During my PhD activity, analysis of elongation in polyurethane and polyurethane-silicone blends were carried on and the bending phenomenon was experienced. Results in merit are presented in Ch.4.

2.3.1.7 Comparing performances of dielectric elastomer actuators

One of the more useful metrics for comparing actuator materials, independent of size, is the energy density of the material. The actuator energy density is the maximum mechanical energy output per cycle and per unit volume of material. While the actual energy output of the material depends on the loading condition, the case where the actuator does no external work is often used to compare different materials without regard to loading conditions. In this case, the energy is actually the internal elastic energy of deformation. For small strains with free boundary conditions and no load, the actuator energy density e_a of the material can be written as

$$e_a = Y s_z^2 = (\varepsilon\varepsilon_o)^2 (V/z)^4/Y \qquad (2.63)$$

Conventionally, the elastic energy density $e_e = ½ Y s_z^2$ is often used. However, for large strains with a linear stress-strain relation, this formula must be modified because as the thickness strain becomes increasingly negative, the film flattens out and the area over which the pressure must be applied increases. A more detailed derivation for large strains gives the formula for the elastic energy density of materials with a linear stress-strain relation as

$$e_e = Y [(s_z - \ln(1+ s_z)] \tag{2.64}$$

This equation agrees with the more common formula at small strains but is significantly higher for strains greater than 20%.

The validity of the electrostatic model and the above equations has been well established (e.g., [63]). It can be clearly seen from the equations that dielectric elastomer performance depends on the macroscopic permittivity of the polymer as well as on its modulus of elasticity. Further, it is clear that it is desirable to have a high electrical breakdown strength in order for the response to be as large as possible.

Beyond these fundamental guidelines for quasistatic operation, there are several other material features that might be optimized for improved dynamic response. These features include

- high bulk resistance and low electrical loss factor for high efficiency,
- low viscoelastic damping for high efficiency,
- good electrical fatigue properties for high durability, and
- good mechanical fatigue properties and low creep.

There are also several features that are of practical consideration in selecting a material for ease of fabrication and a given application:

- good tolerance to temperature and humidity
- ease of processing into thin uniform films with few defects for manufacturability and high yield

As the number of researchers working on dielectric elastomers increase, so too does the variety of polymers under consideration. Tab.2.4, adapted from [63], shows the performance of a variety of polymers using the circular actuation test. This table is not exhaustive nor does it reflect the greatest performance achieved with each class of polymer. However, it does serve to show that good response was achieved with a variety of polymers and also shows why much early work has focused on silicones. It will also be obvious by reviewing this table why acrylics were to become of great interest.

Polymer (Specific Type)	**Elastic Energy Density** [J/cm^3]	**Pressure** [MPa]	**Strain [%]**	**Young's Modulus*** [MPa]	**Electric Field** [V/mm]	**Dielectric Constant** [@1 kHz]	**Coupling Efficiency,** k^2 [%]
Silicone Nusil CF19-2186	0.15	0.72	32	1.0	235	2.8	54
Silicone Dow Corning HS3 (centrifuged to remove particulates)	0.038	0.13	41	0.125	72	2.8	65
Polyurethane Deerfield PT6100S	0.20	3.8	11	17	160	7.0	21
Silicone Dow Corning Sylgard 186	0.10	0.50	32	0.7	144	2.8	54
Fluorosilicone Dow Corning 730 (centrifuged to remove particulates)	0.051	0.29	28	0.5	80	6.9	48
Fluoroelastomer LaurenL143HC	0.016	0.39	8	2.5	32	12.7	15
Polybutadiene Aldrich PBD	0.025	0.41	12	1.7	76	4.0	22
Isoprene Natural Rubber Latex	0.010	0.19	11	0.85	67	2.7	21

*Average engineering modulus at the maximum strain.

Table 2.4. Maximum response of representative elastomers in early research by SRI International.

Parameter	**Acrylics**	**Silicones**	**Comment**
Maximum actuation strain (%)	380	120	Strain in generator and sensing modes can be greater than that in actuation
Maximum actuation pressure (MPa)	8.2	3.0	Blocked stress
Maximum specific energy density in actuation (MJ/m^3)	3.4	0.75	Greatest energy density of all field-activated materials; can theoretically be greater in generator mode
Maximum frequency response (Hz)	> 50,000	> 50,000	Small-strain acoustic measurements; frequency response is very dependent on strain and size; full response of acrylic is generally much lower, due to viscoelasticity (see mechanical loss factor below)
Maximum electric field (MV/m)	440	350	Maximum fields are realizable only in uniform films with few defects
Relative dielectric constant	4.5 – 4.8	2.5 – 3.0	Measured at 1 kHz; small drop-off at higher frequencies
Dielectric loss factor	0.005	< 0.005	Measured at 1 kHz
Elastic modulus (MPa)	0.1 – 3.0	0.1 – 2.0	Elastic modulus is typically nonlinear with respect to strain; these values are averages over a typical range of strain
Mechanical loss factor	0.18	0.05	Loss factor of acrylics varies with strain and other conditions
Maximum electromechanical coupling, k^2	0.9	0.8	Similar to that of the best field-activated materials such as single-crystal piezoelectric ceramics
Maximum overall efficiency (%)	> 80	> 80	Assumes ideal driving electronics; the efficiency depends on the actuation frequency
Durability (cycles)	> 10,000,000	> 10,000,000	Durability is highly dependent on how close the driving voltage is to the maximum field
Operating range (°C)	–10 to 90	–100 to 260	Short-term range; long-term range has yet to be determined

Table 2.5. Performance of best silicones and acrylics.

Material	**Effective Modulus** [MPa]	**Relative Dielectric Constant**	**Dielectric Loss Factor tan d_e**	**Mechanical Loss Factor tan d_m**	**Electro-mechanical Coupling Factor, k^2** [%]	**Overall Maximum Efficiency h_t** [%]
Dow Corning HS3 silicone (centrifuged)	0.1	2.8 at 1 kHz	0.005 at 1 kHz	0.05 at 80 Hz	79	82 at 80 Hz
NuSil CF19-2186 silicone	1.0	2.8 at 1 kHz	0.005 at 1 kHz	0.05 at 80 Hz	63	79 at 80 Hz
3M VHB 4910 acrylic	3.0	4.8 at 1 kHz	<0.005 at 1 kHz	0.18 at 20 Hz	90	80 at 20 Hz

Table 2.6. Efficiency-related characteristics of dielectric elastomer films.

2.3.2 Piezoelectric polymers

Similar to piezoelectric ceramics described in §2.2.1, piezoelectric polymers also exist, showing electric voltage generation if subjected to an external strain and *viceversa*. The electromechanical response, in this class of polymers, is linear, such as in typical piezoelectric ceramics but, in comparison with the responses in inorganic materials, the electromechanical activity in these polymers is relatively low. For a physical and mathematical description of the processes involved please refer to §2.2.1.1 and §2.2.1.2.
Piezoelectric polymers in general, that represent a subclass of ferroelectric polymers, are polymers possessing spontaneous polarization that can be reoriented between possible equilibrium directions by realizable electric field [12]. They can be in a single crystal form or a semicrystalline form in which the ferroelectric crystallites are embedded in an amorphous matrix. Examples of piezoelectric polymers include poly(vinyl fluoride) (PVF), poly(vinylidene fluoride) (PVDF), copolymers of PVDF with trifluoroethylene (TrFE) and odd-numbered nylons.

2.3.2.1 Poly(vinylidene fluoride) (PVDF)

Poly(vinylidene fluoride) (PVDF) exhibits a variety of characteristic mechanical and electrical properties, such as piezoelectricity, pyroelectricity, non-linear optical properties etc. It has a very simple chemical formula, $-CH_2-CF_2-$, intermediate between polyethylene and polytetrafluoroethylene. This simplicity of chemical structure gives both high flexibility and some stereochemical constraint to the main chain of PVDF. Because of these structural characteristics, therefore, PVDF takes many types of molecular and crystal structures, which change depending on the preparation conditions of the sample. Is has at least four major crystalline phases (α, β, γ, δ), two of them, the α-phase and the β-phase are the most relevant phases for practical applications. In β-phase two chains in an all-*trans* planar zigzag conformation are packed into individual orthorhombic unit cells. In this conformation the fluorine atoms are positioned on one side of the unit cell, resulting in a net dipole moment. The β-phase is quite polar, having a net dipole of 2,1 D (debye) and, being it noncentrosymmetric,it is responsible for the PVDF piezoelectricity.
In the α-phase the chain conformations are represented as a sequence of alternating trans and gauche sequences. Each unit cell containing two chains in orthorhombic and adjacent chains are packed such that the dipole moments of the individual carbon-fluorine bonds are

aligned perpendicular to the chain direction, cancelling one other out. The directions of the chains consists of a statistical average of up-up and up-down orientations. When prepared using the melt crystallization or solution cast, in most cases PVDF will form the α-phase, which is a non polar phase. Mechanical stretching is often used in order to convert the α-phase to the piezoelectric β-phase. On the other hand, for P(VDF-TrFE) copolymers with VDF content less than approximately 85 mol%, the β-phase will be formed directly.

In the β-phase crystallites there are ferroelectric domains, which are polar but nonetheless oriented in all crystallographycally allowed directions. This accounts for the absence of any piezoelectric activity. To be made piezoelectric, the domains must be oriented in a strong electric field called “poling field”.

As described in Ch.4 and 5, PVDF used during the PhD activity was a commercial polarized product, thus, piezoelectric.

2.4 References

[1] Moulson A. J. *et al*., Electroceramics, materials, properties and applications, Whiley, London, 1990
[2] Bar-Cohen Y., in Handbook on Biomimetics, Yoshihito Osada Ed., Chapter 8, NTS Inc., 2000
[3] Popielarz R., *Macromolecules*, 34, 5910-591, 2001
[4] Lippman G., *Annales de chimie et de physique*, 24, 1, 45, 1881
[5] Gautschi G., Piezoelectric Sensorics: Force, Strain, Pressure, Acceleration and Acoustic Emission Sensors, Materials and Amplifiers, Springer, 2002
[6] Standard on Piezoeletricity, ANSI/IEEE, 1987
[7] http://electrochem.cwru.edu/encycl
[8] Finkenstadt V. L., *Applied Microbiology and Biotechnology*, 67, 6, 735-745, 2005
[9] Eftekhari A., *Chemistry of Materials*, 22, 2689, 2010
[10] Carpi F. *et al*, Dielectric elastomers as electromechanical transducers, Elsevier, 2008
[11] Zhang, Q. *et al*., in Electroactive Polymers (EAPs) Actuators as Artificial Muscles Reality, Potential and Challenges, 1st ed, Chapter 4, Y. SPIE Press, 2001
[12] Bar-Cohen J., Electroactive Polymer (EAP) Actuators as Artificial Muscles, Reality, Potentiality and Challenges, SPIE Press
[13] Kinase W. *et al*., *Journal of the Physical Society of Japan*, 10, 942, 1955 1955
[14] Shkel Y. M. *et al*., *Journal of Applied Phys*ics, 83, 415, 1998
[15] Landau L. D. *et al*., Electrodynamics of Continuous Media, Pergamons, Oxford, 1970
[16] Kloos G., *Journal of Physics D*, 28, 939, 1995
[17] Stark K. H. *et al*., *Nature*, 176, 1225, 1995
[18] Perline R. E. *et al*., *Sensors and Actuators A*, 64, 77-85, 1998
[19] Carpi F. *et al*., Enhancing the dielectric permittivity of elastomers in Dielectric elastomers as electromechanical transducers, Elsevier, 2008
[20] Debye P., *Zeitschrift für Physik*, 13 , 97, 1912
[21] Havriliak S. *et al*., *Journal of Polymer Science C*, 14 , 99-117, 1996
[22] Zener C., *Proceedings of the Royal Society of London*, Series A, 523-529, 1934
[23] Seanor D. A., *Electrical Properties of Polymers*, Academic Press, New York, 1932
[24] Jonscher A. K., *Journal of Physics D: Applied Physics*, 13, 143-148, 1980
[25] Suo Z. *et al*., *Journal of the Mechanics and Physics of Solids*, 56, 467-486, 2008
[26] Wissler M. *et al*., *Sensors and Actuators A: Physical*, 138, 2, 384-393, 2007
[27] Kofod G. *et al*., *Journal of Intelligent Material Systems and Structures*, 14, 12, 787-793, 2003
[28] Perline R. *et al*., in Dielectric elastomers as electromechanical transducers, pp.3, Elsevier, 2008
[29] Madden J. D. W. *et al*., in Dielectric elastomers as electromechanical transducers, pp.13, Elsevier, 2008
[30] Skov A. L. *et al*., Dielectric elastomers as electromechanical transducers, pp.25, Elsevier, 2008
[31] Kofod G. *et al*., Journal of Intelligent Material Systems and Structures, 14, 787, 2003

[32] Doi M. *et al*., Introduction to polymer physics, Clarendon Press, Oxford, UK, 2001
[33] Sommer-Larsen P. *et al*., *Proceedings of the International Society of Optical Engineering*, San Diego, CA, 5385, 68, 2004
[34] James H. M. *et al*., *Journal of Chemical Physics*, 15, 669, 1947
[35] Langley N. R. *et al*., *Macromolecules*, 1, 353 1968
[36] Dossin L. M. *et al*., *Macromolecules*, 12, 123, 1979
[37] Frisch H. L. *et al*., *Pure Applied Chemistry*, 53, 1557, 1981
[38] Hourston D. J. *et al*., *Polymer*, 37, 3521, 1996
[39] Larsen A. L. *et al*., *e-Polymers*, 050, 2004
[40] Chambon F. *et al*., *Journal of Rehology*, 31, 683, 1987
[41] Larsen A. L. *et al*., *Proceedings of Smart Structures and Materials 2004 (EAPAD)*, SPIE, 5385, 108, 2004
[42] Venkatraman S., *Journal of Applied Polymer Science*, 48, 1383, 1993
[43] Milner S. T. *et al*., *Macromolecules*, 30, 1259, 1997
[44] Degennes P. G., *Macromolecules*, 19, 1245, 1986
[45] Kornbluh R. *et at*., *Proceedings of Smart Structures and Materials 2003 (EAPAD)*, SPIE, 5051, 143-158, 2003
[46] Chang V. S. C. *et al*., *Polymer Bulletin*, 8, 69-74, 1982
[47] Saunders K. J., Organic polymer chemistry, Chapman & Hall Ed., London, 1989
[48] David L. D., *Chemistry in Britain*, 23, 553, 1987
[49] Perline R. *et al*., *Science*, 287, 5454, 836-839, 2000
[50] Kofod G. *et al*., *Proceedings of Smart Structures and Materials 2001 (EAPAD)*, SPIE, 4329, 141-147, 2001
[51] Kornbluh R. *et al*., *Proceedings of Smart Structures and Materials 2000 (EAPAD)*, SPIE, 3987, 51-64, 2000
[52] Kornbluh R. *et al*., *Proceedings of Smart Structures and Materials 1999 (EAPAD)*, SPIE, 3669, 149-161, 1999
[53] Oertel G., Polyurethane Handbook, Macmillen Publishing Co., New York, 1985
[54] Blackwell J. *et al*., in Urethane chemistry and applications, Washington D.C. American Chemical Society, Ch.14, pp.179, 1981
[55] Blackwell J. *et al*., Structure of the hard segments in polyurethane elastomers, IPC Business Press, 1979
[56] Grillo D.J et al., Physical Properties of Polyurethanes from Polyesters and Other Polyols, *Polyurethanes '92 Conference Proceedings*, New Orleans, LA, The Society of the Plastics Industry, Inc., 1992
[57] Musselman S.G. *et al*., Structure Versus Performance Properties of Cast Elastomers, *Polyurethanes '98 Conference Proceedings*, Dallas, TX, The Society of the Plastics Industry, Inc., 1998
[58] Zhou Y. et al., Journal of Applied Physics, 96, 1, 294-299, 2004
[59] Kawai H., *Oyo Butsuri*, 36, 484, 1967
[60] Kawai H., *Oyo Butsuri*, 39, 869, 1970
[61] Watanabe M. *et al*., Journal of Polymer Science Part B: Polymer Physics, 39, 10, 1061, 2001

[62] Watanabe M. *et al*., Journal of Applied Polymer Science, 79, 6, 1121-1126, 2001
[63] Kornbluh R. *et al*., in Smart Structures and Materials 1999: Electroactive polymer actuators and devices, ed. Y. Bar-Cohen, Proc. SPIE, 3669, 149-161

Chapter 3

How to improve DEs performance

Reproduced in part from

"*Enhancing the Dielectric Permittivity of Elastomers*" Carpi, F., Gallone, G., Galantini, F., De Rossi, D., in *Dielectric Elastomers as Electromechanical Transducers*, Carpi, De Rossi, Kornbluh, Perline, Sommers-Larsen Eds., Elsevier 2008

3.1 An introduction

As obtained in Cap.2 (Eq.2.44), it is well known from literature [1, 2, 3, 4, 5] that electromechanical transduction properties of any dielectric elastomer are intrinsically regulated by its the dielectric permittivity. This parameter proportionally controls both the achievable active stresses and strains. Accordingly, a suitable increase of the material permittivity may provide a valuable means to improve the performance of a dielectric elastomer actuator. This chapter provides a brief overview of the most used methods, mainly based on purely physical approaches, currently available for increasing the dielectric permittivity of rubber-like insulators with reference to the activity developed for the PhD thesis.

In order to increase the dielectric permittivity of polymer materials, different methods are currently available. They may be classified in three main groups: random composites, field-structured composites and new synthetic polymers. The first approach is based on the dispersion into the polymer matrix of a filler, either solid (e.g. powder) or liquid. The second method exploits a composite approach as well, although the material is now cured in presence of an external electric field, in order to align dipoles. The third strategy deals with the synthesis of new materials with tailored characteristics. Tab.3.1 shows a list of such methods in terms of involved physical processes and adopted materials, by mentioning specific state-of-the art examples related to either elastomers or not. Some of the methods reported in this table have been already experimented for incrementing the dielectric constant of elastomers used for actuation. On the contrary, other examples relate to different types of materials (not elastomers) and/or different applications. These have been included as well for the sake of completeness and because, in certain cases, they may suggest approaches that worth to be investigated for applications to actuation elastomers. The different considered techniques will be separately discussed in the following sections with reference to Tab.3.2, which reports the most significant results achieved by the studies mentioned in Tab.3.1.

Process		**Filler** (where applies)		**Matrix**			
				Elastomers	**Ref.**	**Non elastomers**	**Ref.**
Random composites	Mixing with inorganic fillers (particles)	Ferroelectric/ piezoelectric ceramics	PMN-PT [$Pb(Mg_{1/3}Nb_{2/3})O_3$-$PbTiO_3$]	Silicone	[6,7]	--	--
			TiO_2	Silicone	[7,8]	--	--
			$BaTiO_3$	Silicone	[7]	Polyacrylates	[9]
		Conductive particles	Fe	Silicone	[10]	Polyester	[10]
						Epoxy resin	[11]
			Cu	--	--	Epoxy resin	[11]
			Cu coated phospholipides	Silicone/polyurethane	[12]	--	--
			Carbon black	Polyurethane	[13]	Polyethylene	[14,15]
			Carbon nanotubes	--	--	Epoxy resin	[16]
						Polycarbonate	[17]
		Organic monomers	Copper phtalocyanine [CuPc]	Silicone	[18]	P(VDF-TrFE)	[19]
		Organic polymers	Poly(copper phtalocyanine) [PolyCuPc]	Polyurethane	[20]	Poly(ethylene-co-vinyl acetate)	[7]
			Polyaniline [PAni]	Polyurethane	[20,21]	P(VDF-TrFE-CFE)	[22,23]
Field-structured composites	Cross-linking in electric field of elastomers with inorganic fillers (particles)	Ferroelectric/ piezoelectric ceramics	SiO_2	Silicone	[24]	--	--
			$BaTiO_3$, $PbTiO_3$	Silicone	[24,25]	Epoxy resin	[26]
Synthesis of new polymers	Functionalization	--		Sulfonated poly(stirene-ethylene/butylene styrene)	[27]	P(VDF-TrFE-CFE)	[22,23]
	Copolymerisation (grafting and/or cross-linking)	--		Silicone with lateral liquid crystalline groups	[28,29]	--	--
				Acrylonitrile-butadiene rubber	[30]		
	Polymer blending	--		Silicone/polyurethane	[12]	--	--

Table 3.1. Non exhaustive synoptic table of different methods used for improving the dielectric constant of polymers, along with related state-of-the-art examples.

System		Loading [%]	ε'_m	ε'_c	ε''_c	$tg\delta_c$	Y_c [MPa]	$E_{break,c}$ [V/µm]	S_m [%]	S_c [%]	Ref.
Dielectrics for Maxwell Stress actuation	Silicone/TiO_2	70 wt	3 @1Hz	10	--	--	10	30	--	--	[7]
	Silicone/PMN	70 wt	3 @1Hz	8	--	--	10	34	--	--	[7]
	Silicone/PMN	30 vol	8 @10Hz	32	32	1	0.13	--			[6]
	Silicone/$BaTiO_3$	70 wt	3 @1Hz	20	--	--	10	26	--	0.4 tr@25V/µm	[7]
	Silicone/TiO_2	30 wt	6 @10Hz	8	~0.8	0.1	0.016	--	1 *tr*@10V/µm	11 tr@10V/µm	[8]
	Silicone/CuPc	20 wt	3 @1kHz	6	--	--	--	25	6 *tr*@26V/µm	12 tr@26V/µm	[18]
	Polyurethane/carbon black	18.76 vol	6 @1Hz	4400	$\sim10^8$	$\sim10^5$	28.7	0.8	~0 *tr*@0.7V/µm	0.035 tr@0.7V/µm	[13]
	Polyurethane/PolyCuPc/PAni	85/15/14 vol	10 @1Hz	800	--	--	80	>20	-2 *lon*@20V/µm	-9 lon@20V/µm	[20]
	Poly(ethylene-co-vinylacetate) [EVA]/PolyCuPc	70 wt	3 @1Hz	~40	--	$\sim10^2$	--	4.6	--	--	[7]
	Acrylonitrile-butadiene rubber	--	14 @10Hz	--	--	--	--	--	--	20 tr@50V/µm	[30]
Dielectrics for electro-strictive actuation	Ferroelectric liquid-crystalline elastomer (FLCE)	--	--	--	--	--	3	--	--	-4 lon@1.5V/µm	[28]
	P(VDF-TrFE)/CuPc (+irradiation)	40 wt	40 @0.1Hz	425	--	0.7	$\sim10^3$	13	--	-2 lon@13V/µm	[19]
	P(VDF-TrFE-CFE)/PAni (+irradiation)	25 vol	60 @1kHz	5000	--	0.6	530	3.85	-0.2 *lon*@16V/µm	-2.65 lon@16V/µm	[22]
	P(VDF-TrFE-CFE)/grafted elastomer	--	--	--	--	--	3	--	--	-0.13 lon@50V/µm	[29]
	S-SBS [sulfonated(styrene-ethylene /buthylene-styrene) tryblock copolymer]	10 wt H_2O 10 wt S	2	50000	$6\cdot10^4$	--	--	--	--	--	[27]
		20 wt H_2O 20 wt S		25000	$3\cdot10^4$	--	--	--	--	--	
		0 wt H_2O 16 wt S		5	--	--	--	--	--	--	
	Silicone/PMN-PT	30 vol	8 @10Hz	30	40	--	0.135	--	--	--	[6]
	Silicone/Fe	50 vol	3 @1Hz	60	20	--	--	--			[10]
	Silicone/SiO_2 structured @1kV/mm	13 vol	2.3 @1Hz	25	--	18	0.06	$1.5\cdot10^3$			[24]
	Polyurethane/PAni	17 wt	6 @1kHz	1120	--	--	80	--	--	--	[21]
	Polyurethane/silicone/Cu-coat.phosph.lip	12 wt	--	30	2	~0.6	--	--			[12]
Dielectrics for different applications	Polyethylene/carbon black	5 wt	3 @10Hz	6	0.07	10^{-2}	--	--	--	--	[15]
	Polyethylene/carbon black	2 vol	3 @10Hz	20	--	--	--	--			[14]
	Poly-ethylene-glycol-diacrylate [PEGDA]/$BaTiO_3$	30 vol	10 @100Hz	40	--	--	--	--	--	--	[9]
	Trimethylolpropane-triacrylate [TMPTA]/$BaTiO_3$	30 vol	3 @100Hz	25	--	--	--	--			
	Tetradecanediol-dimethacrylate [TDDMA]/$BaTiO_3$	30 vol	2 @100Hz	20	--	--	--	--			
	Epoxy resin/Fe	40 wt	5 @100Hz	7.5	7	1	--	--	--	--	[11]
	Epoxy resin/Cu	40 wt	5 @100Hz	12	6	0.5	--	--			[11]
	Epoxy resin/carbon nanotubes	0.05 wt	3 @10Hz	40	$\sim10^3$	25	--	--			[16]

Notes: ε'_m= real relative permittivity of the matrix; ε'_c, ε''_c $tg\delta_c$= real and imaginary relative permittivity and loss tangent of the composite; Y_c= elastic modulus of the composite; $E_{break,c}$= dielectric strength of the composite; S_m, S_c= strain of the matrix and of the composite, respectively; tr= transverse; lon= longitudinal;-- = not available/not applicable.

Table 3.2. Summary of the main results achieved by the studies reported in Tab.3.1.

3.2 Random composites

Since the last three decades, fabrication of composites has become a very common methodology in the field of materials engineering, aimed at achieving a set of specific properties superior with respect to those provided by the single constituents. Such an approach has also been extended to the development of dielectric elastomers with improved dielectric permittivity. For this purpose, fillers of high dielectric constant are usually introduced in the form of powder in the elastomeric matrix before vulcanisation. In general, the resulting composite will have intermediate electric properties with respect to those of matrix and filler. However, a universal composition law capable of providing, given the electric properties of both matrix and filler, reliable predictions of the composite response is still not available. Rather, several mixing rules have been proposed to account for the effective permittivity ε_c of a system consisting of two immiscible phases, as descried in the following.

3.2.1 Dielectric mixing rules

Typically, mixing rules consider an isotropic medium (*Effective Medium Theory*) of dielectric permittivity ε_m and volume fraction v_m filled with spheroids of permittivity ε_f and volume fraction $v_f = 1\text{-}v_m$. They are usually derived in the form of composition equations for the effective permittivity at sufficiently high frequencies (ε_∞) [31]. Among such models, those pertaining to continuous media filled with spherical particles are here specifically considered as a starting point for the following discussion.
It is possible, in general, to identify upper and lower bounds for ε_c such that [32]:

$$\varepsilon_{c,\min} \leq \varepsilon_c \leq \varepsilon_{c,\max} \tag{3.1}$$

where ε_{c_min} and ε_{c_max} are solutions of equivalent series and parallel model circuits, respectively given by:

$$\varepsilon_{c,\min} = \frac{\varepsilon_m \varepsilon_f}{\varepsilon_m v_f + \varepsilon_f v_m} \tag{3.2}$$

$$\varepsilon_{c,\max} = \varepsilon_m v_m + \varepsilon_f v_f \tag{3.3}$$

Beyond such rough limits, further steps in modelling the dielectric properties of a binary mixture have been accomplished in the frame of the so-called Wagner theoretical scheme [31, 33]. As reported by Van Beek [31], under the hypothesis of sufficiently small filler concentrations, it is possible to select suitable intermediate regions surrounding the filler particles where two alternative points of view hold at the same time. The first considers the electric potential as arising from a distribution of spheres with dielectric constant ε_f , enclosed in an insulating medium of different dielectric constant ε_m; the second foresees a larger heterogeneous sphere with overall dielectric constant ε_c embedded in the same insulating medium with dielectric constant ε_m [34]. By equating the two alternative expressions for the electric potential, the so-called Sillars [35, 36] or Landau-Lifshitz [34] mixing rules can be obtained:

$$\varepsilon_c = \varepsilon_m \left[1 + \frac{3\nu_f (\varepsilon_f - \varepsilon_m)}{2\varepsilon_m + \varepsilon_f} \right] \tag{3.4}$$

However, Eq.(3.4) holds just at very low volume fractions of filler (v_f <0.1) and only for fillers having a higher electrical resistivity than the matrix. More accurate predictions can be achieved with by one of the most popular equations, the so-called Maxwell-Garnett [36, 37-40] formula:

$$\varepsilon_c = \varepsilon_m \left(1 + \frac{3\nu_f (\varepsilon_f - \varepsilon_m)}{(1-\nu_f)(\varepsilon_f - \varepsilon_m) + 3\varepsilon_m} \right) \tag{3.5}$$

which in principle should be valid without restrictions about resistivity. However, it is common to find in the literature the mixing rule of Eq.(3.5) expressed in many other equivalent forms, such as:

$$\frac{\varepsilon_c - \varepsilon_m}{\varepsilon_c + 2\varepsilon_m} = \nu_f \frac{(\varepsilon_f - \varepsilon_m)}{\varepsilon_f + 2\varepsilon_m} \tag{3.6}$$

so that it is sometimes referred to as Maxwell-Wagner [41-43] or Rayleigh [31, 33, 44, 45] or Lorentz-Lorenz [31, 46] or Kerner-Böttcher [33, 47] equation. Similarly to Eq.(3.4), these two equations can be derived within the Wagner approach, and indeed it is found that Eq.(3.4) is just an approximation of Eqs.(3.5) e (3.6) [31]. Both these results can also be obtained directly via the Clausius-Mossotti scheme for the polarisability of a medium [31, 46].

By using a quite similar approach, Böttcher suggested to equate the electric field acting into each component of the mixture to the field which would settle in a sphere of the same material, embedded in a medium having the dielectric constant ε_c of the mixture [33]. Calculations lead to the following relation, referred to as Böttcher [33, 45, 48] or Landauer [32, 47, 49] or Polder-Van Santen [50] equation:

$$\nu_m \frac{(\varepsilon_c - \varepsilon_m)}{2\varepsilon_c + \varepsilon_m} + \nu_f \frac{(\varepsilon_c - \varepsilon_f)}{2\varepsilon_c + \varepsilon_f} = 0 \tag{3.7}$$

sometimes also written in the form:

$$\frac{\varepsilon_c - \varepsilon_m}{3\varepsilon_c} = \nu_f \frac{(\varepsilon_f - \varepsilon_m)}{2\varepsilon_c + \varepsilon_f} \tag{3.8}$$

In case of diluted systems Eqs. (3.5) and (3.6) are equivalent.

When the dispersed particles are not spherical in shape, the mixing formulas discussed so far must be revised, in order to take account of their geometry. Typical is the case of particles with a spheroidal or cylindrical geometry, characterised by the ratio of their axes (a/b), which may even become pure rods or discs. The common way to include the information about such kinds of geometries of filler particles is to properly introduce a *depolarization factor A*, which contains the information about the particles shape in terms of their deviation from sphericity. Thus, for example, the widely used Maxwell-Garnett equation is modified into the form [31]:

$$\varepsilon_c = \varepsilon_m \left(1 + \frac{\nu_f \left(\varepsilon_f - \varepsilon_m \right)}{A\left(1-\nu_f\right)\left(\varepsilon_f - \varepsilon_m\right) + \varepsilon_m} \right) \quad \text{for } \nu_f < 0.1 \tag{3.9}$$

It is possible to determinate *A* by calculating it with specific formulas [31] or by referring to published tables [51]. In the case of spheres, *A*=1/3 so that Eq.(3.9) turns back into Eq.(3.5), as expected. Some other formulas, which come from exact solutions of the Waner's theory for very common cases, are (for a complete list see [31]):

Wagner-Rayleigh $\varepsilon_c = \varepsilon_m \dfrac{2\varepsilon_m + \varepsilon_f + 2\nu_f \left(\varepsilon_f - \varepsilon_m \right)}{2\varepsilon_m + \varepsilon_f - \nu_f \left(\varepsilon_f - \varepsilon_m \right)}$ for spheres and $\nu_f < 0.2$ (3.10)

Sillars $\varepsilon_c = \varepsilon_m \left[1 + \nu_f \dfrac{\varepsilon_f - \varepsilon_m}{\varepsilon_m + A\left(\varepsilon_f - \varepsilon_m\right)} \right]$ for spheroids with axes_{main} // E and $\nu_f < 0.1$ (3.11)

Bruggeman $\varepsilon_c = \varepsilon_f \dfrac{3\varepsilon_m + 2\nu_f \left(\varepsilon_f - \varepsilon_m \right)}{3\varepsilon_f - \nu_f \left(\varepsilon_f - \varepsilon_m \right)}$ for lamellae and discs (3.12)

An improvement of these mixing rules was proposed by Bruggeman as an extension of the Wagner scheme, in which the initially low volume fraction of the filler is gradually increased by infinitesimal additions [31, 33]. The Bruggeman integration method leads to a distinct mixing rule, which permits to assess the overall electrical response at much higher content of (spherical) filler than for previous equations [31]. This is particularly attractive for a disordered system, where constituent particles may become very close to each other and even agglomerate, so that deviations from an ideally uniform and dilute system may be substantial even at low filler concentrations ($\nu_f > 0.1$). Thus, the solution of a differential equation obtained from either Eqs.(3.5) or (3.6) (they may be considered equivalent, as a starting point) leads to the Bruggeman's formula [45, 48, 52]:

$$\frac{\varepsilon_f - \varepsilon_c}{\varepsilon_c^{\,1/3}} = \frac{(1-\nu_f)(\varepsilon_f - \varepsilon_m)}{\varepsilon_m^{\,1/3}} \tag{3.13}$$

which is expected to hold for ν_f values up to 0.5, with the constraint that the dispersed spheres do not form a percolative path throughout the medium.

With even larger filler contents, the electric field arising from the neat induced distribution of dipole moments is likely to become more and more important in determining the overall field locally experienced in the matrix. Accordingly, the need for more realistic assumptions in order to obtain a reliable mixing rule is evident. For this purpose, Jayasundere and Smith calculated the electric field within a dielectric sphere embedded in a continuous dielectric medium by also taking into account the polarization of adjacent particles [47]. This approach led to the following equation:

$$\varepsilon_c = \frac{\varepsilon_m \nu_m + \varepsilon_f \nu_f \dfrac{3\varepsilon_m}{(2\varepsilon_m + \varepsilon_f)} \left[1 + 3\nu_f \dfrac{(\varepsilon_f - \varepsilon_m)}{(2\varepsilon_m + \varepsilon_f)} \right]}{\nu_m + \nu_f \dfrac{3\varepsilon_m}{(2\varepsilon_{1m} + \varepsilon_f)} \left[1 + 3\nu_f \dfrac{(\varepsilon_f - \varepsilon_m)}{(2\varepsilon_m + \varepsilon_f)} \right]} \tag{3.14}$$

Interestingly Vo *et al.* proposed a dielectric constant modelling regarding the dependence of the effective dielectric constant of a composite material with respect to the interfacial phases generated between the polymer matrix and the filler particles [53]. Their results show that the composite dielectric constant mainly depends on the ratio between the filler and matrix dielectric constants, and on the degree of interaction between filler and matrix.
As mentioned at the beginning of this section, the mixing rules reported hold for the high frequency values of the permittivity. Nevertheless, an investigation of dielectric properties of an elastomer devoted to the enhancement of its electromechanical properties should focus mainly on the low frequency part of the spectrum. In fact, dielectric elastomer actuators are usually operated at relatively low frequency where, due to the limited bandwidth of elastomers, actuation strains are superior. According to Fricke, in case of spheroids it is possible to formulate a pair of mixing rules for both the relaxed and unrelaxed permittivity of the composite [31]:

$$\begin{cases} \varepsilon_{c,s} = \varepsilon_m + \frac{1}{3}\nu_f \sum_{i=a,b,c} \frac{\sigma_f - \sigma_m}{\left[\sigma_m + A_i\left(\sigma_f - \sigma_m\right)\right]} + \sigma_m \sum_{i=a,b,c} \frac{\sigma_m\varepsilon_f - \sigma_f\varepsilon_m}{\left[\sigma_m + A_i\left(\sigma_f - \sigma_m\right)\right]^2} \\ \varepsilon_{c,\infty} = \varepsilon_m \left\{ 1 + \frac{1}{3}\nu_f \sum_{i=a,b,c} \frac{\varepsilon_f - \varepsilon_m}{\left[\varepsilon_m + A_i\left(\varepsilon_f - \varepsilon_m\right)\right]} \right\} \end{cases} \tag{3.15}$$

where A_a, A_b and A_c are the depolarizing factors along three axes *a*, *b* and *c* (defined in [31]) and σ_m and σ_f are the conductivities of the polymer matrix and filler, respectively. The presence of σ_m and σ_f in Eq.(3.15) should not be surprising, however, since the aforementioned mixing rules and their underlying assumptions are still valid even if both matrix and filler possess finite electrical conductivities. In addition, it is exactly the mobility of some charge carriers which, although limited, gives rise to the interfacial polarisation and the coupled relaxation processes.
All the above equations are based on different assumptions, even if they are derived within the same theoretical scheme. Thus, their predictions may considerably differ from one another. As an example, Fig.3.1 shows a comparison among a set of experimental data from a composite dielectric elastomer and theoretical values expected from classical mixing rules [6]. The composite was a silicone elastomer matrix filled with particles of $Pb(Mg_{1/3}Nb_{2/3})O_3$-$PbTiO_3$ (PMN/PT) with an average size lower than 100μm.

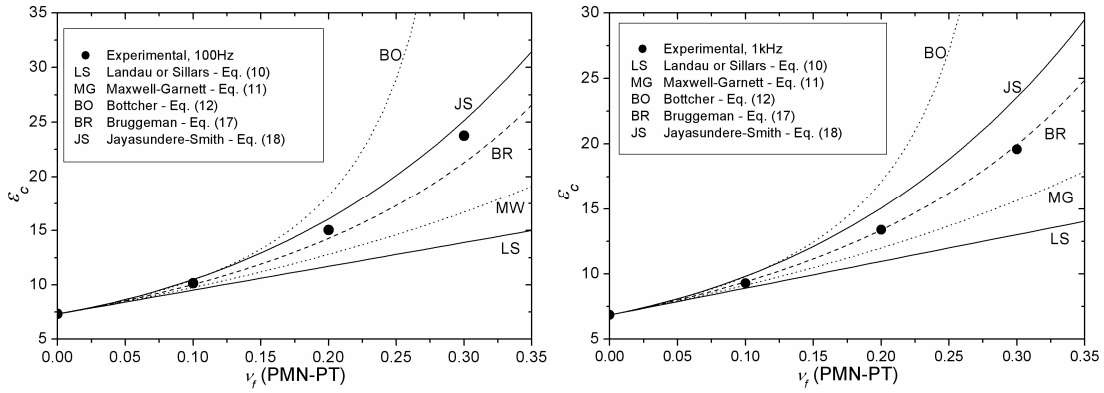

Figure 3.1. Experimental ε_c data (dots) of silicone/PMN-PT composites at 100Hz and 1kHz for various filler contents ν_f compared with specified models (adapted from [6]).

This figure shows that at low filler contents (i.e. diluted systems with ν_f <0.1), predictions from Eqs.(3.4-3.8), (3.13) and (3.14) are similar and in substantial agreement with experimental data. At higher filler contents (concentrated systems) differences among models become relevant. Notably, the Bruggeman model gave the best agreement with experimental data within the entire composition range and particularly at the higher frequency. This can be ascribed to the fact that, with respect to the occurring polarisation processes, the dielectric permittivity at 1 kHz was closer to the unrelaxed value (ε_∞) than at 100 Hz.

In order to compare models predictions with literature experimental data, it must be pointed out that a direct comparison is often not possible, due to a lack of information about the considered volume fractions. In fact, unfortunately, authors too frequently report compositions in terms of weight fractions (without any indication about density) rather than volume percentages, making any possible comparison very difficult.

3.2.2 Dielectric fillers

The use of high permittivity inorganic fillers is a well-established technique to improve the dielectric constant of a polymer matrix [54]. In particular, powders of ferroelectric/piezoelectric ceramics, showing the highest dielectric constants (e.g. ε'_f ~20000 for lead magnesium niobate - PMN), can allow significant increments of permittivity. For instance, a four-fold increase of the permittivity of a silicone elastomer was obtained at 10 Hz by loading the material with 30 vol% lead magnesium niobate – lead titanate (PMN–PT) [6]. Likewise, an increase of the dielectric constant of poly-ethylene-glycol-diacrylate (PEGDA) from ε'_m~10 to ε'_c~40 at 10^2 Hz by filling the material with 30 vol% barium titanate ($BaTiO_3$) was described [9]. Other examples are reported in Tab.3.2.

Despite the considerable improvements of the material dielectric properties that can be achieved by using ceramic fillers, such a method is not always suitable for the sake of improving the actuation properties. In fact, its use has brought so far limited results in this respect [7]. This is due to the fact that ferroelectric ceramics usually are highly stiff, which is likely to cause a loss of strain capabilities in the resulting composite. Nevertheless, taking such an assumption as a general rule can be misleading. In fact, also possible increases of the actuation strains within definite field ranges have been reported [8]. This usually happens for those systems whose mechanical properties can have specific benefits from the composite approach. For instance, this is the case for small interactions between matrix and filler, as recognised in [7] and as it will be discussed in the following of this chapter. With respect to this, Fig.3.2 shows an increase of the strain response achieved from a 100%-pre-strained sample of silicone elastomer, loaded with 30 wt% (7.4 vol%) of a titanium dioxide (TiO_2) powder [8].

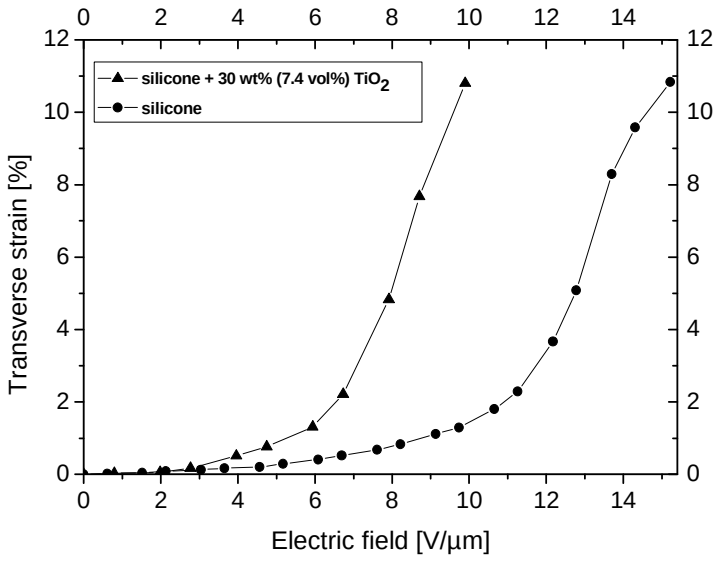

Figure 3.2. Transverse strain vs electric field for samples made of a pure silicone elastomer (lower curve) and its composite with TiO_2 particles (higher curve), tested with a transverse pre-strain of 100% (adapted from [8]).

More interesting results have been reported for organic dielectric fillers. As an example, Zhang et al. [18] mixed a silicone matrix (ε'_m~3) with a copper-phtalocyanine olygomer (ε'_f~10000), obtaining increments of the dielectric constant up to about ε'_c=6 for a filler concentration of 20 wt%, with a related electromechanical strain response of 12 % at 26 V/µm. For this system the electromechanical response increased with the filler content. However, breakdown threshold was reduced, probably due to the formation of aggregates of copper-phtalocyanine particles.

Insulators are not the sole candidate materials as suitable fillers. In fact, dielectric improvements can be achieved with conductive (and semiconductive) fillers too, as described in the following.

3.2.3 Conductive and semiconductive fillers

The need for high permittivity fillers, as suggested by the mixing rules discussed above, has led to test also the effects of loading dielectric elastomers with conductive materials. The use of conductive fillers as a possible means to increase the dielectric permittivity is motivated by the fact that free charges not only contribute to conduction, but also they can give rise to *Maxwell-Wagner polarization*. Nevertheless, as a drawback, such insulator-conductive composite systems are prone to show percolative behaviours, which may result in a dramatic increase of their conductivity for filler concentrations exceeding a certain threshold $\nu_{f,perc}$. The percolation threshold represents the filler concentration at which conducting paths between particles in contact with each other take place throughout the medium. Such a threshold strongly depends on the ratio between particle length and

diameter [55]. Unfortunately, the maximum increase of the composite permittivity is achieved close to the percolation threshold, according to the following relation [56, 57]:

$$\varepsilon'_c = \varepsilon'_m \left(\frac{\nu_{f,perc} - \nu_f}{\nu_f} \right)^{-q} \quad \text{with} \quad 0.8<q<0.9 \quad \text{for } \nu_f \approx \nu_{f,perc} \quad (3.16)$$

The parallel increases of both the real and the imaginary parts of the permittivity are, of course, antagonistic. They can seriously compromise the applicability of such types of systems as electromechanical transduction materials, due to their typically low dielectric strengths.

As a specific type of conductor, metals have been frequently tested. For instance, for mixtures of epoxy resins (ε'_m=5 at ~100Hz) with 40 wt% copper particles or iron particles, values of ε'_c~12 and ε'_c~7.5, respectively, at 10 Hz with a rather limited loss factor (about 6-7) have been reported [11]. As a significant drawback, usually metallic fillers can dramatically increase the composite stiffness. Moreover, they typically show a lack of adhesion with the polymer matrix, with a further degradation of the mechanical properties of samples.

As an alternative to metals, graphitic conductors may provide advantages in terms of a superior surface compatibility with the polymer matrix. For instance, composites consisting of polymers loaded with carbon black particles are very common. The compatibility of carbon black with organic phases is demonstrated by its wide use with vulcanized rubbers for several types of common industrial applications (tires, cables, etc.). As an example, for a carbon black-filled (18.76 vol%) polyurethane (PU) a dielectric constant of 4400 has been described [13]. Likewise, carbon black-filled polyethylene (PE) samples showed large dielectric constants near the percolation threshold, varying from ε'_c~20 for ν_f=1.9 vol% up to ε'_c~10^4 for ν_f=2.5 vol%.

In the light of reducing the stiffening introduced by an inorganic filler and simultaneously exploiting the drastic dielectric enhancement achievable near the percolation threshold (Eq. (3.16)), it is worth of note the work by Zucolotto *et al*. [58]; they reported that, by loading a terpolymer styrene-ethylene-butylene with carbon black modified particles, the percolation threshold can be lowered down to 5wt%, with evident advantages in terms of mechanical properties.

According to their amazing physical properties, and namely high electrical conductivity, carbon nanotubes can also be used as electrically efficient fillers. Percolation threshold for carbon nanotube fillers can be considerably lower with respect to any other type of conducting filler. Accordingly, very small loading percentages (particularly advantageous in order to limit the elastic modulus) can offer interesting improvements of the dielectric permittivity. Nevertheless, attempts in this direction have so far produced composites typically characterized by considerable losses, unsuitable for electromechanical applications. As an example, results concerning epoxy resin/carbon nanotubes composites (0.05 wt%) showing ε'_c=~40 @~10 Hz, but also losses of the order of 10^3 and elastic modulus increments of 20 %, have been reported [16].

In order to improve the compatibility with the polymer matrix, advantages can derive from the use of fillers consisting of organic conductors, in the form of either monomers or polymers. As an example, a work by Zhang et al. [19] reported for an electron-irradiated P(VDF-TrFE) copolymer (already studied [33]) filled with 40 wt% copper-phtalocyanine olygomer a composite dielectric constant of 425 at 0.1 Hz and a loss factor of about 0.7, starting from a matrix dielectric constant of 40.
Conducting and semiconducting polymers, such as polyanilines, polythiophenes, polypyrroles and polyphthalocyanines are frequently studied as possible fillers. For instance, by adding 70 wt% poly(copper phthalocyanine) (ε'_f~10000) to a poly(ethylene-co-vinyl acetate) (EVA) matrix (ε'_m=3), an increase up to 40 at 1Hz of the real dielectric permittivity was reported for the composite [7]. A work of Chwang et al. [21] describes a polyurethane matrix filled with 17wt% polyaniline (Pani) and showing a composite dielectric constant of 1120; the authors underline the benefits of an "in situ polymerization of PAni in PU matrix (ISP-blends)" with respect to a "simple mixing of PAni and PU in aqueous solution (SM-blend)". A more complex system, made of a bi-component matrix of polyurethane and poly(copper phtalocyanine) (Poly(CuPc)) filled with 14 vol% PAni, showed a dielectric constant of about 800 at 1Hz, along with an elastic modulus increase of about four times in comparison with the matrix [20].
Concerning non elastomeric matrices, all-polymer percolative electron-irradiated composites between poly(vinylidene fluoride-trifluororthylene-chlorotrifluoroethylene) (P(VDF-TrFE-CTFE)) and PAni were described [22, 23]; for a 25 vol% PAni loading, the composite showed a dielectric constant of about 5000 at 1 kHz, starting from a value of 60 for the pure matrix.
In general, organic monomers and polymers can contribute to advantageously increase the orientational polarizability of the material. Nevertheless, if they are conductive, they can give rise to percolation phenomena at high concentrations. In fact, organic monomers and polymers can bring great electric losses, due to their high electrons delocalization; such losses typically increase with the doping of the material.

3.2.4 Mechanical properties of random composites

Within an attempt of improving the electromechanical properties of a dielectric elastomer, the purely electrical analysis considered so far should always be parallel to an investigation of the effects on the material mechanical properties. In fact, any attempt of increasing the material dielectric constant should always preserve the mechanical compliance within an acceptable range. Approaches based on random composite can be particularly risky in this respect. The literature on composite systems is rich of models (not reported here) that propose possible composition rules of the elastic modulus. As a general property, it is worth mentioning that, as reasonably expected, such models foresee that the composite elastic modulus is intermediate between those of the constitutive phases. Accordingly, an advantageous increase of the dielectric constant can correspond to a disadvantageous mechanical stiffening. Such phenomena have, of course, antagonistic effects on the electromechanical strain response of the material.

Most of models for mechanical composition rules implicitly assume a perfect adhesion between the constitutive phases. This hypothesis is not always acceptable and it becomes quite unrealistic for specific types of systems, such as in the case of particles-loaded elastomers to be used for actuation, i.e. that have to sustain deformations. In fact, the mechanical properties of composites can actually depend on several factors, such as filler type and geometry, its interaction with the host matrix, along with specific working conditions. Among the latter, eventual pre-strains (exerted by either external loads or internal parts of the device) play a relevant role; for instance, a decrease of the elastic modulus in elongated samples of a silicone elastomer loaded with PMN-PT or TiO_2 has been reported and interpreted as due to the formation of cavitations around the filler particles [6, 8]. An example is presented in Fig.3.3.

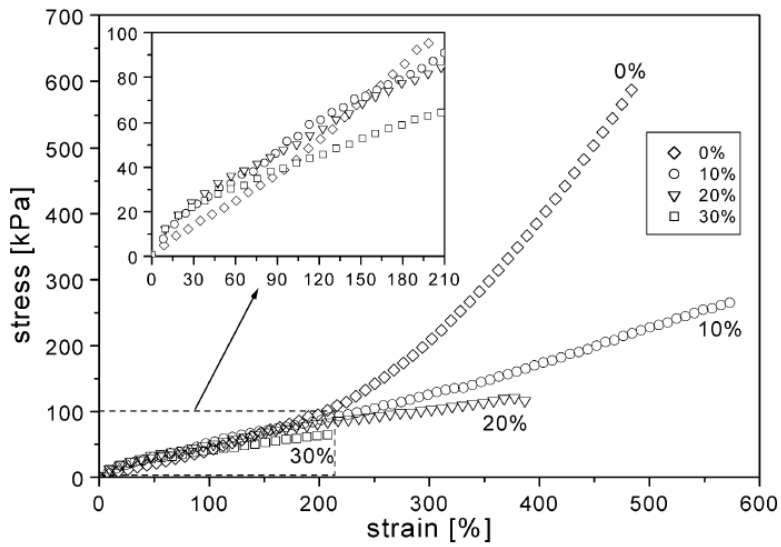

Figure 3.3. Stress–strain curves of silicone/PMN–PT composites for different volume fractions of the filler (adapted from [6]).

The cavitations, which are favoured by a lack of adhesion between the matrix and the particles, become progressively more and more important as the material elongation is increased. As previously introduced, this phenomenon can have a positive effect on the actual electromechanical properties of the composite material. The data reported in Fig.3.2 offer an example of such a situation: the strain response of a sample of pure silicone is lower than that of a sample of the same material loaded with ceramic particles, when both samples are highly (100%) pres-strained; this evidence should be mainly attributed to the (significant) reduction of the elastic modulus, rather than to the (modest) increase of the dielectric constant [8].

3.2.5 Dielectric strength of random composites

One of the typical drawbacks of the random composite approach consists of an observed substantial decrease of the material dielectric strength E_{break}. More generally, it is straightforward to recognise that higher values of ε' typically correspond to lower values of E_{break}. This is a common experimental evidence, that can also be easily assessed from the

large amount of literature data. This fact might be reasonably interpreted as mainly due to interfacial (Maxwell-Wagner) polarization phenomena [6, 8, 13].

Although a general expression capable of reliably relate the dielectric strength and the dielectric constant of composites is currently not available, it is worth reporting at least a couple of simple models that can provide interesting estimates.

The first model deals with a very rough schematisation: let's assume the elastomer as a homogeneous material (that is not the case of random composites!) and a purely elastic body at low strains; for such conditions, it can be demonstrated [59] that in the case of Maxwell-stress actuation the nominal breakdown field of the material is given by the following expression:

$$E_{break} = \frac{V_{break}}{d_0} = e^{-1/2}\sqrt{\frac{Y}{2\varepsilon_0\varepsilon'}} \cong 0.6\sqrt{\frac{Y}{2\varepsilon_0\varepsilon'}} \tag{3.17}$$

where ε' is the dielectric constant of the material, Y is its elastic modulus, V_{break} is the breakdown voltage of the sample and d_0 is its thickness at rest. This relation suggests that by increasing the dielectric constant of the material, its dielectric strength is expected to decrease as $1/\sqrt{\varepsilon'}$. Interestingly, such a trend has frequently been found to provide a satisfying fit of experimental data; as an example, see [60].

A subtler model is offered by the *local field theory* of dielectric media [61]. Let's consider a dielectric material subjected to an applied electric field E; although the space-averaged electric field can be uniform, the actual internal electric field can locally vary from point to point, depending on interactions of local fields generated by dipoles. Accordingly, the local electric field E_{loc} is defined as the field that actually acts on an individual polarisable unit (such as a molecule or an atom); it is also known as the Lorentz local field and it is given by the following expression [62]:

$$E_{loc} = \frac{\varepsilon' + 2}{3} E \tag{3.18}$$

where, in this case, ε' is the dielectric constant of the material surrounding the local polarisable unit (excluding the unit itself). Eq.(3.18) can be used to obtain an expression that relates the dielectric constant and the dielectric strength of the matrix (ε'_m, $E_{break,m}$) with those of the resulting composite (ε'_c, $E_{break,c}$). In fact, let's assume that the value of the local breakdown field of the matrix is the same when the matrix is in its pure and in its composite form; in this case, by equating the right-hand member of Eq.(3.18) evaluated for both these situations, we obtain the desired expression:

$$\frac{\varepsilon'_m + 2}{3} E_{break,m} = \frac{\varepsilon'_c + 2}{3} E_{break,c} \tag{3.19}$$

Moreover, Eq.(3.19) can be further developed by using for ε'_c one of the mixing rules previously described, according to different models. This can provide a useful tool in order to estimate the overall electrical behaviour of the composite system.

As a final remark, it is worth stressing that, despite the reduction of the dielectric strength typically observed in random composite systems, possible relative increases of the

actuation performances at low electric fields demonstrated for some systems (as reported in the previous sections) encourage further investigations for possible uses at low voltages.

3.3 Field-structured electro-active materials

The dielectric constant of a random composite may result further increased by cross-linking the mixture under the action of a proper electric field. In fact, this may provide an alignment along a preferential direction of the intrinsic polar groups of both the material and the filler; this can happen especially if the latter exhibits ferroelectric properties. As a result, an increase of the global polarizability of the material may occur.

As an example, a silicone (poly-dimethyl-siloxane) matrix loaded with 13 vol% SiO_2 cured under a field of 1 kV/mm showed a permittivity $\varepsilon'_c \cong 25$ in comparison with a dielectric constant $\varepsilon'_m \cong 2.3$ for the pure silicone [24]. Likewise, Khastgir et al. [25] described that filling a poly-dimethyl-siloxane sample ($\varepsilon'_m \cong 5$ at 100Hz) with 13.7 vol% barium titanate ($BaTiO_3$) and curing the mixture under a dc electric field of 4kV/cm, a permittivity $\varepsilon'_c \cong 90$ can be achieved.

Concerning non elastomeric systems, a work of Wilson et al. [26] reported, for an epoxy resin loaded with 40 vol% lead titanate ($PbTiO_3$) and cured under a field of few hundreds V/mm, an increase of the dielectric constant at 10^2 Hz from about 5 for the pure matrix, to about 16 for the field-structured composite.

As a general observation, it should be considered that field structuring provides a means to improve the material polarisability (and therefore its dielectric response) just along a definite direction, yielding a marked anisotropy in the material properties. This could not necessarily be a disadvantage for a material to be used for actuation; in fact, depending on the specific arrangement of the material within the actuator configuration, one could exploit this effect in order to increase the electromechanical coupling towards privileged directions, rather than others.

Nevertheless, it is worth of note that the actual electromechanical properties of field-structured systems may result sensibly affected by possible decreases of the breakdown strength. In fact, depending on the nature and geometry of the filler, field structuring may introduce additional pathways for breakdown currents.

According to these observations and given the inherent procedural complications of such a method of material processing, one can clearly recognize that it still poses many issues that need further basic investigations. Thus, deeper studies are currently necessary in order to assess the eventual suitability of such a technique for effectively enhancing the actuation performances of elastomers.

3.3.1 Electrets: quasi-permanent charged dielectrics

As defined in literature [63], [64], electrets, in analogy to the well known magnets, are dielectrics whose charge arrangement persists much longer than the time period over which it is studied. This phenomenon differs from the thermodynamically stable ferroelectricity [65], in ferroelectric polymers, in fact, a stress in the 3-direction mainly decreases the distance between the molecular chains, due to the relatively weak van der Waals and electrostatic interactions between chains in comparison with the strong covalent bonds within the chain. The thickness decrease thus results in an increase of the dipole density and in an increase of the charges on the electrodes, yielding a negative d_{33} coefficient from dipole-density (or secondary piezoelectricity). In cellular polymers (ferroelectrets), stress in the 3-direction also decreases the thickness of the sample, but the thickness decrease occurs dominantly across the voids, the macroscopic dipole moments decrease, and so do the electrode charges, yielding a positive d_{33} (intrinsic or direct (quasi-) piezoelectricity).
Electret polarization can be achieved in different ways discussed in the following, and can bring to two main types of charging, real charges or polarization charges (see Fig.3.4), both of them increasing the dielectric response of the material itself. In particular, real charges are positive or negative carriers trapped at the surface or in the volume of the dielectric. Polarization charges instead, are aligned dipoles or real charges displaced within molecular or domain boundaries (Maxwell-Wagner polarization).
Electret properties were first mentioned by Gray [66] in 1732, within his studies on the perpetual attractive power of different dielectrics, and Faraday [67] in 1839, who theorized about electrets properties due to application of an external electric field. The term "electret" was then coined in 1885 by Heaviside [68] while systematic studies into electret properties began in 1919 thanks to the Japanese physicist Eguchi [69].

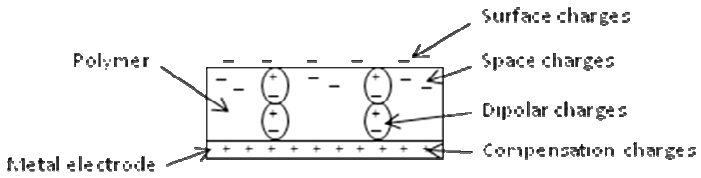

Figure 3.4. Schematic representation of the cross-section of an electret with a combination of surface charges, space charges and aligned dipolar charges.

Methods for forming space-charge electrets and dipolar electrets are different. The charging of space-charge or surface-charge electrets is mostly achieved by injecting or depositing charge carriers by discharges, particle beams, contact electrification (tribocharging) or other techniques through or onto a non-metallized surface. Injection form a deposited metal layer is also possible at relatively high fields. Other methods consist in the generation of carriers within the dielectric by light, radiation or heat and simultaneous charge separation by a field. Dipolar electret, on the other hand, particularly interesting to have enhanced permittivities, are generally polarized by application of an electric field to the material at room temperature or temperatures decreasing form a

properly selected higher to a lower value. Dipolar orientation has also been achieved by corona charging, that is the method used to increase the dielectric constant of some of elastomers used during this PhD activity.

Corona Charging and poling

The corona method depends on charge deposition on a polymer by a corona discharge (see Fig.3.5). The discharge is generated by application of a voltage of a few kilovolts between a needle or knife electrode and a back electrode located behind the sample to be charged. An additional wire mesh located between the needle electrode and the dielectric and biased to a potential of at least a few hundred volts can be used to control the lateral current distribution and the total current to the sample. If the surface potential and the compensation current into the rear electrode are continuously monitored, the equivalent surface-charge density and the conduction current through the sample can be determined during the charging process [70].

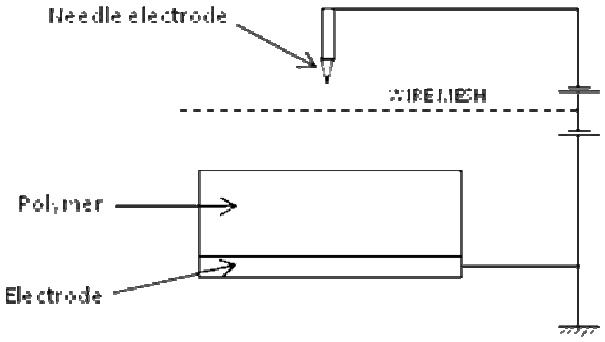

Figure 3.5. Schematization of the corona charging method.

The corona-charging method has the advantage of being simple to implement and fast to operate and, for this motives, it has been chosen as poling method to prepare electrets for this PhD activity. However, since it is performed at room temperature, this poling method produce electrets with a thermal stability inferior to that of thermo-electrets.
During the last century the preparation of electrets via poling techniques has been tested on a large amount of polymers, first of all PVDF and its copolymers [63], to prepare electrets, but more specifically piezoelectrets, in the form of sheets [71] and fibers [72].

Soft cellular electrets

A major break-through in the quest of polymer films with high piezoelectric coefficients and dielectric constants came when it was realized that a piezoelectricity-like effect can also result from electric dipoles at a macroscopic, rather than a molecular level. In 1987, in fact, a new class of polymer electrets was discovered: the foam electrets. In that year Kirjavainen and co-workers at the University of Tampere, Finland, developed a procedure for producing cellular polypropylene films [73] and few years later they charged the internal voids through corona poling [74]. This study soon opened the way for a new series of experiments with different polymers, PP initially, then PVDF, PTFE and PVC. They demonstrated that after the application of a high external electric field, cavities inside the polymer, due to the Paschen breakdown effect, became macrodipoles and could retain

charge/polarization for long period of time. Applying a mechanical stress to these materials change the vertical dimensions of the voids and therefore the dipole moment of the separated +/- charges trapped on the internal surfaces. Consequently, the macroscopic polarization changes, giving rise to a quasi-piezoelectric response. The shape of the cavities can be optimized by means of inflation treatment [75] while it has been proved that biaxially stretched polymer foams are highly anisotropic media and therefore exhibit large d_{33} coefficients but small d_{31} values. Other workers in 2001 [76] investigated the influence of gas in the voids of cellular electret polymers during corona charging in order to enhance their electromechanical performances. They discovered that with elevated ambient gas pressure or with various gases of higher electrical breakdown strength inside the voids, more efficient charge separation inside the sample were possible.
As a consequence of pressure acting onto a cellular electret polymer, a charge signal q is generated on the electrodes [77]:

$$\Delta q = k\Delta F \tag{3.20}$$

$$\Delta \sigma = k\Delta p \tag{3.21}$$

where k is the sensitivity factor (C/N), F is the acting dynamic force (N), p the active dynamic pressure (N/m^2) and σ is the generated charge per unit area (C/m^2).
Similarly to piezoelectric systems, electret polymers produces an electric signal if compressed, being the electric signal linearly dependent by the applied force, and they are suited for dynamic response in the sensor mode (see §2.2.1) but their charge response is related to their voided structure, not to the piezoelectricity of the material. A table of the main parameters characterising the behaviour of piezoelectric and electret material is here reported.

	Sensitivity [pC/N]	**Dielectr.const.** @1Hz	**Density** [g/cm^3]
PVDF	d_{31}=28	12	1.76
Poled PVDF	d_{31}=60	10	1.76
PP	d_{31}<5	2.25	0.90
Foam poled PP	d_{33}=25÷250	1.6	0.55

Table 3.3. comparison of some electret material [78a,b].

The formation of foam structure in polymers

A foamed polymer can be understood as a structure of two phases: the gas and the polymer. To make the phases in a uniform, homogeneous order a third solid component, the nucleator, is significant.
Foaming methods can be divided into chemical and physical foaming. In chemical foaming chemical nucleating agents are added in melt polymer and foaming gas is produced by decomposition of the nucleator at a certain temperature, for example using microwave-activation [79]. Is this the case of polyurethanes that foam by adding water in the components before the cure. Water, reacting with isocyanate groups, forms carbon dioxide that remains trapped inside the matrix giving rise to bubbles. In physical foaming the polymer is saturated with external gas or filled with solids inclusions removed by solvents [80] or mechanical pressure [81].

Generally the polymer and the foaming agent are mixed together and then the nucleator is added (batch foaming), but also a procedure consisting in the simultaneous mixing of the three components is allowed (continuous foaming), depending on the desired final product.

The ***formation*** of foam structures can be illustrated as a three stage process where:

1. foam-cells are created as a result of chemical reaction of the nucleating agents or as a results of gas dissolved into the polymer (bubble nucleation)
2. foam-cells grow or decrease as a result of external pressure or diffusion of the gas from the polymer into the foam bubble at increased temperature or fading of suited inclusions (bubble conversion)
3. foam structure is balanced by cooling the structure (foam stabilization).

The use of the terms foam "bubble" and foam "cell" is introduced in the literature sometimes inconsistently many times with the same meaning. In this study general distinction is made and foam cell is discussed when unstabilized foam embryos is considered. When the foam cell is stabilized, it is considered to be a foam bubble.
A foam-cell can be generated in a polymer by two main processes:

- self-nucleation, when nucleation occurs as a result of gas dissolved in homogenous polymer phase (physical foaming)
- heterogeneous nucleation with nucleators, where chemical nucleators produce gas decomposition (chemical foaming).

Self nucleation generally causes trouble in foam control. The foam structure includes large foam bubbles which are far apart form each other. Heterogeneous nucleation, instead, produces more homogeneous bubbles and foaming occurs at low gas concentrations. The activation energy barrier, as reported in the following, is much lower in heterogeneous nucleation compared to self-nucleation.

Gibbs free energy for homogeneous nucleation is [82]:

$$\Delta G^*_{\text{hom}} = \frac{16\pi\gamma_{bp}^3}{3\Delta P^2} \tag{3.22}$$

where γ_{bp} is the surface energy of the foam bubble polymer interface and ΔP is the pressure of the gas in the cell.
Gibbs free energy for heterogeneous nucleation can be introduced as [82]:

$$\Delta G^*_{het} = \Delta G^*_{\text{hom}} \cdot S(\theta) \tag{3.23}$$

where S(θ) is the contact angle between particle nucleator and gas; it receives values less than 1 and depends on the wetting angle of the third phase.
With the assumption of Eqs.(3.22) and (3.23), the formation of one single cell always increase the system free energy ΔF and decrease in surface tension lowers the energy needed for bubble formation. On the other hand, tightly packed microcellular foam structure is more unstable compared to sparse big bubbled foam [83].

Another equation which favours the collapse of the foam-cells and thus the formation of larger foam bubbles is expressed as follow:

$$\Delta p_{12} = \frac{2\gamma}{\frac{1}{r_1} - \frac{1}{r_2}} \tag{3.24}$$

where r_1 is the radius of foam cell 1, r_2 is the radius of foam cell 2, and Δp_{12} is the pressure difference between cells 1 and 2. According to Eq.(3.24) the gas pressure at equilibrium in the smaller cell is higher compared to the larger one favouring the diffusion of the gas into the larger cell. A lot of chemical and physical processes affect bubble formation, a part of them is treated in [83, 84, 85, 86, 87].

When the external pressure of the saturated polymer is reduced the foam cells start to *grow* rapidly. The bubble growth will be governed by the rate of diffusion of dissolved gas to the polymer-gas interface r_1 as well a by the degree of supersaturation and viscosity of the melt. Effectiveness of the diffusion is heavily temperature dependent and it can be described with Arrhenius equation:

$$D = D_0 \exp(-E_D / RT) \tag{3.25}$$

where D is the diffusion coefficient, D_0 the material dependent diffusion coefficient, E_D the activation energy in diffusion, R the ideal gas law constant and T the temperature.

The concentration of the gas has almost no effect on diffusion in solid polymers because of low interaction and solubility between gas and polymer. Solubility is considerably increased in molten polymers (extrusion foaming). Molecular size, shape and reactivity of the gas has a major influence on diffusion [88, 89], along with the viscosity of the polymer: at high temperature or with low viscosities the expansion of the cells is more complete [84].

According to Han [90], when the saturation pressure is increased, the growth of the foam bubbles is increased, because of the pressure inside the cell seeks equilibrium with the outer gas pressure.

$$\Delta p = 2\sigma / r \tag{3.26}$$

where p represent the difference between the pressure inside the foam bubble and the pressure in the polymer melt, σ is the surface tension of the bubble inner circle and r the radius of the foam bubble.

Beckman et al. [91] have shown that the foam bubble can be decreased by increased saturation pressure in batch foaming with supercritical carbon dioxide. The increase in saturation pressure favours homogeneous nucleation and smaller foam bubbles can be achieved. They also showed bigger and fewer cell generation with short saturation time.

In the foaming of molten polymers smaller bubbles can be achieved by heterogeneous nucleation and the increase in saturation pressure leads to increased bubble growth [90].

Concerning foam *stability*, it is well known that foaming in polymers, unlike in liquids, is more hindered due to a viscoelastic behaviour and a structure that an be “frozen” by lowering the temperature. In the first stage of growing , the bubbles are circular, but when the foam extent is more than 74% the wall of the bubbles start to change their shape and

the structure becomes like a honeycomb (hexagonal packing). The dimension of the structure and the amount of polymer phase can be described by the wall thickness δ (distance between two adjacent bubbles), the average length a (hexagon side) and the Plateau corner radius r (hexagon radius) [92].

$$\frac{\sigma}{r} = \frac{A}{\delta^3} \tag{3.27}$$

with A = Hamaker constant.

Surface active additives and surface effects play an important role in foam stabilization. The effect of surface active additives is based on their movement from lower surface energy areas to higher ones during bubble growth. They form a thin interface between foam bubble and polymer. The growing of the foam bubbles lowers the surface active additive concentration on the surface leading to increased surface tension, which stabilises the foam structure [83].

According to the system free energy the energy barrier of the cell nucleation can be lowered by lowering the surface tension in the interface between the nucleator and the polymer. In three phase polymer foaming the solid particle nucleators should not be wetted by the polymer. If the polymer wets the particle, gas will not create a bubble on the surface. But if the particle is treated with a surface active additive which lowers the interface of particle and polymer, the gas will form a bubble so that the surface active layer spreads along the surface of the growing cell [93].

Fluorocarbon (CFC) foaming agent, prohibited by the European Community, have been recently replaced inert gases such as nitrogen or carbon dioxide [94]. Han [90] showed the effect of polymer malt pressure on solubility of gases at different temperature and demonstrated that the increase of the polymer melt pressure in extrusion foaming cause more complete dissolving of foaming gas in polymer.

Nucleation agents instead, used in heterogeneous foaming are mainly chemical ,nucleators and particles. The most widely used are azo-compounds, which decompose exothermically.

The advantage of endothermally decomposive bicarbonate and citric acid compounds is their temperature binding effect, which assists in receiving uniform and stabilised foam structure. Their processability in different temperatures is also wider.

Mineral particle nucleators, such as calcium-carbonate and talc powders are widely used in biaxially oriented foam films, which are also called “pearlized” or “cavitaed” structures. Pearled film is based on orientation process where the interface around the particles is stretched forming small cavities in the polymer structure. The foam extent of the film is low, but the film becomes highly opaque because of interscratches [95], like in case of VTT PP electret sheets.

3.3.1.1 An electromechanical approach

As other electroactive materials described above (§2.2.1 and §2.3.1), electrets can respond to an external mechanical stimuli with a chance in polarization and vice-versa. In

particular, considering the "actuator model", we can define the actuator sensitivity k_a as [96]:

$$k_{a=}\frac{\Delta x}{\Delta V} \tag{3.28}$$

being Δx the change in film thickness and ΔV the applied electric field. k_a can be derived by first defining the quotient

$$\frac{\Delta p_{ik}}{\Delta V}=\frac{\Delta\left(\frac{1}{2}\varepsilon_0\varepsilon_g E_{ik}^2\right)}{\Delta V} \tag{3.29}$$

where Δp_{ik} is the change in the electrical force per unit area in the kth air layer, being the electret film schematized as in the following picture.

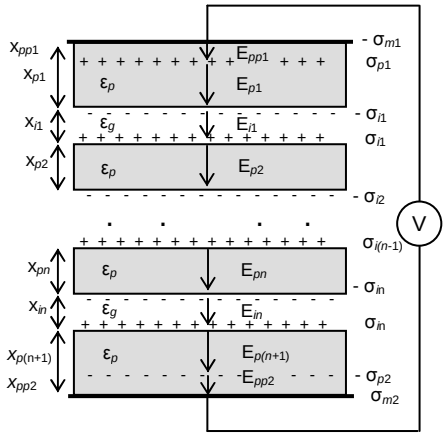

Figure 3.6. Schematic picture of a multiple air gap structure for a corona charged cellular film.

For the short-circuited film, Gauss' law can be used to form the following equations:

$$\begin{cases} \varepsilon_0\varepsilon_p E_{pp1}-0=-\sigma_{ml} \\ \varepsilon_0\varepsilon_p E_{p1}-\varepsilon_0\varepsilon_p E_{pp1}=-\sigma_{pl} \\ \varepsilon_0\varepsilon_g E_{1l}-\varepsilon_0\varepsilon_p E_{p1}=-\sigma_{il} \\ \ldots \\ \varepsilon_0\varepsilon_p E_{p(n+1)}-\varepsilon_0\varepsilon_g E_{in}=\sigma_{in} \\ \varepsilon_0\varepsilon_p E_{pp2}-\varepsilon_0\varepsilon_p E_{p(n+1)}=-\sigma_{p2} \\ 0-\varepsilon_0\varepsilon_p E_{pp2}=\sigma_{m2} \end{cases} \tag{3.30}$$

The potential difference between the film surfaces can be derived according to Kirchhoff's second law:

$$E_{pp1}x_{pp1}E_{p1}(x_{p1}-x_{pp1})+\sum_{j=1}^{n}E_{ij}x_{ij}+E_{pp2}x_{pp2}+E_{p(n+1)}(x_{p(n+1)}-x_{pp2})+E_{pp2}x_{pp2}=V \tag{3.31}$$

Using Eqs.(3.30) and (3.31), the electric field for the kth air layer can be written as

$$E_{ik} = \frac{\varepsilon_0 \varepsilon_p V + x_{pp1}\sigma_{p1} + x_{pp2}\sigma_{p2} + \varepsilon_p \sum_{j=1}^{n} x_{ij}\sigma_{ij}}{\varepsilon_0 \varepsilon_p \sum_{j=1}^{n} x_{ij} + \varepsilon_0 \sum_{j=1}^{n+1} x_{pj}} - \frac{\sigma_{ik}}{\varepsilon_0} \tag{3.32}$$

By differentiating p_{ik} in respect to V and assuming that the relative thickness changes in air voids are equal, the actuator sensitivity k_a is given by

$$k_a = \frac{\Delta x}{\Delta V} = \frac{x_0}{Y} \frac{B - \varepsilon_p \left(\sum_{j=1}^{n} x_{ij}\sigma_{ij} \sum_{j=1}^{n+1} x_{pj} \right) \left(\sum_{j=1}^{n} x_{ij} \right)^{-1}}{\left(\sum_{j=1}^{n+1} x_{pj} + \varepsilon_p \sum_{j=1}^{n} x_{ij} \right)^2} \tag{3.33}$$

where $B = \varepsilon_0 \varepsilon_p{}^2 V + \varepsilon_p x_{pp1}\sigma_{p1} + \varepsilon_p x_{pp2}\sigma_{p2}$ and $\Delta\sigma_{m1}$ is the change of the charge density on the upper electrode. The mean depths x_{pp1} and x_{pp2} of the surface charge are typically very small compared to the thickness of the polymeric layer so their effect on the actuator sensitivity appears to be negligible. Equation … can thus be reduced to

$$k_a = \frac{x_0}{Y} \frac{\varepsilon_0 \varepsilon_p^2 V - \varepsilon_p x_p \sigma_{eff}}{\left(x_p + \varepsilon_p x_i \right)^2} \tag{3.34}$$

The effective charge density σ_{eff} is the charge density on the polymer/air interfaces on both sides of the single air gap. As showed in Eq.(3.34), the sensitivity of a polymeric film, working in the actuation mode, is inversely proportional to the elastic modulus Y and directly proportional to the charge density σ_{eff} on the polymer/air interfaces, depending also on the dielectric constant of the polymer matrix ε_p, considering ε_g=1.

When an external voltage V is applied to the electrodes and increased form 0 to V, the thickness of the film changes by an amount Δx. Since the sensitivity depends on the voltage, Δx is given by

$$\Delta x = \int_0^V k_a dV = \frac{\frac{1}{2}\varepsilon_0 \varepsilon_p^2 V^2 - \varepsilon_p x_p \sigma_{eff} V}{\left(x_p + \varepsilon_p x_i \right)^2} \tag{3.35}$$

Thanks to this background on the argument, we tried to reproduce the cellular technique onto our elastomeric samples. The development of cellular polymers for electromechanical application is quite new at the moment so, after a brief research about the state of the art on the argument, we proceeded with the preparation of silicone and polyurethane rubber foams to be used as soft matrices for actuators using both the physical and the chemical foaming methods. Also commercial elastomeric foams has been used and characterized for a comparison.

3.4 New synthetic polymers

An ideal approach to obtain elastomers with specific improved dielectric properties is represented by a challenging synthesis of new molecular architectures. For instance, they might be obtained either as blends of known polymers or by copolymerisation or by grafting of highly polarisable lateral chains to existing molecules (Tab.3.1). Some of the most significant examples of methods adopted so far in order to synthesize new polymers for actuation are briefly mentioned in the following. The related most important data are reported in Tab.3.2.

Butkewisch and Scheinbeim described a thermoplastic elastomer consisting of a hydrated sulfonated poly(styrene-ethylene/buthylenes-styrene) triblock copolymer, whose dielectric constant was found to vary of four orders of magnitude (from 5 to 50000), depending on both the amount of absorbed water and the sulfonation degree of the styrene groups (Tab.3.2) [97]. Nevertheless, the authors recognised also that this kind of material was too lossy for uses in Maxwell stress actuators, due to a high hydrogen ion conductivity [97].

Another interesting method to modify the dielectric properties of elastomers is the synthesis of liquid-crystalline elastomers, i.e. elastomer chains with grafted highly-polarisable lateral groups [98]. In this type of materials the polarization phenomena can be enhanced by the rearrangement of the lateral group chains and the creation of crystalline regions [98]. Elastomers with grafted crystalline groups were also used by Su et al. [99], in order to develop blends with the electrostrictive copolymer P(VDF-TrFE) (Tab.3.2).

As a different type of material, Jung et al. [100] reported the electromechanical properties of an acrylonitrile-butadiene rubber (NBR) used for dielectric elastomer actuation (Tab.3.2); this study compared the response of NBR with different sate-of-the-art elastomers.

Blending of different polymers can result in new materials with potentially attractive properties. As an example, Huang et al. [101] proposed a blend of polyurethane and phthalocianine, which also included PAni, to obtain ε'_c~800 at 1 Hz for a 14-15-85 vol% PAni-Pc-PU composition.

As a final example, we mention here a study of Chiou et al. [102] dealing with immiscible silicone and polyurethane that formed a system with two physically interpenetrating but chemically separated phases; the system was further modified, by introducing copper-coated phospholipidic tubules, which were found to be arranged along the material interfaces or in the component having the mayor affinity. For a 50-50 vol% PU-PDMS composite filled with 16 vol% tubules, a relative dielectric constant of about 40 at 10 GHz was measured [102].

3.4.1 Polymer blending

In order to overcome restriction due to the composite approach a new technique has been recently adopted [103, 104] to improve the dielectric constant and consequently the electromechanical performance of polymers through physical blending of two or more polymers. Rather than loading the elastomeric matrix with a stiff ceramic o metallic filler, a high polarizable polymeric component is added to the matrix before the cure. A

microscopic blend is thus obtained in which the components remain physically interlaced but chemically unbounded. In order to clarify such a type of compound, the definition of the main structure arising form the mixing of two or more polymer are here reported:

Interpenetrating polymer network (IPN):
A polymer comprising two or more networks which are at least partially interlaced on a molecular scale but not covalently bonded to each other and cannot be separated unless chemical bonds are broken.
A mixture of two or more preformed polymer networks is not an IPN.
[1996, 68, 2305, IUPAC Compendium of Chemical Terminology 2nd Ed., 1997]

Semi-interpenetrating polymer network (SIPN)
A polymer comprising one or more networks and one or more linear or branched polymer(s) characterized by the penetration on a molecular scale of at least one of the networks by at least some of the linear or branched macromolecules.
Note: Semi-interpenetrating polymer networks are distinguished from interpenetrating polymer networks because the constituent linear or branched polymers can, in principle, be separated from the constituent polymer network(s) without breaking chemical bonds; they are *polymer blends*.
[1996, 68, 2305, IUPAC Compendium of Chemical Terminology 2nd Ed., 1997]

Polymer blend
A macroscopically homogeneous mixture of two or more different species of polymer.
Notes:

1. In most cases, blends are homogeneous on scales smaller than several times visual optical wavelengths.
2. For polymer blends, no account is taken of the miscibility or immiscibility of the constituent polymers, i.e. no assumption is made regarding the number of phases present.
3. The use of the term ‘polymer alloy’ for a polymer blend is discouraged [105]

More generally speaking, a polymer blend or polymer mixture is a member of a class of materials analogous to metal alloys, in which at least two polymers are blended together to create a new material with different physical properties.
Recently Vo *et al.* [106] and Todd *et al.* [107] have found and theoretically demonstrated the relationship between the interphase volume fraction and the dielectric constant in blends. In particular they found out that the interphase region between the polymeric agglomerates has dielectric properties different from those of the constituents, due to a reduced mobility of the polymeric chains in proximity of a discontinuity area and to electrostatic interaction that can increment the local polarizability. Similar results were found also for the mechanical [108], thermal [109], acoustical [110] and optical field. The amount of interphase present in a blend and the affinity of the polymeric constituents affect the overall dielectric behaviour of the blend itself.
Most known mixing rules regarding particle composites doesn’t take into account the effect of the interaction between blend constituents and this often results in bad data

modelling, as in the case of Carthy *et al.* [111] that measured dielectric constant higher than expected form theoretical models for a composite constituted by titanium dioxide powder dispersed in a poly(styrene-ethylene-butadiene-styrene) matrix. Other workers in the same years [112] demonstrated how the electronic properties of interfaces between two different solids can differ strikingly from those of the constituent materials. In particular they discovered metallic conductivity at interfaces formed by insulating transition-metal oxides.

3.4.1.1 Modeling the dielectric response of polymer blends

In 1996 Bicerano [113] proposed a series of empirical equations (obtained analysing data form several polymer; standard deviation=3%) to predict the polarization of single molecules or entire polymeric chains. Using the following equations in particular, it is possible to predict the effect of multiple chemical bonds onto the dielectric constant of the material under test:

$$\varepsilon = 1.412014 + \frac{0{,}001887E + N_{dc}}{V_W} \tag{3.36}$$

where E is the cohesive molecular energy that depends on electronic molecular polarization, N_{dc} is the permanent dipole moment of the molecule and V_W is the van der Waal's volume taken here as normalization factor.
The first to study the characteristic of the interphase instead, introducing a parameter to describe the grade of affinity between the components of the blend, were Todd and Shi [114] who developed an Interphase Power Low (IPL) model, different form the previous Lichtenecker-Rother (LR) model, based on the principle:

> The interphase region between the matrix and the filler, in a polymeric blend, is comprised of polymer molecules that are bonded or otherwise oriented at the matrix-filler interface. This restriction affects the molecule's electrical characteristics.

Differently from a common two-component power-law relationship, like the one described in Eq.(3.37),

$$\varepsilon_c^{\beta} = \phi_1 \varepsilon_1^{\beta} + (1-\phi_1)\varepsilon_3^{\beta} \tag{3.37}$$

where ε_c, ε_1, ε_3, are the complex dielectric permittivities of the composite system, the filler and the matrix respectively, ϕ_1 is the volume fraction of filler component and β is a dimensionless parameter representing the shape and orientation of the filler particles, the IPL model used here instead takes into account a third component, the interphase, whose volume is dependent upon the characteristics of the filler and matrix components, and is described by the following equation:

$$\varepsilon_c^{\beta} = \phi_1 \varepsilon_1^{\beta} + \phi_2 \varepsilon_2^{\beta} + \phi_3 \varepsilon_3^{\beta} \tag{3.38}$$

where ε_2 and ϕ_2 are the dielectric constant and volume fraction of the interphase respectively. In this equation ϕ_1 is known while $\phi_3 = [\ 1- \phi_1 - \phi_2\ ]$ and ϕ_2 is dependent upon

the filler volume fraction, the filler surface area and the thickness of the interphase region surrounding each filler particle. For monodisperse, spherical particles the interphase volume fraction ϕ_2 is given by:

$$\phi_2 = \frac{\frac{4\pi\phi_1}{3}\left[\left((r+\Delta r)^3 - r^3\right) - 6f\left(3(r+\Delta r) - \Delta r\right)\Delta r^2\right]}{r^3} \tag{3.39}$$

where r is the radius of the filler particles, Δr is the thickness of the interphase region and f is an overlap probability function that for spherical particles has the form:

$$f = \left(\frac{6\phi_1}{\pi}\right)^3 \tag{3.40}$$

with ϕ_3 filler volume fraction of the spherical particle filled composite. Approximations have been developed to estimate the overlap of such particles using Monte Carlo simulation [115] or alternately analytical solutions to percolation models [116, 117, 118], but the details of these analysis are beyond the scope of this work.

Finally the interphase power-low exponent β is a measure of the geometry of the composite medium with respect to the applied electric field and, except for the extremes values 1 (individual components oriented parallel to the electric field) and -1 (individual components oriented parallel to the electric field), it is given by:

$$\beta = 1 - 2\left[\frac{1}{1 + 1{,}6(a:b) + 0{,}4(a:b)^2}\right] \tag{3.41}$$

In Eq.(3.41) the quantity (*a:b*) is the ratio of the ellipsoid dimension a long the axis parallel to the applied field to the ellipsoid dimension along the axes perpendicular to the applied field. For a sphere, like our case, a = b and this relationship reduces to 1/3 as predicted by Landau, Lifshitz and Looyenga [119, 120].

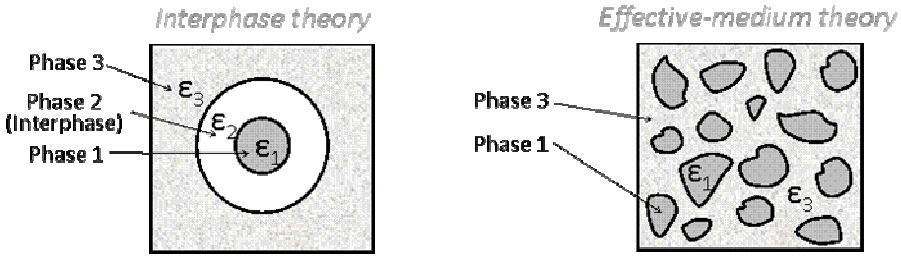

Figure 3.37. Schematic representation of the two different approaches consisting of the well known Effective Medium Theory (§3.2.1) and the new Interphase Theory.

The IPL model predicts a distinct non-linearity in the effective dielectric constant and dielectric loss as a function of filler volume loading. Since the dielectric characteristics of the interphase region contributes to the overall effective dielectric characteristics of the composite system, and the volume fraction of the interphase region changes non-linearly with the volume fraction of filler according to equations reported above, the permittivity of the composite/blend changes non-linearly as a function of filler loading. This effect is shown in Fig.3.38 in which both the effective dielectric constant and the effective dielectric

loss of a model composite system is predicted using the IPL model (Eq.(3.38)) as well as the standard two-component power low model (Eq.(3.37)).

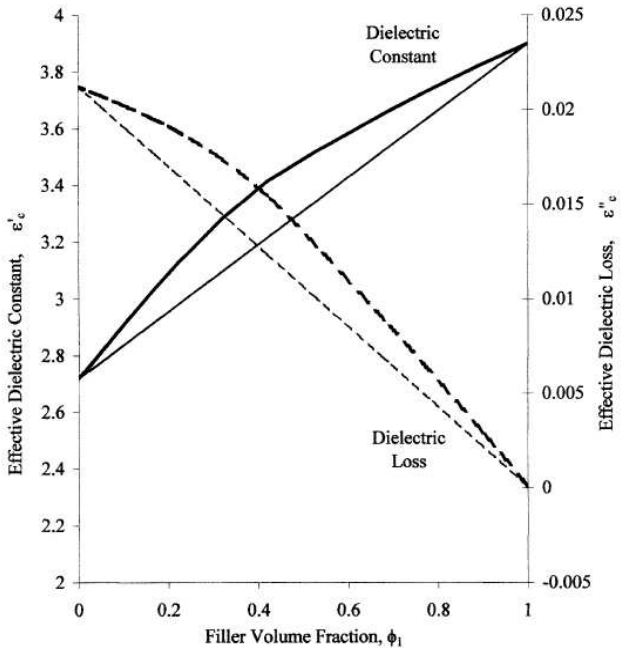

Figure 3.38. Effective dielectric constant (solid lines) and dielectric loss (dashed lines) as a function of filler volume fraction – typical power-law model predictions (light lines) and interphase power-law model predictions (bold lines).

When the interphase dielectric constant is equal to the dielectric constant of the filler and the matrix in this system, a linear prediction is generated. When the interphase dielectric constant is greater than that of the filler and matrix, a maximum is predicted at approximately 40-volume percent filler loading. The interphase region of a composite system has its own unique dielectric characteristics, therefore, the composite system may take an effective permittivity outside the range of the filler and matrix phases if the permittivity of the interphase region falls outside these bounds. The limit of the interphase permittivity deviation from that of the constituent phases is controlled by the chemical structure of the interphase region.

To more fully illustrate the capability of the IPL model to predict the permittivity of a wide range of composite systems, the following figure is reported, illustrating the full scope of possible situations for the dielectric constant of two component composites having an interphase layer.

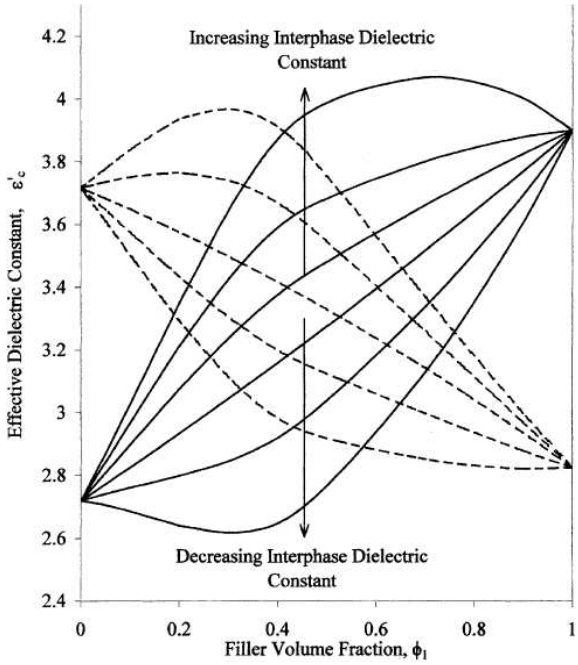

Figure 3.39. Effective dielectric constant of model composite systems as a function of filler volume fraction. Effects of increasing interphase dielectric constant and decreasing interphase dielectric constant for composite systems where $\varepsilon_1>\varepsilon_3$ (solid lines) and composite system where $\varepsilon_1<\varepsilon_3$ (dashed lines).

Analogous is effect of increasing filler surface area and interphase thickness (for an in-depth argumentation on this topic please refer to [114].

3.5 Conclusions

This chapter has presented the most followed techniques, available at present, in order to possibly enhance the dielectric permittivity of elastomers. The most significant state-of-the-art results have been reported. Random composites and field-structured composites represent readily applicable approaches suitable to actually increase the dielectric permittivity of elastomers. Nevertheless, such methods not always can guarantee a real benefit in terms of resulting electromechanical properties. In fact, the possible material stiffening plays an antagonistic role, capable in some cases of exceeding any eventual electrical improvement. As a different approach, the most challenging synthesis of new highly-polarisable polymers may offer, of course, superior opportunities, although at the price of considerably greater development times and costs. A valid alternative to the techniques cited above could be represented by the blend approach that, as shown in §3.4.1 and supported by results (Cap.6), allow to obtain discrete values of dielectric constant maintaining low losses and low elastic modulus. This represents one of the major future challenges for achieving new generations of more efficient dielectric elastomers suitable for more performing actuators, possibly requiring lower driving voltages.
Dielectric, mechanical and electromechanical results obtained during the PhD activity using the described techniques are reported in Cap.5-6 along with a validation of theoretical methods today available.

3.6 References

[1] Carpi F. *et al*, Dielectric elastomers as electromechanical transducers, Elsevier, 2008
[2] Bar-Cohen Y., Electroactive polymer (EAPs) actuators as artificial muscles, SPIE Press, 2004
[3] Perline R. E. *et al*., *Sensors and Actuators A* , 64 , 77-85, 1998
[4] Seanor D. A., Electrical Properties of Polymers, Academic Press, New York, 1982
[5] Birks J. B., Progress in Dielectrics, London Heywood & Company Ltd., 1960
[6] Gallone G. *et al*., Material Science and Engineering C, 27, 1, 110-116, 2007
[7] Szabo J. P. *et al*., in *Smart Structures and Materials 2003: Electroactive Polymer Actuators and Devices (EAPAD)*, Ed. Bar-Cohen Y., Proc. SPIE, 5051, 180-190, 2003
[8] Carpi F. *et al*., *IEEE Transactions on Dielectrics and Electrical Insulation*, 12 , 4, 2005
[9] Popierlarz R. *et al*., *Macromolecules* , 34 , 5910-5915, 2001
[10] Matsumoto M. *et al*., *IEEE Transactions on Dielectrics and Electrical Insulation*, 6, 1, 27-34, 1999
[11] Tsangaris G. M. *et al*., *Material Chemistry and Physics*, 44 , 245-250, 1996
[12] Chiou B. et al., *Journal of Applied Polymer Science*, 89 , 1032-1038, 2003
[13] Cameron C. G. *et al*., in *Smart Structures and Materials 2004: Electroactive Polymer Actuators and Devices (EAPAD)*, Ed. Bar-Cohen Y., 5385 , 51-59, 2004
[14] Benguigui L. *et al*., Journal of Polymer Science Polymer Physics, 25, 127-135, 1987
[15] Foulger S. H., Journal of Applied Polymer Science, 72, 1573-1582, 1999
[16] Kim B. et al., Journal of Applied Physics, 94 , 10, 2003
[17] Potschke P. *et al*., *Polymer*, 44 , 5023-5030, 2003
[18] Zhang X. Q. *et al*., in *Smart Structure and Materials 2004: Electroactive Polymer Actuators and Devices (EAPAD)*, Ed. Bar-Cohen Y., Proc. SPIE, 5385, 78–86, 2004
[19] Zhang Q. M. *et al*., *Nature*, 419, 284-287, 2002
[20] Huang C. *et al*., Applied Physics Letters, 84 , 22, 2004
[21] Chwang C. *et al*., *Synthetic Metals*, 142, 275-281, 2003
[22] Huang C. *et al*., in *Smart Structure and Materials 2004: Electroactive Polymer Actuators and Devices (EAPAD)* , Ed. Bar-Cohen Y., Proc. SPIE, 5385, 87-98, 2004
[23] Li J. *et al*., *Applied Physical Letters*, 84, 16, 2004
[24] Liu B. *et al*., *Journal of Rheology*, 45, 3, 641-657, 2001
[25] Khastgir D. *et al*., *Journal of Polymer Science Polymer Physics*, 37, 3065-3070, 1999
[26] Wilson S. A. *et al*., *Journal of Physics Applied Physics*, 38, 175-182, 2005
[27] Butkewitsch S. *et al*., *Applied Surface Science*, 252, 8277-8286, 2006
[28] Lehmann W. *et al*., *Nature*, 410 , 22, 2001
[29] Su J. *et al*., in *Smart Structure and Materials 2000: Electroactive Polymer Actuators and Devices (EAPAD)*, Ed. Bar-Cohen Y., Proc. SPIE 3987, 65-72, 2000
[30] Jung K. *et al*., *Smart Material Structures*, 16 , S288-S294, 2007
[31] Van Beek L. K. H., in Progress in Dielectrics, Vol. 7, Eds. Birks J. B. London Heywood Books, New York, pp. 69-114, 1967
[32] Nalwa H. S., Ferroelectric Polymers, Marcel Dekker Press Inc., New York, 1995

[33] Böttcher C. J. F. *et al*., Theory of Electric Polarization, 2nd edn, Elsevier Press, New York, 1978
[34] Landau L. D. *et al*., Electrodynamics of Continuous Media, 2nd edn, Pergamon Press, New York, 1984
[35] Sillars R., *Journal of Institution of Electrical Engineers*, 80, 378, 1937
[36] Tuncer E. *et al*., Applied Physics, 89, 12, 8092, 2001
[37] Maxwell-Garnett J. C., Philosophy Transactions Royal Society of the London A, 203, 385, 1904
[38] Maxwell-Garnett J. C., Philosophy Transactions Royal Society of the London A, 205, 237, 1906
[39] Smith G. B., Journal of Physics D Applied Physics, 10, L39, 1977
[40] Shalev V. M., Physical Reports, 272, 61, 1996
[41] Maxwell J. C., Electricity and Magnetism, Clarendon Press, New York, 1892
[42] Wagner K. W., *Archiv für Elektrotechnik*, 2, 378, 1914
[43] Wagner K. W., Die Isolierstoffe der Elektrotechnik, Ed. Schering, H. Springer Press, New York, 1924
[44] Rayleigh J. W., *Philosophical Magazine*, 5, 34, 481, 1892
[45] Nelson S. O. *et al*., *Journal of Physics D Applied Physics*, 23, 346, 1990
[46] Shen L. C. *et al*., *Geophysics*, 50, 4 , 692, 1985
[47] Jayasundere N. *et al*., *Journal of Applied Physics*, 73, 5 , 2462, 1993
[48] Landauer R., *Journal of Applied Physics*, 23, 779, 1952
[49] Sihvola A. H. *et al*., *Journal of Physics D Applied Physics*, 29, 514, 1996
[50] Bruggeman V. D. A. G., *Annalen der Physik*, 5, 24, 636, 1935
[51] O'Konski C. T., *Journal of Physical Chemistry*, 64, 605, 1960
[52] Wilson S. A. *et al*., *Journal of Physics D Applied Physics*, 38, 175, 2005
[53] Vo H. T. *et al*., *Microelectronics Journal*, 33, 409-415, 2002
[54] Mazur K. in Ferroelectric Polymers, Ed. Nalwa, H.S. Marcel Dekker Inc., New York, pp.539-610, 1995
[55] Carmona F. *et al*., *Journal of Physique Letters*, 41, L531-L534, 1980
[56] Dang Z. *et al*., *Applied Physical Letters*, 81, 25, 4814-4816, 2002
[57] Nan C., *Progress in Material Science*, 37, 1, 1-116, 1993
[58] Zucolotto V. *et al*., Polymer Composites, 25, 6, 2004
[59] Carpi F., On the dielectric strength of insulating elastomers for Maxwell-stress actuators, unpublished work under revision
[60] Mc Pherson J. *et al*., Applied Physical Letters, 82, 13, 2121-2123, 2003
[61] Blythe A. R., Dielectric breakdown. Electrical Properties of Polymers, Cambridge University Press, New York, p.140, 1979
[62] Blythe A. R., Dielectrics in static field. Electrical Properties of Polymers, Cambridge University Press, New York, p.15, 1979
[63] Sessler G. M., Electrets, Springer-Verlag, 1980
[64] Seanor D. A., Electrical properties of polymers, Academic Press New York, 1982
[65] James E. M., Physical properties of polymers Handbook, Springer Ed, 2007
[66] Gray, *Philosophy Transactions of the Royal Society of London A*, 37, 285, 1732

[67] Faraday M., Experimental Researches in electricity, Richard and John Edward Taylor, London, 1939
[68] Heaviside O., Electromagnetic induction and its propagation, Electrization and electrification, Natural Electrets, The Electrician, pp.230-231, 1885
[69] Eguchi M., *Proceedings on Physical and Mathematical Society Japan*, 3, 1, 326-331, 1919
[70] Moreno R. A. *et al*., *Journal of Applied Physics*, 47, 3397-402, 1976
[71] Wegener M. *et al*., *Journal of Applied Physics*, 12, 92, 2002
[72] Wegener M. *et al*., *IEEE Tansaction on Ultrasonics, Ferroelectrics, and Frequency Control*, 50, 7, 2003
[73] Kirjiavainen K., US Patent, 4,654,546, 1987
[74] Paajanen M., *Sensor and Actuators*, 84, 95-102, 2000
[75] Wegener M. *et al*., *Journal of Physics D: Applied Physics*, 37, 623-627, 2004
[76] Paajanen M. *et al*., *Journal of Physics D: Applied Physics*, 34, 16, 2001
[77] Pajaanen M. *et al*., *Sensors and Actuators A: Physical*, 84, 1-2, 2000
[78a] Das-Gupta D. K., in Molecular electronics, ed. M.C.Petty, M.R.Bryce, and D.Bloor, Edward Arnold, London, Melbourne, Aukland, pp.47-71, 1995
[78b] Davis G. T. *et al*., *Macromolecules*, 15, 329-333, 1982
[79] Lewis L. N. *et al*., US Patent, 5,438,081, 1995
[80] Venkatram P. S. *et al*., PNAS, 97, 5, 1970-1975, 2000
[81] Ferguson T. W. *et al*., US Patent, 6,818,673 B2, 2004
[82] Colton J. S. *et al*., *Polymer Engineering and Science*, 7, 27, 1987
[83] Klempner D. *et al*., Handbook of polymeric foams and foam technology, Hanser, 1-46, 187-242, 1991
[84] Lee S. T. *et al*, *Polymer Engineering and Science*, 12, 29, 1989
[85] Isayev A. I. *et al*., *Polymer Engineering and Science*, 14, 31, 1991
[86] Pham T. A., International Patent n.WO90/0880, 1990
[87] Ramesh, N. S. *et al*., *Polymer Engineering and Science*, 22, 34, 1994
[88] Krevelen D. W., Properties of polymers, their estimations and correlations with chemical structure, Amsterdam, 1980
[89] Stuck L. G. F., *Journal of Polymer Science Part B: Polymer Physics*, 27, 1989
[90] Han C. D., Multiphase flow in polymer processing, 1981
[91] Goel S. K. *et al*., *Polymer Engineering and Science*, 14, 34, 1994
[92] Kraynik A. M. *et al*., *Journal of Rehology*, 31, 175-205, 1987
[93] Bikerman J. J., Foams, New York, Sprimger Verlag Ltd., 1973
[94] Dwyer F. J. *et al*., *Plastics Engineering*, 29-32, 1990
[95] Nago S. *et al*., *Journal of Applied Polymer Science*, 45, 1527-1535, 1992
[96] Paajanen M. *et al*., *IEEE Transaction on Dielectrics and Electrical Insulation*, 8, 4, 2001
[97] Butkewitsch S. *et al*., *Applied Surface Science*, 252 , 8277-8286, 2006
[98] Lehmann W. *et al*., *Nature*, 410, 22, 2001
[99] Su J. *et al*., in *Smart Structure and Materials 2000: Electroactive Polymer Actuators and Devices (EAPAD)*, Ed. Bar-Cohen, Y., Proc. SPIE, 3987, 65-72, 2000

[100] Jung K. *et al*., *Smart Materials and Structures* , 16, S288-S294, 2007
[101] Huang C.*et al*., *Applied Physical Letters*, 84 22, 2004
[102] Chiou B. *et al*., *Journal of Applied Polymer Science*, 89, 1032-1038, 2003
[103] Carpi F. *et al*., *Advanced Functional Materials*, 18, 2, 234-241, 2008
[104] Gallone G. *et al*., *Polymer International*, 59, 400-406, 2010
[105] 1996, 68, 2305, IUPAC Compendium of Chemical Terminology 2nd Ed., 1997
[106] Vo H. *et al*., *Microelectronic Journal*, 33, 5, 409-415, 2002
[107] Todd M. G. *et al*., *Journal of Applied Physics*, 94, 7, 2003
[108] Veenstra H. *et al*., *Polymer*, 41, 1817-1826, 2000
[109] Samvedi V. *et al*., *Nanotechnology*, 20, 36, 2009
[110] Zhang Q. *et al*., *Japanese Journal of Applied Physics*, 36, 6853-6861, 1997
[111] Mc Carthy D. N. *et al*., *Actuator 2008, 11th International conference on new actuators*, Bremen, 2008
[112] Alves H. *et al*., *Nature Materials*, 2205, 2008
[113] Bicerano J., Prediction of Polymer properties, 2nd ed., New York, Marcel Dekker Inc., 1996
[114] Todd M. G. *et al*., *IEEE Transaction on dielectrics and Electrical Insulation*, 12, 3, 2005
[115] Pike G. *et al*., *Phisical Reviews B*, 10, 1421-1434, 1974
[116] Yi Y. *et al*., *Physical Review E*, 66, 2002
[117] Kuo C. *et al*., *Acta Metallurgica et Materialia*, 43, 397-403, 1995
[118] Wang S. *et al*., *Composites Science and Technology*, 46, 93-103, 1993

II
Experimental Part

Chapter 4

Energy generation and storage

Materials, experimental procedures, results and discussion

4.1 Materials

In order to generate electrical energy from human movements, two electroactive materials were identified for their excellent energy conversion capability and their good mechanical properties, as abrasion resistance, tenacity and suitability to be produced in different shapes. They are the commercial piezoelectric poly(vinylidene fluoride) (PVDF) by *MSI - Measurement Specialities Inc.* [1] and the electret polypropylene (PP Emfit film) by *Emfit Ltd* [2]. For a in-depth argumentation on this materials please refer to §2.3.2 and §3.3.1.
The PVDF film was purchased with silver electrodes included, while electret PP had not metallic electrodes. For this motive, a silver paint (Electrodag® PF-418 by *Acheson Industries Ltd.* [3]) was bought and airbrushed onto the electret PP film that was finally coated with a shielding dielectric ink (Electrodag® PF-455 by *Acheson Industries* [3]) in order to improve the mechanical resistance of the sample.
The selected materials, opportunely shaped, were used to perform preliminary tests of energy transduction and to develop a first prototype of wearable converter inserted in a shoe and able to collect charges and switch on a LED during the human walk.
With respect to the results obtained during the PhD activity, it will be possible to design and develop new configurations and materials suited for wearable applications and optimized in order to maximize the conversion of mechanical-to-electrical energy.

4.1.1 Poly(vinylidene fluoride)

The PVDF piezo film by MSI is a flexible, lightweight, tough engineering plastic available in a wide variety of thicknesses and large areas.

Figure 4.1. PVDF sample by *MSI* as received.

Its properties, as a transducer, include:

- Wide frequency range - 0.001 Hz to 10^9 Hz
- Vast dynamic range (10^{-8} to 10^6 psi or 10^{-6} torr to 10^3 bar)

- Low acoustic impedance
- High elastic compliance
- High voltage output - 10 times higher than piezo ceramics for the same force input
- High dielectric strength - withstanding strong fields (75 V/μm) where most piezo ceramics depolarize.
- High mechanical strength and impact resistance (10^9 - 10^{10} Pascal modulus).
- High stability - resisting moisture (<0.02% moisture absorption), most chemicals, oxidants, and intense ultraviolet and nuclear radiation.
- Can be fabricated into unusual designs.

One major advantage of piezo film over piezo ceramic is its low acoustic impedance which is closer to that of water, human tissue and other organic materials. For example, the acoustic impedance ($Z_0=\rho\upsilon$) of piezo film is only 2.6 times that of water, whereas piezo ceramics are typically 11 times greater. A close impedance match permits more efficient transduction of acoustic signals in water and tissue.

Piezo film does have some limitations for certain applications. It makes a relatively weak electromechanical transmitter when compared to ceramics, particularly at resonance and in low frequency applications. The copolymer film has maximum operating/storage temperatures as high as 135 °C, while PVDF is not recommended for use or storage above 100 °C. Also, if the electrodes on the film are exposed, the sensor can be sensitive to electromagnetic radiation. Good shielding techniques are available for high EMI/RFI environments.

PVDF piezo film has low density and excellent sensitivity, and is mechanically tough. The compliance of piezo film is 10 times greater than the compliance of ceramics. When extruded into thin film, piezoelectric polymers can be directly attached to a structure without disturbing its mechanical motion. Piezo film is well suited to strain sensing applications requiring very wide bandwidth and high sensitivity. As an actuator, the polymer's low acoustic impedance permits the efficient transfer of a broadband of energy into air and other gases.

In the following, a summering table collecting the main properties of the PVDF used for the first tests, is reported.

Property	**Value**	**Units**
t	52, 110	10^{-6} m
d_{31}	23	10^{-12} C/N
d_{33}	-33	10^{-12} C/N
k_{31}	12	%
Y	3	10^9 N/m^2
ε	12	-
ρ	1,78	10^3 Kg/m^3
Electrodes	Ag ink	-
Producer	Measurement Specialities Inc.(*MSI*) 1000 Lucas Way, Hampton, VA 23666 www.meas-spec.com	
Contact	robin.fletcher@meas-spec.com	

Table 4.1. General properties of PVDF piezo film by *MSI*.

4.1.2 Electret Polypropylene foam

The electret film by Emfit is based on a polyolefin material, isotactic polypropylene (PP), manufactured in a continuous biaxial orientation process that stretches the film in two perpendicular directions (machine direction and the transverse direction). The structure of Emfit film consists of flat voids separated by thin polyolefin layers. The voids are made by compounding small particles, usually mineral particles (for example calcium-carbonate and talc powder), which functions as rupture nuclei and form closed lens-like cavities to the film during the biaxial orientation. The biaxially oriented film is further swelled with patented high-pressure gas injection technology. The swelling process more than doubles the thickness and elasticity of the film by increasing the size of air-voids inside it. Electromechanical response with properly swelled cellular film is over 10-fold compared to the situation where the film is charged before swelling.
Operating in a reciprocal fashion, changes in thickness of the Emfit film generate a corresponding charge and hence, voltage to appear on the electrodes. The transducers behaves like an "active" capacitor, consequently, the loading of the signal by the input impedance of the measuring device must be considered.

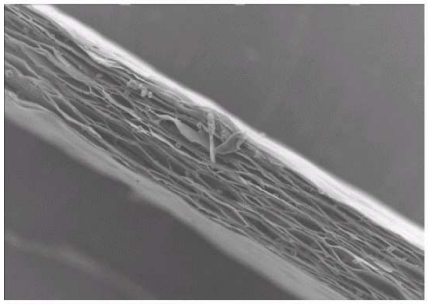

Figure 4.2. SEM micrography of section of electret PP film by *Emfit*.

In the following, a summering table collecting the main properties of the electret PP used for the first tests, is reported:

Property	**Value**	**Units**
t	70	10^{-6} m
d_{33}	25-250	10^{-12} C/N
Y	0,5	10^{6} N/m^2
ε	1,6	-
ρ	0.7	10^{3} Kg/m^3
Sensibility	> 100	N/cm^2
Electrodes	none	-
Producer	Emfit Ltd. Konttisentie 8B, 40800 Vaajakoski,FIN www.emfit.com	
Contact	heikki.raisanen@emfit.com	

Table 4.2. General properties of electret PP cellular film by *Emfit*.

4.1.3 Silver ink

Electrodag 418 SS™ conductive screen printable ink by Acheson consists of very finely divided silver particles in a thermoplastic resin. It is specifically designed for use in the production of low voltage circuitry on flexible substrates such as polycarbonate and as a cross-over on UV-curable dielectric inks, but may also be used on PVC and other solvent sensitive substrates.
Typical applications include membrane touch switches, keyboards, heating elements, flexible circuitry and shielding against electromagnetic interference.
It shows different advantages including:

- it is applicable with manual, semi-automatic and high speed screen printing equipment. For this PhD activity an air-brush was used
- It has a good screen residence time
- It has good mechanical strength at low temperatures and drying cycles
- It is compatible with polycarbonate film, polyester film, PVC-film, paper and cardboard.

In the following, a summering table collecting the main properties of the silver ink used for the first tests, is reported:

Property	**Value**	**Units**
Sol. content	65,5 – 67,5	%
Appearance	Silver	-
Viscosity	10.000 – 30.000	10^{-3} Pa·s
Density	2	10^{3} Kg/m^{3}
Coverage	15	m^{2}/Kg at 10 μm
Reccommended thickness	8 -12	10^{-6} m
Cure	80 – 140	°C (15 min)
Solvent	MEK, acetone etc	-
Resistivity	< 0,03	Ohm/square/25 μm
Producer	Acheson Industries Ltd. 9679 ZG Scheemda, Netherlands www.achesonindustries.com	

Table 4.3. General properties of the Electrodag 418 SS™ silver ink by *Acheson Industries Ltd*.

4.1.4 Dielectric ink

Electrodag PF-455B™ dielectric ink by Acheson consists of an acrylate paint with superior humidity resistance. It is supplied ready for use and does not require dilution. Typical applications include insulating crossovers. It shows different advantages including:

- Non-conductive
- Excellent humidity resistance
- Excellent printability
- Fast UV cure
- Excellent adhesion
- Good dielectric strength

The main product characteristics are summarized in the following table.

Property	**Value**	**Units**
Appearance	Translucent green	-
Viscosity	13.500	10^{-3} Pa·s
Density	1,02	10^{3} Kg/m^3
Coverage	98	m^2/Kg at 10 μm
Breakdown Voltage	2.500 – 3.000	V/25μm AC
Cure	0,5	J/cm^2 (UV light)
Solvent	MEK, acetone etc	-
Resistivity	> $2 \cdot 10^9$	Ohm/square/25 μm
Producer	Acheson Industries Ltd. 9679 ZG Scheemda, Netherlands www.achesonindustries.com	

Table 4.4. General properties of the Electrodag PF-455B™ dielectric ink by *Acheson Industries Ltd*.

4.2 Experimental procedures

After the first couple of months dedicated to the research of suitable materials and the study of the state of the art regarding the techniques today available to generate and harvest energy using wearable devices (Cap.1), the experimental activity began. The main steps of the work have been, in order:

1. Chemical-physical characterization of the material as received
2. Identification of the most suitable place to put the transduction devices
3. Designing of the most efficient configuration
4. Cut and shape of the materials as supplied
    - Electrodes deposition
    - Electric contact settings
    - Electrode shielding
    - Insertion into the shoe
5. Electro-mechanical in-lab tests (validation of theoretical models)
6. Electro-mechanical worn tests.

4.2.1 Chemical-physical characterization of the materials as received

In order to verify the effective crystallinity of the PVDF film, before to start with electromechanical tests, both X-Ray diffractometry (XRD) and Differential Scanning Calorimetry (DSC) were performed on samples with different thicknesses. The results are reported below.

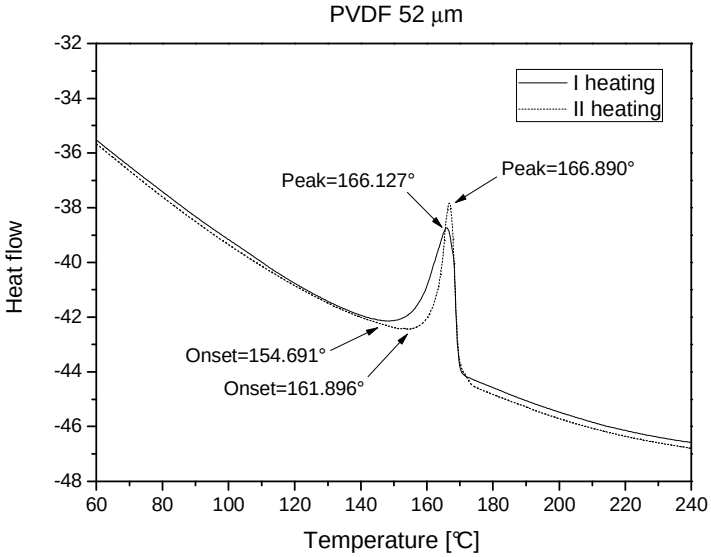

Figure 4.3. DSC analysis of PVDF film (110μm thickness).

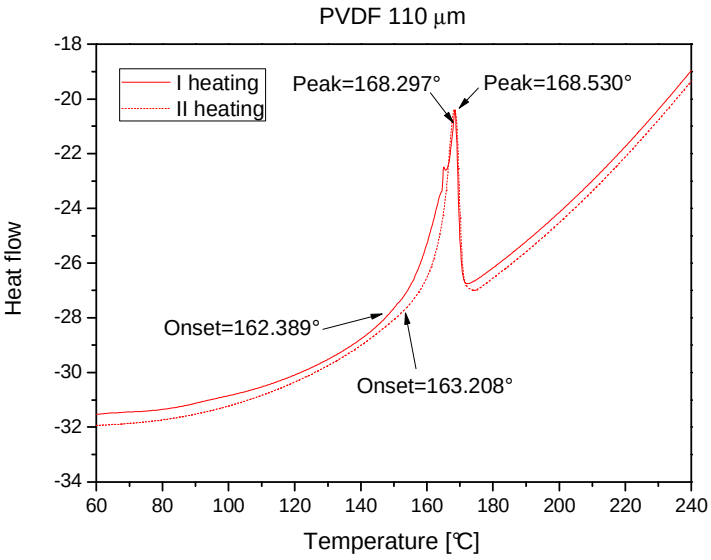

Figure 4.4. DSC analysis of PVDF film (52μm thickness).

As shown in the Fig.4.3 and 4.4 (data collected with a Q200 Differential Scanning Calorimeter by *TA Instrument*), no substantial differences exist between the two PVDF films with different thickness. Just a small peak appears at 165° for the PVDF film 110μm thick, probably arising form a small amount of non-polar α phase left. As it known in fact, a PVDF film, in order to become piezoelectric, had to be heated and polarized under high electric field while it is contemporarily stretched to align dipoles. This type of treatment produces a crystalline polarized PVDF phase called β phase. Other phases (α and γ

phases), not crystalline and not polarized, are not piezoelectric. For this motive, the peak at about 165° for the PVDF 110 μm film could be due to a non perfect conversion of α phase into β phase since thicker films are subjected to a small amount of stretching cycles with respect to the thinner ones (52 μm). In order to assure the presence of the crystalline β phase for the PVDF we proceeded carrying on X-Ray Diffractometry on samples. The results obtained are reported below.

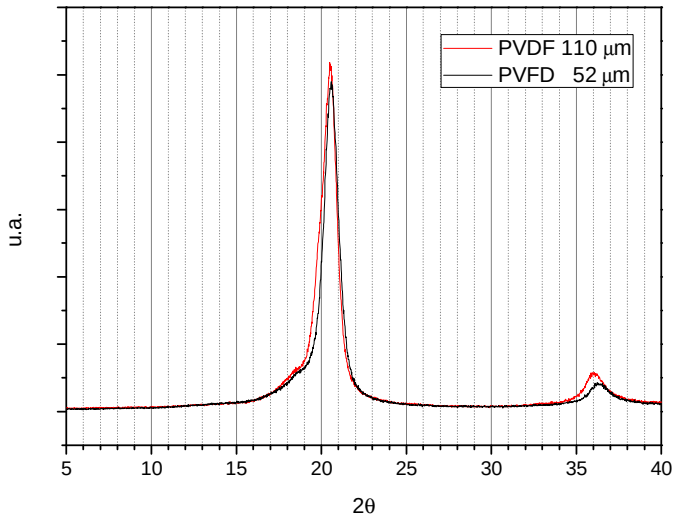

Figure 4.5. X-Ray analysis of PVDF films with different thickness.

The graph reported in Fig.4.5, obtained with a Kristalloflex 810 spectrometer from Siemens [4], confirm what obtained with the thermal calorimetry, that is: no substantial differences exist between the PVDF films with different thickness. Thanks to the Bragg law, a comparison between the theoretical and experimental diffractive angles has been done and the results obtained are reported in the following (Tab. 4.6-4.8).
When a monochromatic X-Ray beam (35 kV) of wavelength λ (0,5÷2,5 Å in this case) hits a crystal, constructive interference can be generated if the incidence angle is a particular angle called θ, which varies in relation to the interplanar distance inside the crystal. Indicated with the Miller indices (*hkl*) the set of parallel diffractive crystal planes [5], the Bragg law states:

$$n\lambda = 2d_{hkl}\sin\theta \qquad (4.1)$$

where n is the diffraction order. As mentioned earlier, PVDF has three main phases, α (orthorhombic), β (orthorhombic) and γ (monoclinic). Their lattice constants (Tab.4.5) and the mathematical procedure (Eq.(4.2)) to obtain the θ angle are report below.

Phase	***a* [Å]**	***b* [Å]**	***c* [Å]**
α	8.58	4.91	2.56
β	4.96	9.64	4.96
γ	4.96	9.58	9.23

Table 4.5. Lattice constants for the three PVDF phases [5].

The orthorhombic lattice planes responsible for the diffraction are (*2 0 0*), (*0 2 0*), (*0 0 2*) and (*1 1 1*) and they are related to *d* through:

$$\frac{1}{d_{hkl}^2} = \frac{h^2}{a^2} + \frac{k^2}{b^2} + \frac{l^2}{c^2} \tag{4.2}$$

The *d* values and the corresponding θ angles are collected in the tables below.

h	***k***	***l***	***d***	***θ***	***2θ***
2	0	0	2.480	18.096	36.191
0	2	0	4.820	9.196	18.392
0	0	2	2.480	18.096	36.191
1	1	1	3.296	13.516	27.032

Table 4.6. *d* and θ values for the PVDF α phase.

h	***k***	***l***	***d***	***θ***	***2θ***
2	0	0	4.290	10.344	20.687
0	2	0	2.455	18.286	36.573
0	0	2	1.280	36.998	73.997
1	1	1	2.194	20.549	41.099

Table 4.7. *d* and θ values for the PVDF β phase.

h	***k***	***l***	***d***	***θ***	***2θ***
2	0	0	2.480	18.096	36.191
0	2	0	4.790	9.254	18.508
0	0	2	4.615	9.608	19.217
1	1	1	3.975	11.173	22.346

Table 4.8. *d* and θ values for the PVDF γ phase

From the data collected in the tables above it is clear that the θ angles of Fig.4.5 correspond to the main diffractive angles of PVDF in its polar β phase, that are 20.687° and 36.573°. Two visible, although less intense, peaks appear at 36.191° and 18.392° and from Tab.4.6 we can affirm that they belong to the non-polar α phase.

As supposed from the analysis of the DSC spectra, both PVDF films, 52 and 110 μm thick, consist of piezoelectric PVDF in the polar β phase, that is necessary to have an electric response during worn tests. A few amount of non-polar α phase is present in the thicker film, but this will not affect the electromechanical behaviour of the material.

4.2.2 Identification of the most suitable place to put the transduction devices

On the wake of Starner et *al*. [6], who identified the walk as best source for energy generation by human body (Tab.4.9), we decided to arrange the transduction devices inside the insole of a shoe, a boot supplied by Diadora designed for fire-fighters in particular.

Human source	**Total power** [W]
Breathing band	0,83
Blood pressure	0,93
Exhalation	1
Body heat (Carnot efficiency)	2,4 – 4,8
Finger motion	6,9 – 19
Arm motion	60
Footfalls	67

Table 4.9. Table reporting the amount of energy supplied by human body.

Two free spaces were found, one under the plant of the foot (about 75 cm^2 for 0,2 cm thickness) and one under the heel (28 cm^2 for 1,5 cm thickness) (Fig.4.6).

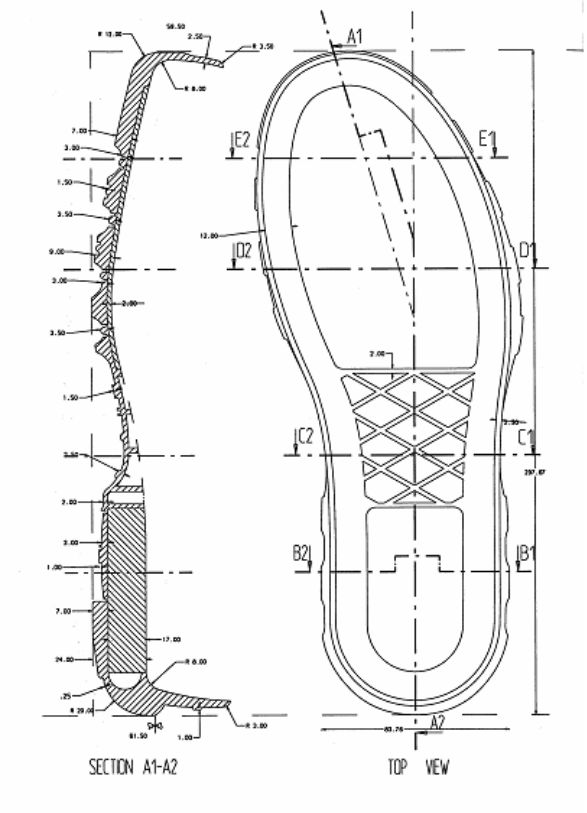

Figure 4.6. Technical drawing of the boot supplied by *Diadora*.

4.2.3 Designing of the most efficient configuration

In order to maximize the conversion between the mechanical energy generated with each footstep and the electrical energy supplied by the transducer, two different configurations were designed, one for the plant and one for the heel free spaces within the sole. They are reported in the figure below.

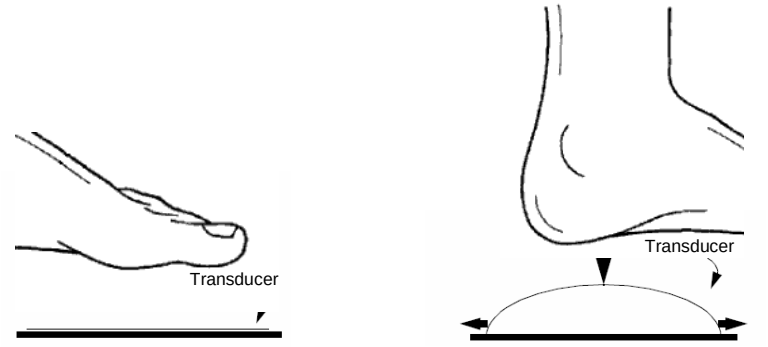

(a) (b)

Figure 4.7. Possible in-shoe configurations; (a) planar configuration; (b) "bridge" configuration.

4.2.4 Cut and shape of the materials as supplied

Sheets of PP and PVDF, as supplied, were cut in two different shapes, as shown in Fig.4.8, in order to maximize the area subjected to the stress during the walk.

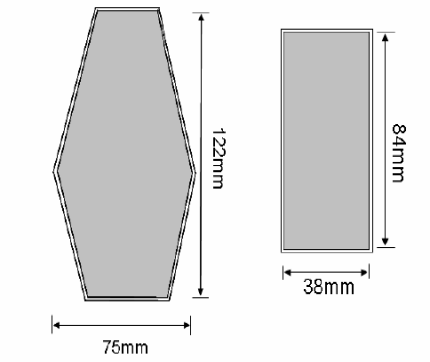

Figure 4.8. Shape and dimension of PVDF and PP transducers after cutting and electrodes deposition.

Silver electrodes, constituted by a conductive silver ink (Electrodag 418 SS™) dissolved in acetone, were deposited onto the PP samples using an airbrush. About 2 mm of PP without metallization was maintained along the edge in order to avoid electrical contact between the two opposite sides of the transducer. The same was for the PVDF samples whose edges was cleaned, after cutting, using nitric acid (65 vol% HNO_3).

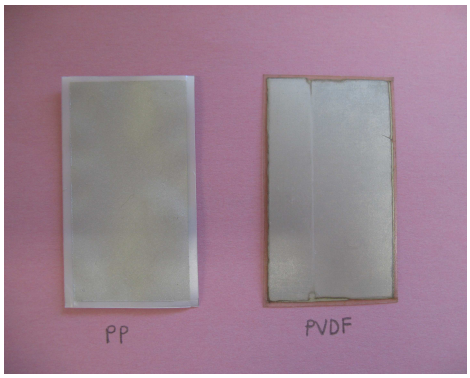

Figure 4.9. PP and PVDF transducers after electrodes deposition.

Electrical contacts were added, both onto PVDF and PP, using metallic wires and conductive adhesive tape and, finally, in order to limit electrodes abrasion and to assure electromagnetic shielding, a layer of dielectric paint (Electrodag PF-455B™) was used to cover the overall device. During experimentation, also metallic rivets were used as electrical contact between the transducer and the measurement instrumentation, but they caused electrical conduction between the two opposite sides of the sample so they were soon neglected.
Samples were then inserted into the shoe using respectively a flat and a "bridge" configuration for the heel and the plant of the sole (Fig.4.7). The final energy generation system developed is showed in Fig.4.10.

(a) (b)

Figure 4.10. PVDF transducers inserted into the boot sole (a) and boot external appearance (b).

Combinations of more than one transducers connected in series were tried also, but a suitable electronic circuit for the harvesting of charges of opposite sign, generated simultaneously, must be develop before to proceed in that way.

4.2.5 Electro-mechanical in-lab tests (validation of theoretical models)

In order to mechanically characterize the PVDF and PP transducers, preliminary tests to verify the transduction capability of the materials were performed.

Compression. In the following graph the electric voltage generated by the PP (70 μm thick) and PVDF samples (52 and 110 μm thick) is reported with respect to time. For both the two different materials, the response, in term of generated voltage, is instantaneous, this means that the charge and discharge of the film, acting as a planar plate capacitor, is very fast. Both PVDF and PP, are sensitive to transitory solicitation instead of stationary solicitations.

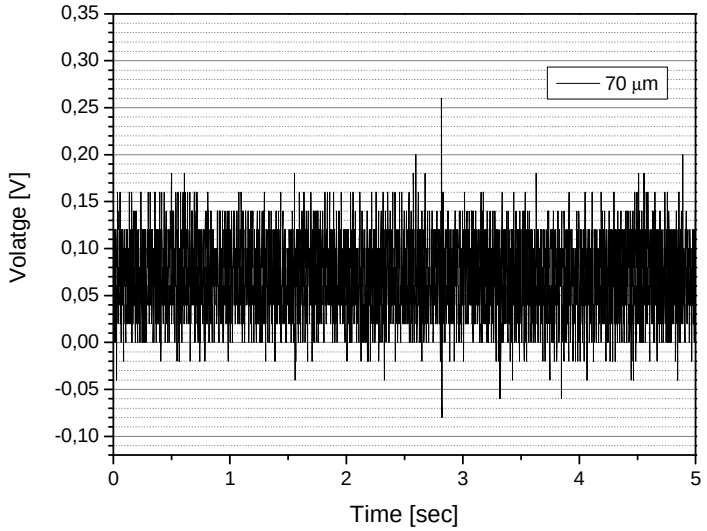

Figure 4.11. Compressive test performed on PP sample using F = 1,5Kg.

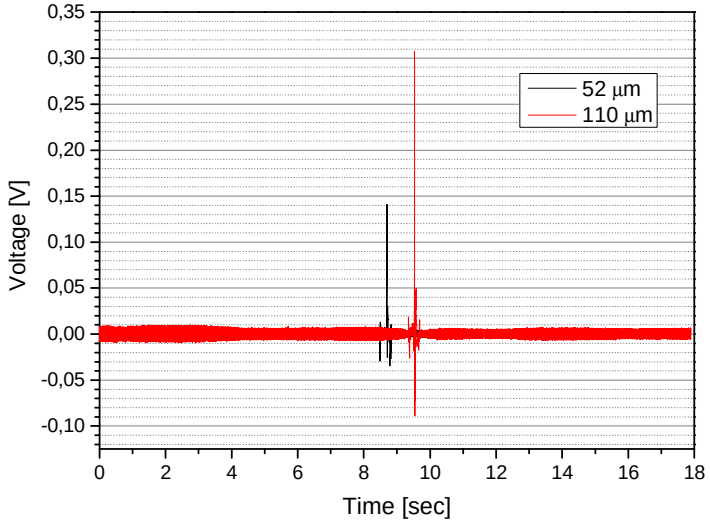

Figure 4.12. Compressive test performed on PVDF samples using F = 1,5Kg.

In order to verify the results obtained from the first preliminary compressive test, the definition of polarization (*P*) and voltage (*V*) for a piezoelectric material subjected to a compressive stress was considered [7].

$$P = \frac{Q_{pol}}{A} = \sigma \cdot d_{33} = \frac{F}{A} \cdot d_{33} \tag{4.3}$$

$$V = \frac{Q_{pol}}{C_0} = \frac{F \cdot d_{33} \cdot h}{\varepsilon_0 \varepsilon_r A} \tag{4.4}$$

where P is the polarization, Q_{pol} the polarization charge, C_0 transducer capacity, A the transducer active area covered with the electrodes (A = 2,8 cm × 4,9 cm = 13,72 · 10^{-4} m^2), F is the applied force (F = 1,5 Kg · 9,8 m/s^2 = 14,7 N), d_{33} the piezoelectric coefficient ($d_{33,PVDF}$ = 23; $d_{33,PP}$ ~ 25), h the transducer thickness, 70, 52 and 110 μm respectively), ε_0 the vacuum permittivity (8,85·10^{-12} F/m) and ε_r the relative dielectric constant of the transducer material (ε_{PVDF} = 12 and ε_{PP} = 1,6). Substituting the values into Eq.(4.4) we obtained the results reported in the following tables.

h [μm]	$\mathbf{V}_{(theoretical)}$	$\mathbf{V}_{(experimental)}$
70	1÷10	<0,26>

Table 4.10. Comparison of experimental and theoretical compressive values obtained with PVDF samples.

h [μm]	$\mathbf{V}_{(theoretical)}$	$\mathbf{V}_{(experimental)}$
52	0,12	<0,14>
110	0,25	<0,31>

Table 4.11. Comparison of experimental and theoretical compressive values obtained with PVDF samples.

As reported in the table above (Tab.4.10), the model doesn't fit with experimental data collected during the compressive test on PP. This is due probably to a discrepancy between the declared d_{33} coefficient (25-250 pC/N, see Tab.4.2) and the real one. In any case, the output signal generated by the PP sample is less intense and more noisy with respect to that of PVDF and for these reasons this material will be not considered for the rest of the activity. The accordance between theoretical and experimental value is good for PVDF sample instead (Tab.4.11). For higher thickness we have higher voltage generation, according to Eq.(4.4). This means that data supplied by the company are correct and we can proceed using this material to develop wearable transducers.

Bending. After compressive measurements, samples were subjected to two bending tests in order to find the best configuration for an optimized "generated energy/applied stress (or strain)" ratio. To do that, an Instron machine by *Zwick/Roell* [8], mod. ProLine table-top Z005, was used. Its main characteristics are reported in the table below.

Max Load	5	[kN]
Load cell (strain gage)	100	[N]
Crosshead max speed	500	[mm/min]
Crosshead min speed	0,01	[mm/min]

Table 4.12. Zwick/Roell ProLine Z005 main specifications.

For the acquisition of the electrical signals generated during this first tests, a data acquisition module NI USB-6251 (8 differential channels, 16 single ended channels) by *National Instruments* [9] was used. Having the NI-DAQ module a high input impedance (>10^9 Ohm), an electrical resistance (10^6 Ohm) was added in parallel to the transducer. In this way the NI-DAQ impedance can be neglected and the recorded voltages have to be multiply for a factor δ as reported in the following relation [10]

$$V_0 = V_S \cdot \delta = V_S \cdot \frac{R}{R + \frac{1}{j2\pi f C_0}} \tag{4.5}$$

$$C_0 = \varepsilon_0 \varepsilon_r \frac{A}{d} \tag{4.6}$$

where V_0 is the effective voltage, V_S is the voltage measured with the NI-DAQ module and the added resistance R, as reported in the equivalent circuit below (Fig. 4.13), C_0 is the transducer capacitance and f is the frequency of the generated signal.

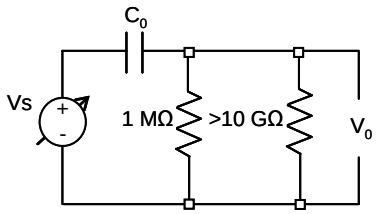

Figure 4.13. Acquisition electrical circuit scheme.

In the following, a picture showing the two configurations used (Fig.4.14) and the graphs containing the data collected (Fig.4.15-16) are reported.

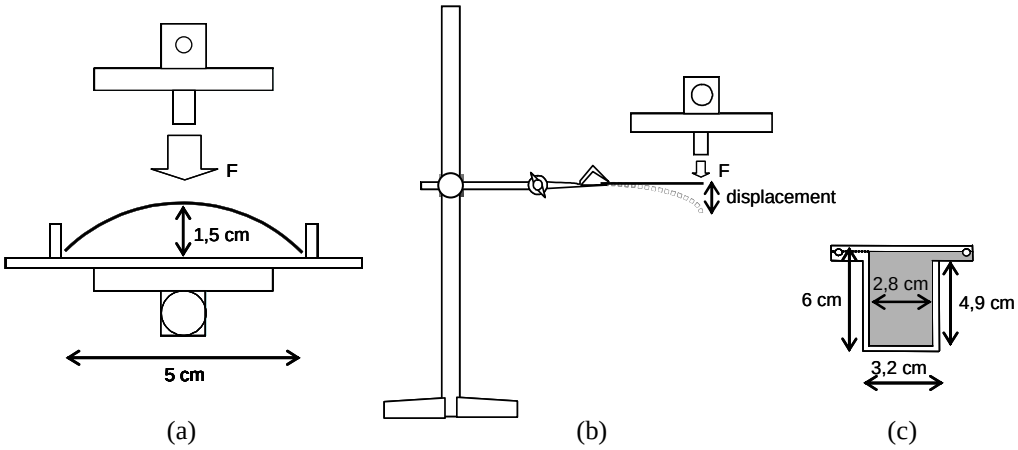

Figure 4.14. (a) "Bridge configuration"; (b) bending configuration; (c) sample dimensions.

The maximum speed of 500 mm/min was used to test PVDF samples of two different thicknesses. The displacement of the crosshead was respectively 3, 5, 7 and 10 mm for the bending configuration and 3, 5 and 10 mm for the bridge configuration. Different measurements were carried on samples and different frequencies were used (1 or 2 Hz), but no dependence on frequency was observed from the results obtained. For clarity, only two graphs are reported for the PVDF sample of thickness 110 μm showing the voltage

response with respect to time during the machine solicitation. A typical electromechanical response for a PVDF sample in the “bridge” and bending configuration is shown in Fig.4.15-4.16, while a summery of the voltages generated for the different displacements is reported in Fig.4.17-4.18 for the bending and bridge configuration respectively.

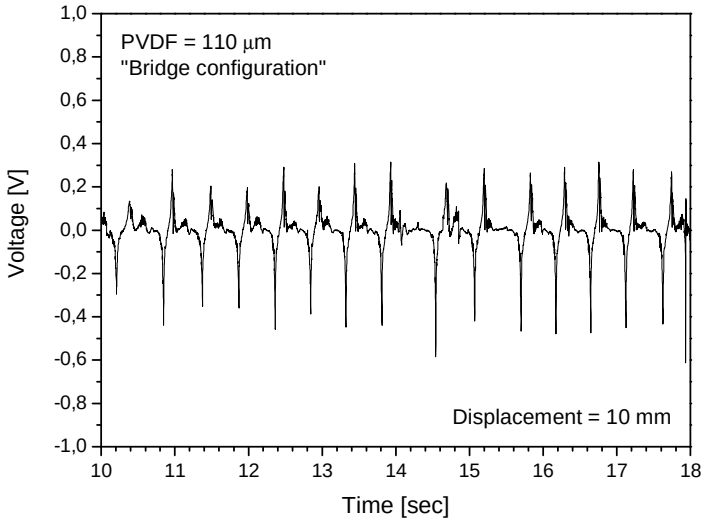

Figure 4.15. Typical electromechanical response of a PVDF sample in “bridge” configuration.

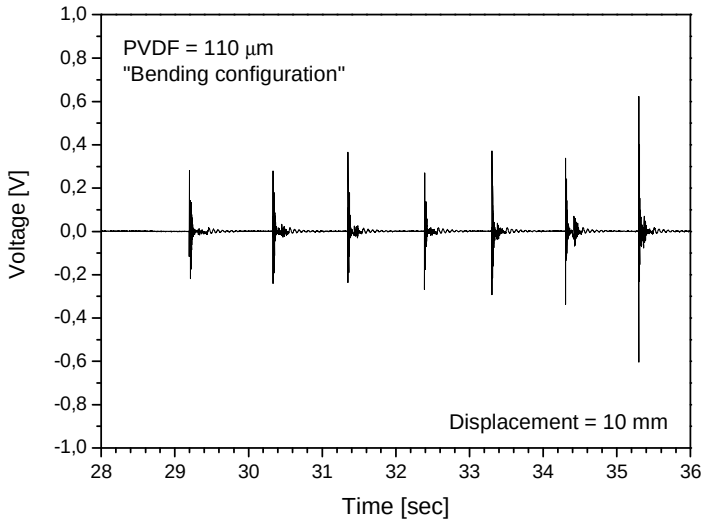

Figure 4.16. Typical electromechanical response of a PVDF sample in “bending” configuration.

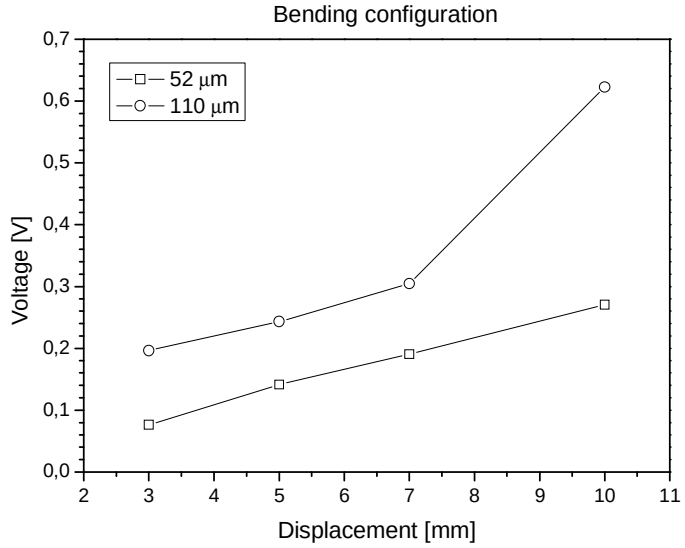

Figure 4.17. Electromechanical responses of a PVDF sample in "bending" configuration.

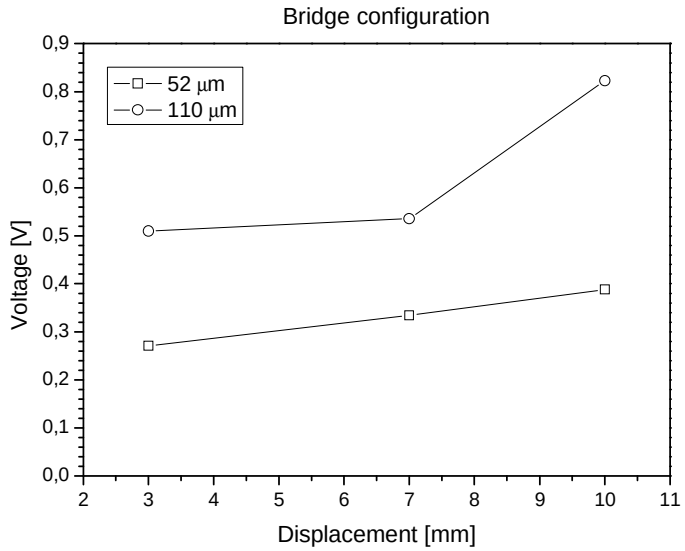

Figure 4.18. Electromechanical response for a PVDF sample in "bridge" configuration.

As for compressive test, for bending configuration also a theoretical model predicting the response of piezoelectric plate is available [11]. The model predicts the voltage generated by a plate of thickness h, length L and width w subjected to a displacement Δ and it is reported in the following.

$$V = \frac{Q_{tot}}{C} = \frac{3}{4}\hbar_{31} \cdot \frac{h^2}{L^2} \cdot \Delta \tag{4.7}$$

where $\hbar_{31} = g_{31} \cdot Y$, $g_{31}=d_{31}/\varepsilon$ being the piezoelectric stress constant and Y is the elastic modulus of the beam. The model can be obtained as follows.
Define the strain s of the beam as:

$$s(x,z) = \frac{z}{R} \tag{4.8}$$

where R is the radius of curvature of the beam and z the distance form the neutral plane:

$$R(x) = \frac{L^3}{3(L-x)\Delta} \tag{4.9}$$

with x = distance form the fixed end. Thus for a cantilever of thickness h:

$$s(x,z) = \frac{3}{4}\frac{h}{L^3}(L-x)\Delta \tag{4.10}$$

Thanks to the piezoelectric coupling along the *31* direction, the charge induced due to the strain at point x is:

$$Q_{dx} = \varepsilon w E_{31}(x)dx = \varepsilon w \hbar_{31} s_1(x,z)dx \tag{4.11}$$

being E_{31} the electric field along the 31 direction and:

$$Q_{tot} = \int_0^L Q_{dx} \tag{4.12}$$

Substituting Eq.(4.11) in Eq.(4.12) and considering the definition of the voltage V induced by the section $w \cdot z \cdot dx$ onto the external surface $h/2 \cdot dx$ we have:

$$V = \frac{Q_{tot}}{C} = \frac{\varepsilon \cdot \hbar_{31} \cdot w \cdot \int_0^L s_x(x, \frac{h}{2})dx}{C} \tag{4.13}$$

where s is defined as in Eq.(4.10) and $C=\varepsilon(wL/h)$. Integrating Eq.(4.13) we obtain Eq.(4.7)

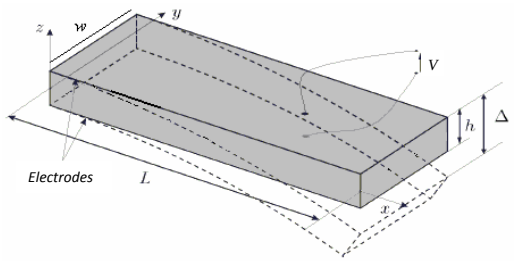

Figure 4.19. Sketch of PVDF plate in a bending configuration.

Parameter	Units	Value
g_{31}	Vm/N	$216 \cdot 10^{-3}$
Y	N/m^2	$2 \cdot 10^9$
h	m	$52, 110 \cdot 10^{-6}$
L	m	$5 \cdot 10^{-2}$
Δ	m	$3, 5, 7, 10 \cdot 10^{-3}$

Table 4.13. PVDF sample geometrical and physical characteristics [12].

Substituting the values of Tab.4.13 in Eq.(4.7), Tab.4.14 and Tab.4.15 have been filled reporting the theoretical *vs* experimental voltages for the bending configuration.

Displacement Δ [mm]	$\mathbf{V_{exp}}$ [V]	$\mathbf{V_{th}}$ [V]
3	0,076	1,05
5	0,14	1,75
7	0,19	2,45
10	0,27	3,50

Table 4.14. Comparison between experimental and theoretical voltages for a PVDF sample (52μm thick) - bending test.

Displacement Δ [mm]	$\mathbf{V_{exp}}$ [V]	$\mathbf{V_{th}}$ [V]
3	0,19	4,70
5	0,24	7,84
7	0,3	10,98
10	0,62	15,68

Table 4.15. Comparison between experimental and theoretical voltages for a PVDF sample (110μm thick) - bending test.

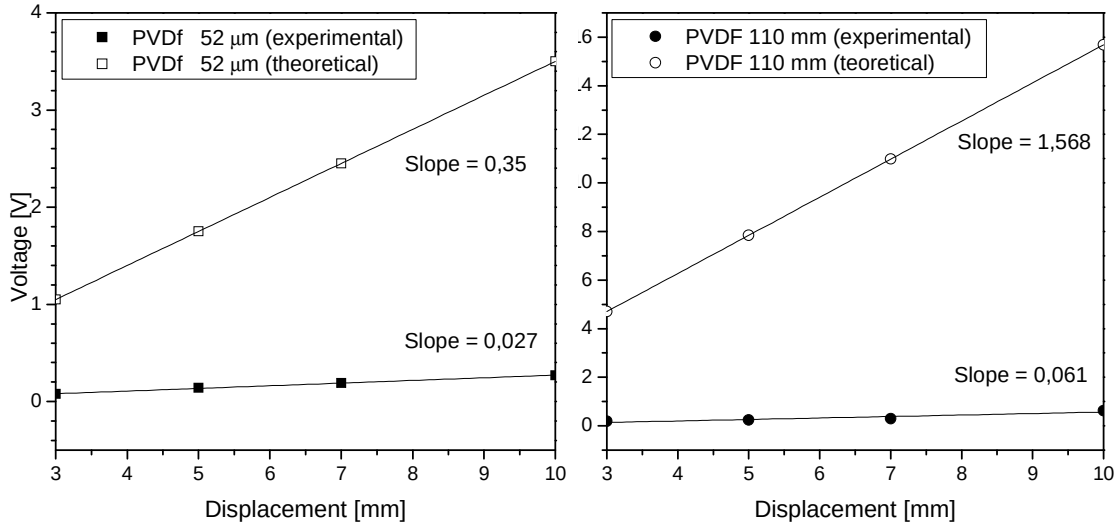

Figure 4.20. Comparing experimental *vs* theoretical data (induced voltage) for two PVDF samples in bending configuration (lines are as a guide for the eyes).

As for the compressive model described by Eq.(4.4), also the model for the bending of the PVDF cantilever shows a direct proportionality between the thickness of the film and the voltage produced for a specific displacement Δ, nevertheless the theoretical values of the voltage obtained with the bending model do not agree exactly with the experimental ones (factor ×12 ca. for the 52 μm film and ×30 ca. for the 52 μm film). A lot of parameters are involved, most of which are in a quadratic form, so that big errors can arise for small variations of the values. A model providing a better approximation of experimental data have to be developed, maybe considering the kinetic energy by which the piezo-transducer is solicited.

4.2.6 Electro-mechanical worn tests

After a preliminary characterization of the selected materials and the study of the most suitable configurations to adopt in order to harvest electrical energy from passive human movements (§4.2.2-4.2.5), a first prototype of device integrated into the shoe has been developed (Fig.4.10). Results obtained with the worn test are reported below.

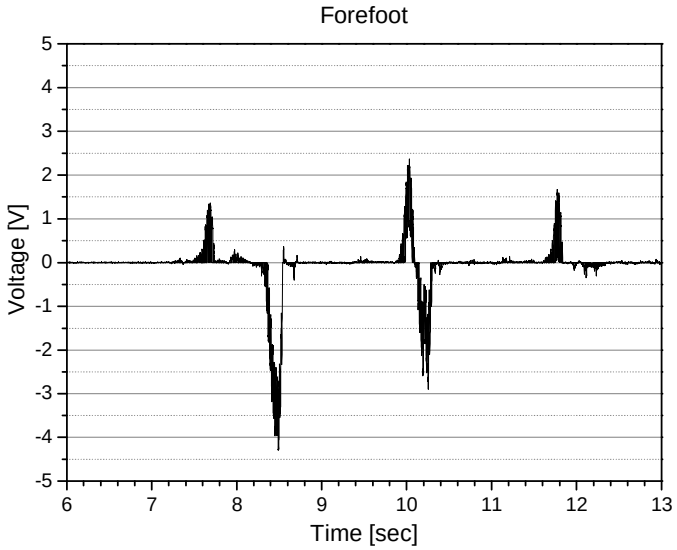

Figure 4.20. Electromechanical response of PVDF transducers inserted in a shoe(forefoot) – walking.

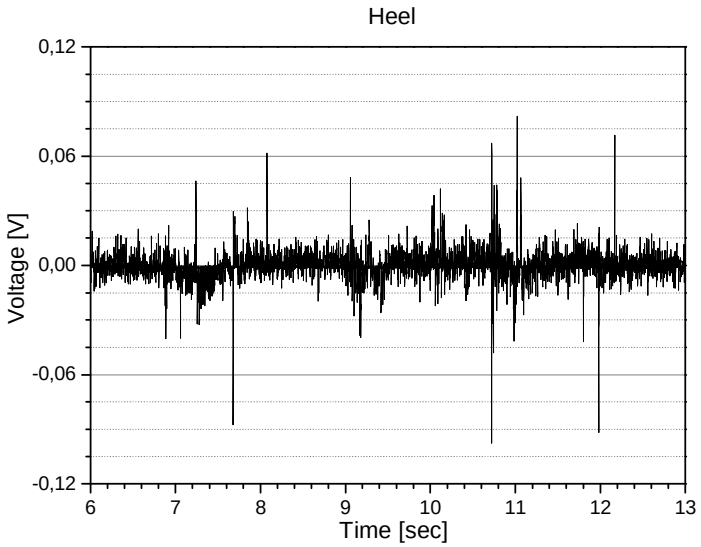

Figure 4.21. Electromechanical response of PVDF transducers inserted in a shoe(heel) – walking.

As shown in Fig.4.20-21, PVDF transducers, as designed and developed during this PhD activity, are able to convert mechanical to electrical energy during the human walk. In particular, several repeated tests demonstrated that the transducer positioned under the forefoot can provide more energy (1,5 ÷ 4 V) with respect to that under the heel (0,045 ÷ 0,1 V). This results has two main causes, one linked with dimensions, the transducer

positioned under the forefoot, in fact, is bigger than that under the heel, the other due to the different stresses exerted onto the two transducers, the solicitation generated by the heel, in fact, is quite intense but short, that generated by the forefoot is longer in time and involve a bigger sample area. In future a new planar configuration can be developed for the heel transducer too.

In order to enhance the efficiency of transduction of the PVDF converters, a study on the possibility to reduce the resonance frequency of the embedded system was carried on. The idea was that of modify the system in order to approach its natural frequency to the frequency of a walk (~ 2 Hz) or of a run (~ 4 Hz). In this way the signal/noise ratio would be reduced and the mechanical and electrical response of the PVDF amplified. To do that, a rectangular PVDF sample (3cm×1cm×110μm) was solicited by a fast impulse and than left free to return to an equilibrium state. The frequency of oscillation of the sample is reported in the figures below for a free sample, a sample fixed onto an aluminium foil (0,47mm×14cm) and a sample fixed onto an aluminium foil with an inertial mass added onto one end.

Voltages were acquired by means of a digital oscilloscope mod. TDS3000B by *Tektronix* [13], they are shown in the following figures and summarized in Tab.4.16.

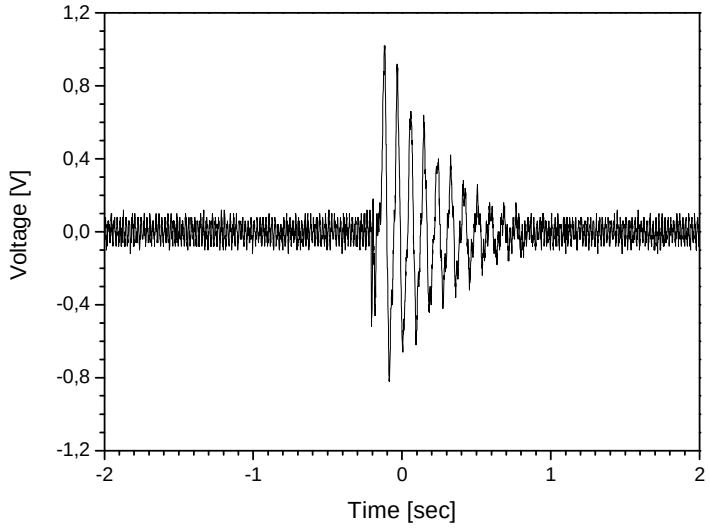

Figure 4.22. Damped oscillations for a PVDF sample fixed onto an Al foil.

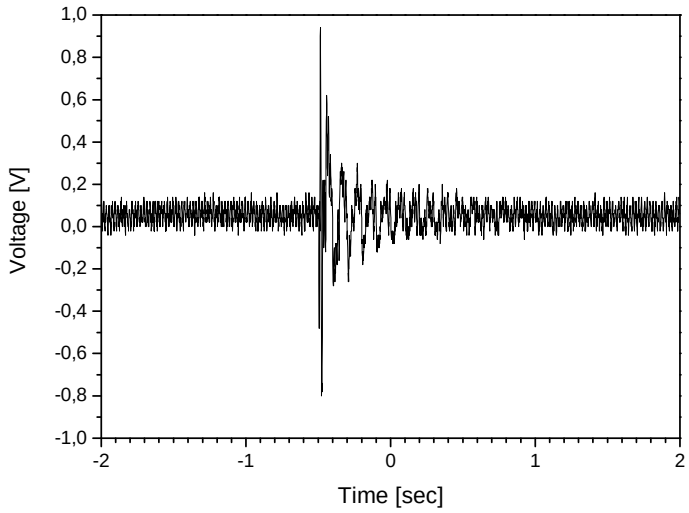

Figure 4.23. Damped oscillations for a PVDF sample fixed onto an Al foil. Added inertial mass = 0,4g.

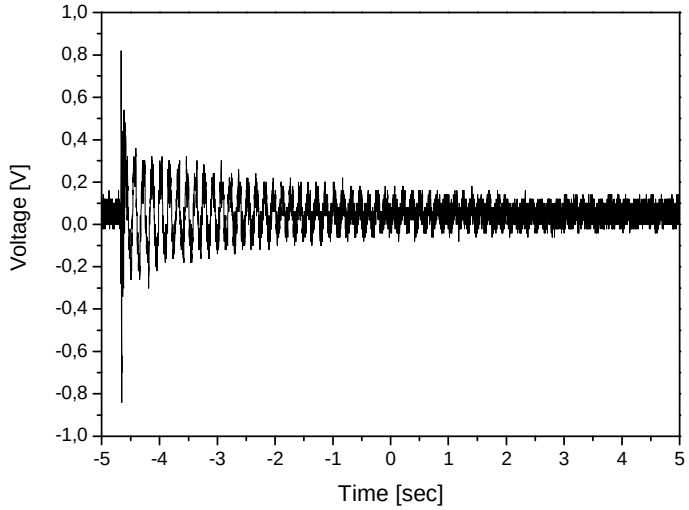

Figure 4.24. Damped oscillations for a PVDF sample fixed onto an Al foil. Added inertial mass = 2,6g.

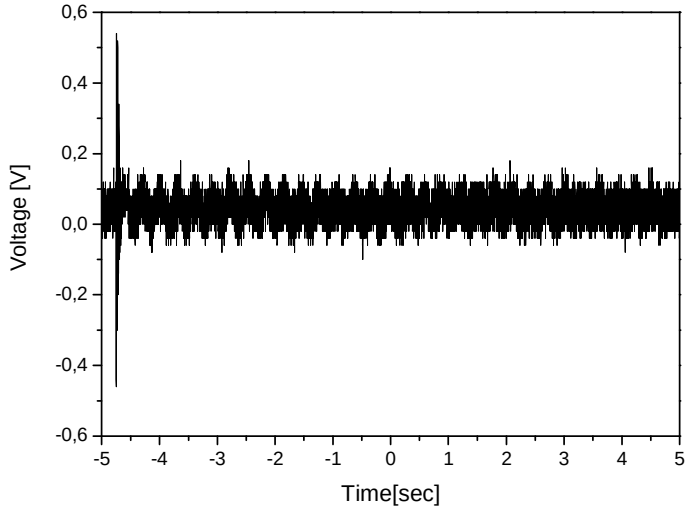

Figure 4.25. Damped oscillations for a PVDF sample fixed onto an Al foil. Added inertial mass = 15,8g.

	Free	**Al foil**	**Al foil + 0,4g**	**Al foil + 0,7g**	**Al foil + 1,28g**	**Al foil + 2,6g**	**Al foil + 5,8g**	**Al foil + 15,8g**
T [sec]	0,02	0,1	0,1	0,1	0,11	0,15	0,2	0,3
f_n [Hz]	50	10	10	10	9,09	6,7	5	3,3

Table 4.16. Resonance frequencies and oscillation periods for a PVDF sample in a bending configuration.

As shown in the previous figures, modifying the transduction system by adding a mass it is possible to reduce the period of each oscillation (T= peak-to-peak distance) and preserve the oscillation during time. Fig.4.23 in the following reports the variation of the resonance frequency (f_n) and the period (T) for the PVDF sample with different inertial masses added onto the system.

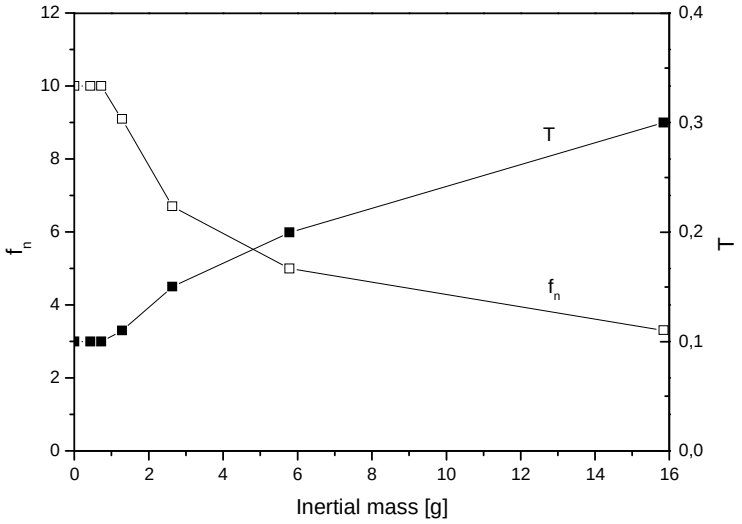

Figure 4.26. Resonance frequencies and oscillation periods *vs* inertial mass weight for a PVDF sample in a bending configuration.

From the data collected with this final tests it is possible to affirm that, although the generated voltages and charges are low and discontinuous in time, an improvement of the performance of the system is possible by a mechanical optimization of the structure.

4.3 Demonstrator

Thanks to a collaboration with the University of Pavia, Dept. of Electronic Engineering, an electronic circuit able to collect the generated charges and to gather them into a storage capacitor has been developed. The scheme of the circuit is reported in Fig.4.27 while the values of the parameters used are listed in the table below.

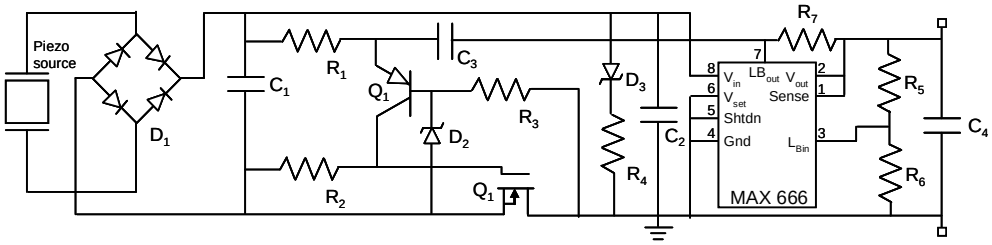

Figure 4.27. Storage-circuit.

Element	Value	Units
D_1	500	mA
D_2	2,4	V
D_3	LED	-
C_1	0,1-2,2	µF
C_2	0,1	µF
C_3	0,1	µF
R_1	510	KΩ
R_2	1	MΩ
R_3	10	KΩ
R_4	100	KΩ
Q_1	2N3906	-
Q_2	VN2222L	-

Table 4.17. Circuit elements.

Voltages generated by two PVDF transducers inserted in a shoe collected using circuit of Fig.4.27 are reported in the following.

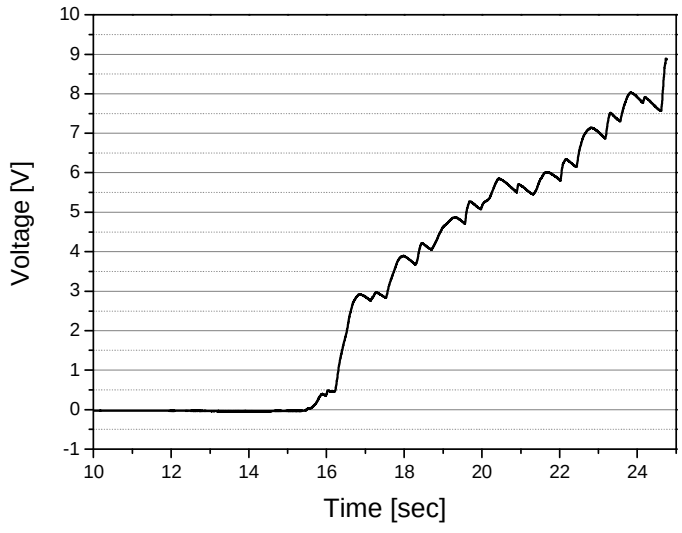

Figure 4.28. Collected charge during walk (15 steps) for C_1=0,1µF.

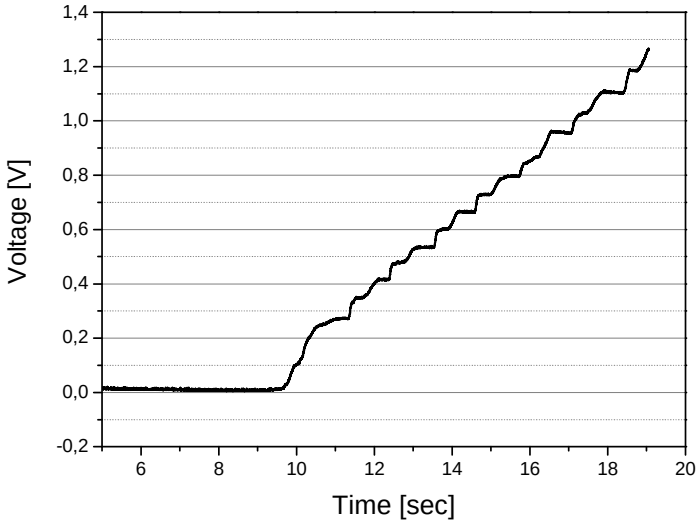

Figure 4.29. Collected charge during walk (15 steps) for C_1=2,2μF.

Fig.4.28 and 4.29 show as different capacitors can harvest different amount of charge with different rate. In particular, comparing two capacitors, respectively 0,1 and 2,2 μF, the first will be faster to charge and to discharge (charge after each step decays quickly), while the second one will be slower to fill but it will retain charge longer.
The energy developed by the two systems is calculated below and it has been used to light a LED (2 V, 10-15 mA):

$$E = \frac{1}{2}CV^2 = \frac{1}{2} \cdot 0{,}1 \cdot 10^{-6} F \cdot 64V^2 = 3{,}2\mu J \tag{4.8}$$

$$E = \frac{1}{2}CV^2 = \frac{1}{2} \cdot 2{,}2 \cdot 10^{-6} F \cdot 1{,}44V^2 = 1{,}6\mu J \tag{4.9}$$

The energy developed is low for both cases so, in order to insert this type of devices into garment, it is useful to choose the appropriate application, as for example, wireless data transmission in the case of low energies; while to recharge a battery bigger capacitors are needed and the circuitry for the accumulation have to be optimized for the low frequencies.
Following the development of the first electrical circuit for the accumulation of charges (Fig.4.27), a new advanced circuit was designed (Fig.4.28) for a more sophisticated LED lighting. It is reported in the figure below.

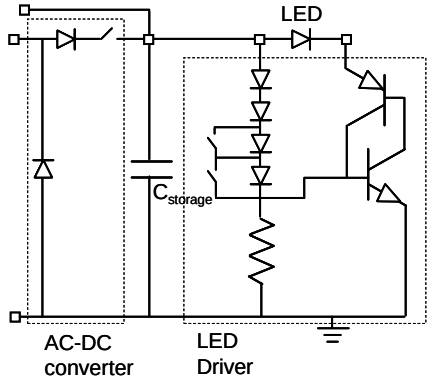

Figure 4.28. LED lighting circuit.

Thanks to this circuit it is possible to regulate the threshold voltage at which the capacitor $C_{storage}$ have to discharge onto the LED.
In order to maximize the harvesting of the generated power from the piezoelectric element, a study on the influence of the load resistance *RL* (load resistance) should be done. In the following figure (Fig.4.29) the scheme of a possible circuit for this type of characterization is reported.

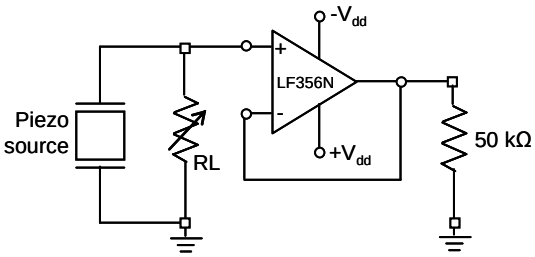

Figure 4.29. Best *RL* identification circuit.

4.4 Conclusions

From data collected during this first part of activity regarding the energy generation and storage from passive human power, the following assessments can be stated:

- it is possible to convert the passive human power (mechanical energy) generated during the walk into electrical energy.
- piezoelectric PVDF is more efficient as transducers with respect to PP: PP films responds to thickness change rather than bending and can be used for sensing applications only, not for charge generation.
- experimental data collected with PP samples don't fit the theoretical model developed for piezoelectric material, probably due to the different nature of generated charges (see §3.3.1).

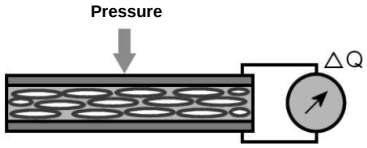

Figure 4.30. PP sensor mechanism.

- generated charge is to low and discontinuous at the moment to recharge a battery.
- further studies regarding the most suitable geometries for the specific applications must be carried out (optimize resonance frequency).
- an harvesting circuit optimization for the low frequencies is needed, following the available examples for piezoceramic systems [14].
- it may be worth to investigate the possibility of obtaining thicker PVDF films (not currently available on the market) with enhanced transduction capability, reinforcing them with nanotubes for example, as suggested by Ramaratnan [15].

4.5 References

[1] http://www.meas-spec.com/
[2] http://www.emfit.com/
[3] http://www.achesonindustries.com
[4] http://www.siemens.com/entry/cc/en/
[5] Nalwa H. S., Ferroelectric Polymers, Marcel Dekker, Inc, New York, 1995
[6] Starner T., *IBM Systems Journal*, 35, 3&4 (1996)
[7] Gonzalez J. L. *et al*., *Proceedings of the 4th IEEE International Conference on Materials and Engineering for Resources*, Piscataway, 202-207, 2001
[8] http://www.zwick.com/it.html
[9] http://www.ni.com/
[10] Floyd T. L., Electronics Fundamentals: Circuits, Devices, and Applications, Amazon, UK, 2003
[11] Chen S-N *et al*., *Mechatronics*, 16, 379-387, 2006
[12] Measurements Specialities, Inc., Piezo Film Sensors Technical Manual
[13] http://www.tek.com
[14] Paci D. et al, IEEE International Conference on Electronics, Circuits and Systems (ICECS), 177-181, 2008
[15] Ramaratnam A. *et al*., *Journal of Intelligent Material Systens and Structures*, 17, 199-208, 2006

Chapter 5

Wearable Sensing
Materials, experimental procedures, results and discussion

During the second year PhD, the activity regarding the development of sensing devices for the acquisition of physiological parameter (ECG, breath rate, muscle activity) or for haptic and tactile applications to robots was developed. Such devices must be adaptable to textiles to be worn in clothes.
In the following pages the two main topics faced, concerning piezoelectric and piezocapacitive sensing for wearable applications, are discussed.

I PIEZOELECTRIC SENSING

As discussed in §2.3.2, piezoelectric materials are able to respond to a mechanical strain with a generation of charges so they have been chosen as transduction materials for wearable applications.

5.1 Materials

5.1.1 Poly(vinylidene fluoride)

Due to our knowledge and past experience on poly(vinylidene fluoride) (PVDF) and thanks to its excellent transduction capability (high d_{31} and d_{33} piezoelectric coefficients), along with mechanical resistance and good processability, PVDF, was the preferred material to develop the experimental activity on wearable sensing. Since it was necessary to knit the PVDF into textile fabrics with industrial machines (Fig.5.2), a suitable piezoelectric PVDF bi-oriented film by *Piezotech* [1] was purchased in the form of ribbon (Fig.5.1). Geometrical and physical characteristics of the material are reported in the figure and table below.

Property	**Value**	**Units**
$t_{\text{without electr.}}$	28	10^{-6} m
$t_{\text{with electr.}}$	40	10^{-6} m
d_{31}	10	10^{-12} C/N
d_{32}	10	10^{-12} C/N
d_{32}	22	10^{-12} C/N
k_{31}	12	%
Y	2	10^{9} N/m^2
ε	12	-
ρ		10^{3} Kg/m^3
Electrodes	Al	-
Producer	Piézotech S.a.S. 9 Rue de Colmar, 68220, Hésingue, France www.piezotech.fr	

Table 5.1. Main physical characteristics of PVDF ribbon by *Piézotech*.

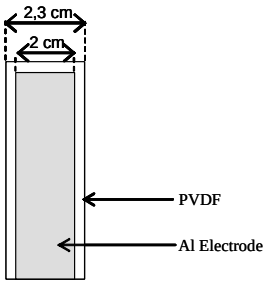

Figure 5.1. PVDF ribbon by *Piezotech*.

5.1.2 Textile substrates

In collaboration with the Universtity of Lodz (TUL), who made available the machines, two suitable knitting were selected, they are shown in the figure below.

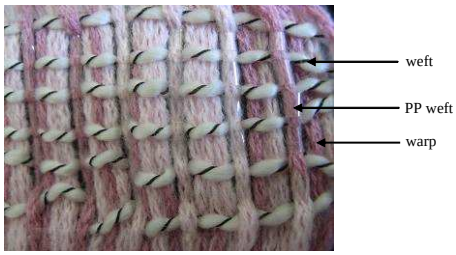

Figure 5.2. Textiles fabrics by *TUL*.

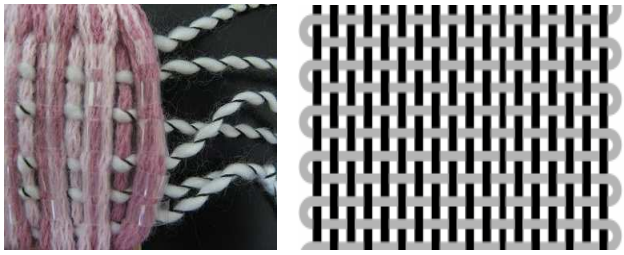

Figure 5.3. Weft knitted by the shuttle loom.

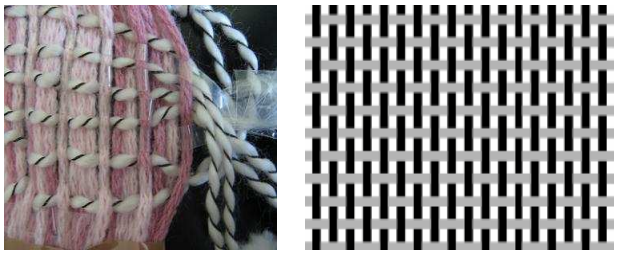

Figure 5.4. Weft knitted by the rapier loom.

Fig.5.3 shows a detail of a fabric with the weft knitted by the shuttle loom. In this way there is only a piezoelectric sensor for the entire selected textile area and it is essential to be sure that the ribbon is oriented in the same direction (same side up) to avoid signal cancellations. The overall signal can be stronger but less selective.
Fig.5.4 show instead a detail of a fabric with the weft knitted by the rapier loom. In this way there are different piezoelectric sensors for a selected textile area. Each sensor is

independent and can control different point/muscles onto the body. For these motives, the knitting of Fig.5.4 was chosen for the sensing activity.
In order to find the best textile substrates in which embed the piezoelectric sensors, four different fabrics were selected: polypropylene, cotton, wool and linen, to be used as substrates structured as in Fig.5.4.

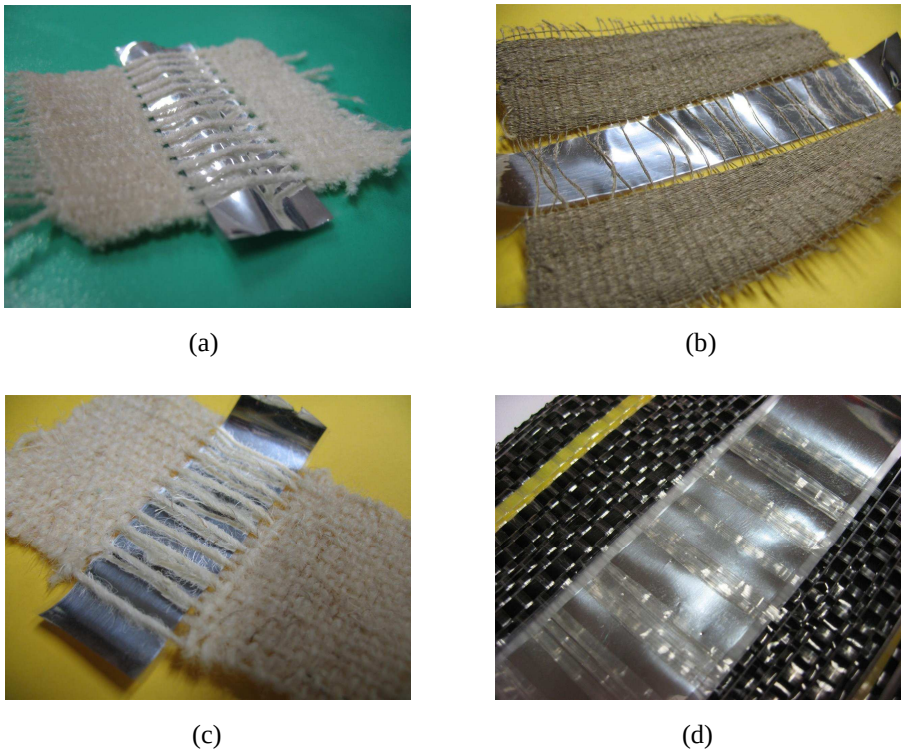

(a) (b)

(c) (d)

Figure 5.5. Embedded PVDF sensors in cotton (a), linen (b), wool (c) and PP (d) textile substrates.

5.2 Experimental procedures

The experimental activity concerned in:

1. Identification of the most suitable place to put the transduction devices
2. Electro-mechanical in-lab tests
3. Electro-mechanical worn tests.

5.2.1 Identification of the most suitable place to put the transduction devices

With the intent to detect physiological signals like ECG, breath rate and muscle activity, four preferred areas were selected to put sensors within garments. They are showed in the following picture (Fig.5.6) and correspond respectively to:

- breathing rate: chest
- ECG: chest, wrist
- muscle activity: biceps, calfs
- arm motion: joints (elbows, knees)

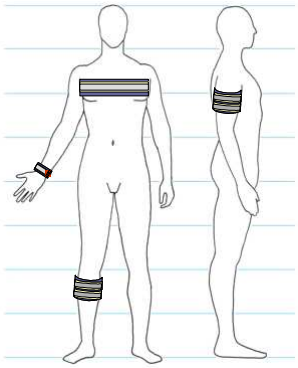

Figure 5.6. Schematic drawing of the possible locations for piezoelectric sensors.

Waiting for the production of first textiles prototypes by TUL, the two simplified configuration, reported in Fig.5.8 and 5.9 in the following, were adopted to test the response of PVDF ribbon and record physiological parameters (see §5.2.3).

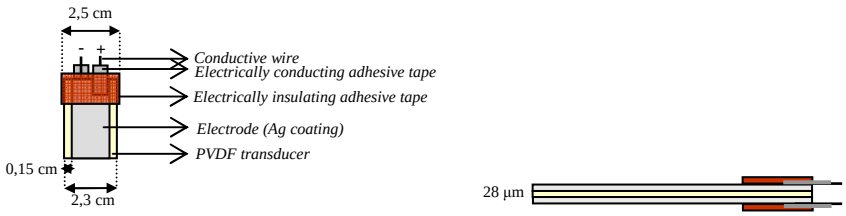

Figure 5.7. Sketch of a PVDF ribbon; detail of the electric contact.

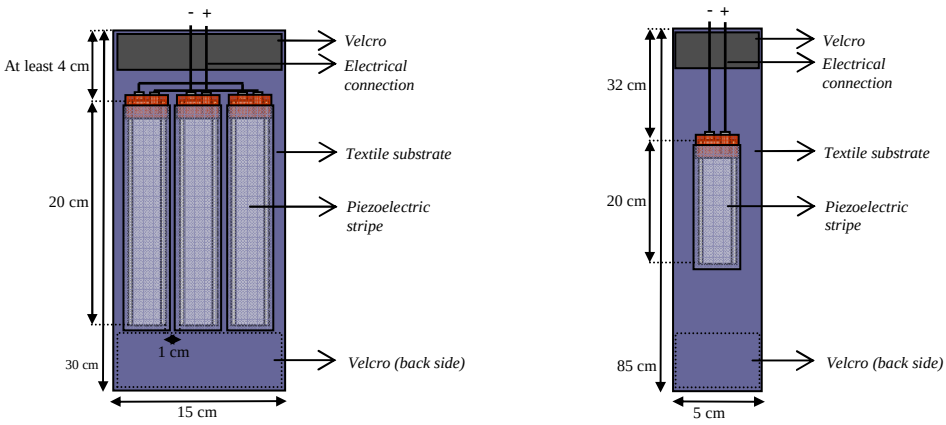

Figure 5.8. Sketch of an array configuration of piezo stripes inserted in a textile for detection of (a) muscle activity (biceps, calf, etc) and (b) breath monitoring.

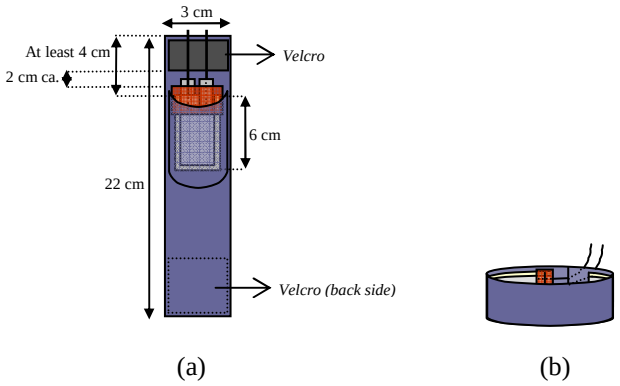

Figure 5.9. Sketch of a single piezoelectric stripe (a) to use as "wrist sensor" (b).

5.2.2 Electro-mechanical in-lab tests

In order to test the response of the fabric to a mechanical stress/strain solicitation, electromechanical tests using an electromagnetic motor as a force source were firstly performed. The sample was set as shown in Fig. 5.10 in order to reproduce a solicitation as similar as possible to the body movements, arm bending in particular and samples shown in Fig.5.5 were used.

The experimental set-up consisted in:

- an electromagnetic mini-shaker, mod. 4810 by *Brüel&Kiær* [2] (maximum force 10 N, frequency range DC to 18kHz)
- a load cell (GSS XFTC-101, maximum force 50N) for the detection of the force exerted
- a digital oscilloscope, TDS3014B by *Tektronix* (100 MHz, 1.25 MS/s) to visualize and register the output voltages
- an electronic system and a software (*Simulink*) for the piloting of the mini-shaker

Two different frequencies of solicitation were applied, 1 and 0,5 Hz respectively, the sample was fixed at two extremities and the mini-shaker tip (convex tip) was applied in the middle of the PVDF ribbon, as shown in the figure below. The displacement of the tip was 5 mm and the force applied 10 N.

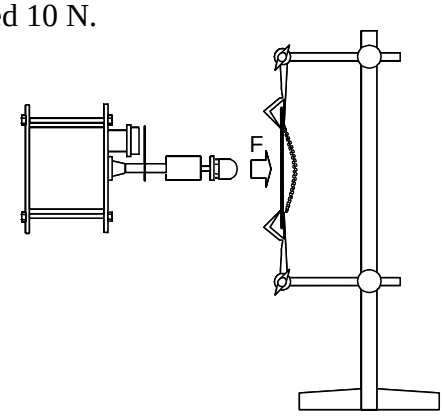

Figure 5.10. Sketch of the experimental set-up used for the constrained bending of PVDF sensors inserted into textiles.

Results obtained, at 1 and 0,5 Hz respectively, for the four different textiles substrates are reported below.

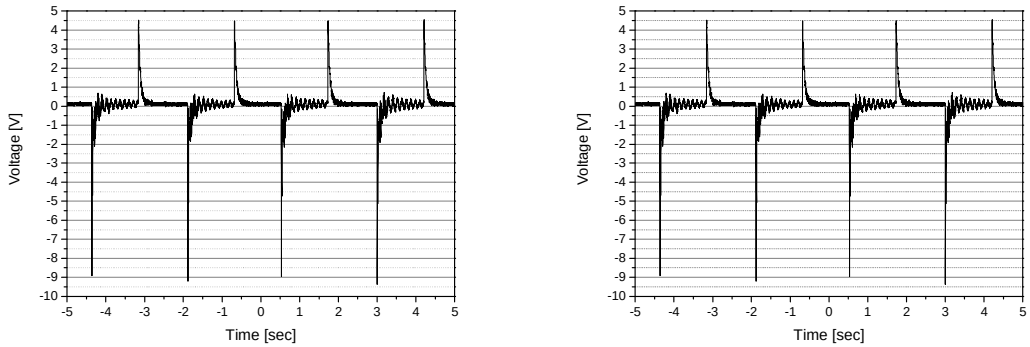

Figure 5.11. Electromechanical bending response for a PVDF sample in cotton fabric.

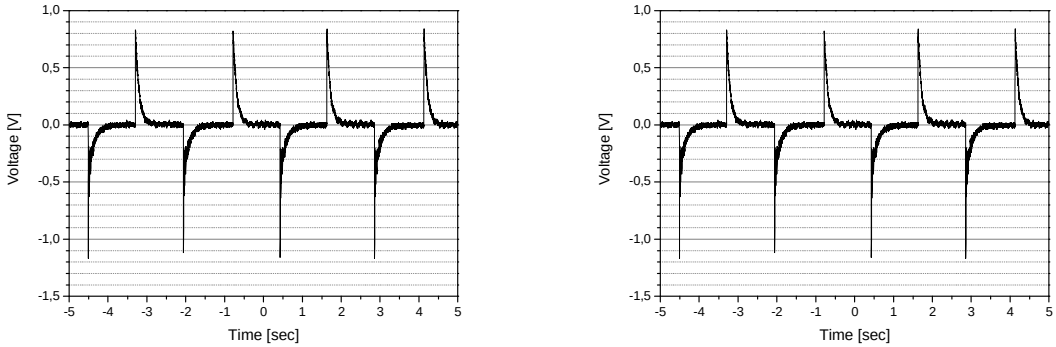

Figure 5.12. Electromechanical bending response for a PVDF sample in linen fabric.

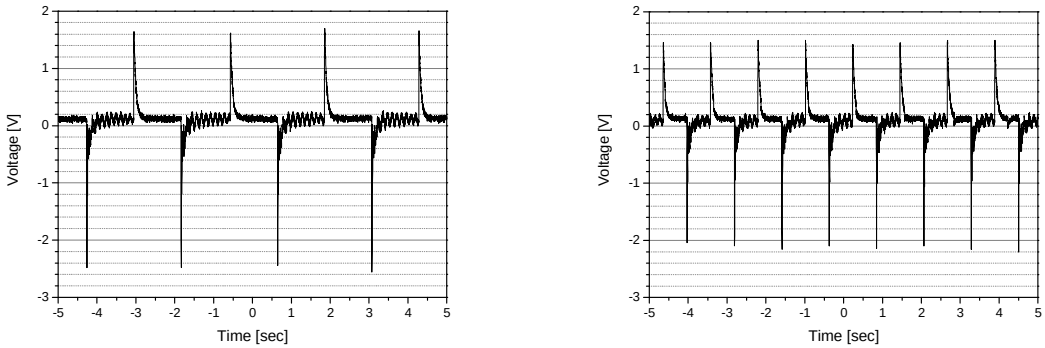

Figure 5.13. Electromechanical bending response for a PVDF sample in wool fabric.

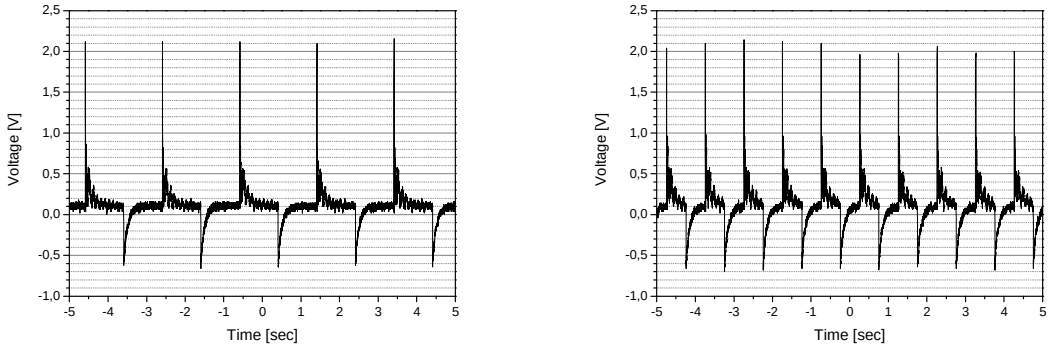

Figure 5.14. Electromechanical bending response for a PVDF sample in polypropylene fabric.

As shown in the graphs above, there are no differences in the output voltages generated by samples solicited with the two distinct frequencies.
Considering the results obtained, an estimation of the average energy produced by each sample can be made as follow:

$$C_{PVDF} = \frac{A}{d}\varepsilon_0\varepsilon_{PVDF} \tag{5.1}$$

$$E = \frac{1}{2}CV^2 \tag{5.2}$$

Considering that samples are different in length:

$$E_{density} = E / Volume \tag{5.3}$$

Substituting the corresponding values in Eq.5.1 for the four different samples we have:

Textile substrate	**PP**	**Linen**	**Wool**	**Cotton**
<E>/Vol [J/m^3]	0,4	0,12	0,53	6,14

Table 5.1. Medium electric energy densities generated during a single solicitation.

As expected from the graphs reported in Figs.4.11-4.14, the cotton fabric supplies more energy with respect to the other. This probably is due to the fact that the cotton substrate is soft and deformable and can follow the deformation of the PVDF stripe without constrain it.

5.2.3 Electro-mechanical worn tests

After first electromechanical characterization, preliminary test on the feasibility to detect physiological signals using PVDF embedded stripes have been performed. They consisted into fix the fabric onto the clothes of the user and register the response as a consequence of the arm bending (Fig.5.15) and the normal breathing activity (Fig.5.16). From the figures reported below it is clear that recordering physiological activity is possible.

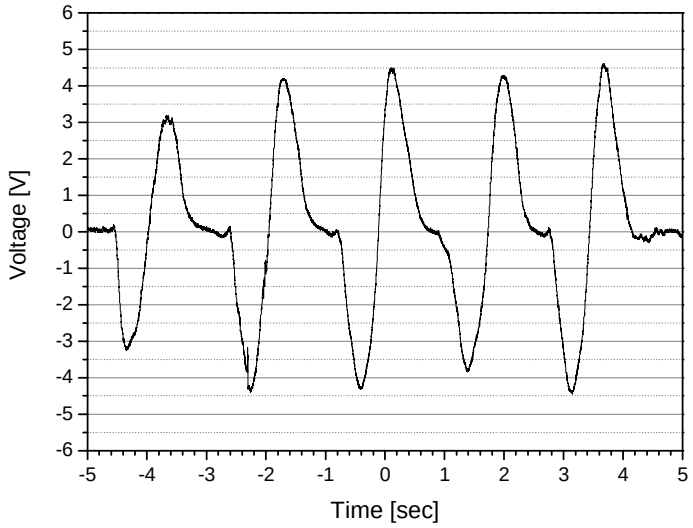

Figure 5.15. PVDF sample inserted in PP textile; elbow bending.

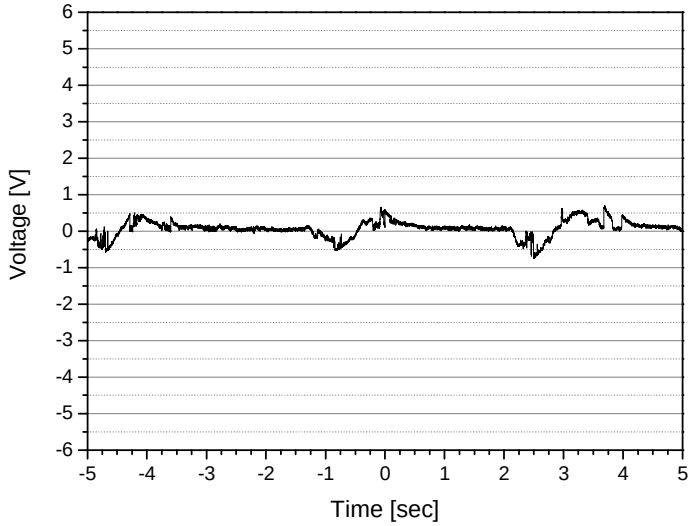

Figure 5.16. PVDF sample inserted in PP textile; breathing rate.

Next step consisted in using more sophisticated samples (Fig.5.8a) in order to obtain selective signals, referred to muscles for example. The results obtained are reported in the following figure.

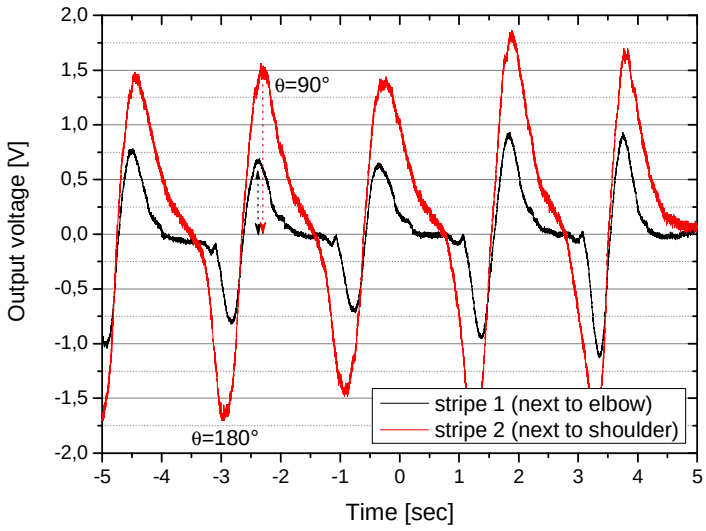

Figure 5.17. PVDF sample inserted in cotton textile; biceps activity, bending of the arm.

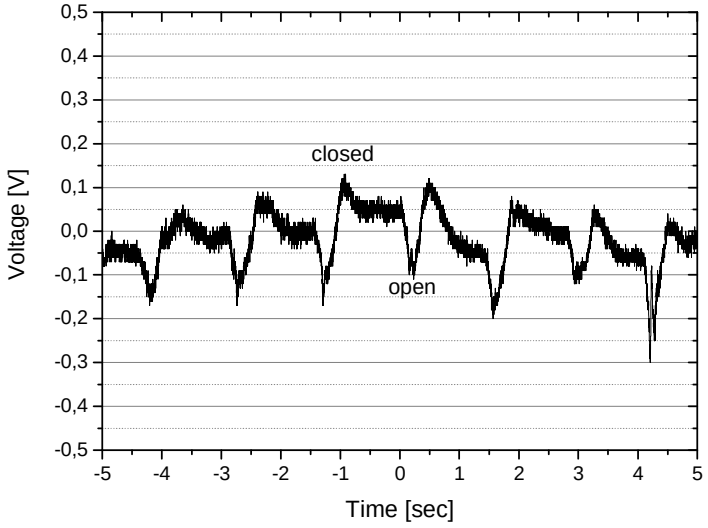

Figure 5.18. PVDF sample inserted in cotton textile; biceps activity, opening-closure of the hand.

Data reported in Fig.5.17 shows the signals corresponding to the muscle activity of the biceps during the bending of the forearm. The sensorized fabric used for the test (Fig.5.8a) made possible to discern between two different areas of the biceps, so two muscles, one next to the elbow and the other next to the shoulder. This type of test could be useful to monitor posture or body movement for patients with neuromotor disorders.

Fig.5.18 instesad report the response of a single-stripe sensorized fabric used to monitor the biceps activity during the opening-closure of the hand. Just few muscles of the biceps are involved in the activity (the most part of work is done by fore harm muscles) but the signal is visible and clear, so also weak muscle activity can be detect with this type of sensors.

Finally, electromechanical worn tests were carried on using the best performed fabrics (PVDF in cotton, §5.2.2) using systems reported in Fig.5.8b and 5.9. Breathing rate and heart rate were measured respectively. Heart rate, in particular, was measured through sensors placed onto chest and wrist, at rest and during physical activity (stairs climbing). Signals acquired are reported in the following figures.

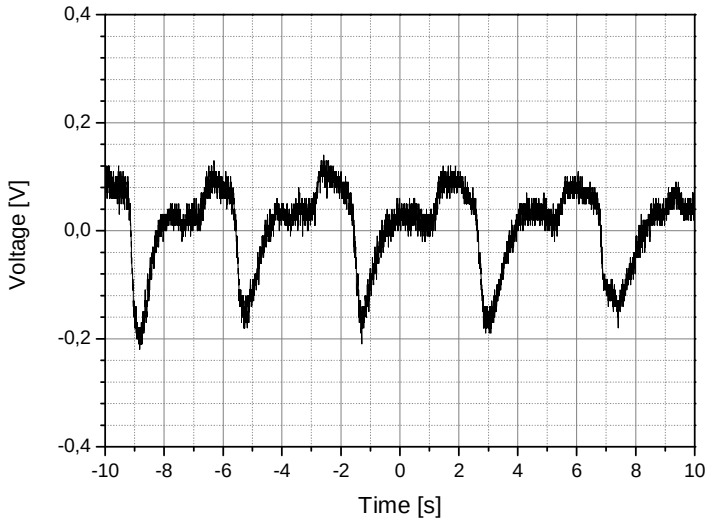

Figure 5.19. PVDF sample inserted in cotton textile (chest); breath rate monitoring.

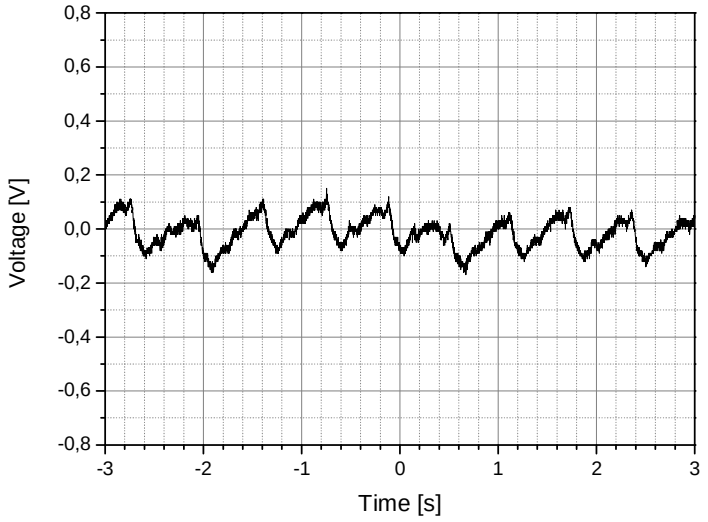

Figure 5.20. PVDF sample inserted in cotton textile (chest); heart rate monitoring at rest.

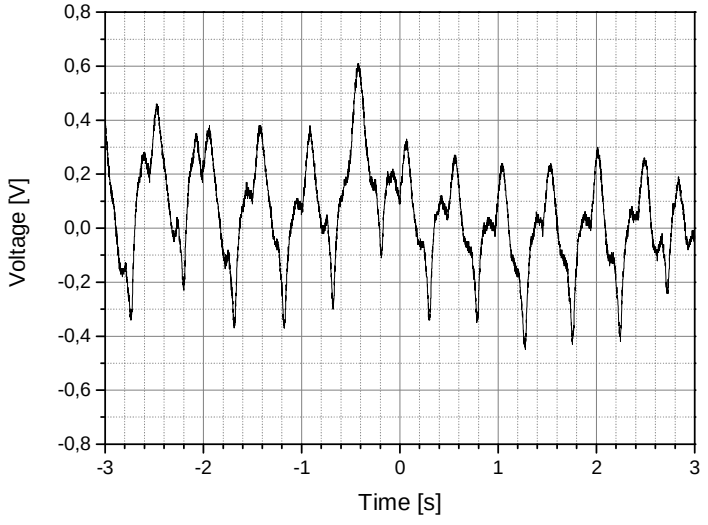

Figure 5.21. PVDF sample inserted in cotton textile (chest); heart rate during physical activity.

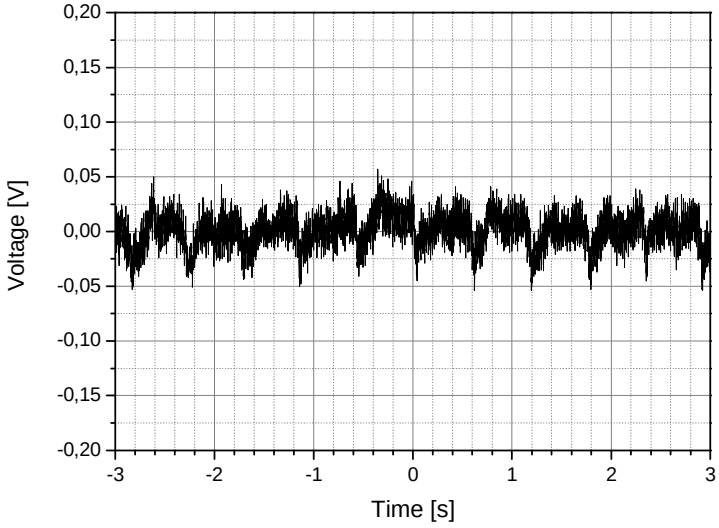

Figure 5.22. PVDF sample inserted in cotton textile (wrist); heart rate at rest.

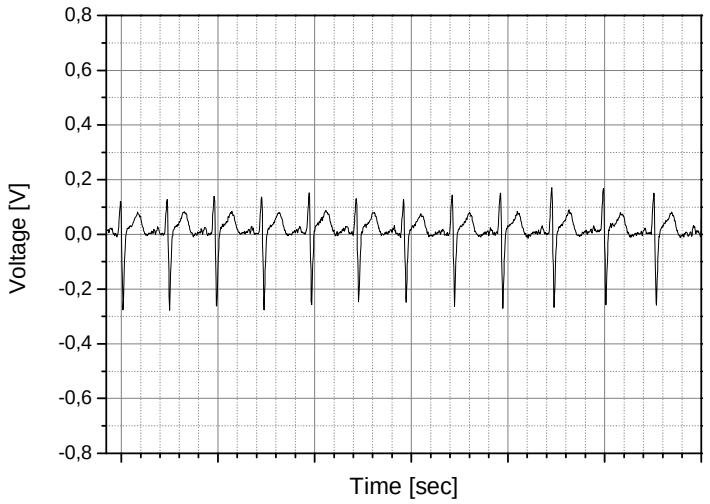

Figure 5.23. ECG by commercial Ag/AgCl *3M* electrodes; heart rate during physical activity.

Thanks to electro-mechanical worn tests it was demonstrated the possibility to use PVDF embedded fabrics to monitor physiological parameters with a good accuracy (see Tab.5.2).

	Breath rate: signal amplitude	**Heart rate: signal amplitude**
PVDF embedded sensor	<0,35>	<0,6>
Commercial sensor	-	<0,4>

Table 5.2. comparison between commercial and PVDF sensors.

Further improvements could be done in terms of filtering software [3, 4] to improve the signal-to-noise ratio.

II PIEZOCAPACITIVE SENSING

Another way to detect pressure changes with wearable electroactive devices consists into using parallel plate capacitors with dielectric elastomer as dielectric medium and compliant electrodes able to follow the deformation imposed by the extern onto the capacitors. Being the dielectric elastomer a soft medium, a pressure applied onto the capacitor plates reduces the distance (*d*) between plates and brings a change in capacitance (*C*). With respect to piezoresistive sensors, also widely used in literature for wearable applications [5, 6, 7], piezocapacitive pressure sensors are less sensitive to temperature changes and electromagnetic fields and do not show hysteresis phenomena [8, 9].
This was the object of this part of activity about wearable sensing with piezocapacitive devices.

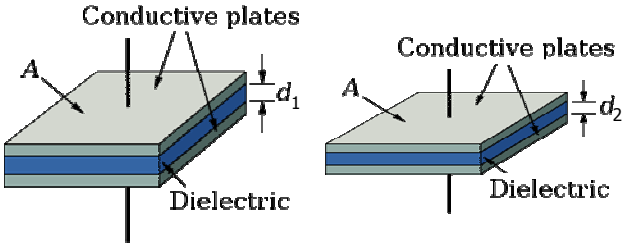

(a) (b)

Figure 5.24. piezocapacitive effect: $C_{(a)} < C_{(b)}$.

In order to have high strain/stress sensitivities (*s*) an high capacitance, and thus an high relative permittivity of the dielectric medium, is needed. Given the capacitance of a parallel plate capacitor as:

$$C = \varepsilon_0 \varepsilon_r \frac{A}{d} \tag{5.4}$$

and the change in thickness and in capacity respectively as [10]:

$$\Delta d = d_0 \frac{\Delta P}{E} \qquad \text{and} \qquad \Delta C = C_0 \frac{\Delta P}{E - \Delta P} \tag{5.5}$$

with ΔP=change in pressure and E=elastic modulus of the dielectric material, thus the sensitivity is:

$$s = \frac{\Delta C}{\Delta d} \tag{5.6}$$

where ε_0 is the vacuum permittivity, ε_r is the relative dielectric permittivity and A the area of the capacitor plates, we can affirm that the higher the capacitance, the higher the sensitivity for a small change in thickness of the capacitor [10].
In order to prepare a dielectric elastomer with a high permittivity(ε_r)/elastic modulus(E) ratio, to enhance the C preserving the softness, the composite approach (§3.2) was used. A selection of silicone and polyurethane elastomers, along with ferroelectric ceramics, was carried out. They are described in the following paragraphs.

5.3 Materials

5.3.1 Silicones

Two silicone materials were chosen, one in bulk (Ecoflex®, by *Smooth-On* [11]) and one foam (Soma Foama® by *Smooth-On* too).

Ecoflex rubbers are platinum-catalyzed silicones that are versatile and easy to use. They are mixed 1A:1B by weight or volume and cured at room temperature with negligible shrinkage. Rubber also cures without a "tacky" surface. Low viscosity ensures easy mixing and de-airing, or you can choose to mix and dispense using our convenient dispensing cartridges. Cured rubber is very soft, very strong and very "stretchy", stretching many times its original size without tearing and will rebound to its original form without distortion.

Soft Ecoflex® rubbers are based on Smooth-On's Dragon Skin® technology and are currently available in four different hardness': Shore A-5, Shore 00-10, 00-30 and 00-50. They are suitable for a variety of applications including making prosthetic appliances, cushioning for orthotics and special effects applications (especially in animatronics where repetitive motion is required).

No particular handling was necessary with this type of material. Desired quantity of elements A was weighed and then part B was added as a consequence. Plastic (PP) petri were used and degassing (10 minutes) was applied before cure in order to avoid bubbles formation. The samples was left in a plane, room temperature place for 2 days before demolding.

For Ecoflex-ceramic composites the same procedure was adopted. The ceramic powder, opportunely dried, was added in the desired weight percent after the mixing of the A and B elements.

Depending on what type of sample was needed (planar for dielectric, elongation and electromechanical tests; cylindrical for compressive tests) petri with diameter 5,5 cm or small becker (5 ml, 2 cm diameter) were used.

Property	**Value**	**Units**
Components	A, B	-
Mixing ratio	1:1	by weight or volume
Density	1,07	g/cm^3
Pot life	48	min
Cure time	4	h
Temperature range	-19 to 232	°C
Dielectric strength	> 350	V/mm
Hardness	30	ShoreA
Producer	Smooth-On Inc. 2000 Saint John Street, Easton PA 18042 www.smooth-on.com	

Table 5.3. General properties of Ecoflex silicone by *Smooth-On*.

The other silicone based elastomer used is the Soma Foama 15 by *Smooth-On* too (**Soma Foama** in the following). It is a soft, two-component platinum silicone flexible foam that is versatile and easy to use. Mixed 2 Parts A : 1 Part B by volume, foam can be poured into a mold or over other surfaces. Pot life (working time) is 50 seconds at room temperature (73°F / 23°C) and handling time is 20 minutes at room temperature and full cure is 1 hour. Foam expands 4 times its original volume and develops a uniform 15 lb./cu. ft. cell structure (240 kg/m³). Cured foam is high heat resistance (will resist up to 350°F / 176°C), water resistant, UV resistant and resists oxidation and ozone degradation. Soma Foama can be used for a variety of industrial and special effects applications including making foam filled appliances, padding/seat cushioning, orthotics/orthopedics, potting and encapsulation of electrical circuits and vibration dampening.
No particular handling was necessary with this type of material. Desired quantity of elements A was weighed and then part B was added as a consequence. Plastic (PP) petri and steel tongue were used to mix the elements. The samples was left in a plane, room temperature place for 1 hour before demolding. No degassing was applied.
For Soma Foama-ceramic composites the same procedure was adopted. The ceramic powder, opportunely dried, was added in the desired weight percent preferably in the A component and mixed energetically in order to favour powder dispersion before the sudden increase of the viscosity due to B addition. When an homogeneous mixture were obtained, part B was added.

Property	**Value**	**Units**
Components	A, B	-
Mixing ratio	2:1	by volume
Density	0,24	g/cm^3
Pot life	30	s
Cure time	1	h
Temperature range	≤ 176	°C
Volumetric expansion	400	%
Producer	Smooth-On Inc. 2000 Saint John Street, Easton PA 18042 www.smooth-on.com	

Table 5.4. General properties of Soma Foama foam silicone by *Smooth-On*.

5.3.2 Polyurethanes

Two polyurethane materials were chosen, one in bulk (Poly74-20, by *Polytek* [12]) and one foam (EspakSoft, by *Prochima* [13]).

Poly74-20 Liquid Rubber (**Polytek** in the following) consists of Part A and Part B that, after mixing, cure at room temperature to flexible, high-strength, mold rubber. Polytek Rubber make durable, easy releasing molds for casting plasters and waxes without release agents, but are also excellent for casting cement, epoxy, polyester, urethane and acrylic with proper release agents. Allow to cure at room temperature, 77°F (25°C). Ultimate properties are reached in about seven days, but molds may be used with care after curing for 48 hours. Heat accelerates the cure - low temperatures slow the cure. Avoid curing in areas where the temperature is below 60°F (15°C). Both Parts A and B react with atmospheric moisture and, therefore, should be used up as soon as possible after opening.

Before resealing, Poly Purge™, a heavier-than-air dry gas, can be sprayed into open containers to displace moist air and extend storage life. Tools should be scraped clean before the rubber cures. Denatured ethanol is a good cleaning solvent, but is highly flammable and must be handled with extreme caution.

Care must be taken preparing Polytek samples due to the presence of isocyanates (part A) and fume hood and gloves must be used during the preparation. Desired quantity of elements A was weighed and then part B was added as a consequence. Plastic (PP) petri were used and degassing (10 minutes) was applied before cure in order to avoid bubbles formation. The samples was left in a plane, room temperature place for 2 days before demolding.

For Polytek-ceramic composites the same procedure was adopted. The ceramic powder, opportunely dried, was added in the desired weight percent after the mixing of the A and B elements.

Depending on what type of sample was needed (planar for dielectric, elongation and electromechanical tests; cylindrical for compressive tests) petri with diameter 5,5 cm or small becker (5 ml, 2 cm diameter) were used.

Property	**Value**	**Units**
Components	A, B	-
Mixing ratio	1:2	by weight
Density	1,01	g/cm^3
Pot life	30	min
Cure time	48	h
Storage temperature	15 to 22,5	°C
Hardness	20	ShoreA
Producer	Politek Development Corp. 55 Hilton Street, Easton, PA 18042 www.polytek.com	

Table 5.5. General properties of Polytek74-20 polyurethane by *Polytek*.

Espak Soft is a liquid polyurethanic bicomponent, freon free, which allows to obtain a soft closet cell foam at room temperature. It is particularly suitable for the realization of light and soft products like scenographic elements, technical articles, sportive articles, molds, dolls etc. The volume increase is 12-14 times in free foaming. Density can be increased foaming in closed molds depending on material quantity. A compact semi-lucid skin is formed onto the external surface. Nevertheless, water absorbance up to 20 weight% can be found. This is due to the rupture of external cells, most along the expansion direction.

No particular handling was necessary with this type of material. Desired quantity of elements A was weighed and then part B was added as a consequence. Plastic (PP) petri and steel tongue were used to mix the elements. The samples was left in a plane, room temperature place for 1 hour before demolding. No degassing was applied.

For Espak Soft-ceramic composites the same procedure was adopted. The ceramic powder, opportunely dried, was added in the desired weight percent preferably in the A component and mixed energetically in order to favour powder dispersion before the sudden increase of the viscosity due to B addition. When an homogeneous mixture were obtained, part B was added.

Property	Value	Units
Components	A, B	-
Mixing ratio	2:1	by weight
Density	0,055	g/cm^3
Pot life	15 - 20	s
Cure time	5 10	min
Volumetric expansion	1200-1400	%
Producer	Prochima Via G. Agnelli 6 - 61030 Calcinelli (PU) www.prochima.it	

Table 5.6. General properties of Espak Soft polyurethane by *Prochima*.

5.3.3 Ferroelectric ceramics

Among the broad field of electroactive ceramics, the Lead Magnesium Niobate Lead Titanate (**PMN-PT** in the following) was chosen as high dielectric constant material to increase the permittivity of elastomeric matrices for its good dielectric properties and stability.

PMN-PT is classified as a relaxor ferroelectric. Relaxors exhibit very high dielectric constants (ε>20000), diffuse ferroelectric-to-paraelectric phase transitions, and electrostrictive strain vs. electric field behaviour. Strain varies quadratically with electric field for an electrostrictor rather than linearly as for a piezoelectric. For transducer applications, electrostrictors must operate under a DC bias field to induce piezoelectric behaviour. Operation under bias is characterized by field dependent piezoelectric and electromechanical coupling coefficients.

In the past, PMN materials used for Sonar applications have suffered from low coupling, high loss, and poor reliability. TRS has developed PMN-PT formulations and processing methods that overcome these limitations [14].

Since it contains lead it should be handled with care. The PMN-PT powder was kept in a cool, dry place and the necessary quantities were dried in an oven (80°, 4 hours) before being used, in order to remove any water adsorbed.

Property	Value	Units
Components	PbO TiO2 $MgNb_2O_6$	72,6 wt% 7 wt% 20,4 wt%
Density	7,9	g/cm^3
Grain size	3 to 6	μm
Elastic modulus	1÷10	10^9 Pa
Melting point	1310 to 1350	°C
ε' @ 1kHz	18000	-
Appearance	White powder	-
Producer	TRS Ceramics, Inc. Suite J, 2820 East College Avenue, PA 16801 www.trstechnologies.com	

Table 5.7. General properties of PMN-PT powder by *TRS Ceramics*.

5.4 Experimental procedures

The experimental activity concerned in:

1. Dielectric characterization of composite samples
2. Dynamical-mechanical characterization of composite samples

5.4.1 Dielectric characterization of composite samples

Wideband dielectric spectroscopy was carried out on disc-shaped samples of the composites and the pure matrices (diameter of 11mm and thickness less than 1mm) at 20°C in the frequency range 10Hz-100MHz by means of a vector network analyser (mod. ZVRE by Rohde & Schwarz, Germany). The adopted procedure was based on the method proposed by Pelster [15] and has already been reported in detail elsewhere [16].
In the following the real and imaginary part of the samples permittivity are reported for each composition.

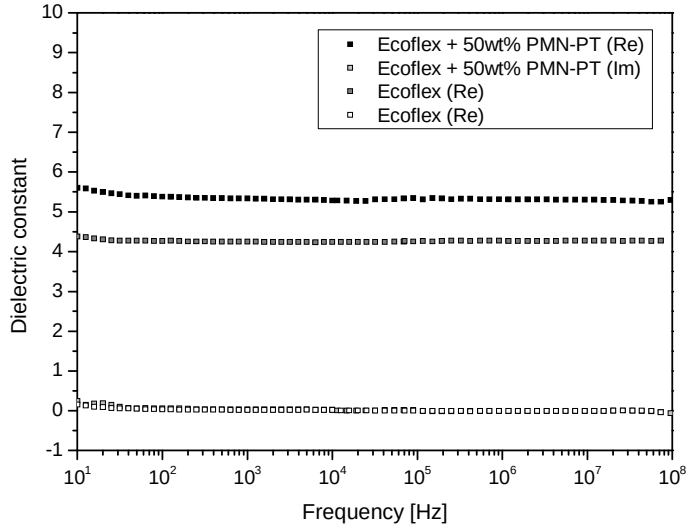

Figure 5.25. Dielectric constant *vs* frequency for Ecoflex samples.

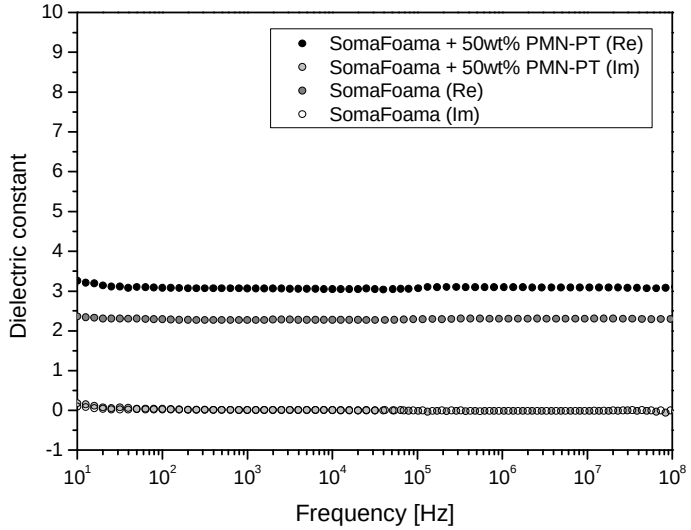

Figure 5.26. Dielectric constant *vs* frequency for SomaFoama samples.

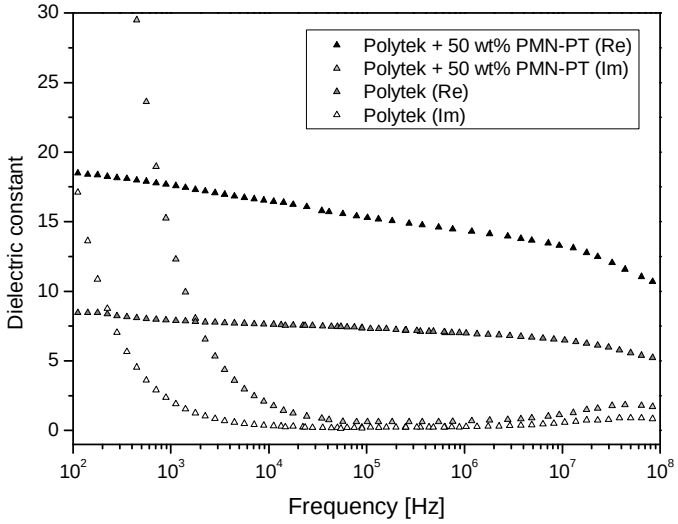

Figure 5.27. Dielectric constant *vs* frequency for Polytek samples.

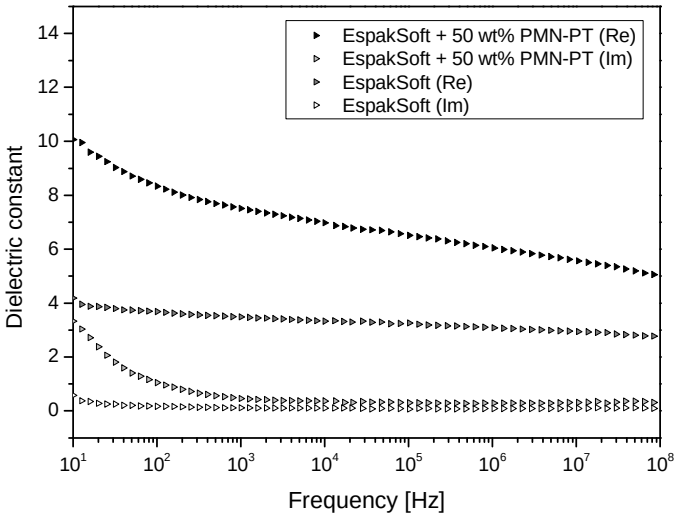

Figure 5.28. Dielectric constant *vs* frequency for EspakSoft samples.

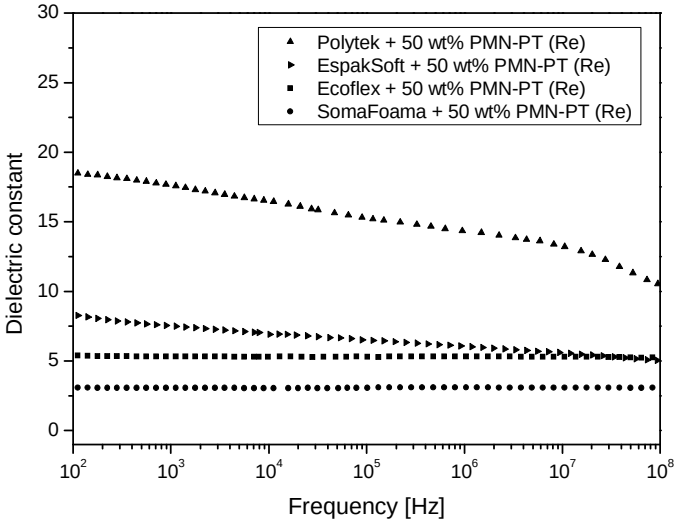

Figure 5.29. Comparison of the dielectric constant real part of silicone and polyurethane samples.

Frequency [Hz]	**Polytek**	**Polytek + 50 wt% PMN-PT**	**Increm. [%]**	**EspakSoft**	**EspakSoft + 50 wt% PMN-PT**	**Increm.** [%]
10	8	19	*+137*	4	10	*+150*
$250 \cdot 10^3$	7,5	16	*+113*	3,3	6,5	*+97*
10^8	5	10,5	*+110*	2,7	5	*+85*

Table 5.8. Dielectric constant values at 10, $250 \cdot 10^3$ and 10^8 Hz for polyurethane tested samples and relative increment with respect to the pure matrix.

Frequency [Hz]	**Ecoflex**	**Ecoflex + 50 wt% PMN-PT**	**Increm. [%]**	**SomaFoama**	**SomaFoama + 50 wt% PMN-PT**	**Increm.** [%]
10	4,37	5,6	*+28*	2,35	3,25	*+38*
$250 \cdot 10^3$	4,27	5,31	*+24*	2,31	3,08	*+33*
10^8	4,2	5,3	*+26*	2,3	3	*+30*

Table 5.9. Dielectric constant values at 10, $250 \cdot 10^3$ and 10^8 Hz for silicone tested samples and relative increment with respect to the pure matrix.

As summarised in Tab.5.8-5.9, by adding ceramic fillers into both silicone and polyurethane matrix the values of ε are increased. In particular, the Polytek polyurethane containing 50 wt% of PMN-PT shows the higher ε increment in term of absolute value (ε=19), while the Espak Soft corresponding sample shows the higher per cent increment (+150%) with respect to the pure material. Silicone based dielectric elastomers show less evident but still significant increases.

5.4.2 Dynamical-Mechanical characterization of composite samples

Composites and pure matrices were dynamical-mechanically tested by means of a dynamometer (model EPLEXOR® 100N by *GABO Qualimeter Testanlagen GmbH* [17], Germany), which was used, here and later during the development of wearable actuators, for measuring visco-elastic material properties depending on temperature, frequency and mechanical load. In particular both the real and imaginary part of the elastic modulus *E* were determined. Specimens in the form of cylinders 15 mm thick and about 15 mm wide were compressed in the range -5 to -30% at 20°C and 10 Hz frequency along the cylinder axis dimension. A dynamic strain of 2% was imposed during the overall test in order to verify if the filler loading damage the mechanical properties of the elastomer in terms of increased elastic modulus.

In the following an exemplifying graph showing the real and imaginary part of the elastic modulus *E* for a Ecoflex-based composite is reported. This is the sample that suffered most the presence of the ceramic filler. Other samples were not affected at all no particular increments of the elastic modulus have been registered for them.

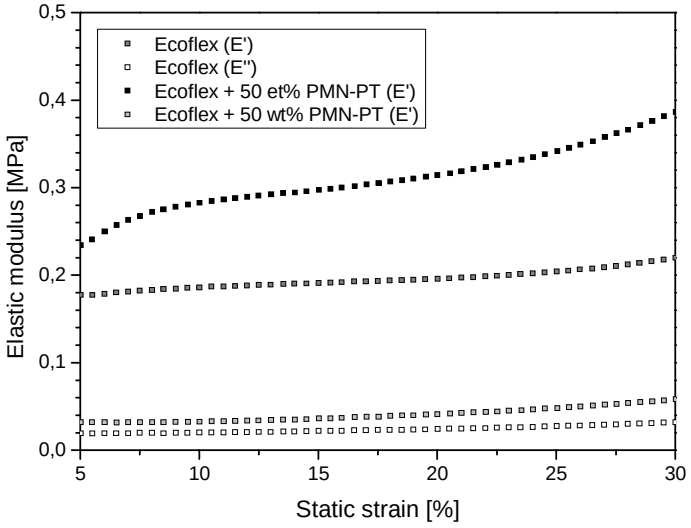

Figure 5.30. Elastic modulus in compression *vs* applied static strain for Ecoflex samples.

	Ecoflex	**Ecoflex + 50 wt% PMN-PT**	**Increment** [%]
Storage modulus [MPa]	0.193	0.304	*57*
Loss modulus [MPa]	0.022	0.038	*73*
Applied Static Stress [Mpa]	0.027	0.035	*29*

Table 5.10. Values of storage modulus, loss modulus and applied static stress for a Ecoflex sample before and after loading at 17,5 % static strain.

5.5 Conclusions

At the end of the activity concerning the development and characterization of electroactive PVDF devices to be employed as sensors for wearable applications, it can be affirmed that:

- it is possible to detect movement and physiological parameters (heart rate, breath rate, muscle activity) with good accuracy using PVDF sensors.
- PVDF sensors in the form of ribbon can be knitted into garments.
- conductive gel is not necessary for the developed PVDF sensors.
- PVDF sensors could be used as energy generators also.
- further improvements, in term of signal-to-noise ratio, could be achieved by using suited electronic filtering.
- results obtained indicate that a further study on the production of PVDF sensors in the form of fiber may be considered and that it would represent the new frontier in term of wearable electronics.

The second topic concerning the development and characterization of elastomeric materials suited for applications as dielectric materials in piezocapacitive devices, was successfully carried out. Soft silicone- and polyurethane-based matrices were loaded with PMN-PT ferroelectric ceramic and the resulting composites were dielectrically and mechanically analysed. Concluding, it can be affirmed that:

- by using opportune PMN-PT weight concentrations, it is possible to enhance the dielectric constant ε of both silicone and polyurethane matrices up to more than 2 times from the initial value (+150% increment for the Espak Soft sample containing PMN-PT).
- elastic modulus of obtained samples, measured in compressive conditions, is not particularly affected by the presence of the ceramic filler (higher E increase +57% for the Ecolfex sample containing PMN-PT).
- along with ε, also the sensitivity of the developed piezocapacitive sensors can be improve up to 2 times.
- a study (rheological characterization) of the influence of the viscous (dissipative) contribute of E to the overall response of this kind of devices has to be carried out, in order to develop even more efficient materials (reduce response times).
- the development of a PU/SI compatible-compliant-high electrically conductive material to be used as electrode (capacitor plates) has to be investigated.

5.6 References

[1] http://www.piezotech.fr/
[2] http://www.bksv.com/
[3] Sameni R. *et al*., *Proceedings of the IEEE Engineering in Medicine and Biology 27th Annual Conference*, Shangai, China, 2005
[4] Zhang W. *et al*., *Proceedings of the 7th World Congress on Intelligent Control and Automation*, Chongqing, China, 2008
[5] De Rossi D. *et al*., *Conference proceedings of the Annual International Conference of the IEEE Engineering in Medicine and Biology Society*, 6830-3, 2009
[6] Jeong J. W. *et al*., *World Congress on Medical, Physics and Biomedical Engineering (IFMBE)*, Munich, Germany, 25/5, 282-284, 2009
[7] Huang C-T. *et al*., *Sensors and Actuators A, Physical*, 141, 2, 396-403, 2008
[8] Maggiali M. *et al*., *Mechatronics*, Ireland, Limerick, 2008
[9] Gorjanc T. C. *et al*., *US Patent n. 2010/0282000*, 2010
[10] Chiang C-C *et al*., *Sensors and Actuators A*, 134, 382-388, 2007
[11] http://www.smooth-on.com/
[12] http://www.polytek.com/cart/
[13] http://www.prochima.it/
[14] http://www.trstechnologies.com/
[15] Pelster R., *IEEE Transactions on Microwave Theory and Tech*nology, *43*, 7, 1494, 1995
[16] Gallone G. *et al*., *Material Science & Engineering C*, *27*, 110, 2007
[17] http://www.gaboqualimeter.com/

Chapter 6

Wearable actuation
Materials, experimental procedures, results and discussion

I POLYMER BLENDING

During the overall PhD research, the main pursued activity has been the development of soft dielectric elastomers to use as actuators (electromechanical transducers) for wearable applications. The idea was to find a way to decrease the driving voltages needed to pilot such devices and make them more suitable for wearable applications. To do this, a systematic study on the permittivity and the elastic moduli of the materials selected as dielectric matrices was carried out, trying to increase the first without compromise the second. The blend approach and the structural modification under high electric fields were chosen as methods to increase the permittivity (as widely discussed in Ch.3). Good results has been achieved for both the approaches, as shown in the following paragraphs.

6.1 Materials

6.1.1 Silicones

Two silicone elastomers were chosen as matrices for actuating applications, one by *Smooth-On*, **Ecoflex** [1], and the other one by *BJB Enterprises Inc.*, TC-5005 A/B-C [2].

For a detailed description of Ecoflex silicone please refer to §5.3.

The second silicone used was the commercial TC-5005 A/B-C silicone (**BJB** in the following). It is a room temperature vulcanizing rubber intended primarily for making silicone skins, but it is also used as general purpose, high strength rubber. The main features of this product are its excellent physical properties such as high tear resistance, low viscosity and easily pouring, temperature resistance, high elongations and translucency.

It consists of three components, A, B, and C, the last one being the softener. BJB A/B is processed by adding curing agent B at a ratio of 10 parts by weight to 100 parts by weight of A. The BJB C component can be added as much as 50% to the total weight of BJB A/B (we chose 45 wt% for all formulations). This will increase the elongation and lower the amount of force needed to elongate the product.

No particular handling was necessary with this type of material. Plastic (PS) petri were used for the samples preparation and degassing (10 minutes) was applied soon after mixing before cure in order to avoid bubbles formation. Samples were left on a plane place for 1 day at room temperature before demolding.

For BJB/polyurethane blends a different procedure was adopted, which is reported in detail in §6.1.4.

Property	Value	Units
Components	A, B and C	-
Mixing ratio	B = 10wt% A C = 45wt% A+B	by weight
Density	1,14	g/cm^3
Pot life	40	min
Cure time	24	h
Elongation (A/B+C)	1000	%
Hardness	10	ShoreA
Producer	BJB Enterprises Inc. 14791 Franklin Avenue, Tustin, California www.bjbenterprises.com	

Table 6.1. General properties of TC-5005 A/B-C silicone by *BJB Enterprises Inc*.

6.1.2 Polyurethanes

Two polyurethane elastomers were chosen as matrices for actuating applications, Polytek by *Polytek* [3] and CLC by *Crosslink Technlogy Inc.* [4].

For a detailed description of Polytek polyurethanes (**Polytek** in the following) please refer to §5.3.2.

The CLC-005 (in the following **CLC**) urethane elastomers were developed by Crosslink Technology Inc. to accommodate applications requiring soft, abrasion resistant materials. These castable urethanes provide ease of processing, fast gel time and excellent cured properties. They are especially suited for casting, potting, rapid tooling and other cast urethane components. Aliphatic versions of these formulations provide improved performance.

Care must be taken when preparing CLC samples due to the presence of isocyanates (part B) and fume hood and gloves must be used during the preparation. Desired quantity of elements A was weighed and then part B was added as a consequence. Glass petri were used to avoid chemical reaction between the mold and the isocyanates and degassing (10 minutes) was applied before cure in order to avoid bubbles formation. The samples was left on a plane place for 2 days at room temperature before demolding.

For CLC-ceramic composites the same procedure was adopted. The ceramic powder, opportunely dried, was added in the desired weight percent after the mixing of the A and B elements.

Depending on what type of sample was needed (planar for dielectric, elongation and electromechanical tests; cylindrical for compressive tests) petri with diameter 5,5 cm or small becker (5 ml, 2 cm diameter) were used as molds.

Property	Value	Units
Components	A, B	-
Mixing ratio	100:18	by weight
Density	1,05	g/cm^3
Pot life	20	min
Cure time	48	h
Hardness	5	ShoreA
Producer	Crosslink Technology Inc. 6680 Finch Ave., West, Toronto, Canada www.crosslinktech.com	

Table 5.6. General properties of CLC polyurethane by *Crosslink Technology Inc*.

6.1.3 Conjugated/highly polarizable molecules

Due to positive results obtained previously by preparing dielectric blends with silicone elastomers and poly(3-hexylthiophene-2,5-dyil) (P3HT) [5], other three high dipole polymers were selected in order to test their effect onto the dielectric response of few matrices. They are reported below along with a brief description of their main physical and chemical characteristics. Conjugated and high dipole polymers such as polyphtalocyanines (Pc), poly(3,4-ethylenedioxythiophene) poly(styrenesulfonate) (PEDOT:PSS) and others have not been taken into account due to their scarce stability (they oxidize easily), their hygroscopicity and their difficulty to process (insoluble, etc) (Ch.3).

6.1.3.1 Thiophene

Thiophene is a heterocyclic compound consisting of a flat five-membered ring. It is aromatic as indicated by its extensive substitution reactions.

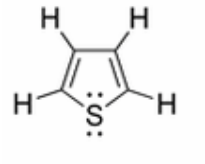

Figure 6.4. Thiophene chemical structure.

At room temperature, thiophene is a colorless liquid with a mildly pleasant odor reminiscent of benzene, with which thiophene shares some similarities. The high reactivity of thiophene toward sulfonation is the basis for the separation of thiophene from benzene, which are difficult to separate by distillation due to their similar boiling points (4 °C difference at ambient pressure). Like benzene, thiophene forms an azeotrope with ethanol.
The molecule is flat; the bond angle at the sulphur is around 93 degrees, the C-C-S angle is around 109, and the other two carbons have a bond angle around 114 degrees. The C-C bonds to the carbons adjacent to the sulphur are about 1.34Å, the C-S bond length is around 1.70 Å, and the other C-C bond is about 1.41 Å.
Thiophene is considered aromatic, although theoretical calculations suggest that the degree of aromaticity is less than that of benzene. The "electron pairs" on sulfur are significantly delocalized in the pi electron system. As a consequence of its aromaticity, thiophene does not exhibit the properties seen for conventional thioethers. For example the sulfur atom resists alkylation and oxidation.

Property	**Value**	**Units**
Formula	C_4H_4S	-
Dipole moment	0,52	D
Purity	> 99	%
Density	1,051	g/cm^3
MW	84,14	u.m.a.
T_m	-38	°C
Aspect	Colorless liquid	-
Producer	Sigma Aldrich Inc. 3050 Spruce St., St. Louis, MO 6310 www.sigmaaldrich.com	

Table 6.5. General properties of Thiophene by *Sigma Aldrich Inc.*

6.1.3.2 Poly(3-hexylthiophene-2,5-diyl) (P3HT)

Polythiophenes (PTs) result from the polymerization of thiophenes, a sulfur heterocycle, that can become conducting when electrons are added or removed from the conjugated π-orbitals via doping.

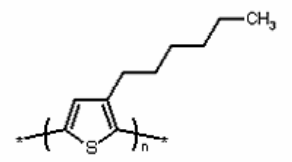

Figure 6.1. Poly(3-hexylthiophene-2,5-diyl) (P3HT) chemical structure.

Electrons are delocalized along the conjugated backbones of conducting polymers, resulting in an extended π-system with a filled valence band. By removing electrons from the π-system ("p-doping"), or adding electrons into the π-system ("n-doping"), a charged unit called a bipolaron is formed. The bipolaron moves as a unit up and down the polymer chain, and is responsible for the macroscopically observed conductivity of the polymer. Generally, the conductivity of PTs is lower than 10^3 S/cm ($\sigma_{Cu} \sim 5\times10^5$ S/cm). In this case the P3HT used was not doped [6] and we consider it just for its high dipole moment (μ = 1.9 D) which assures high polarizability.

The extended π-systems of conjugated PTs produce some of the most interesting properties of these materials, among which their optical properties. Conjugation relies upon overlap of the π-orbitals of the thiophene rings, which, in turn, requires them to be coplanar.

Property	**Value**	**Units**
Formula	$C_{10}H_{14}S$	-
Purity	90 to 94	%
Density	1,09	g/cm^3
MW	50000	u.m.a.
T_m	238	°C
Structure	Regioregular; undoped (non-conductive)	-
Aspect	Flakes	-
Producer	Rieke Metals Inc. 1001 Kingbird Rd., Lincoln, NE www.riekemetals.com	

Table 6.2. General properties of P3HT by *Rieke Metals Inc.*

6.1.3.3 Polyaniline (emeraldine base) (PANI)

Polyaniline (PANI) is a conducting polymer of the semi-flexible rod polymer family. Polymerized from the aniline monomer, polyaniline can be found in one of three idealized oxidation states:

1. Leucoemeraldine: white/clear and colorless
2. Emeraldine: green for the emeraldine salt, blue for the emeraldine base
3. (Per)nigraniline: blue/violet

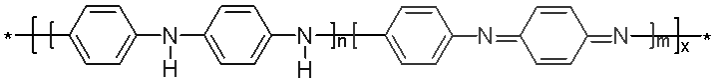

Figure 6.2. PANI emeraldine base chemical structure.

In Fig.1, *x* equals half the degree of polymerization (DP). Leucoemeraldine, with n = 1 and m = 0, is the fully reduced state. Pernigraniline is the fully oxidized state (n = 0, m = 1) with imine links instead of amine links. The emeraldine (n = m = 0.5) form of polyaniline, often referred to as emeraldine base (EB), is neutral, if doped it is called emeraldine salt (ES), with the imine nitrogens protonated by an acid. Emeraldine base is regarded as the most useful form of polyaniline due to its high stability at room temperature and the fact that, upon doping with acid, the resulting emeraldine salt form of polyaniline is electrically conducting. Leucoemeraldine and pernigraniline are poor conductors, even when doped with an acid.

The color change associated with polyaniline in different oxidation states can be used in sensors and electrochromic devices. Though colour is useful, the best method for making a polyaniline sensor is arguably to take advantage of the dramatic conductivity changes between the different oxidation states or doping levels.

In order to prevent electrical losses, due to doping process, and complications in the preparation procedure (doped PANI is insoluble in most of the common solvents), PANI was used in the emeraldine base form (Fig.6.2).

Property	**Value**	**Units**
Formula	$C_{24}H_{18}N_4$	-
Dipole moment	1,53	D
Density	0,804	g/cm^3
MW	100000	u.m.a.
T_m	> 350	°C
Structure	undoped (non-conductive)	-
Aspect	Powder	-
Producer	Sigma Aldrich Inc. 3050 Spruce St., St. Louis, MO 6310 www.sigmaaldrich.com	

Table 6.3. General properties of PANI by *Sigma Aldrich Inc.*

6.1.3.4 Pyrrole

Pyrrole is an heterocyclic aromatic organic compound, a five-membered ring. It is a colourless volatile liquid that darkens readily upon exposure to air.

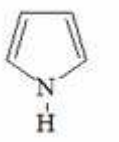

Figure 6.3. Pyrrole chemical structure.

The N*H* proton in pyrroles is moderately acidic with a pK_a of 16.5. Pyrrole can be deprotonated with strong bases such as butyllithium and sodium hydride. The resulting alkali pyrrolide is nucleophilic. Treating this conjugate base with an electrophile such as methyl iodide gives N-methylpyrrole.
The resonance contributors of pyrrole provide insight to the reactivity of the compound. Like furan and thiophene, pyrrole is more reactive than benzene towards electrophilic aromatic substitution because it is able to stabilize the positive charge of the intermediate carbocation.

Property	**Value**	**Units**
Formula	C_4H_5N	-
Dipole moment	1,81	D
Purity	98	%
Density	0,967	g/cm^3
MW	67,09	u.m.a.
T_m	-23	°C
Aspect	Yellow liquid	-
Producer	Sigma Aldrich Inc. 3050 Spruce St., St. Louis, MO 6310 www.sigmaaldrich.com	

Table 6.4. General properties of Pyrrole by *Sigma Aldrich Inc.*

6.1.4 Blends

Different combination of silicones, polyurethanes and conjugated/high dipole polymers were prepared during the experimental activity (taking into account the miscibility limitations of each component into the others). They are listed in the following with a brief description of the procedure adopted for their preparation.

Matrix	**Filler [vol%]**			
	BJB (SI)	**Ecoflex** (SI)	**Polytek** (PU)	**CLC** (PU)
BJB (SI)	/	/	5-10-15-20 30-40-60-***70***	20-25-***30***
Ecoflex (SI)	/	/	15-20-30-***40***	10-***20***
Polytek (PU)	***95***-90-85-80-70-60-40-30	***85***-80-70-60	/	/
CLC (PU)	***80***-75-70	***90***-80	/	/

Table 6.6. Formulations tested and miscibility thresholds (in bold).

6.1.4.1 BJB / highly polarizable molecules blends

Three different high dipole polymers were added to BJB in different amounts [7] in order to be compared with blends obtained with BJB and poly(3-hexylthiophene-2,5-diyl) (P3HT) during the past master thesis [5, 6].
The combinations prepared are listed in the table below.

P3HT [wt%]	**PANI** [wt%]	**Pyrrole** [wt%]	**Thiophene** [wt%]
0	0	0	0
1	1	1	1
3	3	3	3
5	5	5	5

Table 6.7. Highly polarisable molecules amounts in BJB silicone.

Except for the liquid thiophene and pyrrole, PANI and P3HT have been added to the silicone matrix after dissolution in chloroform by heating for about half an hour at 50°C. After, component A, B and C of BJB were added to the solution and the blend was left curing at ambient temperature for 36 hours al least.
For thiophene and pyrrole blends, the selected amount were added directly to the silicone pot and stirred vigorously.

6.1.4.2 Ecoflex / Polytek blends

Care must be taken when preparing samples containing Polytek polyurethane due to the presence of isocyanates (part A), and fume hood and gloves must be used during the preparation in order to avoid skin contact.
Due to the high reactivity of Polytek products, it is necessary to complete the mixing as quickly as possible. The best order of component mixing for the blend Ecoflex plus Polytek is reported below:

- (Ecoflex A + Polytek B) = Blend A (pre-mix)
- (Ecoflex B + Polytek A) = Blend B (pre-mix)
- (Blend A + Blend B)

By following this sequence the reactivity of the polyurethane is decreased and the viscosity of the system remain low enough to permit an efficient mixing of the parts.
The blend is degassed under vacuum for at least 10 minutes, then the cure proceeds at ambient temperature for about 72 hours.
The following combinations by volume of Polytek polyurethane into the Ecoflex silicone the were prepared:

- Ecoflex 85vol% + Polytek 15vol%
- Ecoflex 80vol% + Polytek 20vol%
- Ecoflex 70vol% + Polytek 30vol%
- Ecoflex 60vol% + Polytek 40vol%

Other combinations resulted not feasible due probably to a miscibility limit of the two elastomers into each other. In such cases the systems remained uncured.
Glass Petri have been used for all the formulations tested to avoid chemical reaction between the mould and the component of the blend.

6.1.4.3 Ecoflex / CLC blends

Care must be taken when preparing samples containing Crosslink Technology polyurethane due to the presence of isocyanates (part B), and fume hood and gloves must be used during the preparation in order to avoid skin contact.
Since the high reactivity of Crosslink Technology products, it is necessary to complete the mixing as quickly as possible. The best order of component mixing for the blend BJB A/B-C plus CLC is reported below:

- (Ecoflex A + CLC A) = Blend A (pre-mix)
- (Ecoflex B + CLC B) = Blend B (pre-mix)
- (Blend A + Blend B)

By following this sequence the reactivity of the polyurethane is decreased and the viscosity of the system remains low enough to permit an efficient mixing of the parts.
The blend is degassed under vacuum for at least 10 minutes then the cure proceeds at ambient temperature for about 72 hours.

The following combinations by volume of CLC polyurethane into the Ecoflex silicone the were prepared:

- Ecoflex 80vol% + CLC 20vol%
- Ecoflex 90vol% + CLC 10vol%

Other combinations were not feasible due probably to a miscibility limit of the two elastomers into each other. In these cases the systems remained uncured.
Glass Petri have been used for all the formulations tested to avoid chemical reaction between the mould and the component of the blend.

6.1.4.4 BJB / CLC blends

Care must be taken preparing samples containing Crosslink Technology polyurethane due to the presence of isocyanates (part B), and fume hood and gloves must be used during the preparation in order to avoid skin contact.
Since the high reactivity of Crosslink Technology products, it is necessary to complete the mixing as quickly as possible. The best order of component mixing for the blend BJB A/B-C plus CLC is reported below:

- (BJB A + BJB C + CLC A) = Blend A (pre-mix)
- (BJB B + CLC B) = Blend B (pre-mix)
- (Blend A + Blend B)

Following this sequence the reactivity of the polyurethane is decreased and the viscosity of the system remains low enough to permit an efficient mixing of the parts.
The blend is degassed under vacuum for at least 10 minutes than the cure proceeds at ambient temperature for about 72 hours.
The following combinations by volume of CLC polyurethane into the BJB silicone the were prepared:

- BJB 80vol% + CLC 20vol%
- BJB 75vol% + CLC 25vol%
- BJB 70vol% + CLC 30vol%

Other combinations resulted not feasible due probably to a miscibility limit of the two elastomers into each other. In these cases the systems remained uncured.
Glass Petri have been used for all the formulations tested to avoid chemical reaction between the mould and the component of the blend.

6.1.4.5 BJB / Polytek blends

Care must be taken preparing samples containing Polytek polyurethane due to the presence of isocyanates (part A), and fume hood and gloves must be used during the preparation in order to avoid skin contact.
Since the high reactivity of Polytek products, it is necessary to complete the mixing as quickly as possible. The best order of component mixing for the blend BJB A/B-C plus Polytek is reported below:

- (BJB A + BJB C + Polytek B) = Blend A (pre-mix)
- (BJB B + Polytek A) = Blend B (pre-mix)
- (Blend A + Blend B)

Following this sequence the reactivity of the polyurethane is decreased and the viscosity of the system remain low enough to permit an efficient mixing of the parts.
The blend is degassed under vacuum for at least 15 minutes, then the cure proceeds at ambient temperature for about 72 hours.
The miscibility of the BJB silicone and the Polytek polyurethane is higher with respect to the other combinations tested so the following percentages by volume were prepared:

- BJB 95vol% + Polytek 5vol%
- BJB 90vol% + Polytek 10vol%
- BJB 85vol% + Polytek 15vol%
- BJB 80vol% + Polytek 20vol%
- BJB 70vol% + Polytek 30vol%
- BJB 60vol% + Polytek 40vol%
- BJB 40vol% + Polytek 60vol%
- BJB 30vol% + Polytek 70vol%

The formulation 50/50 vol% was not feasible due probably to a miscibility limit of the two elastomers into each other, the same for the combinations that provided an amount of PU higher than 70 vol%. In these cases the systems remained uncured.
Polystyrene Petri have been used for all the formulations tested without problems of demoulding or chemical reaction with the component of the blend.

6.1.4.6 BJB / Polytek / highly polarisable molecules (P3HT) blends

Finally, five blends of Polytek (PU) in BJB (SI) plus P3HT were prepared. The blend BJB 70 vol% + Polytek 30 vol% was chosen as matrix among the others since it showed the best performance in terms of mechanical and dielectric response and reproducibility.
The following combination by weight of P3HT in the SI/PU blend were prepared:

- BJB 70vol% + Polytek 30vol% + 0,3 wt% P3HT
- BJB 70vol% + Polytek 30vol% + 0,6 wt% P3HT
- BJB 70vol% + Polytek 30vol% + 1,0 wt% P3HT
- BJB 70vol% + Polytek 30vol% + 1,5 wt% P3HT
- BJB 70vol% + Polytek 30vol% + 2,0 wt% P3HT

having just foung in a previous work [6] that the blend BJB + 1,0 wt% P3HT had good performance in terms of dielectric, mechanical and electromechanical response.
Care must be taken preparing samples containing Polytek polyurethane due to the presence of isocyanates (part A), and fume hood and gloves must be used during the preparation in order to avoid skin contact.
As described in §6.1.4.1, P3HT flakes were dissolved in chloroform before the mixing with the elastomeric matrix. Due to the presence of the strong solvent, glass petri were used for the preparation and the cure of the blends. In particular, a tailored glass mold was

prepared having rectangular chambers (4×10 cm) so that the simultaneous preparation of all the chosen formulations was possible.
Due to the high reactivity of Polytek products, it is necessary to complete the mixing as quickly as possible. The best order of component mixing for the blend BJB A/B-C plus Polytek plus P3HT is reported below:

- (BJB A + P3HT in $CHCl_3$) = Blend A
- Almost complete chloroform evaporation
- (Blend A + Polytek A) = Blend 2
- (BJB B + BJB C + Polytek B) = Blend 3
- Blend 2 + Blend 3

By following this sequence the reactivity of the polyurethane is decreased and the viscosity of the system remains low enough to permit an efficient mixing of the parts.
The blend is degassed under vacuum (a trap is used to avoid damage from $CHCl_3$ residues) for at least 15 minutes, then the cure proceeds at ambient temperature for about 72 hours.

6.2 Experimental procedures

Different blends were prepared during the experimental activity in order to test the influence of interphase onto the dielectric and electromechanical response of several elastomeric mixtures. Results obtained were compared with that of pure materials and composites to show differences and to verify theoretical models. The main steps of the activity have been, in order:

1. Infra-red (IR) spectroscopy of the materials as received and of the prepared blends
2. Dielectric characterization (Wide band dielectric spectroscopy)
3. Morphological characterization (SpotLight FT-IR, SEM)
4. Thermo-Dynamical-Mechanical characterization (DMTA)
5. Electromechanical characterization of best performing samples

6.2.1 Infra-red (IR) spectroscopy of materials as received and their blends

Qualitative FT-IR spectra were collected by using a Nicolet 380 FT-IR spectrometer by *Thermo Electron Corporation* [8].
Dielectric elastomers, before and after curing, were analyzed in order to find analogies and differences among each others. Their spectra were compared and used to solve some problems occurred during experimental activity, as in the case of CLC polyuretane by Crossilink Technology whose cure was partially inhibited by using polystyrene petri instead of glass petri. See comments in the following for a better deepening of the problem.
IR spectra of blends were used to investigate the presence or absence of new bonds occurring between the different phases.

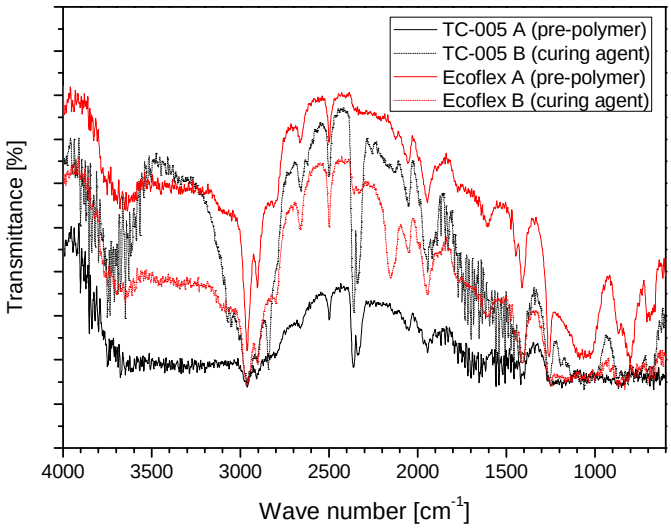

Figure 6.5. IR spectrum of BJB and Ecoflex silicone components.

As it often happens for commercial polymer products, FT-IR spectra of the neat components contain a lot of peaks not well defined. Among all, however, typical absorptions of silicones can be identified (anti-symmetric stretching absorption of Si-O-Si at 1078 cm^{-1} and others) and they are reported in the table below (bold characters are used to highlight the typical absorptions of tested substances.

Wave number [cm^{-1}]	**Part**	**Corresponding chemical group**	**Type of absorption**
818	A, B	**C-H *in* CH_3 + Si-C**	rocking + stretching
1078	A, B	**Si-O-Si**	a. stretching
1260	A, B	**C-H *in* Si-CH_3**	in plane deform.
700-1420-3000	A, B	C-H *in* CH_3	in plane deform.
1930	A, B	C=C	a. stretching
2150	B	C≡C	stretching
2500	A, B	O-H	stretching
2800/3000	A, B	C-H *in* CH_3	s./a. stretching
3500/3700	A, B	O-H	stretching

Table 6.8. Main absorption peaks in Ecoflex silicone components by *Smooth-On*.

Wave number [cm^{-1}]	**Part**	**Corresponding chemical group**	**Type of absorption**
818	A, B	**C-H *in* CH_3 + Si-C**	rocking + stretching
1078	A, B	**Si-O-Si**	a. stretching
1260	A, B	**C-H *in* Si-CH_3**	in plane deform.
700-1400-3000	A, B	C-H *in* CH_3	in plane deform.
1930	A, B	C=C	a. stretching
2350	A, B	C-O_2 *in* CO_2	stretching
2500	A, B	O-H	stretching
2800/3000	A, B	C-H *in* CH_3	s./a. stretching
3500/3700	A, B	O-H	stretching

Table 6.9. Main absorption peaks in BJB silicone components by *BJB Enterprises*.

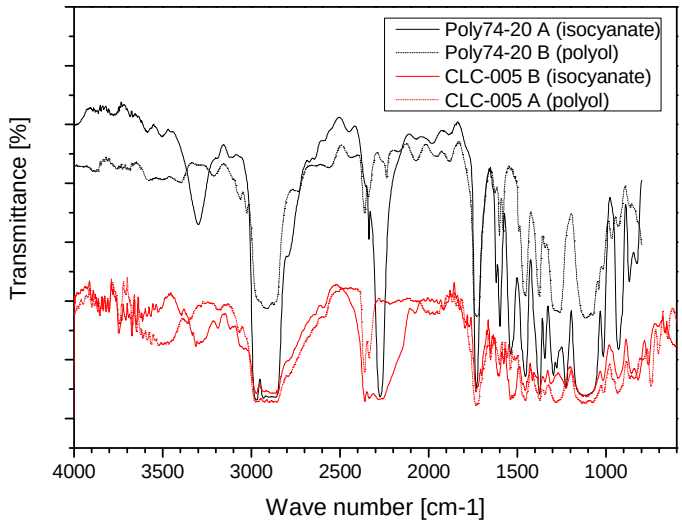

Figure 6.6. IR spectrum of Polytek and CLC polyurethane components.

FT-IR spectra for Polytek and Crosslink Tech. polyurethane components contains less and more defined peaks than those of silicones. Typical absorptions of polyols and isocyanates for the two different products are reported in the table below.

Wave number [cm^{-1}]	**Part**	**Corresponding chemical group**	**Type of absorption**
809	A, B	C-H *in* CH_2	rocking
1000	A, B	**N-C *in* CH-NH_2**	stretching
1110	A, B	**C-O**	stretching
1450	A, B	**C=C**	stretching
1531	A, B	N-H	in plane deform.
1731/1223	A, B	**C=O**	stretching
2273	A	**-N=C=O**	a. stretching
2350	B	C-O_2 *in* CO_2	stretching
2800/3000	A, B	C-H *in* CH_2	s./a. stretching
3300/900	A	N-H 2°	stretching/wagging
3500	B	O-H	stretching

Table 6.10. Main absorption peaks in Polytek polyurethane components by *Polytek*.

Wave number [cm^{-1}]	**Part**	**Corresponding chemical group**	**Type of absorption**
809	A, B	C-H *in* CH_2	rocking
1000	A, B	**N-C *in* CH-NH_2**	stretching
1110	A, B	**C-O**	stretching
1450	A, B	**C=C**	stretching
1531	A, B	N-H	in plane deform.
1731/1223	A, B	**C=O**	stretching
2150	B	C≡C	stretching
2273	B	**-N=C=O**	a. stretching
2350	A, B	C-O_2 *in* CO_2	stretching
2800/3000	A, B	C-H *in* CH_2	s./a. stretching
3300/900	A	N-H 2°	stretching/wagging
3500/3700	B	O-H	stretching

Table 6.11. Main absorption peaks in CLC polyurethane components by *Crosslink Technology*.

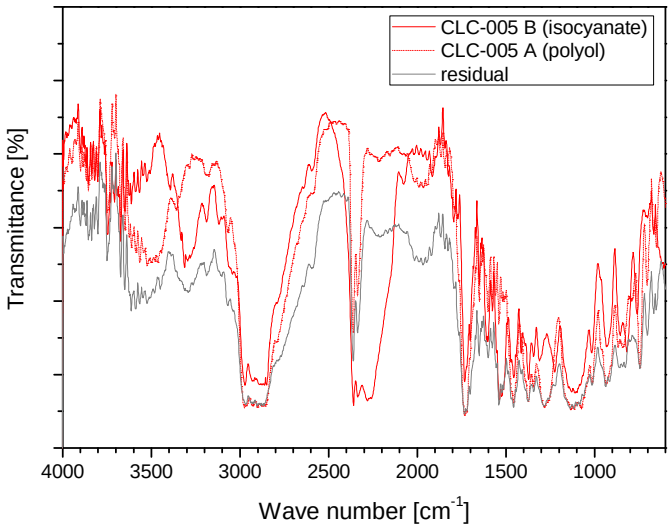

Figure 6.7. IR spectrum of CLC polyurethane components and residual after curing in polystyrene moulds.

In order to analyse the nature of residuals found after the cure of CLC polyurethane in polystyrene petri, the FT-IR spectra reported in Fig.6.7 were acquired. The analysis shows that residuals consisted mainly of polyol component and that it was due probably to the fact that isocyanate groups reacted with hydrogens of CH_2 in polystyrene inhibiting instead of reacting with hydrogen in polyol as asual. Samples for dielectric and mechanical tests were therefore prepared using glass petri.

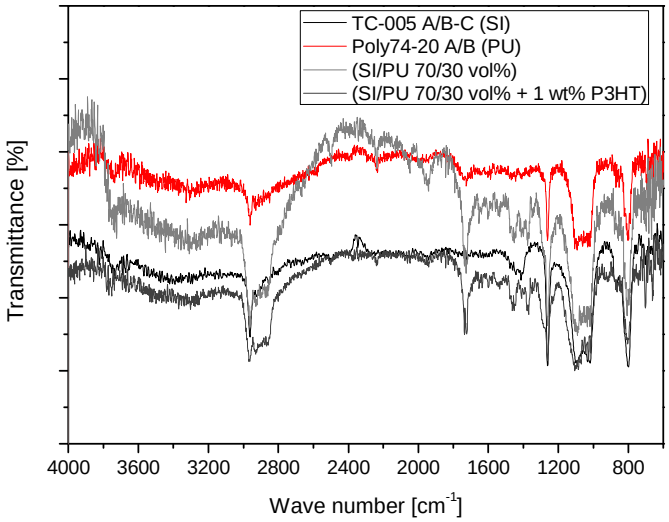

Figure 6.8. IR spectrum of BJB, Polytek, their 70/30 vol% blend and the blend with 1 wt% P3HT.

Fig.6.8 shows FT-IR spectra of cured BJB silicone, Polytek polyurethane and their 70/30 vol% blend. The three cited matrices are compared with each other and with the blend containing 1 wt% of P3HT. From the data collected it is not possible to assess if new bonds had formed between silicone, polyurethane and P3HT, but it is evident that the two SI/PU

blends are very similar to each other, along with two peaks centred at 700 cm^{-1} due to the out of plane deformation of C-H bonds in the thiophene group.

6.2.2 Wide band dielectric spectroscopy

Samples were prepared as described in §5.4.1 and a vector network analyser (mod. ZVRE by Rohde & Schwartz) was used for the measurements according to [9]. Dielectric spectra of both real and imaginary part of permittivity were thus acquired and they are reported in the following.

6.2.2.1 Pure silicone and polyurethane dielectric analysis

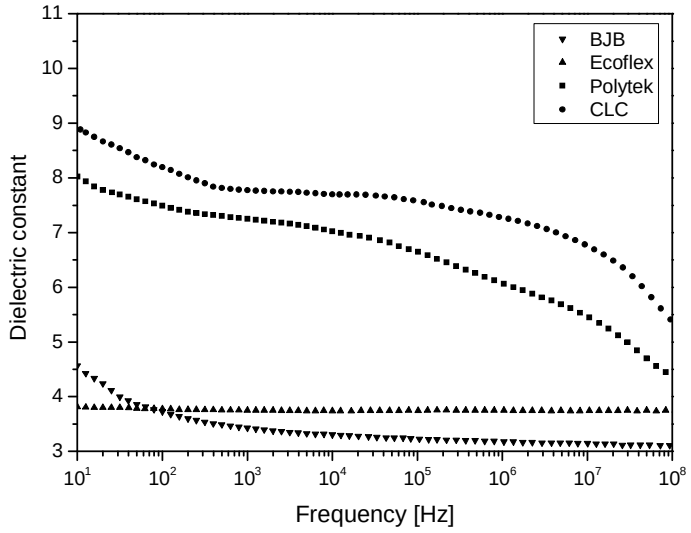

Figure 6.9. Real part of the dielectric permittivity for the pure silicone and polyurethane matrices.

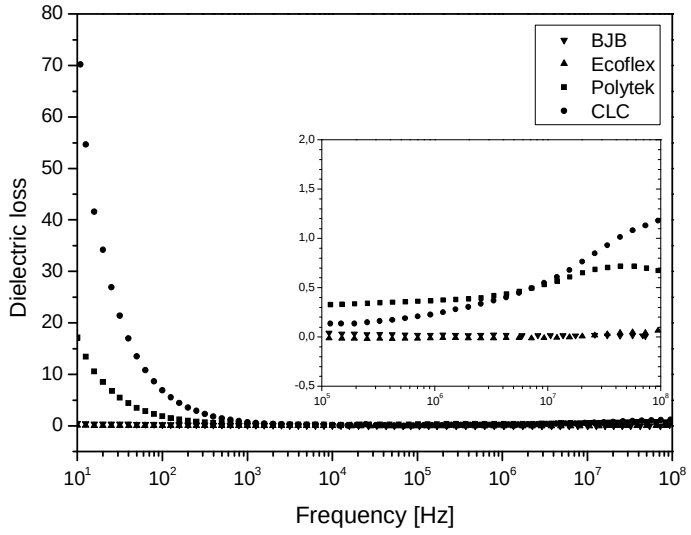

Figure 6.10. Imaginary part of the dielectric permittivity for the pure silicone and polyurethane matrices.

Due to their different chemical nature, silicones and polyurethanes show different dielectric responses. Polyurethane in particular, with their higher dipolar groups (μ_{C-N}= 1.15 D; $\mu_{C=O}$ = 2.3 D [10]) present higher polarity and thus higher dielectric constant (8 and 9 at 10Hz respectively) along with intense relaxations whose presence is visible in the

extreme left and right part of the spectrum (see Fig.6.9 and the detail of Fig.6.10). On the contrary, silicones, mainly containing Si-O (μ_{Si-O} = 0.24 D) and Si-C (μ_{Si-C} = 0.7 D) groups [10, 11], have lower dielectric constants (3,8 and 4,5 at 10 Hz respectively) with weak or absent relaxations. Imaginary part of permittivity, depending on electronic, dipolar and losses, is higher for polyurethanes in the low frequency region and often it is useful to investigate the presence of water absorbed inside the bulk material (ε_{H_2O} at 10 Hz ~ 90, μ_{H_20} = 1,84 D [12]).
Dielectric spectra of pure matrices were used to be compared with those of blends in order to find differences and understand the role of interfaces.

6.2.2.2 Silicone matrix loaded with highly polarizable molecules

In the following the dielectric constants of silicone BJB containing 1, 3, and 5 wt% of conjugated highly polarizable molecules are shown.

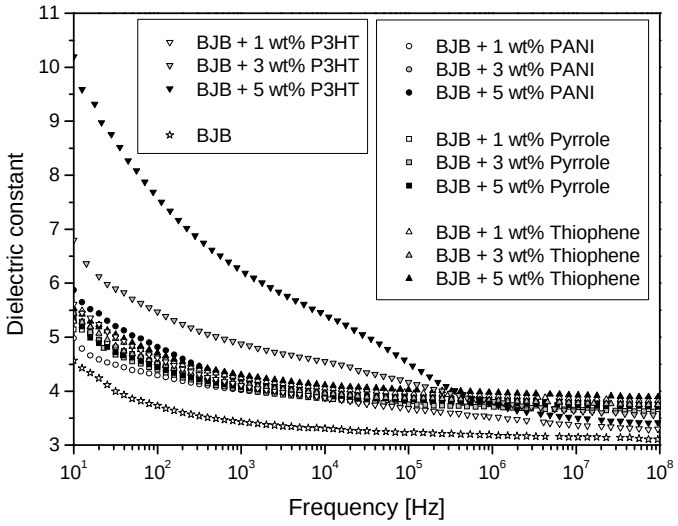

Figure 6.11. Real part of the dielectric permittivity for the silicone/highly polarizable molecules blends.

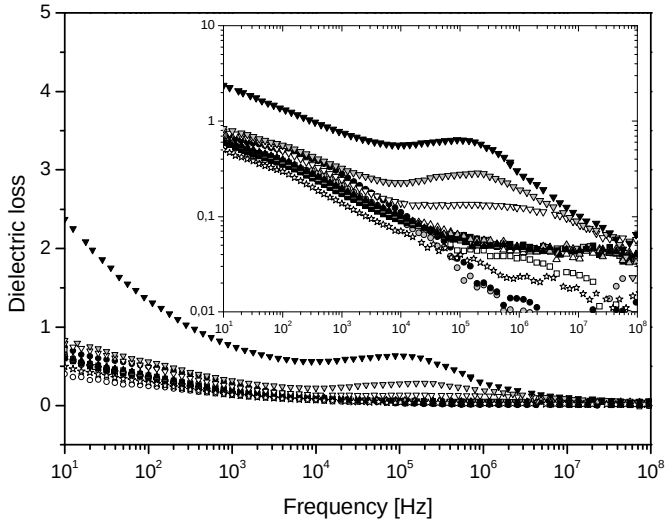

Figure 6.12. Imaginary part of the dielectric permittivity for the silicone/highly polarizable molecules blends.

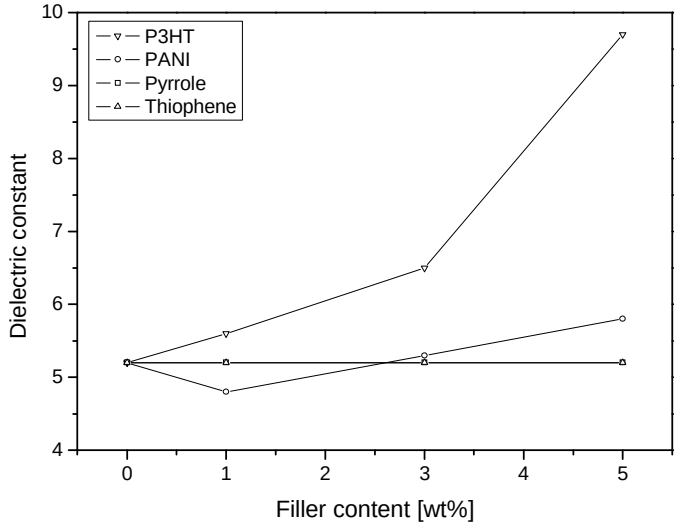

Figure 6.13. Dependence of the dielectric constant at 10 Hz on the filler content for the silicone (BJB)/highly polarizable molecules blends.

As it is clear from Fig.6.13, neither thiophene nor PANI nor pyrrole produce increment of ε higher than that shown using P3HT at the tested loading factors. P3HT, in fact, is the only filler, among those tested, that was able to increase the overall dielectric constant of the blend up to 10,2, starting from a value of 4,5 for the pure matrix. For this reason, this kind of approach, using highly polarizable molecules to increase the dielectric constant of silicone matrices, was abandoned.

6.2.2.3 Ecoflex / Polytek blends

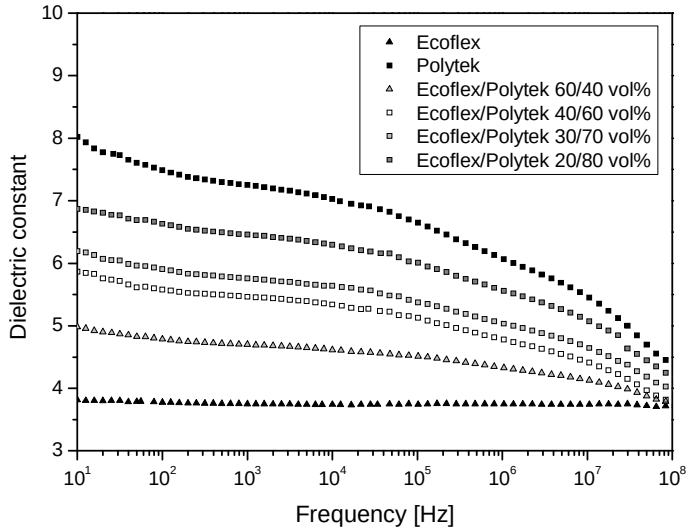

Figure 6.14. Real part of the dielectric permittivity for the Ecoflex/Polytek blends.

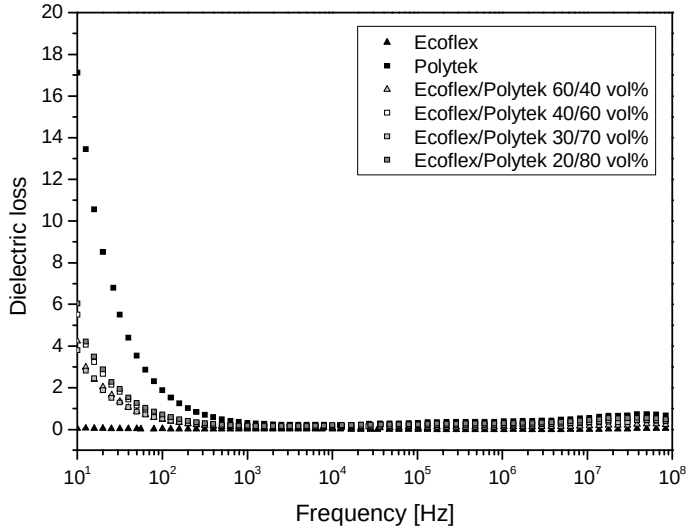

Figure 6.15. Imaginary part of the dielectric permittivity for the Ecoflex/Polytek blends.

Similarly to what happens when an high dielectric constant filler is added to a lower dielectric constant material [13], the resulting dielectric constant of the prepared blends resulted comprised among the values of the two pure constituents, for all the formulations tested. This effect is described by the Effective Medium Theory (§3.2.1 and [13]) and doesn't give interesting results for low dielectric constant materials as those studied. We can conclude that the blending of Ecoflex silicone and Polytek polyurethane hasn't brought to notable dielectric results.

6.2.2.4 Ecoflex / CLC blends

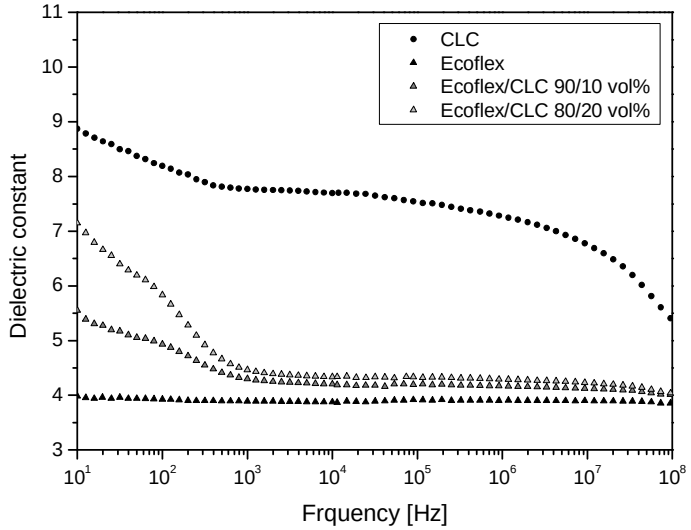

Figure 6.16. Real part of the dielectric permittivity for the Ecoflex/CLC blends.

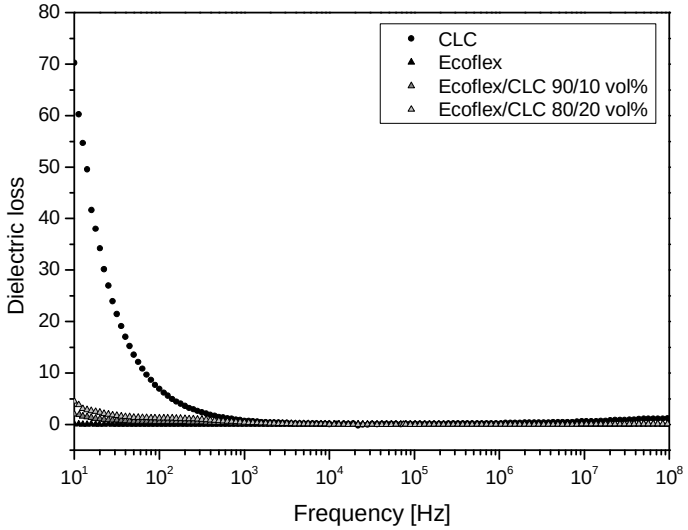

Figure 6.17. Imaginary part of the dielectric permittivity for the Ecoflex/CLC blends.

As in the case of Ecoflex/Polytek, also for Ecoflex/CLC the blends dielectric constants are comprised among those of the pure matrices, even if a definite relaxation appears at about 10^2 Hz. This suggests that, increasing the miscibility threshold of CLC in Ecoflex, a positive increment of the ε, over that of the pure CLC, could, in principle, be possible.

6.2.2.5 BJB / CLC blends

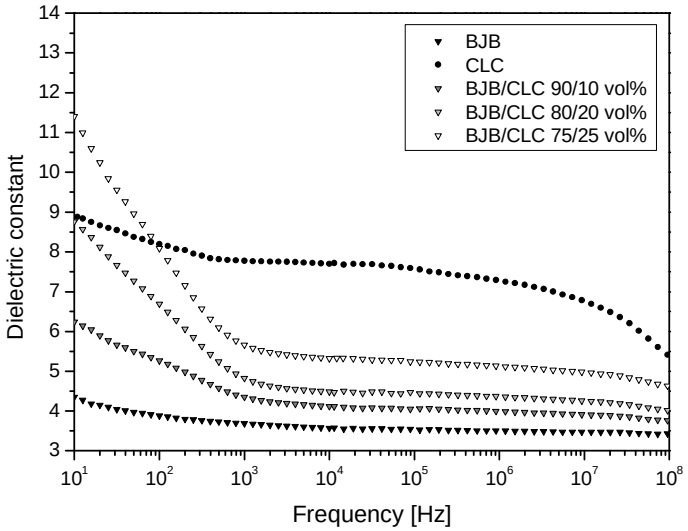

Figure 6.18. Real part of the dielectric permittivity for the BJB/CLC blends.

Differently from the cases previously studied, blends of BJB/CLC show an interesting behaviour with respect to the pure matrices at low frequencies. The dielectric constant of the blend containing 75 vol% of silicone in polyurethane, in fact, is higher than that of the polyurethane itself, that is the component with the highest permittivity between the two blend constituents. This phenomenon can't be explained with the Effective Medium Theory (§3.2.1 and [13]). To deeply understand the response of such a kind of system, the

Interfacial Theory must be considered. As broadly discussed in §3.4.1, this new approach takes into account the influence of the interphase between the two components of the blends. This interphase generally shows proper and unique dielectric properties, different from those of the initial constituents, and thus, possibly higher than those of the highest of the two. Since the model predicts a maximum in the dielectric constant of the blend in correspondence of about the 40% volume fraction of the component having the higher ε between the two (depending on the system under study), we can expect a further increase in the dielectric response for new formulations prepared using higher CLC polyurethane content. The miscibility of the two components into each others have to be increased somehow to obtain this effect [14, 15].

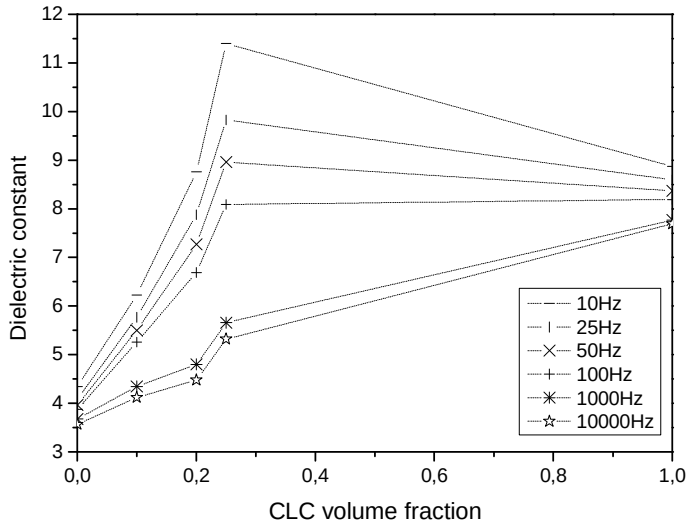

Figure 6.19. Dependence of the dielectric constant on the CLC content for the BJB/CLC blends at different frequencies.

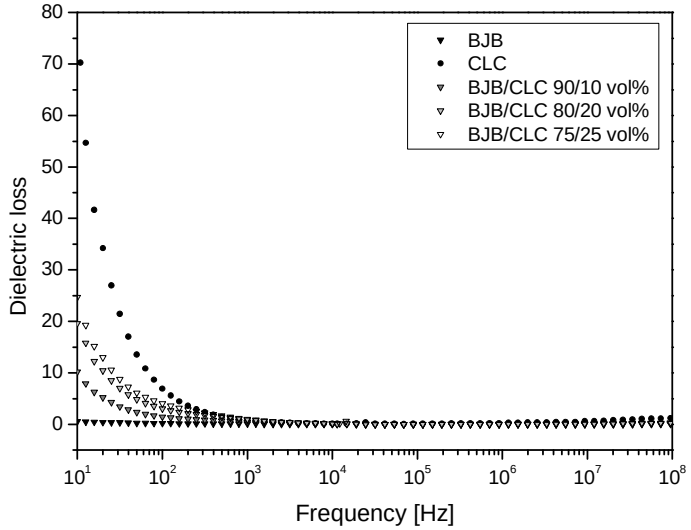

Figure 6.20. Imaginary part of the dielectric permittivity for the BJB/CLC blends.

6.2.2.6 BJB / Polytek blends

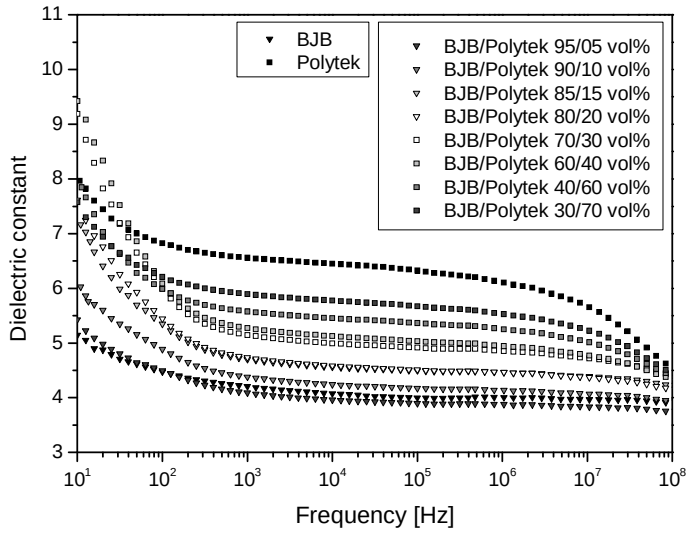

Figure 6.21. Real part of the dielectric permittivity for the BJB/Polytek blends.

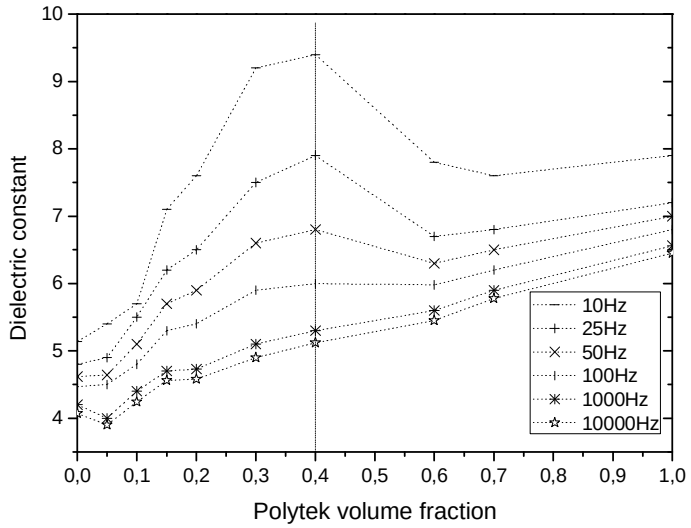

Figure 6.22. Dependence of the dielectric constant real part on the Polytek content for the BJB/Polytek blends at different frequencies.

As in the case of the BJB/CLC blends, also for two of the combination of BJB/CLC tested (70/30 vol% and 60/40 vol% respectively) the dielectric response of the blend overcomes that of the pure polyurethane at low frequencies.

The results obtained with this series of blends are in agreement with the Theory of Interphase (Fig.3.39 in §3.4.1) which takes into account interactions between the blends constituents and predicts a maximum for the ε_{blend} as previously discussed.

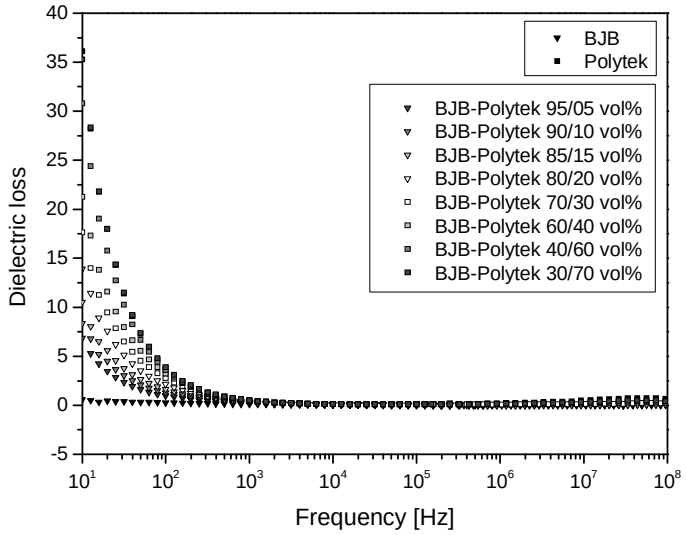

Figure 6.23. Imaginary part of the dielectric permittivity for the BJB/Polytek blends.

6.2.2.7 BJB / Polytek / P3HT blends

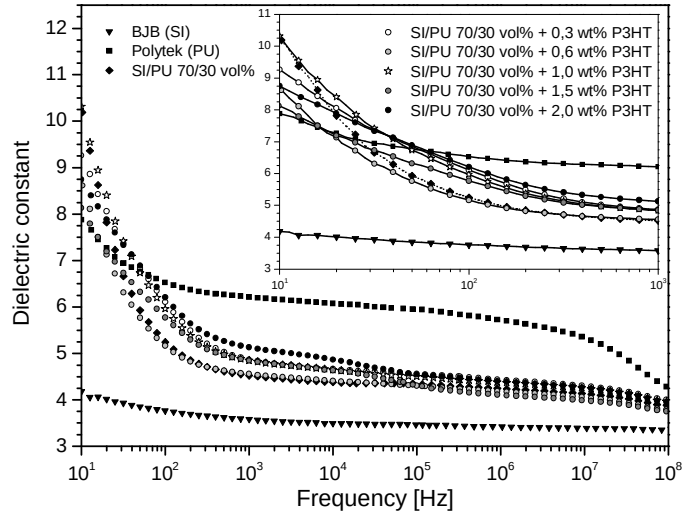

Figure 6.24. Real part of the dielectric permittivity for the BJB/Polytek/P3HT blends.

Thanks to the good dielectric results obtained with the BJB/Polytek blends, the formulation at 70 vol% SI content was selected for further investigations aboutr the interface approach and to increase the dielectric response. Blends of BJB/Polytek and CLC/BJB, although they gave good results, were not used since more difficult to handle.

The BJB/Polytek 70/30 vol% formulation was used to prepare a new series of blends loaded with the highly polarizable P3HT, already described in the previous paragraphs. The dielectric results obtained show a further increase of the dielectric constant with respect to the starting BJB/Polytek 70/30 vol% blend for the concentration of P3HT of 0,3, 1 and 2 wt% in the range 10-10^2 Hz, as shown in Fig.6.24.

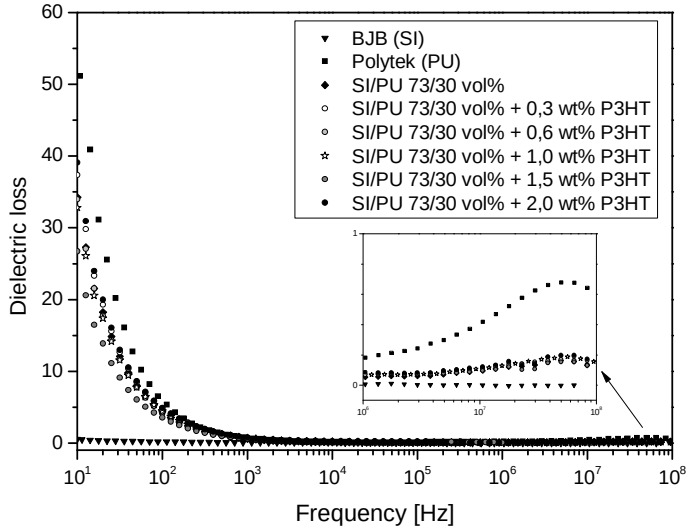

Figure 6.25. Imaginary part of the dielectric permittivity for the BJB/Polytek/P3HT blends.

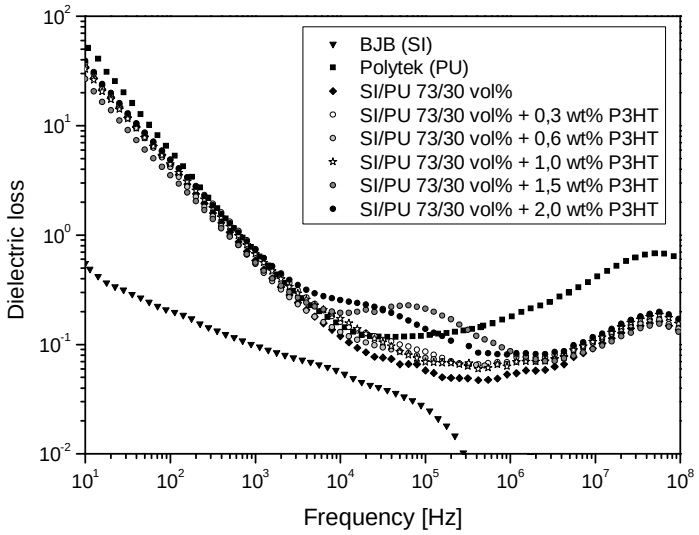

Figure 6.26. Imaginary part of the dielectric permittivity for the BJB/Polytek/P3HT blends (magnification).

Figs.6.25-6.26 report the dielectric losses of the prepared blends, putting into evidence the relaxations phenomena occurring in the samples after the loading with P3HT (Fig.6.26). Two peaks are evident for the samples containing respectively the 1,5 and 2,0 wt% of P3HT, one centred at 10^5 and the other at about $3 \cdot 10^4$ Hz.

6.2.3 Morphological characterization

The blend BJB/Polytek 60/40 and 70/30 vol%, selected as the best candidate materials among those prepared, thanks to their high ε and easiness to be handled, were morphological characterized in order to well define the role of interphases.

6.2.3.1 Spotlight FT-IR spectroscopy

A first preliminary analysis with the Spotlight 200 FT-IR Microscope by Perkin-Elmer [16] was performed. Morphological and chemical results are reported in the following. Samples were broken in liquid nitrogen to obtain brittle fractures of their section.

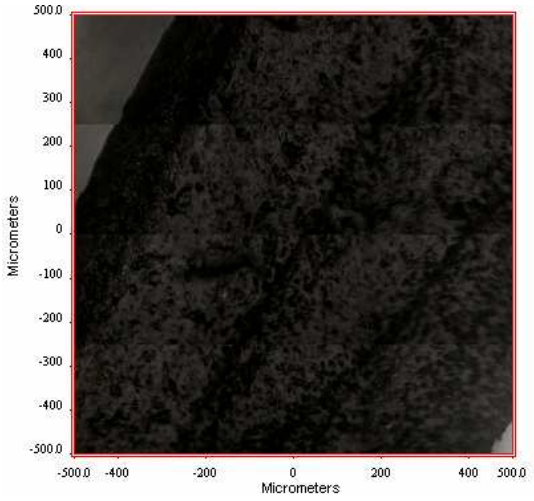

Figure 6.27. Optical image of the blend BJB/Polytek 60/40 vol%.

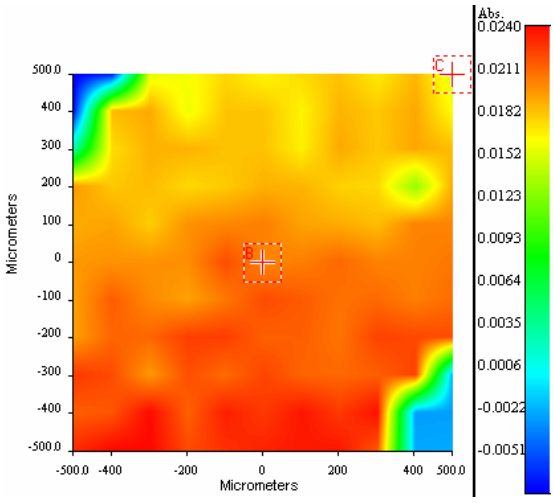

Figure 6.28. Chemical map of the blend BJB/Polytek 60/40 vol%.

Fig.6.27 and 6.28 show a heterogeneous structure of the section of the sample containing at least two predominant phases. One distributed through the bulk (characterized by a yellow to red gradient) and one in proximity of the external surfaces and concentrated in a single internal point at 400-200μm (green).

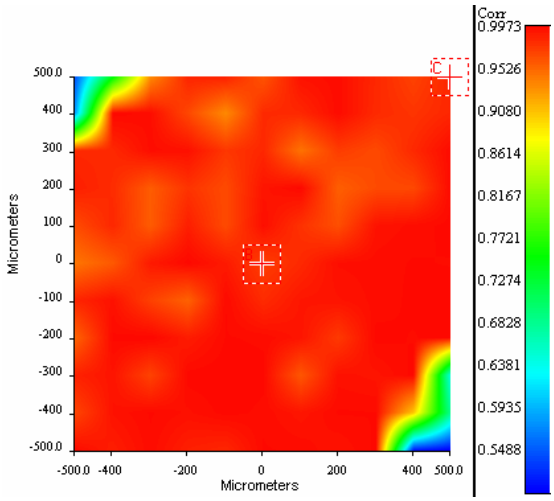

Figure 6.29. Correlation map of the blend BJB/Polytek 60/40 vol% with respect to the BJB.

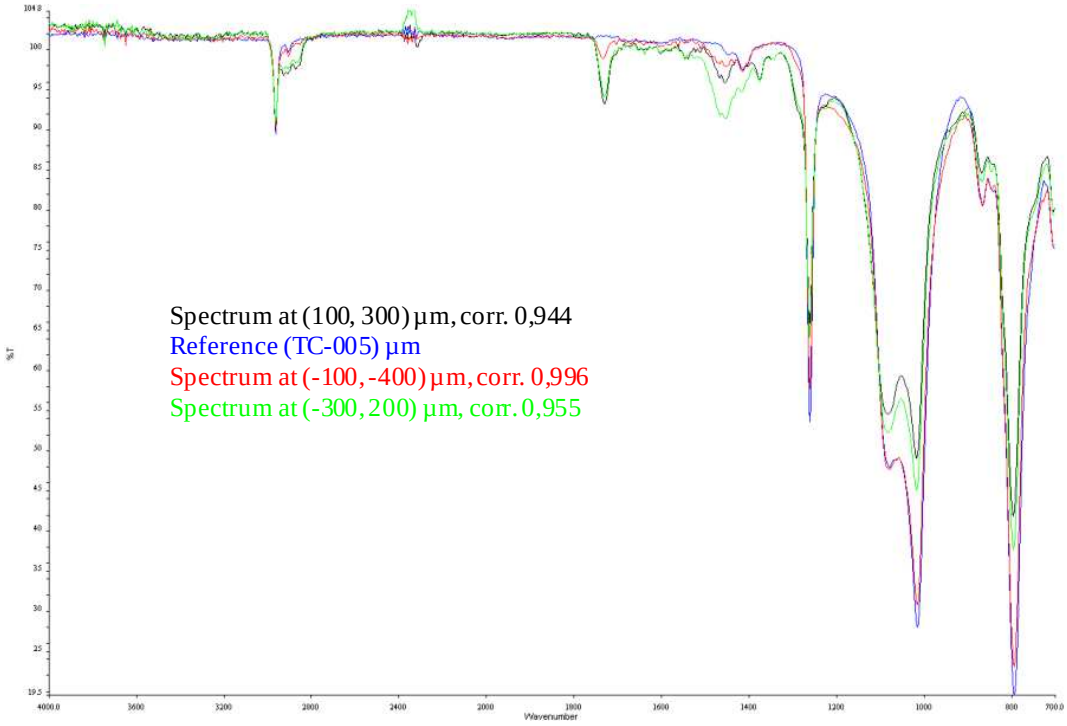

Figure 6.30. FT-IR Spotlight spectra of the blend BJB/Polytek 60/40 vol% taken in three different points.

From Fig.6.29 and the spectrum reported in Fig.6.30 it seems that the bulk material is constituted mainly of silicone, except for some yellow areas (corr. 0,94) distributed through the section.

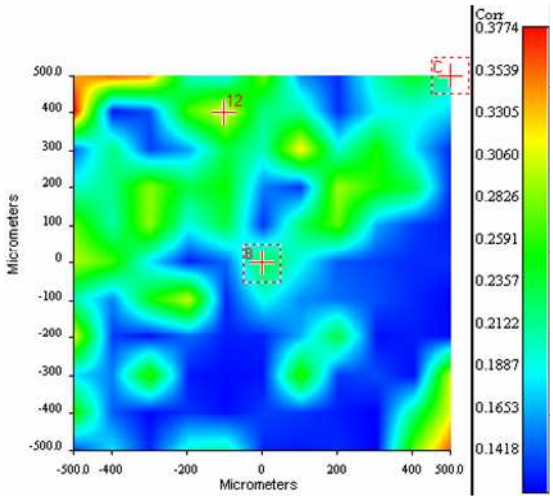

Figure 6.31. Correlation map of the blend BJB/Polytek 60/40 vol% with respect to the Polytek.

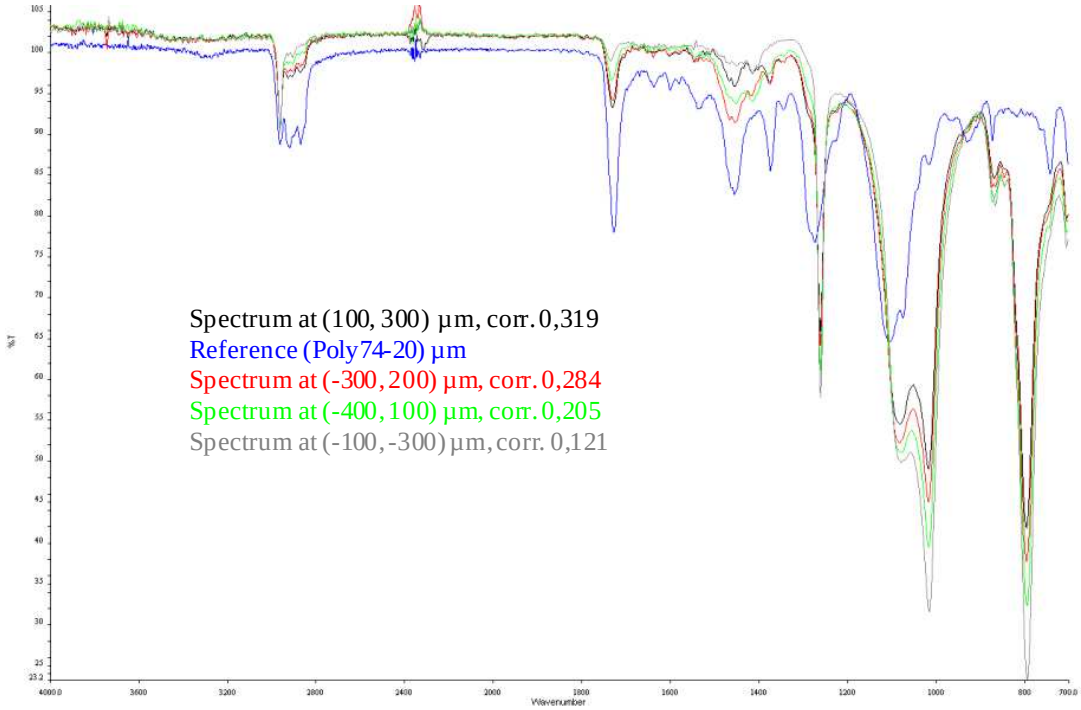

Figure 6.32. FT-IR Spotlight spectra of the blend BJB/Polytek 60/40 vol% taken in four different points.

By analysing the presence of polyurethane instead, as reported in Fig. 6.31 and 6.32, it emerges that, as supposed, the bulk is constituted by a mix of silicone and polyurethane more or less homogeneously distributed across the section.

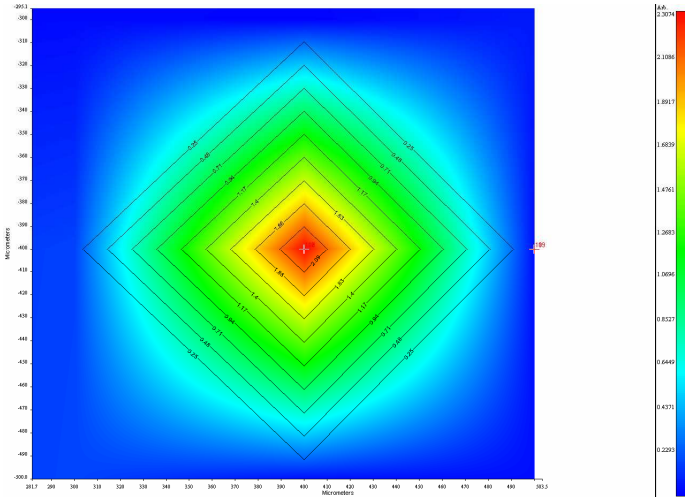

Figure 6.33. Band ratio of a detail of the blend BJB/Polytek 60/40 vol%.

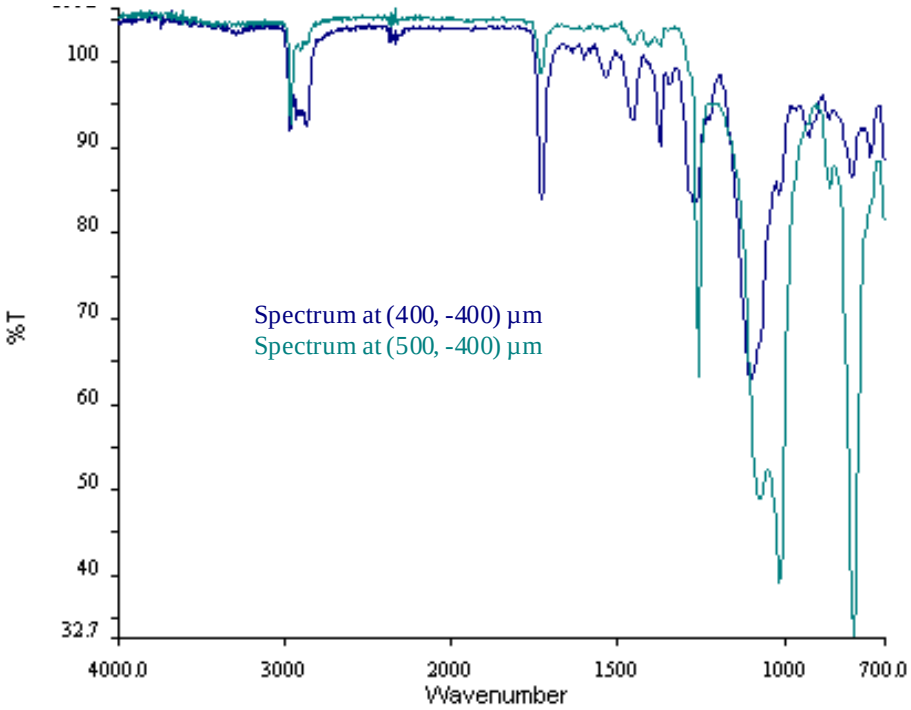

Figure 6.34. FT-IR Spotlight spectra of the blend BJB/Polytek 60/40 vol% taken in two different points.

Fig.6.33 and relatives spectra report the magnification of a detail in order to show the effective presence of a gradient of concentration along the diameter of the inclusions.

6.2.3.2 Scanning Electron Microscopy (SEM)

A scanning electron microscope mod. JSM-5600LV by *Jeol* was used to collect images of the sample sections at different magnifications. Energy Dispersive X-ray spectroscopy was also carried out in order to discriminate among the different SI and PU concentrations.

Ecoflex/Polytek blends

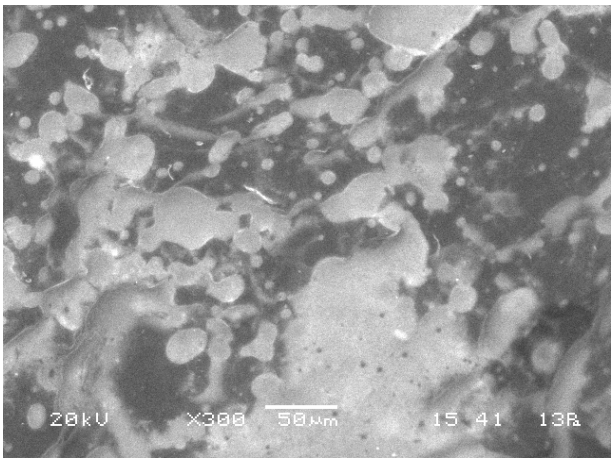

Figure 6.35. SEM image of the blend Ecoflex/Polytek 15/85 vol%.

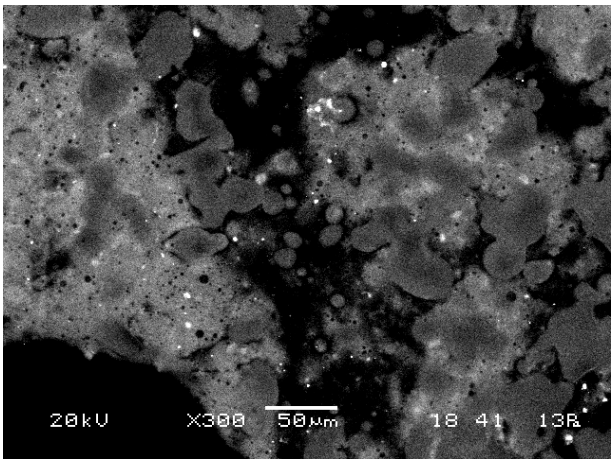

Figure 6.36. SEM image of the blend Ecoflex/Polytek 20/80 vol%.

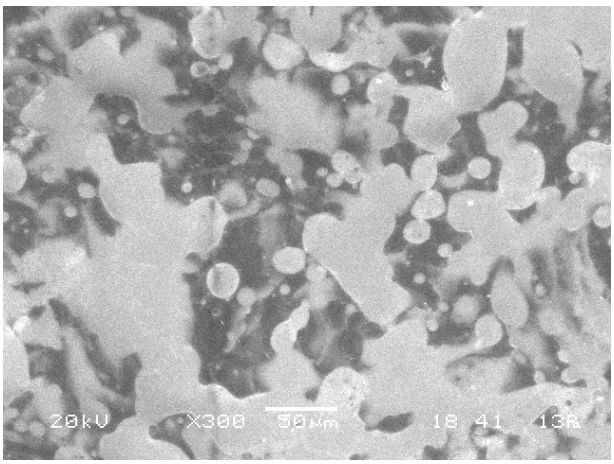

Figure 6.37. SEM image of the blend Ecoflex/Polytek 30/70 vol%.

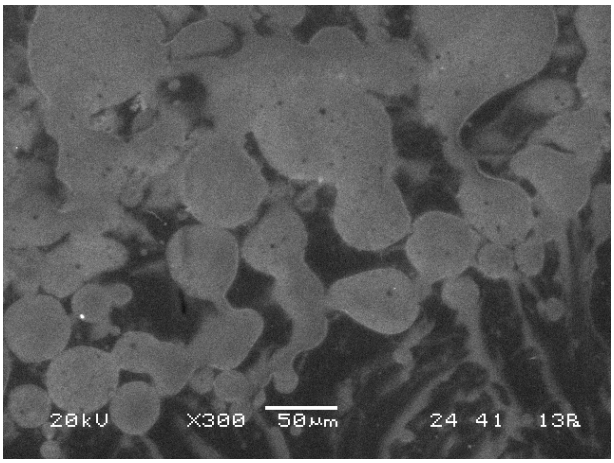

Figure 6.38. SEM image of the blend Ecoflex/Polytek 40/60vol%.

Fig.6.35-38 show the Ecoflex/Polytek blends section at 300x. The bulk material appears as constituted by two principal phases, one marked by a light grey colour (SI inclusions) and the other dark grey (PU matrix). The inclusions are characterized by a circular shape and tend to merge as the concentration increases.

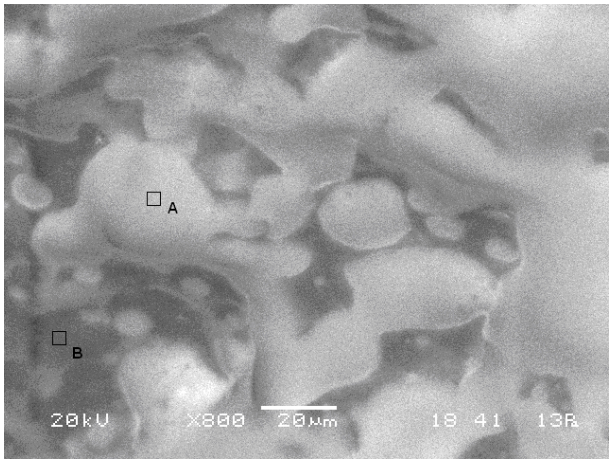

Figure 6.39. SEM image of the Ecoflex/Polytek 30/70 vol%.

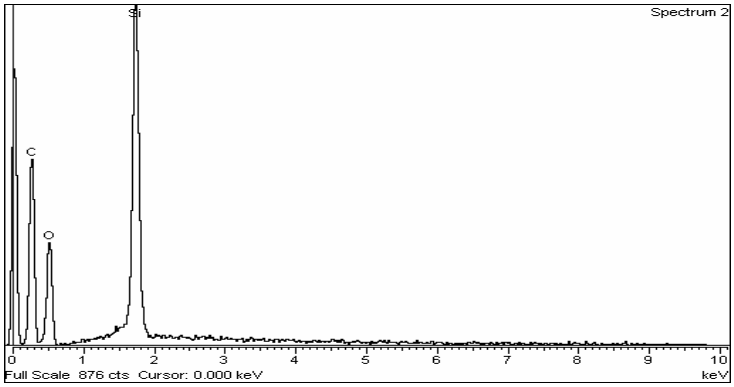

Figure 6.40. EDS (Energy Dispersive X-ray spectroscopy) spectra of the blend Ecoflex/Polytek 30/70 vol% in point *B*.

Fig.6.40 shows the chemical spectrum of a darker region characterized by the presence of Si, C and O atoms. This confirms that it is constituted by a mix of polyurethane and silicone, as expected from the volume ratios of the components inside the blend.

Concentrations by weight relative to the blends studied are collected in Tab.6.12 for the matrices and inclusions respectively. As one can notice from Tab.6.12, concentrations of C and O are higher for the matrix (dark grey regions, PU presence) with respect to the inclusions which resulted mainly constituted by silicones.

	Blend 15/85 vol%		**Blend 20/80 vol%**		**Blend 30/70 vol%**		**Blend 40/60 vol%**	
[wt%]	Matrix	Inclusion	Matrix	Inclusion	Matrix	Inclusion	Matrix	Inclusion
C	58	50	53	33	52	38	58	36
O	26	24	35	35	36	30	24	30
Si	16	26	12	32	12	32	18	34

Table 6.12. Weight percentages for the main elements (C, O, Si) in the Ecoflex/Polytek samples analyzed.

Ecoflex/CLC blends

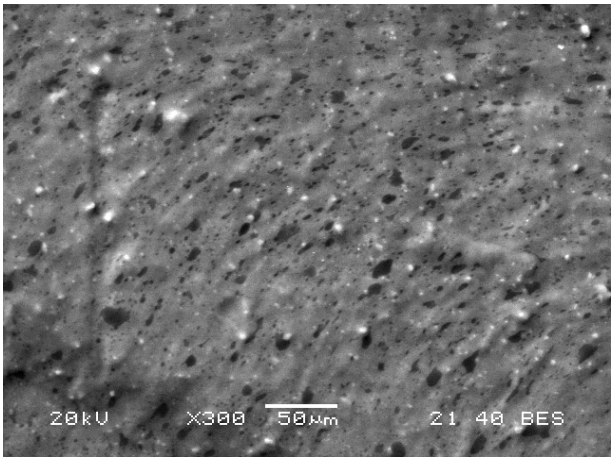

Figure 6.41. SEM image of the blend Ecoflex/CLC 80/20 vol%.

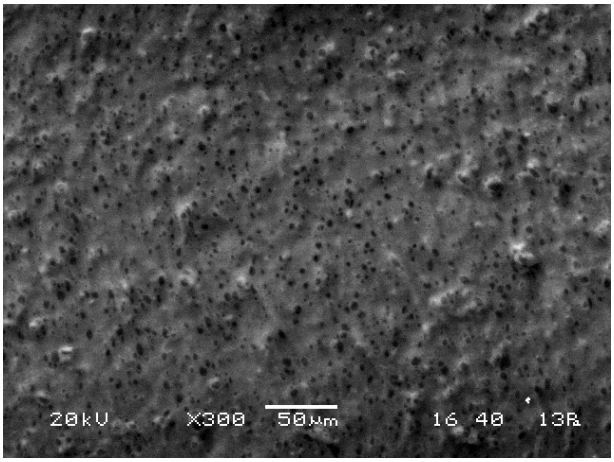

Figure 6.42. SEM image of the blend Ecoflex/CLC 90/10 vol%.

Fig.6.41-42 show the Ecoflex/CLC blends section at 300x. Also in this case the bulk material appears as constituted by two principal phases, one marked by a light grey colour (matrix) and the other dark grey (PU inclusions). The inclusions are smaller than those seen in the Ecoflex/Polytek blends and they are characterized by an irregular shape (see detail in Fig.6.43).

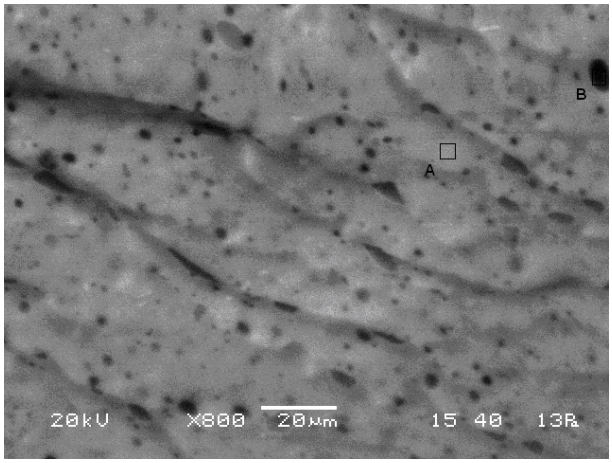

Figure 6.43. SEM image of the Ecoflex/CLC 90/10 vol%.

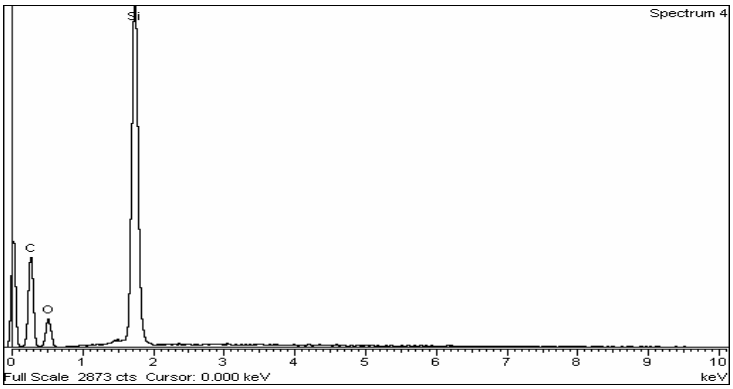

Figure 6.44. EDS (Energy Dispersive X-ray spectroscopy) spectra of the blend Ecoflex/CLC 90/10 vol% in point *B.*

Fig.6.44 shows the chemical spectrum of a darker region characterized by the presence of Si, C and O atoms. This confirms that it is constituted by a mix of polyurethane and silicone, as expected from the volume ratios of the components inside the blend. Concentrations by weight relative to the blends studied are collected in Tab.6.13 for the matrices and inclusions respectively. As one can notice from Tab.6.13, concentrations of C and O are higher for the inclusions (dark grey regions, PU presence) with respect to the matrix, which resulted mainly constituted by silicones.

	Blend 80/20 vol%		**Blend 90/10 vol%**	
[wt%]	Matrix	Inclusion	Matrix	Inclusion
C	36	n.a.	31	59
O	26	n.a.	31	21
Si	38	n.a.	38	20

Table 6.13. Weight percentages for the main elements (C, O, Si) in the Ecoflex/Polytek samples analyzed (n.a. not available).

BJB/CLC blends

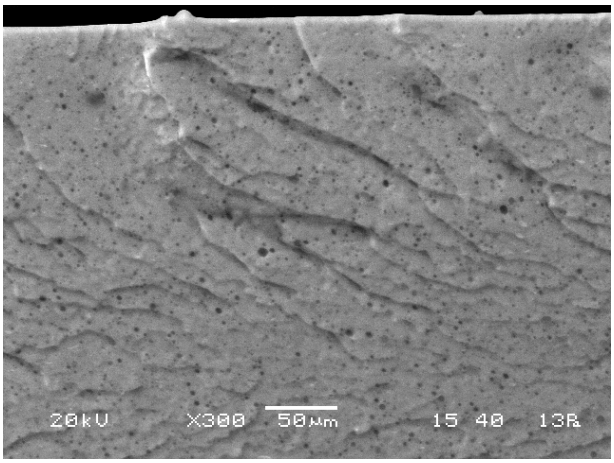

Figure 6.45. SEM image of the blend BJB/CLC 70/30 vol%.

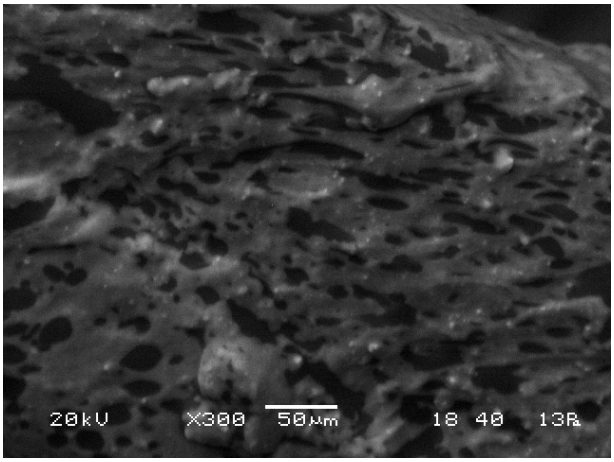

Figure 6.46. SEM image of the blend BJB/CLC 75/35 vol%.

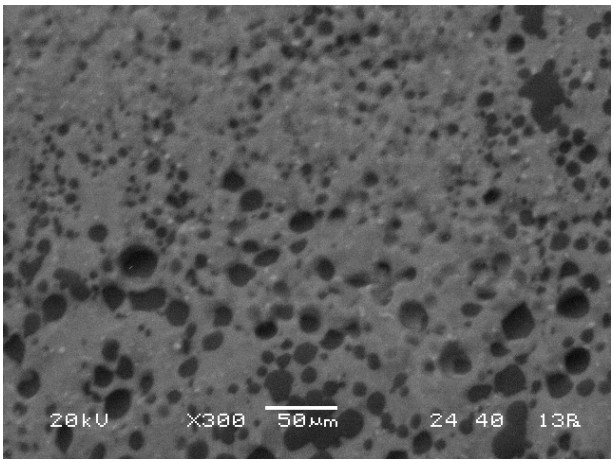

Figure 6.47. SEM image of the blend BJB/CLC 80/20 vol%.

Fig.6.45-47 show the BJB/CLC blends section at 300x. As for the first two cases, the bulk material appears as constituted by two principal phases, one marked by a light grey colour (SI matrix) and the other dark grey (PU inclusions). The inclusions have a broad size

distribution and they are characterized by prevalent circular shape even if sharp and irregular profiles are also observable (see magnification reported in Fig.6.48).

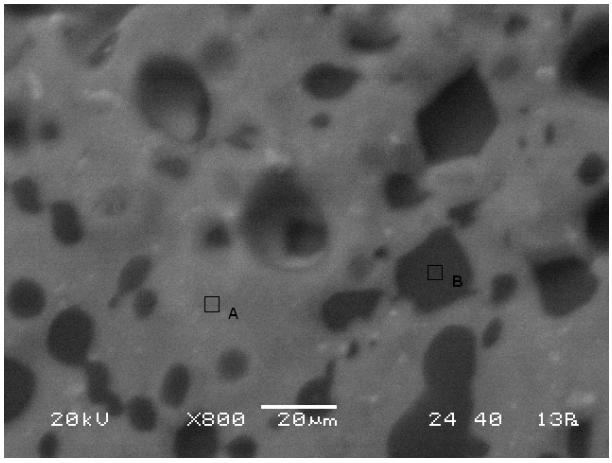

Figure 6.48. SEM image of the BJB/CLC 70/30 vol%.

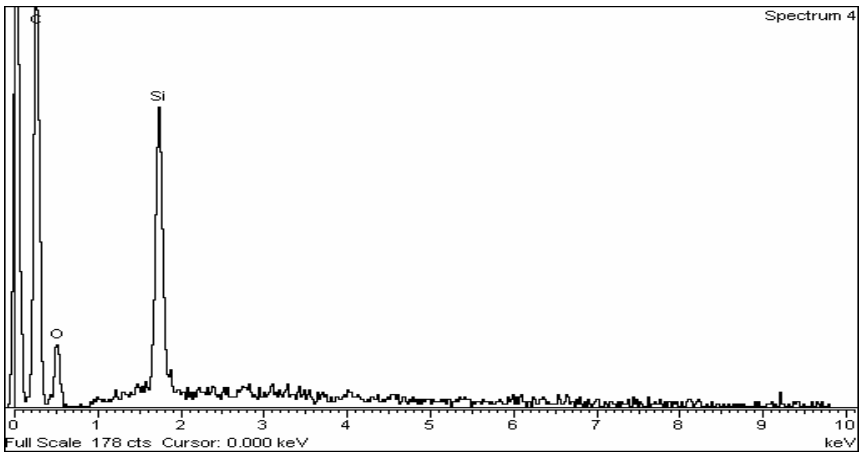

Figure 6.49: EDS (Energy Dispersive X-ray spectroscopy) spectra of the blend BJB/CLC 70/30 vol% in point *B*.

Fig.6.49 shows the chemical spectrum of a darker region characterized, also in this case, by the presence of Si, C and O atoms. This confirms that it is constituted by a mix of polyurethane and silicone, as expected from the volume ratios of the components inside the blend. Concentrations by weight relative to the blends studied are collected in Tab.6.14 for the matrices and inclusions respectively. As one can notice from Tab.6.14, concentrations of C and O are higher for the inclusions (dark grey regions, PU presence) with respect to the matrix, which resulted mainly constituted by silicones.

	Blend 70/30 vol%		**Blend 75/35 vol%**		**Blend 80/20 vol%**	
[wt%]	Matrix	Inclusion	Matrix	Inclusion	Matrix	Inclusion
C	44	70	32	65	32	71
O	18	22	25	23	30	27
Si	38	8	43	12	38	2

Table 6.14. Weight percentages for the main elements (C, O, Si) in the BJB/CLC samples analyzed.

BJB/Polytek blends

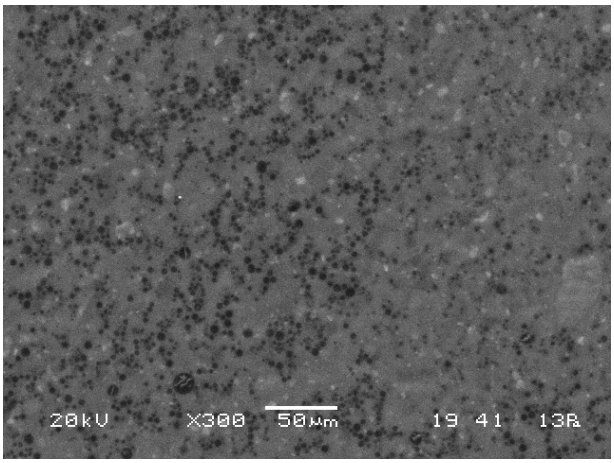

Figure 6.50. SEM image of the blend BJB/Polytek 80/20 vol%.

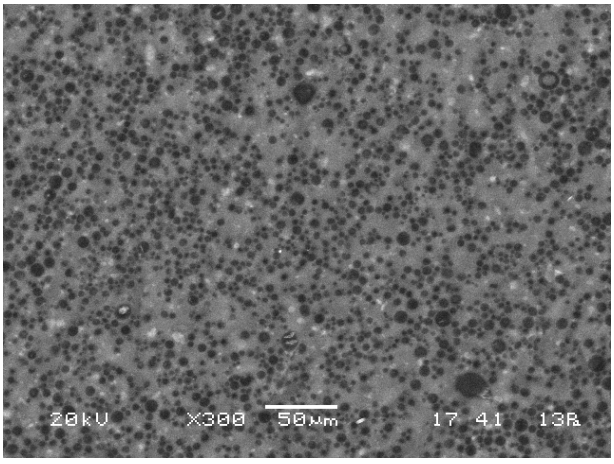

Figure 6.51. SEM image of the blend BJB/Polytek 70/30 vol%.

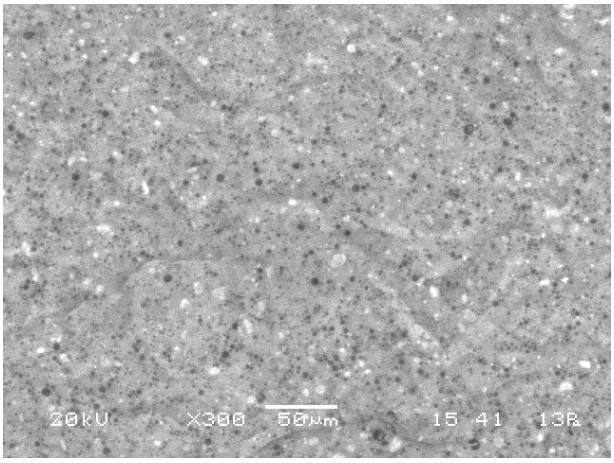

Figure 6.52. SEM image of the blend BJB/Polytek 60/40 vol%.

Fig.6.50-52 show the BJB/Polytek blends section at 300x. As for the first three cases, the bulk material appears as constituted by two principal phases, one marked by a light grey colour (matrix) and the other dark grey (inclusions). The inclusions have a small sized distribution and they are characterized by circular shape (see magnification in Fig.6.53).

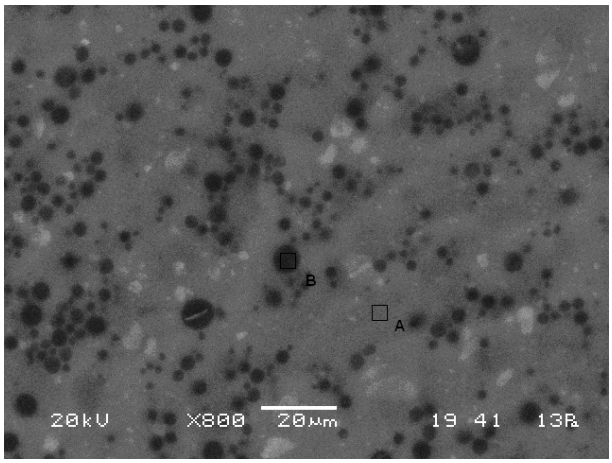

Figure 6.53. SEM image of BJB/Polytek 70/30 vol%.

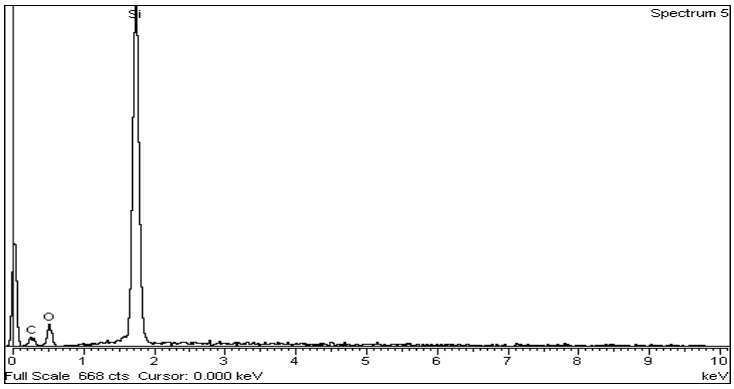

Figure 6.54. EDS (Energy Dispersive X-ray spectroscopy) spectra of the blend BJB/Polytek 70/30 vol% in point *A*.

Fig.6.54 shows the chemical spectrum of a light grey region characterized, as in the previous cases (even if not reported), by a strong presence of Si, along with weak C and O absorptions. This confirms that it is constituted by a mix of polyurethane and silicone, as expected from the volume ratios of the components inside the blend. Concentrations by weight relative to the blends studied are collected in Tab.6.15 for the matrices and inclusions respectively. As one can notice from Tab.6.14, concentrations of C and O are smaller for the inclusions (dark grey regions, PU presence) with respect to the matrix, which resulted mainly constituted by silicones.

	Blend 80/20 vol%		**Blend 70/30 vol%**		**Blend 60/40 vol%**	
[wt%]	Matrix	Inclusion	Matrix	Inclusion	Matrix	Inclusion
C	37	62	26	57	37	53
O	19	15	27	22	31	30
Si	44	23	47	21	32	17

Table 6.15. Weight percentages for the main elements (C, O, Si) in the BJB/Polytek samples analyzed.

BJB/Polytek/P3HT blends

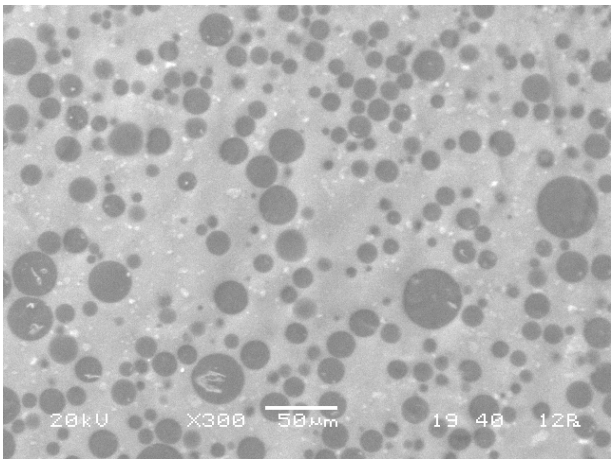

Figure 6.55. SEM image of the blend BJB/Polytek 70/30 vol%.

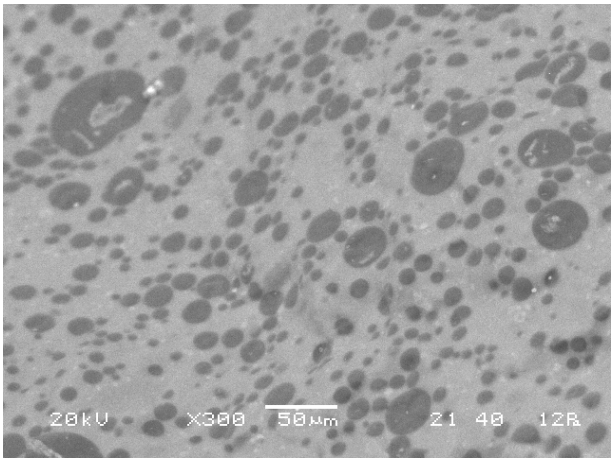

Figure 6.56. SEM image of the blend BJB/Polytek 70/30 vol% + 0,6 wt% P3HT.

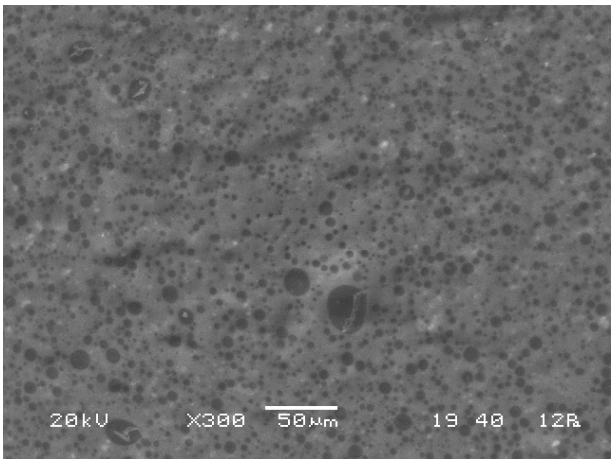

Figure 6.57. SEM image of the blend BJB/Polytek 70/30 vol% + 1,0 wt% P3HT.

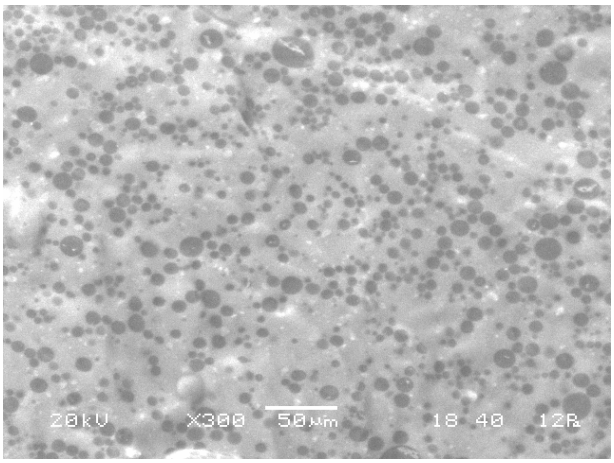

Figure 6.58. SEM image of the blend BJB/Polytek 70/30 vol% + 2,0 wt% P3HT.

Fig.6.55-58 show the BJB/Polytek/P3HT blends section at 300x. Differently from the first four cases, here the bulk material appears as constituted by two principal phases, one marked by a light grey colour (SI matrix), the other dark grey (PU inclusions) and a third middle-grey phase is visible in proximity of the PU inclusions (see detail in Fig.6.59). The inclusions have a quite broad size distribution and they are characterized by circular shape (see detail in Fig.6.59). Comparing the images pertaining to blends with different amounts of P3HT, it can be noted that inclusion size seems to be dependent on the conjugated polymer content. In particular, for the 1 wt% P3HT loading the area of the inclusions fall down from 24 μm^2 to about 11 μm^2 (Table 6.16).
Blends containing P3HT, prepared using chloroform, are not directly comparable with that consisting only of BJB and Polytek (Fig.6.50-52).
As a conclusion it can be affirmed that the P3HT has a certain influence on the microscopic distribution of the SI and PU phases inside the blend acting as "dispersant" for the two elastomeric constituents (increasing of the surface tension and decreasing of the dimension of PU inclusions in SI) while the chloroform inhibits the polymerization promoting the formation of larger inclusion areas (compare Fig.6.51 with Fig. 6.55-58).

	Area [%]	**<Area>** [μm^2]	**<Perimeter>** [µm]	**<Axes>** [µm]	**<Curvature>**
SI/PU 70/30 vol%	34,58	8	12,3	1,7 - 4	1,06
+ 0,6 wt% P3HT	31,55	24	24,6	2,5 – 8,2	0,98
+ 1,0 wt% P3HT	32,61	11	15,4	2,1 – 4,8	0,98
+ 2,0 wt% P3HT	31,78	24,6	23,3	2,7 – 7,5	1,24

Table 6.16. Total area, average area, perimeter, axes and curvature for inclusions of P3HT in the blend BJB/Polytek 70/30 vol%.

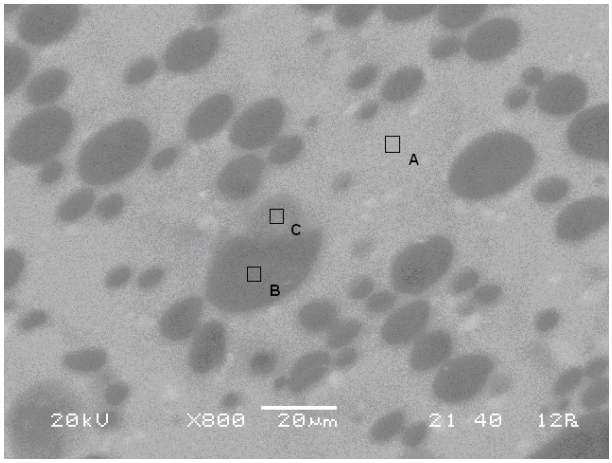

Figure 6.59. SEM image of the blend BJB/Polytek 70/30 vol% + 2,0 wt% P3HT.

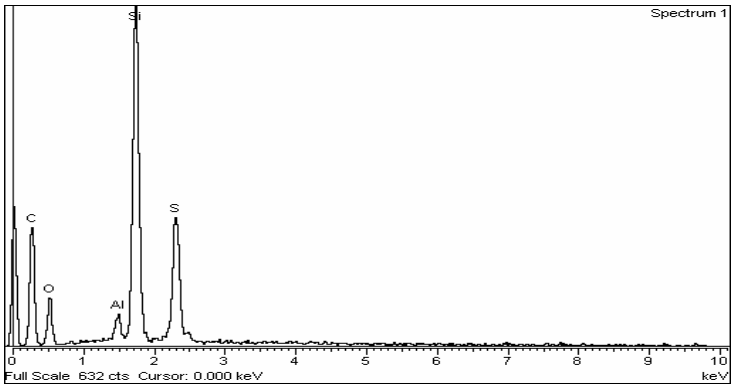

Figure 6.60. EDS (Energy Dispersive X-ray spectroscopy) spectra of the blend BJB/Polytek 70/30 vol% + 2,0 wt% P3HT in point *C*.

Fig.6.60 shows the chemical spectrum of the middle-grey inclusion characterized by a strong presence of S atoms along with C and O atoms. This suggests that it is constituted prevalently by polyurethane and P3HT. Concentration by weight relative to the blends studied are collected in Tab.6.17 for the matrices and inclusions respectively.

	Blend 70/30 vol%		**+ 0,6 wt% P3HT**		**+ 1,0 wt% P3HT**		**+ 2,0 wt% P3HT**		
[wt%]	Matrix	Inclusion	Matrix	Inclusion	Matrix	Inclusion	Matrix	Inclusion	Detail
C	50	72	42	68	47	60	50	68	59
O	29	17	32	19	30	20	23	19	21
Si	21	11	26	13	23	20	27	13	13
S	n.d.	n.d.	n.d.	n.d.	0.06	n.d.	n.d.	n.d.	6

Table 6.17. Weight percentages for the main elements (C, O, Si, S) in the BJB/Polytek samples analyzed (n.d.: not detectable).

Blends of BJB and conjugated highly polarizable molecules (PANI, pyrrole and thiophene) are not been studied with SEM microscope since they contains very low amount of filler that is not detectable by the instrument.

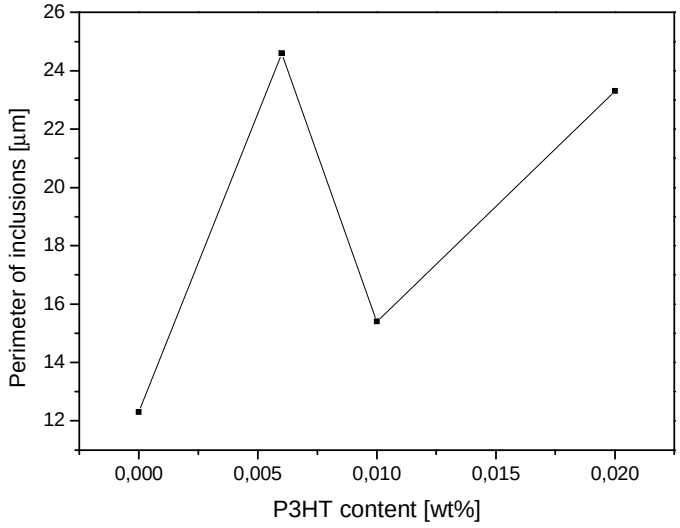

Figure 6.61. Dependence of the perimeter of the inclusions of the BJB/Polytek/P3HT blend on the P3HT content.

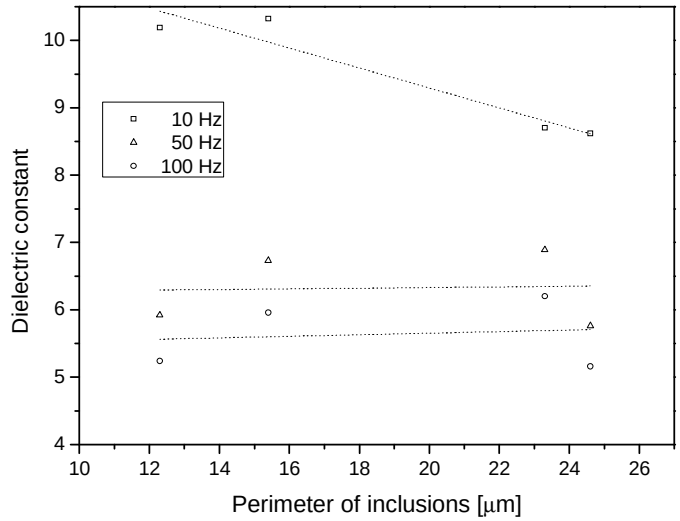

Figure 6.62. Dependence of the dielectric constant real part of the BJB/Polytek/P3HT blend on the perimeter of the inclusions at different frequencies (dotted lines are as a guide for the eyes).

Figs.6.61 reports the dependence of the perimeter of the inclusions with respect to the P3HT content, showing that for the 1 wt% concentration of conjugated polymer the average perimeter has a minimum (~ 13 μm) and thus predicting a higher dispersion of the PU-riches micro-phases into the silicone matrix. As a consequence of perimeter reduction, the dielectric constant shows a maximum, due to the higher interfaces amount between the two micro-phases (Fig.6.62).

As it appears for the Ecoflex/Polytek blends (Fig.6.35-39), and differently from other tested formulations, inclusions of the polymer, present in less volume percentage, merge after a certain road threshold. This transition phase, between a *dispersed* and a *continuous* filler/matrix morphology is defined *co-continuous* [17] and its origin is described by the Spinodal Decomposition [18, 19].

> (…) Spinodal Decomposition is a mechanism by which a solution of two or more components can separate into distinct regions (or phases) with distinctly different chemical compositions and physical properties. This mechanism differs from classical nucleation in that, phase separation due to spinodal decomposition is much more subtle and occurs uniformly throughout the material – not just at discrete nucleation sites (…)
> (…) Since there is no thermodynamic barrier to the reaction inside the spinodal region, the decomposition is determined solely by diffusion (…) [20]

From a more practical standpoint, Spinodal Decomposition provides a means of producing a very finely dispersed microstructure that can significantly enhance the physical properties of the material, in this case enhancing the dielectric response (large interphaces). Such a microstructure could be investigated by a measurement of the interfacial tension between the two components, silicone and polyurethane. Such an analysis, called Breaking Thread Method [21], calculates the interfacial tension between two different materials as directly proportional to the viscosity of the matrix and the grow rate of the distortion and inversely proportional to the wavelength of the distortion itself. It is not part of the present work, but it could be the object of future studies regarding the analysed blends. For a deep argumentation on the topic please refer to [17, 21].

6.2.4 Dynamic-mechanical characterization

In order to study the dynamic-mechanical properties of BJB/Polytek/P3HT blends, two different analysis were performed, one scanning in temperature (at 100 Hz, -100°<T<50°, heating rate 2 °C/min, static strain 5%, dynamic strain<1%) and one varying the static strain applied (at 100 Hz, T=20°C, 10%<static strain<400%, dynamic strain 5%). A dynamometer model EPLEXOR® 100N by *GABO Qualimeter Testanlagen GmbH* [22], Germany was used. Results of elongation tests are reported below for the different blends.

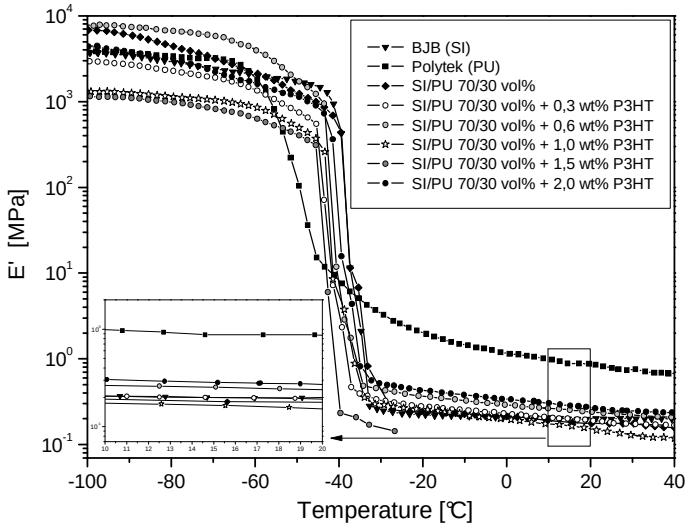

Figure 6.63. Elastic modulus real part *vs* temperature for the BJB/Polytek blends.

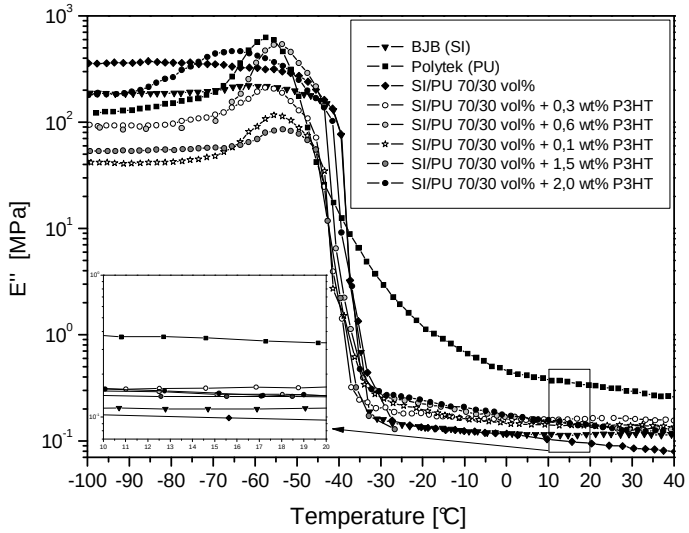

Figure 6.64. Elastic modulus imaginary part *vs* temperature for the BJB/Polytek blends.

The snap decrease of the elastic modulus *E*, both real and imaginary part, showed in Fig.6.63-64 for silicone-based elastomers, and less emphasized for the pure polyurethane, is due to a second order transition, the glass transition of the materials.

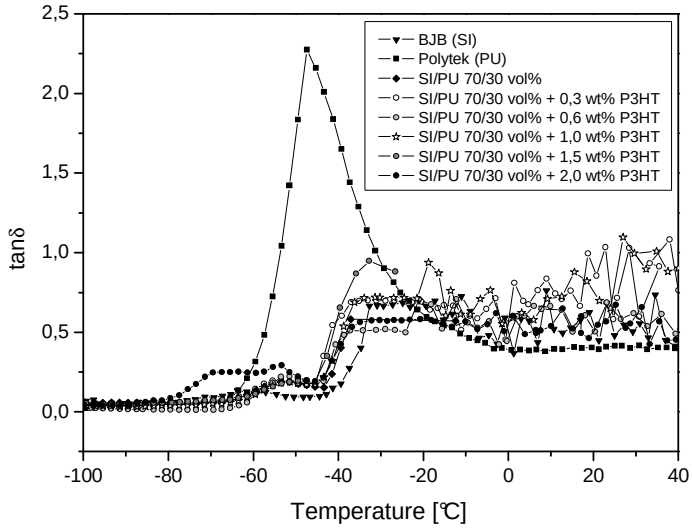

Figure 6.65. Tanδ *vs* temperature for the BJB/Polytek blends.

Data collected in Fig.6.63-65 show that not particular differences in the elastic modulus occur for the samples tested. Both real and imaginary parts of *E* for the blends lie, in fact, next to those of the two constituents, all below the relatively stiffer polyurethane and next to the extremely soft silicone.

To notice the fact that above the 0 °C temperature, the SI/PU 70/30 pure blend presents both real and imaginary part of *E* lower than those of pure silicone and polyurethane. For other blends containing P3HT, there is not a direct proportionality between the P3HT content and the mechanical response.

As stressed for the dielectric properties, the interphase characteristics between the blend components strongly affect the final behaviour of the blend itself. In particular, if the dielectric polarizability of interphase is high, a great volume fraction of interphase may lead to an increased dielectric and mechanical response, the opposite for a bad affinity. The morphology of the blend also is determinant in understanding the mechanical response of a blend, as described in [23, 24] and [25, 26] for dispersed and co-continuous blends respectively. The last showing long elongated interconnected structures that do not break up because of the flow [26].

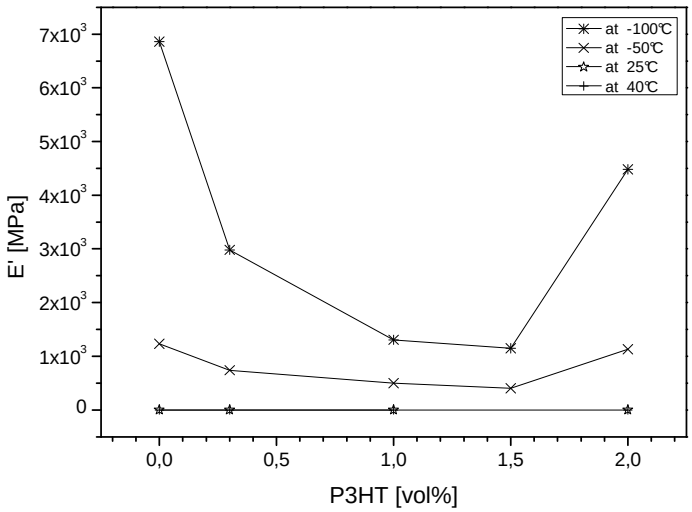

Figure 6.66. Elastic modulus real part *vs* P3HT content for the BJB/Polytek blends at different temperatures.

In particular, if analysed at low temperatures, in correspondence of the 1 and 1,5 wt% P3HT, the lower increase of modulus, with respect to the samples containing 0,3, 0,6 and 2 vol% of P3HT, is shown.

In the graphs below, the elastic modulus, real and imaginary part, is reported in function of static strain, for the samples prepared.

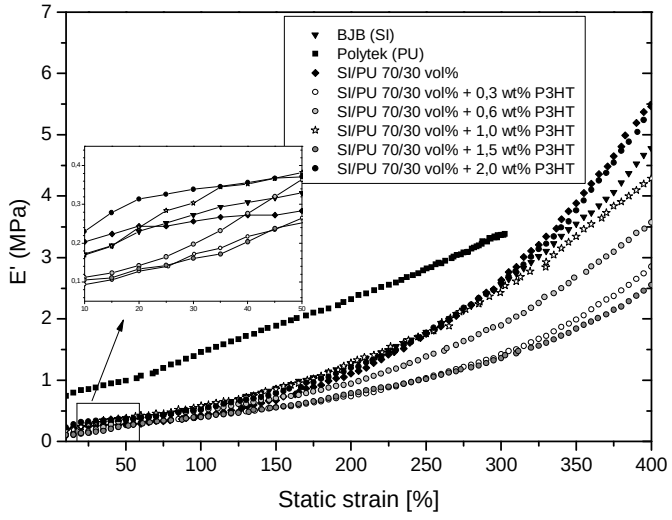

Figure 6.67. Elastic modulus real part *vs* static strain for the BJB/Polytek blends.

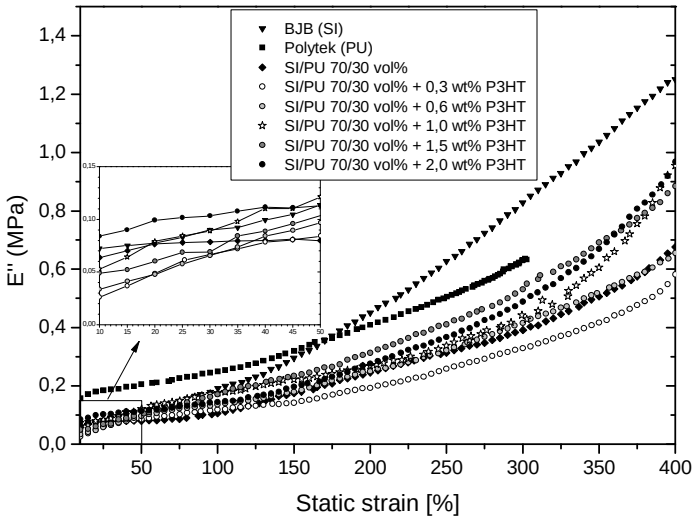

Figure 6.68. Elastic modulus imaginary part *vs* static strain for the BJB/Polytek blends.

Differently from tests performed in temperature, in this case blends moduli lie mostly under that of the two constituents especially for what concerns the imaginary part of the elastic modulus. In order to attribute a predominant viscous or elastic behaviour to the various samples, the loss factor reported in Fig.6.69 has to be taken into account.

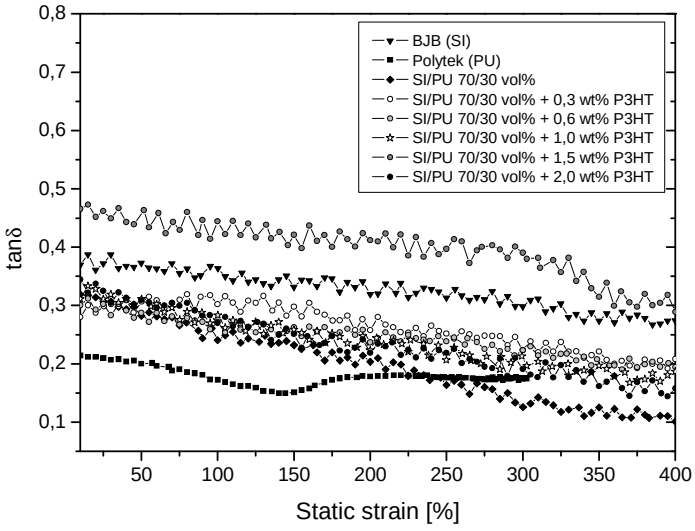

Figure 6.69. Tanδ *vs* static strain for the BJB/Polytek blends.

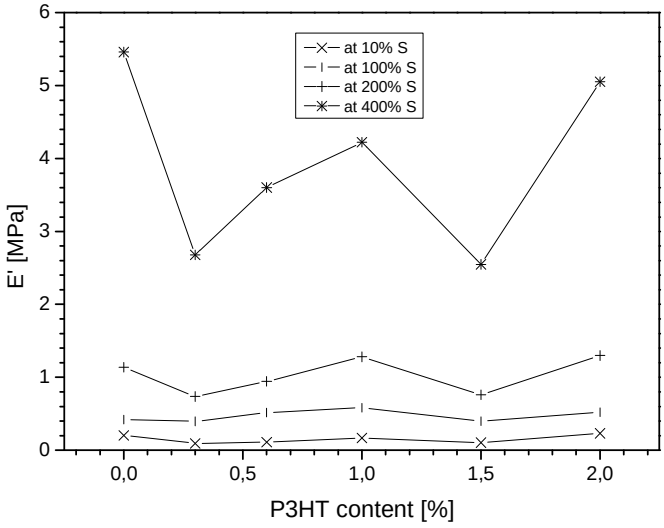

Figure 6.70. Elastic modulus real part *vs* P3HT content for the BJB/Polytek blends at different static strain.

Fig.6.70 reports the mechanical response of the SI/PU blends containing P3HT, studied by varying the static strain applied. An enhancement of the elastic modulus real part *E'* is shown for increasing applied strains; in particular, *E'* shows a maximum in correspondence of the 1 wt% P3HT. This is due probably to the peculiar morphology of this blend, that presents finely dispersed PU inclusions in the soft silicone matrix (Fig.6.57) [27].

6.2.5 Electromechanical characterization

Having selected the BJB/Polytek/P3HT blends as the best performing composition, among those prepared during the experimental activity, they were subjected to electromechanical tests in order to assess their transduction properties.

Compliant electrodes were fabricated on rectangular material strips of 40×20×1 mm, by smearing a carbon based conductive grease (Nyogel 755G, Tecnolube Seal, U.S.A.). Isotonic transverse strains were measured at 20°C as follows: each sample was vertically arranged and a contact displacement transducer (7006, Ugo Basile, Italy [28]) was connected to its lower end, while the higher part was clamped. For each sample a passive vertical pre-strain of 100% was applied by a proper load, in order to obtain a lower elastic modulus. A dc high-voltage power supply (HV-DC 205A-30P, Bertan, U.S.A.) was used to induce active strains in the pre-strained samples, by applying increasing step-wise voltages along their thickness. For each voltage, the steady-state transverse displacement of the material was recorded along its longer (vertical) dimension.

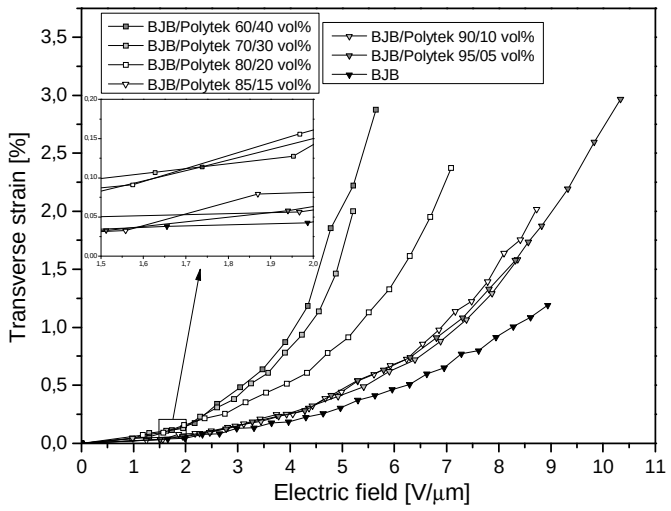

Figure 6.71. Electromechanical response of BJB/Polytek blends.

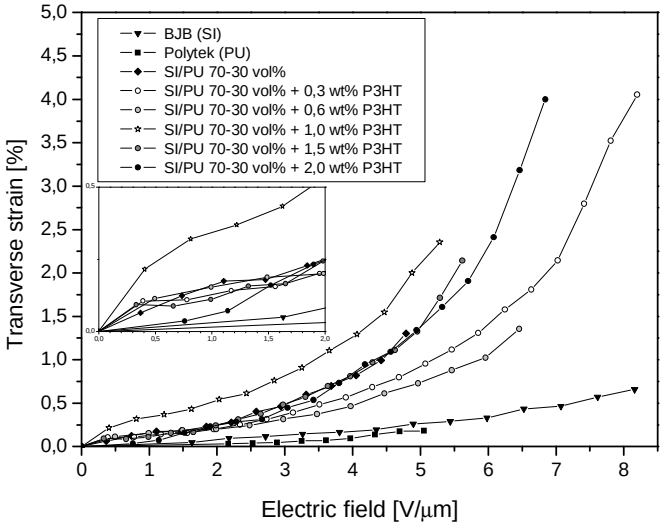

Figure 6.72. Electromechanical response of BJB/Polytek blends at different P3HT loading.

	BJB (SI)	**Polytek** (PU)	**SI/PU 70/30 vol%**	**SI/PU 70/30 vol% + 1 wt% P3HT**	**Increment** [%] **with respect to SI**	**Increment** [%] **with respect to PU**
Dielectric constant @ 10 Hz	4,2	7,3	9,75	10	*+138*	*+37*
Dielectric constant @ 10^4 Hz	3,5	6,12	4,40	4,70	*+34*	*-23*
Strain [%] @ 5 V/μm	0,25	0,20	1,5	2,12	*+748*	*+960*
Elastic energy density [J/m^3]	19	46	99	165	*+768*	*+258*

Table 6.18. Actuative performance for the BJB/Polytek/P3HT blend containing 1 wt% P3HT with respect to the pure constituents.

Data showed in Fig.6.72 reveal that the blend BJB/Polytek/P3HT 1 wt% has the best results in terms of achievable strain. Comparison with the constituents are reported in Tab.6.18 and 6.19.

	ε' @10Hz	**p** [kPa] @5V/μm	**Y** [MPa] @100% pre-strain	**Strain** [%] Linear model @5V/μm	**Strain** [%] Experimental @5V/μm
BJB	4,5	0,9	0,5	0,9	0,25
Polytek	8	1,8	1,4	0,63	0,2
BJB/Polytek 70/30 vol%	10,25	2,26	0,4	2,82	1,3
BJB/Polytek 70/30 vol% + 1 wt% P3HT	10,4	2,3	0,6	1,9	2,2
BJB + 1 wt% P3HT	5,5	1,2	0,05	12	2

Table 6.19. Electromechanical properties of the best performing samples and of the pure constituents.

The simple model considered (Eq.(2.23)) agrees quite well with the measured electromechanical strains for all samples with experimental values of strain generally lower than those predicted by the theory, except for the BJB/Polytek blend with 1 wt% of conjugated polymer. The greatest deviation from the model was obtained for the BJB with 1 wt% P3HT samples prepared in the past [6]. The evident inadequacy of the model may be simply ascribed to the use of ε' at 10 Hz, instead of static ε (as required in the model) along with the fluctuations of the dielectric permittivity due to the presence of P3HT (that brings to losses) and interphases, whose contribute is not taken into account into the theoretical model.

II SOFT ELECTRETS

Parallel to the main activity based on the increment of the performance of bulk dielectric elastomer to be employed as actuators in wearable devices, a new route has been undertaken, in the last year of activity, regarding the development of foam elastomers, characterized by low weight and low elastic moduli, to be polarized under strong electric fields. This process, called *corona charging*, produces electret materials able to retain induced charge (and thus polarization) as long as the material itself and the boundary conditions allows (see §3.3.1).
This is the first time that such a type of study is reported and the result obtained indicate that electret elastomers may represent a new way for obtaining dielectric elastomers with improved transduction performance to be used as actuators in robotic and wearable devices.

6.3 Materials

Two commercial elastomeric foams (one silicone-based and the other polyurethane-based) and one hand-made polyurethane foam were used as matrices for the preparation of electret elastomers.

6.3.1 Silicones

One silicone-based foam was used in this final part of the work. It is the already mentioned Soma Foama® 15 by *Smooth-On* [29]. For a detailed description of this material please refer to §5.3.

6.3.2 Polyurethanes

One of the two polyurethane elastomer used in this final part of the work is the already mentioned Espak Soft by *Prochima* [30] (for a detailed description of this material please refer to §5.3.2). The other is the Polytek by *Polytek* [31] (§5.3.2) opportunely prepared in order to obtain a cellular structure, as described in the following.

6.4 Experimental procedures

6.4.1 Preparation of cellular elastomer foams

Soma Foama Silicone foam by Smooth-On and Espak Soft polyurethane foam by Prochima were used as indicated by the producer.
In order to obtain a cellular structure in Polytek polyurethane instead, three ways were tried as in the following:

- loading with soluble inclusions (paraffin removed by etching)
- no degassing before cure
- loading with distilled water

The first two being classified as *physical foamization* [32, 33, 34] and the last as *chemical foamization* [35]. It is well known, in fact, that the chemical reaction of water with

isocyanate group produces carbon dioxide that remains in part trapped into the matrix in the form of gas bubbles:

$$R - NCO \leftrightarrow R - NH_2 + CO_2(g)$$

The other two techniques consist just in the inclusion of a filler in the matrix to be opportunely removed after the cure in order to leave a hole. In the case of paraffin, the removal by using a solvent (3 subsequent washings with trichloroethylene or n-heptane) has proven to be an inefficient method that caused a mechanical degradation of the matrix and its oxidation. For this reason, this process was soon abandoned. On the other hand, the non-degassing of the matrix caused a non uniform dispersion of air bubbles through the sample section. Air bubbles, in fact, were distributed preferentially in proximity of the upper surface of the sample while in the bottom part there were any. After several test to prepare foams with the three methods cited (Fig.6.73), that of chemical foamization was selected as the best method and samples were prepared using different amount of water (10, 20, 30, 40 and 50 wt% deionized water).

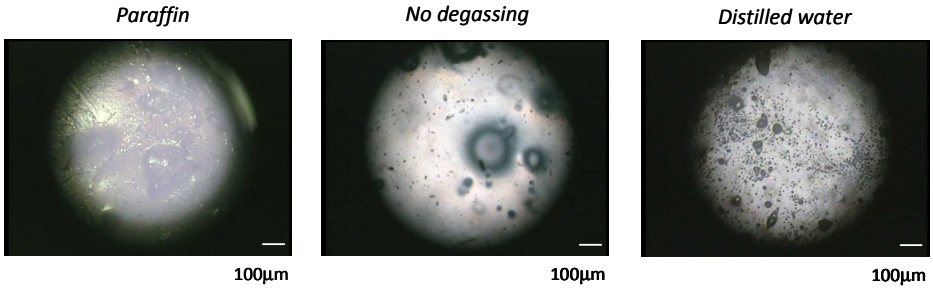

Figure 6.73. Optical images of the Polytek polyurethane during the three different foaming processes.

6.4.1.1 Foaming with deionized water

In order to obtain a uniform distribution of gas bubbles inside the matrix the samples were prepared as in the following:

- mixing of water (10, 20, 30, 40, 50 wt%) in Polytek B (polyol)
- adding Polytek A (isocyanate)
- mixing with an electromagnetic mixer for 10 min (creation of an emulsion)
- cure of the emulsion at ambient temperature for 48 hours
- degassing of the foam with a vacuum pump for 24 hours in order to extract residual water

Samples obtained were opportunely shaped for morphological, dielectric, mechanical and electromechanical analysis.

6.4.2 Morphological characterization

6.4.2.1 Optical and electronic imaging

In order to morphologically characterize the three foams, some pictures were collected.

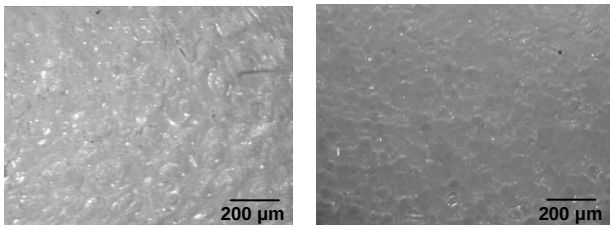

Figure 6.74. Soma Foama (left) and Espak Soft (right) cellular structure respectively (cross section).

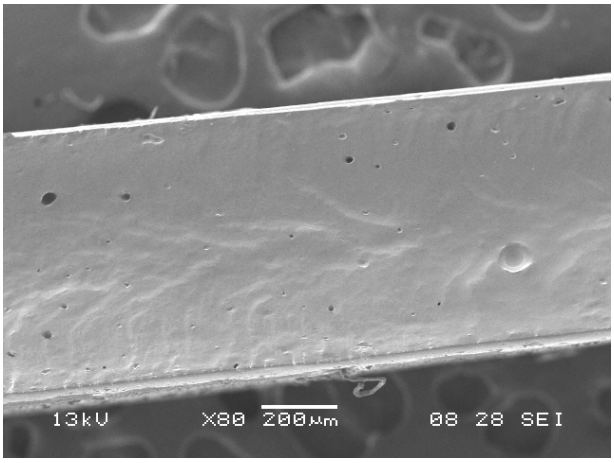

Figure 6.75. SEM micrograph of Polytek / deionized water 10 wt% sample section (in N_2).

As shown in Fig. 6.74 Soma Foama and Espak Soft foams have a very dense cell structure, while the Polytek foam, prepared in lab adding water to the reagents, presents far fewer empties not connected with each others. These empties are more or less homogeneously distributed inside the bulk and have a quite large size distribution (10-50µm). In order to characterize the Polytek foam and to be sure that the pores are present inside the overall material, we proceeded with the analysis of the specific surface area.

6.4.2.2 Specific surface area determination

The BET theory was used to extrapolate the specific surface area of the Polytek foam prepared in lab. The sample, opportunely cut and weighed, was subjected to an N_2 flux from 0 to 1 atm at T=77K (-200°C) (ASAP 2010 Physisorption Analyzer, by *Micromeritics*). The small N_2 gaseous molecules can permeate inside the bulk discontinuities and, as a consequence of the absorbed and desorbed N_2 volume, pores with diameters between 1,9 and 300 nm can be detected (it is a complementary analysis to the SEM micrography that furnishes an underestimation of the present holes, just the interconnected ones).

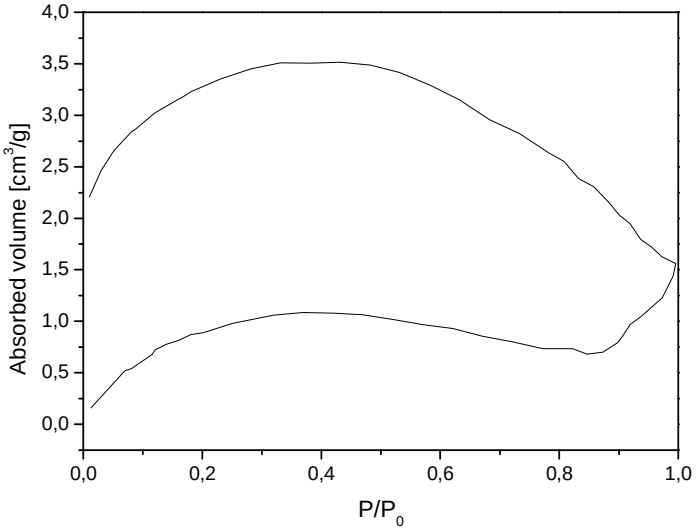

Figure 6.76. Absorbed volume for a Polytek sample (section).

The graph reported in Fig.6.76 shows the hysteresis loop of adsorbed/desorbed N_2 inside the bulk material, assessing that the structure of the sample is porous and that the N_2 desorption is someway prevented. This can be ascribed to a particular morphology of the pores or to a close-cell structure of the foam so that the gas can enter inside the bulk, but it hard desorbs when the pressure is decreased.

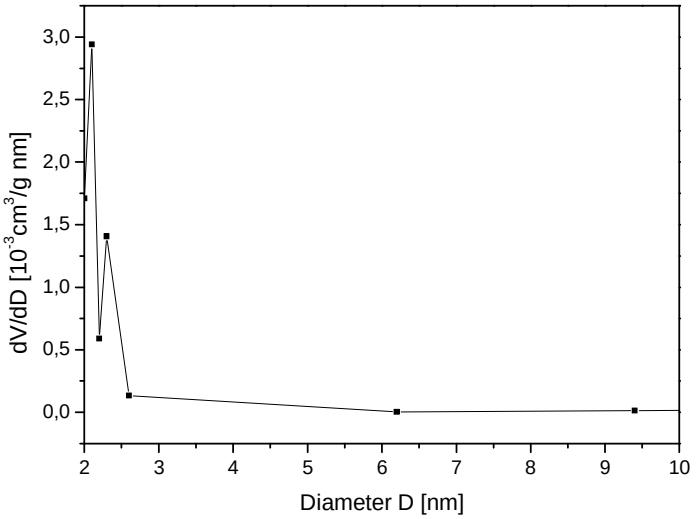

Figure 6.77. Pores diameter distribution for a Polytek sample (section).

Fig.6.77 shows that two are the main pore diameters in the range 2,9-300 nm, 2,1 nm and 2,6 nm. Other structural information are reported in the following table.

	Value	**Units**	**Method**
Surface Area (*S*)	4,0	[m^2/g]	BET
Empty volume	0,0023	[m^3/g]	BJH
<Pore diameter (*D*)>	2,2	[nm]	BJH

Table 6.20. Structural foam parameters.

In particular, the surface area S of the sample is calculated from [17]:

$$S = \frac{v_m \cdot N \cdot a}{V_M} \tag{6.1}$$

where N is the Avogadro's number, a is the area of one adsorbed nitrogen molecule ($16{,}2 \times 10^{-20}$ m^2), and V_M is the molar volume of the gas. With the assumption that the pores in the sample can be taken as an interconnected cylinder and only the surface of the pore wall is considered, the pore diameter D may be estimated by:

$$D = 4 \cdot \frac{V}{S} \tag{6.2}$$

Where V is the total volume of the pores in the sample.
Thanks to this first morphological characterization, it is possible to affirm that the prepared Polytek polyurethane foam effectively presents a porous structure and it can be used as a foam for electret applications.

6.4.3 Corona charging and poling

Corona charging and poling of samples (Polytek foam prepared by adding 10 wt% deionized water) was performed by using a concentrated electric field (5 V/μm). Samples were subjected to corona charging and poling in order to polarize the bulk material (injection of charges inside the material and subsequent polarization) as described in the previous chapters (§3.3.1) [36].

6.4.3.1 Dielectric strength determination

A dc high-voltage power supply (HV-DC 205A-30P, Bertan, U.S.A.) was used to apply increasing step-wise voltages along the sample thickness in order to identify the threshold limit and preserve further samples from electric rupture.
Five samples for each of the three foams (§6.4.2.1) were subjected to increasing electric fields and a threshold limit of 5 V/μm was identified for them.

Figure 6.78. Poling cell, first (left) and final (right) version.

6.4.3.2 Corona charging and poling of foamed samples

The same equipment used for the determination of the dielectric strength of samples (Fig.6.78) was employed for the charging and poling procedure also. It consists in two metallic electrodes, one "infinite" and one almost point, between which the sample is set. The foam has one side in contact with the large plate electrode while the other electrodes (a bundle of 12 steel needles) are at 0,5 mm from the opposite side. The first cell was built

with polystyrene supports and a tin foil was used as bigger electrode. The second cell instead consisted in a plexiglass cylindrical case with a steel disk in the bottom and metallic wires directly settled to the electrodes in order to reduce signal-to-noise ratio and assure a good electrical contact between the power supply and the cell. Tests reported in this work were performed in air, but future test in controlled atmosphere are planned, so to reduce problems due to electrical discharge in air (presence of humidity). Thanks to the Paschen law, in fact, we know that there is a minimum in the electrical strength of a gas at a certain pressure in a given gap (Tab.6.21) and that it is valid both for the external and the internal (void) gas used for the charging and poling [37]. The Paschen law is based on the Townsend breakdown mechanism in gas-filled gaps and it is reported in the equation below:

$$V_{threshold} = \frac{Bpd}{C + \ln(pd)} \tag{6.3}$$

where

$$C = \ln\left(\frac{A}{\ln\left(1 + 1/\gamma\right)}\right) \tag{6.4}$$

A and *B* are experimentally defined constants, C is given by Eq.(6.4), *p* is the gas pressure, *d* the gap dimension and γ is the so-called second ionization coefficient, which is usually poorly known.

Gas	$V_{threshold}$ [V]	$Pd_{threshold}$ (@ 1 atm)	$d_{threshold}$ [μm]
Ar	137	0,9	11,8
N_2	251	0,67	8,8
Air	327	0,567	7,5
N_2O	418	0,5	6,6
O_2	450	0,7	9,2

Table 6.21. Electrical breakdown data of various gases.

Used poling time were 15 seconds, 3 and 5 minutes.

6.4.4 Wide band dielectric spectroscopy

Samples were prepared as described in §5.4.1 and a vector network analyser (mod. ZVRE by Rohde & Schwartz was used for the acquisitions according to [9]. Dielectric spectra of both real and imaginary part of the permittivity were thus acquired for samples subjected to different poling times (15 sec, 3 min and 5 min) and they are reported in the following.

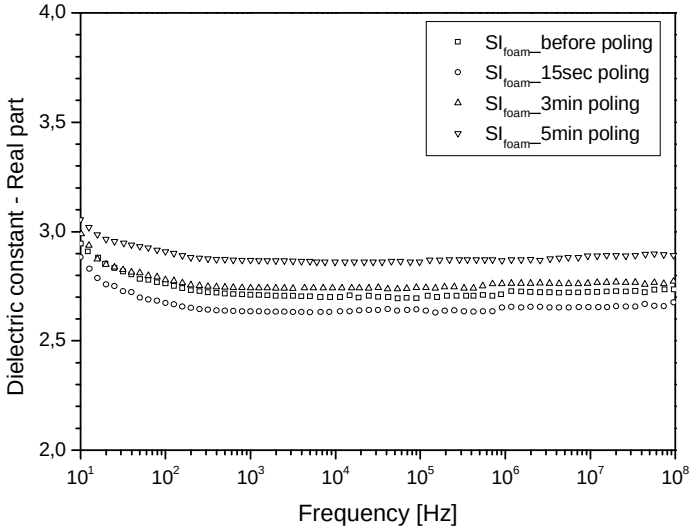

Figure 6.79. Real part of the dielectric permittivity for the Soma Foama commercial silicon foam.

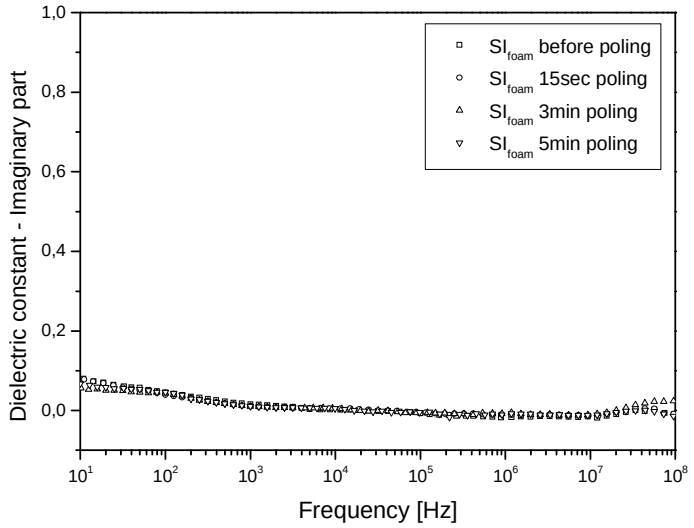

Figure 6.80. Imaginary part of the dielectric permittivity for the Soma Foama commercial silicon foam.

Small increments (from 2,8 up to 2,9 at 10^2 Hz) of the dielectric constant real part are visible after an exposure time of 5 minutes for the Soma Foama silicone foam. The imaginary part doesn't change at all. Shorter exposure times seem to have negative influence onto the dielectric response of the sample.

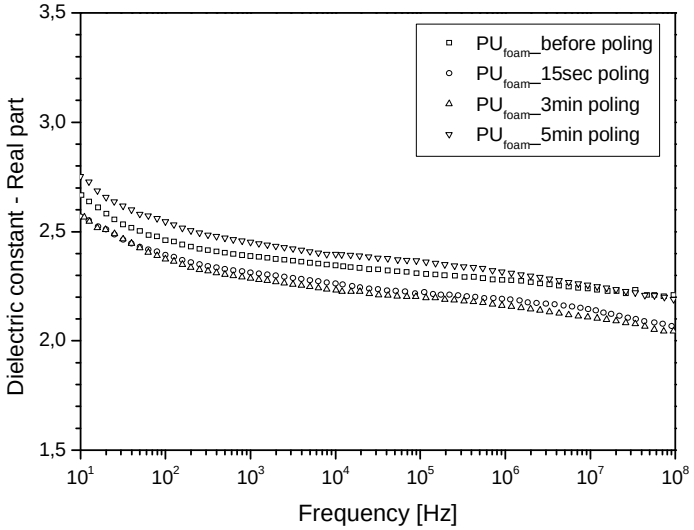

Figure 6.81. Real part of the dielectric permittivity for the Espak Soft commercial polyurethane foam.

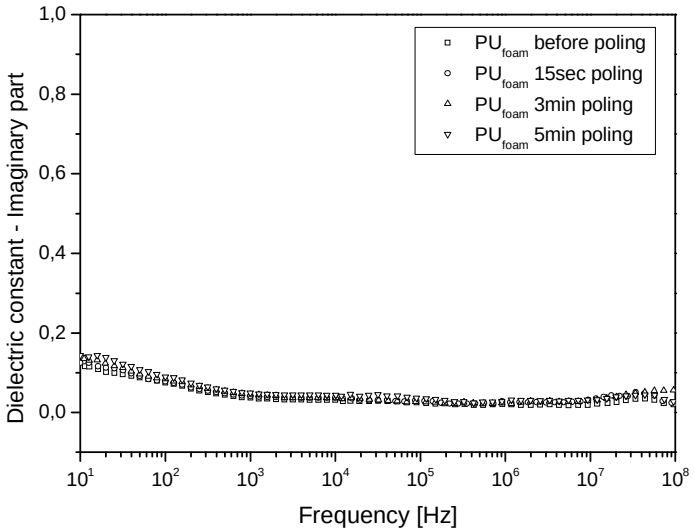

Figure 6.82. Imaginary part of the dielectric permittivity for the Espak Soft commercial polyurethane foam.

Small increments (from 2,45 up to 2,55 at 10^2 Hz) of the dielectric constant real part are visible after an exposure time of 5 minutes for the Espak Soft polyurethane foam too. The imaginary part doesn't change at all. Shorter exposure times seem to have negative influence onto the dielectric response of the sample in this case also.

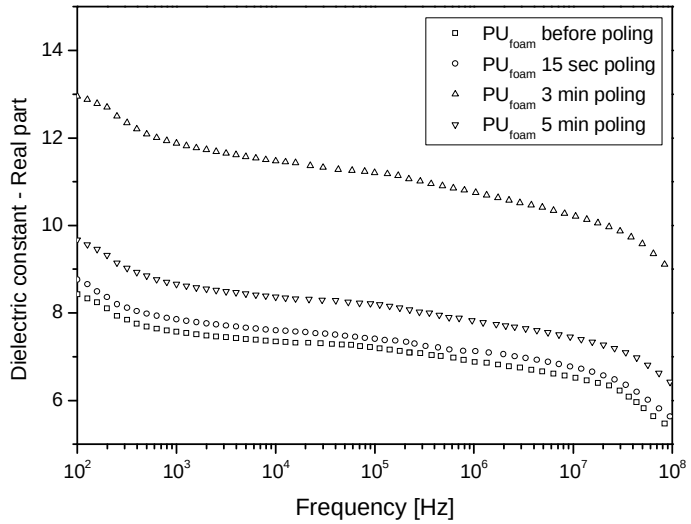

Figure 6.83. Real part of the dielectric permittivity for the Polytek foam prepared in lab.

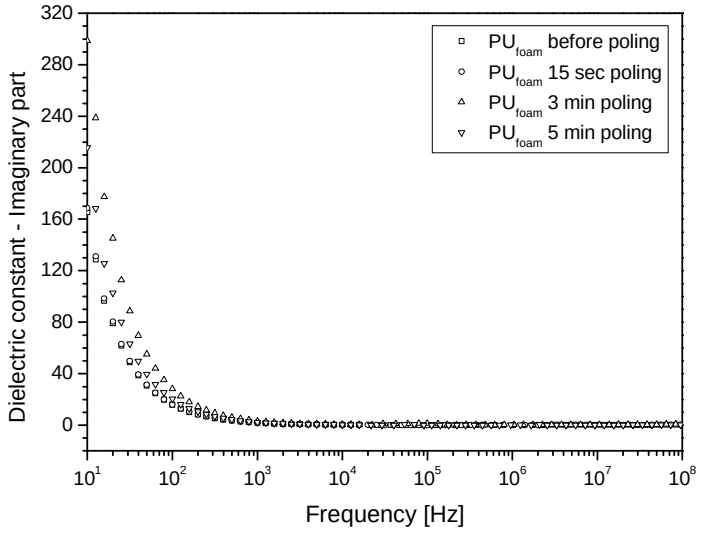

Figure 6.84. Imaginary part of the dielectric permittivity for the Polytek foam prepared in lab.

Significant increments (from 8,5 up to 13 at 10^2 Hz) of the dielectric constant real part are visible after an exposure time of 3 minutes for the Polytek polyurethane foam. The imaginary part doesn't change at all. Shorter and longer exposure times seem to have negative influence onto the dielectric response of the sample (Fig.6.85). Different situation is for the Soma Foama and the Espak Soft foams that show the largest increments of dielectric constant for an exposure time of 5 minutes.

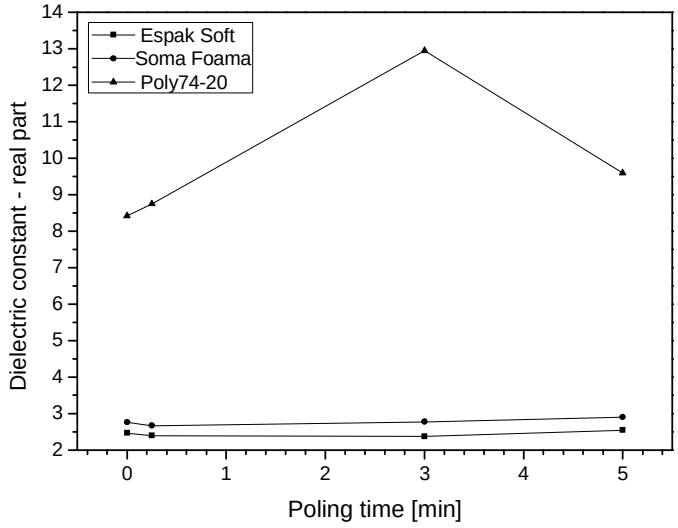

Figure 6.85. Dielectric constant real part *vs* poling time for silicone and polyurethane foams at 100 Hz.

Tests to verify the stability of charging and poling in time were performed on samples. Results are reported in the following graph for the best performing Polytek polyurethane foam.

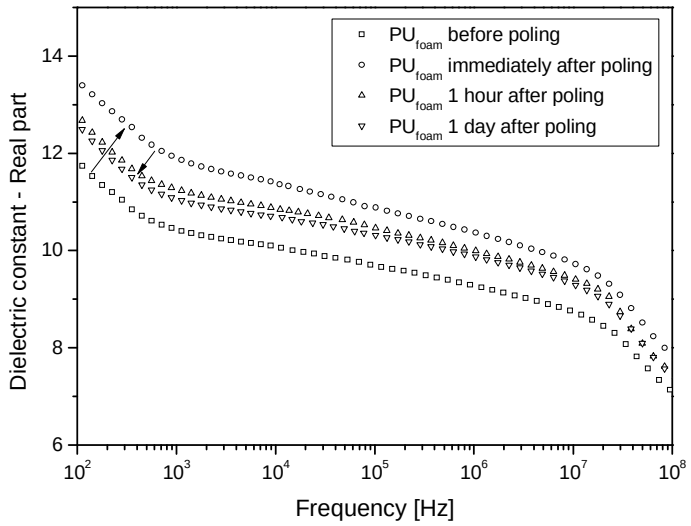

Figure 6.86. Real part of the dielectric permittivity for the Polytek foam prepared in lab.

As shown in Fig.6.86 and 6.87, charges, and consequently polarization, in the Polytek foam are retained just for few minutes into the material. After one hour at rest, the dielectric constant, in fact, decreases of about the 12% with respect to the maximum value reached immediately after the charging and poling treatment (Fig.6.87). In order to preserve charges in time, a work has been published [38] considering the possibility of poling the sample at high temperatures. As the charging temperature is increased, in fact, even deeper traps can be filled because of changes in relative capture and escape probabilities. This could be a possible way to try to preserve polarization charges also in elastomeric foam electrets. Song *et al*. [39], instead, studied the role of water (humidity) on

the charge retained by hydrophobic and hydrophilic composite materials, showing that for the firsts the contact with water had no particular effect on charge stability while for the seconds the contact with the H_2O polar molecules had resulted detrimental.

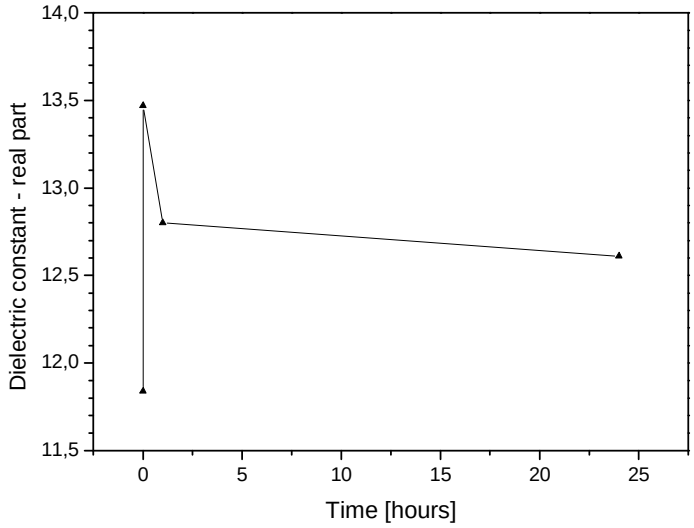

Figure 6.87. Dielectric constant real part *vs* time for the corona poled Polytek foam at 100 Hz.

6.4.5 Dynamic-mechanical analysis

In order to study the dynamic-mechanical properties of Polytek foam, a static and a dynamic strain of respectively 100% and 5% were applied onto a sample and a frequency sweep ranging from 0,1 to 100 Hz was carried out at 25 °C. A dynamometer model EPLEXOR® 100N by *GABO Qualimeter Testanlagen GmbH* [22], Germany was used, similar to previous dynamic-mechanical characterizations (§6.2.4). Results of elongation tests are reported below.

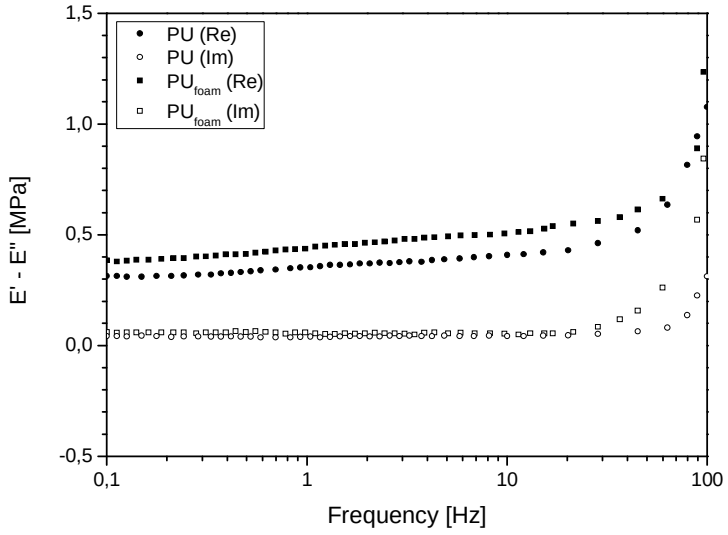

Figure 6.88. Real part of the dielectric permittivity for the Polytek foam prepared in lab.

Both the real and the imaginary part of elastic modulus *E* for the Polytek polyurethane foam, before and after foamization, show a monotonic increasing trend with respect to frequency. No phase transitions and relaxations appear in the range 0,1÷100 Hz. A slight increment of the Polytek elastic modulus is shown (about 20%), with respect to the non-foamed sample. No worsening of the electromechanical properties are expected since the elastic modulus remains below 1 MPa for the entire frequency range analysed.

6.4.6 Electromechanical analysis

The Polytek foam poled at 5 V/μm for 3 min was selected as the best performing among those tested during the dielectric end mechanical characterization, and it was subjected to electromechanical tests, in order to assess its transduction properties after poling. Samples were prepared as described in §6.2.5 and data, collected for the samples before and after poling, are compared in the following graphs.

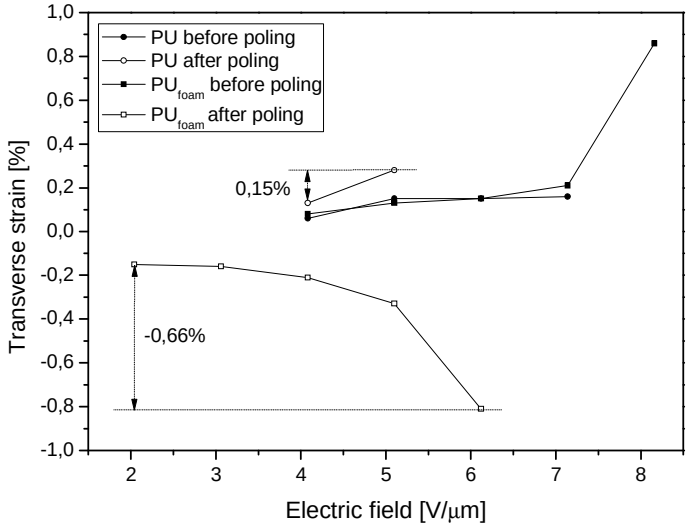

Figure 6.89. Electromechanical response of Polytek foam before and after poling.

Unlike the samples described and analysed in §6.2.5, Polytek foam samples after charging and poling react to the applied electric field with a shortening rather than a lengthening. The strain measured, in fact, is negative.

In general, both the bulk and the foam polyurethane, after the charging and poling process, increase their achievable strain for a given electric field. Polytek foam after poling, for example, reacts to an electric field of 2 V/μm with a strain of 0,15% in module, while the respective un-poled sample starts to strain at 4 V/μm with an elongation of 0,08%.

This peculiar bending behaviour of polyurethane based actuators has been widely described elsewhere [40, 41, 42, 43, 44] and its origin has been mainly related to the ionic content inside the bulk material. Such ionic species, often present within the polyurethane due to its strong polarity, can migrate under the application of an external electric field, generating a gradient in the elastic modulus and a consequent bending (closure) of the actuator in the direction of the stiffer side. The removal of ionic contaminants from the polyurethane by electro-dialysis reduces the degree of deformation, while the addition of

small amount of lithium bromide changes the bending direction. Further studies on the role of ionic content and electric field polarity and frequency are currently under investigation.
The electromechanical results obtained in this part of activity have been encouraging, the charging and poling process, in fact, have enhanced the achievable strain of Polytek polyurethane foam during actuation. Nevertheless, the role of permittivity in electret materials has not yet been clarified. From theory in fact it is known that with the increasing of the electric field above the coercive field, more and more dipoles are poled and less and less dipoles are left which can be poled, so the dielectric constant decreases with the electric field. Finally, the whole material saturates and the dielectric constant goes to a minimum. In the present work, however, for different poling times, no monotonic behaviour of the dielectric constant has been found, except for the Polytek foam. Maybe, a fundamental role in this argumentation is played by the direction of the electric field used during the poling and that used during the electromechanical activation. Opposite driving fields could, in fact, partially or totally neutralise the effect of poling. A possible way to solve the problem could be that of poling the material at elevated temperature and, immediately after poling, freeze the system possibly maintaining the dipole orientation and alignment with a drawing process [45]. Other workers demonstrated how different electronegative or electropositive impurities can affect the dielectric constant of materials by increasing or decreasing it [46, 47, 48]. Zhang et al. finally [49] proved that, for polyurethane foams, with the decreasing of inner voids dimension in the film thickness direction, the air breakdown electric field of the voids can be reached during the corona charging without applying an excessively large voltage. Thus, the charging of the film is enhanced with the reduction of void dimensions. However, if the voids dimensions are too small, a higher electric field strength is necessary again.

6.5 Conclusions

By considering the results obtained during this first part of activity regarding the development and characterization of EAP to be employed as actuators for wearable applications, the following assessments can be stated:

- Largest increments of ε' mainly appear at low frequencies (<100Hz), where processes of interfacial polarization take place.
- Blends of silicone and polyurethane, opportunely formulated in order to maximize the interfacial area between the two immiscible "phases" (SI/PU 60/40 vol%), show dielectric constant and actuating strains higher than that of the pure components (Tab.6.18).
- Results obtained with the blend approach are in agreement with the theoretical model described by the Interfacial Theory.
- Formulations of Ecoflex/CLC, Ecofex/Polytek and BJB/CLC don't show significant increments of ε and strains since the reciprocal of the miscibility of the two components did not allow to reach a wide range of volume fractions. In fact, a volume fraction of about (depending on the system under study) 0,4 of the component with the highest ε (polyurethane in this case) would bring to a maximum in the ε of the blend, as described in the Interfacial Theory, and already demonstrated for the other prepared blends (BJB/Polytek).
- Possibly, if the miscibility thresholds of the Ecoflex/CLC-00, Ecofex/Polytek and BJB/CLC blends was increased, good results could be obtained also with them in terms of dielectric constant.
- P3HT, when added in 1 wt%, enhances the dielectric and electromechanical response of the SI/PU blends maintaining the elastic modulus *E* mostly unchanged.
- Next activity will be turn to the synthesis of new silicone and polyurethane elastomers with intrinsic polarities and low elastic modulus.
- New formulation of PU/P3HT blends and SI/PU/P3HT blends could be prepared and studied thanks to results obtained during this PhD.
- A study on the rheology of the silicones and polyurethanes used during this PhD thesis could allow to deeply understand how the viscosity influence the morphology of the blends (promoting or preventing mixing).
- Following the example of Gupta [50], suitable surfactants and convective mixing could be used to control the grade of dispersion of one phase into the other.

The activity concerning the development of elastomeric electrets foam also brought to interesting results. In brief:

- It is possible to create electret elastomers with enhanced dielectric and electromechanical performance.
- The corona charging and poling have effect on the performance of the bulk along with the foam structure.

- The highest ε and strain increments have been found for the Polytek polyurethane foam sample subjected to an electric field of 5 V/μm for 3 minutes.
- The corona charging and poling of Polytek polyurethane foams produces electrects able to respond to lower electric fields in terms of attainable strains (an electric field of 2 V/μm produces a strain of about 1,5% in the foam PU while, to have the same strain, the bulk PU needs at least 4 V/μm if it has been poled and about 5 V/μm are needed for the foam and bulk PU before poling).
- The charging and poling of the PU stimulate a bending behaviour which is known to be a typical feature of polyurethanes. Differently from traditional DE actuators, in fact, PU, if subjected to external electric fields, maybe due to a gradient in the elastic modulus, bend instead of elongate. This behaviour is always present in PU actuators, but the introduction of empty cavities in the bulk by means of the foamization process, and the further injection of charges by the corona charging and poling, empathises this effect.

Further study in this field will regard the retaining of polarization charges in times and the consequent reduction of polarization decay by using for example higher poling temperatures [38] or hydrophobic additives [39].
Another possible way to increase the electromechanical performances of elastomeric foam electrets could be that of injecting high dielectric gas into voids during the charging and poling treatment, in order to obtain increased dielectric strength inside voids and to be able to apply higher electric fields [37]. Finally, a controlled gas diffusion expansion of the cellular electret could be performed to enhance the electromechanical response of the material as described in [51].

6.6 References

[1] http://www.smooth-on.com/
[2] http://www.bjbenterprises.com/
[3] http://www.polytek.com/cart/
[4] http://www.crosslinktech.com/
[5] Galantini F., Sviluppo e caratterizzazione di elastomeri dielettrici ad elevate permittività mediante compositi tra matrici siliconiche e filler organici ed inorganici, *Master Thesis*, A.A.2004-2005
[6] Carpi F. *et al*., *Advanced Functional Material*, 18, 235-241, 2008
[7] Galantini F. *et al*., *ACTUATOR 10 International Conference and Exhibition on New Actuators and Drive System*, Bremen, 2010
[8] http://www.thermoscientific.com/
[9] R. Pelster, *IEEE Trans. Microw. Theory Tech*., *43*, 7, 1494, 1995
[10] Brandrup J. *et al*., Polymer Handbook, John Wiley & Sons, 2005
[11] Varma R. *et al*., *Inorganic Chemistry*, 3, 12, 1754-1757, 1964
[12] Lyashchenko A. K. *et al*., *Journal of Molecular Liquids*, 125, 130-138, 2006
[13] Carpi F. *et al*, Enhancing the Dielectric Permittivity of Elastomers in *Dielectric elastomers as electromechanical transducers*, Elsevier, 2008
[14] Todd G. *et al*., *IEEE Transactions on Dielectrics and Electrical Insulation*, 12, 3, 2005
[15] Todd G. *et al*., *Journal of Applied Physics*, 94, 7, 2003
[16] http://www.perkinelmer.com/it/
[17] Li J. *et al*., *Macromolecules*, 35, 2005-2016, 2002
[18] Cahn J. W., *Acta Metallica*, 9, 795, 1961
[19] Cahn J. W. et al., The Journal of Chemical Physics, 28, 2, 1958
[20] Hilliard J. E., Spinodal Decomposition in *Phase Transformations*, p.497, American Society of Metals, Metals Park, 1970
[21] Elemans P. H. M. *et al*., *Journal of Rehology*, 34, 8, 1990
[22] http://www.gaboqualimeter.com/
[23] Garboczi E. J., *et al*., *Mechanics of Materials*, 33, 455-470, 2001
[24] Ozmusul M. S. *et al*., *Polymer Composites*, 23, 1, 2002
[25] Veenstra H. *et al*., *Polymer*, 41, 1817-1826, 2000
[26] Potschke P. *et al*., *Journal of Macromolecular Science Part C*, 43, 1, 2003
[27] Souheng W., *Polymer*, 26, 1885-1863, 1985
[28] http://www.ugobasile.com/
[29] http://www.smooth-on.com/
[30] http://www.prochima.it/
[31] http://www.polytek.com/
[32] Ferguson T. W., United States Patent n.6,818,673 B2, 2004
[33] Shastri V. P. *et al*., *Proceedings of the National Academy of Sciences*, 97, 5, 2000
[34] Kirjavainen K., United States Patent n.4,654,546, 1987
[35] Singh S. N., Blowing Agents for Polyurethane Foams, RAPRA, 2002

[36] Giacometti J. A. *et al*., *Brazilian Journal of Physics*, 29, 2, 1999
[37] Paajanen M. *et al*., *Journal of Physics D: Applied Physics*, 34, 2482-2488, 2001
[38] Bamji S. S. *et al*., *Journal of Electrostatics*, 6, 4, 373-379, 1979
[39] Song S. M. *et al*., *12th International Symposium on Electrets ISE*, 63-66, 2005
[40] Watanabe M. *et al*., *Japanes Journal of Applied Physics Part2*, 38, 8A, 872-874, 1999
[41] Watanabe M. *et al*., *Journal of Polymer Science Part B: Polymer Physics*, 39, 1061-1069, 2001
[42] Kyokane J. *et al*., *Syntetic Metals*, 103, 2366-2367, 1999
[43] Kurita Y. *et al*., United States Patent n.5,977,685, 1999
[44] Tartarisco G. *et al*., *Material Science and Engineering C*, 29, 6, 1835-1841, 2009
[45] Champa A. *et al*., *European Polymer Journal*, 33, 10-12, 1645-1649, 1997
[46] Chu S-Y *et al*., *Materials Letters*, 58, 752-756, 2004
[47] Chen T-Y *et al*., *Journal of Materials Science Letters*, 21, 1683-1685, 2002
[48] Wo L. *et al*., *Journal of Physics C: Solid State Physics*, 16, 2803-2812, 1983
[49] Zhang X. *et al*., *Journal of Material Science*, 44, 2459-2465, 2009
[50] Gupta R. *et al*., *Ind. Eng. Chem. Res*., 38, 2418-2424, 1999
[51] Paajanen M. *et al*., *11th International Symposium on Electrets ISE*, 191-194, 2002

Chapter 7

Conclusions

Thanks to both the good results achieved in these three years with the technique of blending applied to dielectric elastomer actuators and the discrete levels of reliability obtained with the configurations of polymeric sensing and energy generation, a substantial step further, in terms of materials and technologies, for the development of a wearable multifunctional prototype, has been taken (a detailed descriptions of the results obtained for the three separated areas, energy generation and storage, sensing and actuating, are reported at the end of each chapter).

From the materials point of view, the trend just started about elastomeric polarized (electret) foams proved to be quite promising, both in terms of dielectric and electromechanical response enhancement. It is a novelty in the field of actuation, and it will be thus another focal point for activities in the forthcoming time.

Energy generation by using piezoelectric PVDF transducers has not completely yielded the desired results, but improvements in the energy conversion could be reach by means of more thick polymeric transducers and suited circuitry for the recovery of charges at low frequencies.

During the next months, thanks to undergoing and just started projects, which allowed the establishment of stimulating collaboration with several European groups specialized in material science and ICT (Information, Communication and Technology), the work developed in these three years can be pursued. An activity for the synthesis of polyurethane elastomers, in order to prepare more efficient electromechanical transducers materials by maximizing the ratio ε/Y will be carried on. The possibility of extruding the best "performing " elastomers in the form of fibers to further improve their integration into wearable systems, will be considered, since this type of configuration for dielectric elastomers has not yet been realized and it would represent a remarkable achievement from a technological standpoint.

Possible applications will then regard the implementation of dielectric elastomer actuators in clothes in order to modify the texture / porosity of textiles along with the production of actuating fibers, as mentioned before. Thanks to the bending properties of the polyurethane EAP studied during the PhD thesis, drug delivering systems (micro-pumps) could be design and developed to be embedded in garments along with sensing devices that could be used for robotic applications (artificial skin, haptic systems).

Appendix

Scientific Production

Papers in peer-reviewed journals

1. De Rossi D., Carpi F., Galantini F., Functional Materials for Wearable Sensing, Actuating, and Energy Harvesting, *Advanced in Science and Technology*, vol. 57, pp 247-256, 2008
2. Gallone G., Carpi F., Galantini F., De Rossi D., Levita G., Enhancing the Electro-Mechanical Response of Maxwell Stress Actuators, *Advances in Science and Technology*, vol. 61, pp. 46-53, 2008
3. Carpi F., Gallone G., Galantini F., De Rossi D., Silicone-Poly(hexyl-thiophene) blends as elastomers with enhanced electromechanical transduction properties, *Advanced Functional Materials*, vol. 18, pp. 235-241, 2008
4. Gallone G., Galantini F., Carpi. F., Perspectives for new dielectric elastomers with improved electromechanical actuation performance: composites *versus* blends, *Polymer International*, vol. 59, 3, pp. 400-406, 2010
5. Galantini F., Gallone G., Carpi F., Transducers materials for wearable sensing techniques: a breaf overview, *Sensors Letters*, submitted.

Chapter or part in a book

6. Gallone G., Carpi F., Galantini F., De Rossi D., Enhancing the dielectric permittivity of elastomers in *Dielectric elastomers as electromechanical transducers Fundamentals, materials, devices, models & applications of an emerging electroactive polymer technology*, pp. 51-68, 2008

Papers in international conferences (Oral contributions)

7. Carpi F., Gallone G., Galantini F., De Rossi D., Enhancement of the electromechanical transduction properties of a silicone elastomer by blending with a conjugated polymer, *10th SPIE Conference - EAP Actuators & Devices (EAPAD)*, vol. 6927, pp. 1-11, San Diego, California, USA, 10 March 2008
8. Gallone G., Carpi F., Galantini F., De Rossi D., Levita G., Enhancing the Electro-Mechanical Response of Maxwell Stress Actuators, *CIMTEC, 3rd International Conference on Smart Materials, Structures and Systems*, Acireale (CT), 8-13 June 2008
9. Galantini F., Gallone G., Carpi F., Improving performance of electro-active polymers (EAPs) *via* Corona Charging, *EuroEAP, First international conference on Electromechanically Active Polymer (EAP) transducers & artificial muscles*, Pisa, 8-9 June 2011
10. Gallone G., Galantini F., Carpi F., Intrinsic bimorph bending response of a polyurethane DEA, *First international conference on Electromechanically Active Polymer (EAP) transducers & artificial muscles*, Pisa, 8-9 June 2011

Short papers in international conferences (Poster contributions)

10. Carpi F., Frediani G., Mannini A., Gallone G., Galantini F., De Rossi D., Artificial muscles based on dielectric elastomer actuators: achievements and challenges, *Primo Congresso Nazionale di Bioingegneria*, pp. 727-728, Pisa, 3-5 July 2008
11. Galantini F., Gallone G., Levita G., Soft elastic modulus and high dielectric constant: a synergistic matching for elastomeric actuators, *ACTUATOR 10, International Conference and Exhibition on New Actuators and Drive System*, Bremen, 14-16 June 2010
12. Galantini F, Gallone G., Carpi F., Levita G., De Rossi D., Soft elastomeric electrets for electroactive polymers, *ISE14, 14th International Symposium on Electrets*, Montpellier, 28-31 August 2011

Partecipations in a project

European Projects:

PROETEX Protection e-Textiles: Micronanostructured fibre systems for Emergency-Disaster Wear, 6PQ, 2006-2009, over

FLEXIFUNBAR Multifunctional barriers for flexible structures, textiles, leather and paper, 6PQ, 2004-2008, over

Fondazione CARIPI:

New Polymer Systems with Electric and Optical Functionalities via Nano and Micro Adhesive Dispersion to Produce Materials and Devices for Smart Applications (POLOPTEL), 2011-2014, ongoing

COST Action:

European Scientific Network for Artificial Muscles (ESNAM), 2010-2014, ongoing

Collaborations

Technical University of Lodz (TUL), Polonia; contact person: Dr. M. Cybula

Ghent University (UGhent), Belgio; contact person: Dr. L. Van Langenhove

Università di Pavia (Dip. di Ing. Elettronica), Italia; contact person: Ing. Dott. D. Miatton

Università di Genova (Dip. di Informatica, Sistemistica e Telematica (DIST)), Italia; contact person: Prof. G. Cannata

Acknowledgements

I finally reached the last (but not least!) page. The page dedicated to all the persons who helped me during this years of research and personal growth.

First of all, I would like to thank my supervisor Dott. Giuseppe Gallone, for his scientific support and his humanity, his patience and his precious advices, he followed me during my entire activity leaving me free to undertake new routs and teaching me to have critical spirit towards myself and my results. Thanks to him I could work for three years in a serene and stimulating environment.

I would like to show my gratitude to Dott. Ing. Federico Carpi also, for his great energy and for letting me join his growing research team, involving me in always more interesting and cutting-edge activities.

Then I owe my deepest gratitude to my dear *super*visors Prof. Danilo De Rossi e Prof. Giovanni Levita for their high example and their inestimable experience and for giving me the opportunity to use laboratories and equipments.

A warm thanks to my colleagues Silvia and Shirley who shared with me these three beautiful years. Thanks for our pleasant moments together and for the interesting conversations and matches. I wish them a joyful and bright future.

Thank to all the staff of the DICCISM Material Groups (present and past members!) for the good work played together.

Many thanks to my dear friends, Daniela and Giorgia for always being there, in the important moments of my life, even if our careers took us away from home and we are far away from each others. I feel you always near.

A warm hug to my family, especially those who are no longer here to rejoice with me, for having let me become the person that I am.

And finally, a special thanks to my companion Franco, who taught me to look at things differently, for his extraordinary stimulus to life and knowledge, for his example and, especially, his love. Thanks.